

# **Proportioning of Self Compacting Concrete Mixes Based on Plastic Viscosity Approach- Experimental and Numerical Investigations**

## **THESIS**

Submitted in partial fulfilment  
of the requirements for the degree of  
**DOCTOR OF PHILOSOPHY**

by

**SRI KALYANA RAMA J**

**ID NO. 2013PHXF0603H**

Under the Supervision of

**Dr. M. V. N. SIVAKUMAR**

**&**

Under the Co-Supervision of

**Prof. A. VASAN**



**BITS Pilani**  
Pilani | Dubai | Goa | Hyderabad

**BIRLA INSTITUTE OF TECHNOLOGY AND SCIENCE, PILANI**

**2018**

**BIRLA INSTITUTE OF TECHNOLOGY AND SCIENCE, PILANI**

**CERTIFICATE**

This is to certify that the thesis entitled **Proportioning of Self Compacting Concrete mixes based on Plastic Viscosity Approach-Experimental and Numerical Investigations** and submitted by **SRI KALYANA RAMA J** ID No **2013PHXF0603H** for the award of PhD of the Institute embodies original work done by him/her under my supervision.

Signature of the Supervisor

**Dr. M V N SIVAKUMAR**

Assistant Professor

Dept. of Civil Engineering

NIT Warangal

Signature of the Co-supervisor

**Prof. A VASAN**

Associate Professor,

Dept. of Civil Engineering

BITS Pilani-Hyderabad Campus

Date:

Date:

**This thesis is dedicated to the *Lotus Feet of Lord Krishna***

---

# ACKNOWLEDGEMENTS

---

I wish to express a deep sense of gratitude to my supervisors **Dr. M. V. N. Sivakumar** and **Prof. A. Vasan** for their valuable guidance, suggestions, encouragement and moral support throughout the entire duration of this research work. It is indeed an honour to be their Ph. D student.

My sincere thanks and appreciation to **Prof. P. N. K. Rao**, Professor, Department of Civil Engineering, BITS Pilani, Hyderabad Campus and **Prof. V. Vinayaka Ram**, Associate Professor, Department of Civil Engineering, BITS Pilani, Hyderabad Campus, who are Doctoral Advisory Committee (DAC), for their valuable suggestions, kind assistance and continuous moral support.

I am thankful to **Prof. Sridhar Raju**, Head, Department of Civil Engineering, BITS Pilani, Hyderabad Campus, **Prof. A. Jagadeesh**, former Head, Department of Civil Engineering, BITS Pilani, Hyderabad Campus, **Dr. Anausa Guharay**, Convener Department Research Committee (DRC), Department of Civil Engineering, BITS Pilani, Hyderabad Campus and **Dr. Murari R R Varma**, former Convener DRC Department of Civil Engineering, BITS Pilani, Hyderabad Campus for their continuous moral support, assistance and encouragement.

I would also express my gratitude to **Prof. K. Srinivasa Raju**, Professor, Department of Civil Engineering, BITS Pilani Hyderabad Campus, for his kind and affectionate enquiries about the work and timely encouragement.

I would also like to thank **Dr. Chandu Parimi**, Assistant Professor, Department of Civil Engineering, BITS Pilani Hyderabad Campus for his valuable inputs on numerical analysis and **Dr. Mohan S C**, Assistant Professor, Department of Civil Engineering, BITS Pilani Hyderabad Campus for his valuable inputs on conducting experiments.

Gratitude is also accorded to BITS, Pilani-Hyderabad campus, for providing all the necessary facilities to complete this research work. My special thanks to, **Prof. G. Sundar**, Director, BITS, Pilani-Hyderabad campus, **Prof. V. S. Rao**, former acting Vice-Chancellor and Director, BITS, Pilani-Hyderabad campus, for allowing me to pursue my research work successfully. My sincere thanks to **Prof. Souvik Bhattacharya**, Vice-Chancellor, BITS Pilani and **Prof. Bijendra Nath Jain**, former Vice-Chancellor, BITS Pilani, **Prof. Sanjay**

**Kumar Verma**, Dean, Academic Research Division, BITS, Pilani, **Prof. Vidya Rajesh**, Associate Dean, Academic Research Division, BITS, Pilani-Hyderabad campus, **Prof. P. Yogeewari**, Associate Dean, Sponsored Research and Consultancy Division, BITS Pilani-Hyderabad campus, for providing the necessary infrastructure and other facilities.

I also express my gratefulness to **Dr A Ramachandra Murthy**, Principal Scientist, Fatigue and Fracture testing group, CSIR-Structural Engineering Research Centre, Chennai for his valuable inputs on the technical aspects of the research work, continuous monitoring and moral support.

I also thank **Prof Bhushan Lal Karihaloo**, Professor, School of Engineering, Cardiff University for his valuable suggestions which improved the technical aspects of the research work.

I sincerely thank **Mr. P. Sai Saran**, Assistant Manager, IJM Concrete, and former Senior Quality Executive, ACC Ltd. for his valuable inputs on the experimental part of research work. I am also grateful to him for implementing one of the mix designs practically.

Special thanks to **Dr. Arkamitra Karan** and **Dr. Rajitha K** of Civil Engineering Department, BITS Pilani-Hyderabad Campus for their valuable advice and moral support throughout the study.

I am also grateful to **Mr. Ravi Kiran** (BASF chemicals), **Mr. Srinivasa Rao** (JSW and Penna Cements), **Dr. L H Rao** (Retd Scientist, NCBM) for their valuable inputs and support.

Special thanks and appreciation to **Dr. Abhijeet Gandage**, **Mr. Darshan R. Chauhan**, **Mr. Sai Kubair K**, **Mr. Jobin George**, **Mrs. Reshmi Nambiar**, **Mr. Darshan Pujara**, **Mr. P. Chaitanya**, **Mr. P. Sai Krishna**, **Mr. Chirag Garg**, **Mr. Shubham Walia**, and **Mr. Ritesh Reddy** for their support and help.

Special thanks and appreciation to **Mr. Rajesh**, **Mr. Shankar**, **Mr. Basha** and **Mr. Hemanth**, of Civil Engineering Department, BITS Pilani-Hyderabad Campus for their help and support in smooth conducting of experiments.

I would also acknowledge **DST-FIST** for their financial assistance in procuring experimental setup which helped the final phase of research work in conducting experiments.

Acknowledgements to **Mr. Ramchandra N, Mr. Bharadwaj B, Mr. Ganesh B. V. L, Mr. Sudheer V, Ms. Swagatika M, Ms. Preeti Jha**, for their joyful support.

I would also personally thank my well-wisher and mentor **Mr. V Ramesh**, Associate Professor, V R Siddhartha Engineering College for his continuous enquiry about the work.

I would like to thank members of Xerox and Printing Sections for their ready services.

Last but not least, this work would not have been completed without the moral support I got from my grandfather **Mr. J. Suryanarayana Murthy**, my parents **Mr. J. V. G. Krishna** and **Mrs. J. Padmavathi**, my wife **Mrs. J. V. P. Pratyusha**, my sisters **Mrs. Bala Savitha** and **Ms. Anagha**, uncle **Mr. J. Chandra Mouli**, my aunt **Mrs. J. L. G. Prasunamba**, my brother-in-law **Mr. Chakradhar S** and my in-laws **Mr G N S V Ramana** and **Mrs G N V Padma**.

I would also thank each and every one who directly or indirectly helped me in the successful completion of my research work.

---

## ABSTRACT

---

With the increase in population, there is a demand for large-scale construction of high rise structures. To meet the quality of standards highly skilled labour is required to complete the construction project efficiently on time. Achieving this is a great challenge with the routine trend of timely compacting and vibrating of the concrete. Sometimes this will lead to obstruction of concrete while pumping into congested reinforcement due to delay in the process. To address this and increase the efficiency of concreting, Self-Compacting Concrete (SCC) is to be adopted because of the ease it has got in pumping concrete into congested portions. Not needing any compaction or vibration is an added advantage of using SCC. SCC is mainly preferred to conventional concrete because of its enhanced fresh and hardened properties.

Choosing alternate supplementary cementitious materials will also decide the overall economy of the construction project. There is an ecological imbalance due to the use of Ordinary Portland Cement (OPC) for making concrete. This, in turn, will release the CO<sub>2</sub> into the atmosphere and alters the health of people. With so much waste being generated, processing the same and using it as an alternate to OPC is very much essential to make eco-friendly concretes.

Nowadays the common problem faced by many of the concrete plants is the shortage of river sand as fine aggregate material. This led to the utilization of locally available materials from quarries as fine aggregate. Crushed Rock Fines (CRF) is the result of that which is an alternative to the river sand. With the percentage of fines present in CRF is more compared to river sand, it shows a better performance in terms of fresh properties.

The present study deals with the formulation of SCC mix design based on the chosen plastic viscosity of the mix and measured the plastic viscosity of the cement pastes incorporating supplementary cementitious materials with CRF and river sand as a fine aggregate. Four different combinations including two binary and one ternary mix are adopted for the current study. SCC with 100% OPC, SCC with 80% OPC and 20% Fly ash, SCC with 75% OPC and 25% GGBS, SCC with 50% OPC and 25% Fly ash and 25% GGBS are the chosen combinations for the entire course of study. Initially, plastic viscosity of the cement pastes is measured using Brookfield Viscometer. The obtained plastic viscosity values are entered as an input into the programming tool to proportion the SCC mixes. Several combinations of

mixtures are generated for each of the four cases and an appropriate combination based on the European Federation of Producers and Contractors of Specialist Products for Structures guidelines is chosen for further experimental investigation.

Influence of plastic viscosity of the mix on the fresh and hardened properties are investigated for SCC mixes with varying water to cement ratios. It is observed that for an increasing plastic viscosity of the mix, slump flow, T500 and J-ring spread increased but V-funnel and L-box decreased. Compressive, split tensile and flexural strengths decreased with the increase in plastic viscosity.

To enhance the mechanical characteristics of SCC mixes, influence of varying fibre fraction is also studied for the Ternary SCC mixes. The volume fraction of fibres and aspect ratio of fibres are entered as an input into the programming tool to obtain combinations of SCC mixtures. Hooked end steel fibres with volume ranging from 0.1% to 0.5% are chosen for the experimental investigation. Results indicated that the compressive, split tensile and flexural strengths increased with the increase in fibre volume fraction but the fresh properties slump flow, T500 and J-ring spread, V-funnel and L-box decreased.

Further, the study is extended in evaluating the fracture energy of Ternary SCC mixes with and without fibres. Fracture energy increased with the increase in fibre volume and post-peak responses are captured more accurately with the presence of fibres.

The present study also explored the possibility of formulating input parameters required for Concrete Damage Plasticity Model (CDPM) to evaluate the fracture properties of concrete. ABAQUS/CAE is used as a numerical tool for the entire course of the study. Stress-strain models Hsu & Hsu and Saenz are chosen to generate the strength and damage values of concrete in compression and tension. Further, the effect of dilation angle and eccentricity on the fracture energy is also discussed. A correction factor is proposed for Saenz model to accurately calculate the fracture properties of concrete. The proposed methodology is validated with the existing experimental works and it is observed that results are encouraging and the proposed methodology is suited for all concretes of grades up to M50.



---

# TABLE OF CONTENTS

---

|  |     |
|--|-----|
| ACKNOWLEDGEMENTS.....  | i   |
| ABSTRACT.....  | iv  |
| TABLE OF CONTENTS.....   | vi  |
| LIST OF TABLES.....  | ix  |
| LIST OF FIGURES.....   | x   |
| LIST OF SYMBOLS.....   | xiv |
| ABBREVIATIONS AND ACRONYMS.....  | xvi |
| CHAPTER 1 INTRODUCTION.....  | 1   |
| 1.1. Background of the study.....  | 2   |
| 1.2. Organization of thesis.....   | 5   |
| CHAPTER 2 LITERATURE REVIEW.....   | 7   |
| 2.1. Introduction to Rheology of SCC.....  | 8   |
| 2.1.1. Newtonian and Non-Newtonian Fluids.....   | 8   |
| 2.1.2. Models to Describe the Flow Behaviour.....                                      | 11  |
| 2.1.2.2. Power law.....  | 11  |
| 2.1.2.3. Bingham model.....  | 11  |
| 2.2. Proportioning SCC with Various Supplementary Cementitious Materials.....          | 13  |
| 2.2.1. Origin and History of SCC.....  | 13  |
| 2.2.2. Uses and Applications of SCC.....   | 13  |
| 2.2.3. Cement Replacement Materials.....   | 14  |
| 2.2.4. Crushed Rock Fines as Fine Aggregate.....                                       | 18  |
| 2.2.5. Mix design of SCC with various supplementary cementitious materials.....        | 18  |
| 2.2.6. Role of superplasticizers on the fresh properties of SCC.....                   | 27  |
| 2.2.7. Role of fibres on fresh and hardened properties of SCC.....                     | 29  |
| 2.3. Fracture properties of SCC.....   | 31  |
| 2.4. Numerical Evaluation of Conventional and SCC Using Various Plasticity Models..... | 34  |
| 2.4.1. Failure Criteria of Concrete.....   | 35  |

|  |   |     |
|--|---|-----|
| 2.5.   | Gaps Identified in Literature .....   | 39  |
| 2.6.   | Objectives of the Proposed Research .....   | 39  |
| CHAPTER 3 CHARACTERIZATION OF MATERIALS .....                                      |   | 41  |
| 3.1  | Introduction .....  | 42  |
| 3.2  | Physical and Chemical Properties of the Materials.....                              | 43  |
| 3.3  | Chemical Analysis.....  | 44  |
| 3.3.1  | X-Ray Diffraction .....   | 44  |
| 3.3.2  | X-Ray Fluorescence.....   | 47  |
| CHAPTER 4 DEVELOPMENT OF SCC MIXES BASED ON PLASTIC VISCOSITY OF CEMENT PASTE..... |   | 53  |
| 4.1.   | Introduction .....  | 54  |
| 4.2.   | Measuring Plastic Viscosity for Various Cement Paste Compositions.....              | 54  |
| 4.3.   | Role of Water to Cement Ratio on Compressive Strength of Concrete.....              | 57  |
| 4.4.   | Development of Plastic Viscosity Based Mix Design for SCC .....                     | 57  |
| 4.4.1.   | For low concentrations.....   | 58  |
| 4.4.2.   | For high concentrations.....  | 59  |
| 4.4.3.   | Methodology for proportioning SCC mixes .....                                       | 61  |
| 4.4.4.   | Effect of addition of fibres .....  | 71  |
| CHAPTER 5 EXPERIMENTAL INVESTIGATION ON SCC WITH AND WITHOUT FIBRES .....          |   | 75  |
| 5.1.   | Mixing Sequence of SCC Mixes with and without Fibres.....                           | 76  |
| 5.2.   | Test methods for fresh and hardened properties of SCC .....                         | 76  |
| 5.3.   | Fresh Properties of SCC Mix without Fibres .....                                    | 79  |
| 5.4.   | Hardened Properties of SCC Mix without Fibres .....                                 | 87  |
| 5.5.   | Fresh Properties of SCC Mixes with the Addition of Hooked End Steel Fibres .....    | 93  |
| 5.6.   | Hardened Properties of SCC Mixes with the Addition of Hooked End Steel Fibres ..... | 102 |
| 5.7.   | Evaluating Fracture Properties of SCC Mixes Using Three Point Bend Tests .....      | 108 |

|   |     |
|---|-----|
| 5.7.1. Fracture Energy.....   | 110 |
| CHAPTER 6    NUMERICAL STUDIES ON FRACTURE PROPERTIES OF SCC<br>USING CDP MODEL .....                                   | 118 |
| 6.1. Introduction .....   | 119 |
| 6.2. Concrete Damaged Plasticity Model.....   | 119 |
| 6.3. Modeling Stress-Strain Curves .....  | 121 |
| 6.3.1. Formulation of Stress-Strain Curves in Compression .....   | 121 |
| 6.3.2. Formulation of Stress-Strain Curves in Tension.....  | 128 |
| 6.4.1. Birtel and Mark .....  | 130 |
| 6.4.2. Lopez-Almansa <i>et al.</i> .....  | 131 |
| 6.5. Evaluation of Fracture Properties.....   | 133 |
| 6.5.1. Characteristic length .....  | 133 |
| 6.6. METHODOLOGY AND RESULTS .....  | 134 |
| 6.6.1. Mesh convergence studies .....   | 134 |
| 6.6.2. Influence of Notch-to-depth ratio ( $a/D$ ) on fracture properties.....  | 139 |
| 6.6.3. Influence of Eccentricity and Dilation Angle on fracture properties.....   | 142 |
| 6.6.4. Comparative analysis of Hsu & Hsu and Saenz model on fracture properties for<br>various grades of concrete ..... | 147 |
| 6.6.5. Influence of varying tensile damage value on fracture energy .....   | 152 |
| CHAPTER 7    CONCLUSIONS .....  | 154 |
| CONTRIBUTIONS FROM THE STUDY .....  | 156 |
| SCOPE FOR FUTURE WORK .....   | 157 |
| REFERENCES .....  | 158 |
| PUBLICATIOIOS FROM THE PRESENT STUDY .....  | 180 |
| RESUME .....  | 181 |
| APPENDIX A    C++ code for proportioning SCC mixes with and without fibres .....  | 182 |
| APPENDIX B    MATLAB Codes for generating compression and tension data for Concrete<br>Damage Plasticity Model.....     | 188 |

---

## LIST OF TABLES

---

|  |     |
|--|-----|
| Table 2.1 Typical viscosities of some common materials .....                                   | 9   |
| Table 3.1 Chemical and physical properties of Ordinary Portland Cement, fly ash and GGBS ..... | 50  |
| Table 3.2 Chemical composition of blended cements .....  | 50  |
| Table 3.3 CSH gel volumes for various combinations of blended cements .....                    | 51  |
| Table 3.4 Bogue's Compounds Content (By % Wt) for Various Combinations.....                    | 51  |
| Table 4.1 Mix combinations .....   | 54  |
| Table 4.2: Plastic Viscosity values in Pa s for various combinations of cement paste.....      | 56  |
| Table 4.3 Measured plastic viscosity of cement pastes for Case I to Case IV .....              | 56  |
| Table 4.4 Packing fractions for different types of packing of particles.....                   | 60  |
| Table 4.5 Mix proportions of SCC mixes-PV:9 w/b:0.57 .....                                     | 66  |
| Table 4.6 Mix proportions of SCC mixes-PV: 7 and 11 w/b: 0.57 .....                            | 67  |
| Table 4.7 Mix proportions for SCC mixes with river sand as fine aggregate .....                | 68  |
| Table 4.8 Mix proportions of SCC mixes-PV: 9 and 13 w/b: 0.5 .....                             | 70  |
| Table 4.9 Plastic Viscosity of mix with fibres .....   | 72  |
| Table 4.10 Mix proportions of SCC mixes with the addition of fibres for w/b = 0.5 .....        | 74  |
| Table 6.1 Summary of CDP Parameters .....  | 121 |
| Table 6.2 Correction Factor Values .....   | 124 |
| Table 6.3 Tensile stress-strain data for CDP Model .....                                       | 129 |
| Table 6.4 Tensile damage data for CDP model .....  | 132 |
| Table 6.5 Summary of FE modelling for various mesh element types and sizes .....               | 135 |
| Table 6.6 Summary of FE modelling for various notch-to depth- ratios.....                      | 139 |
| Table 6.7 Validation of numerical work - 1.....  | 141 |
| Table 6.8 Validation of numerical work - 2.....  | 151 |

---

## LIST OF FIGURES

---

|  |    |
|--|----|
| Figure 2.1 Classification of fluids with $\tau$ as a function of $\gamma$ (Rao A, 2010) .....  | 10 |
| Figure 2.2 Conventional concrete vs SCC mix (Okamura and Ouchi,2003).....  | 19 |
| Figure 2.3 Deviatoric cross section of failure surface as per CDP model .....  | 37 |
| Figure 3.1 Particle Size distribution of Aggregates .....  | 45 |
| Figure 3.2 Combined Gradation as per IS 383:2016 .....   | 45 |
| Figure 3.3 Raw Materials used for SCC mixes.....   | 46 |
| Figure 3.4 X-Ray Diffraction Patterns for OPC .....  | 48 |
| Figure 3.5 X-Ray Diffraction Patterns for Fly ash .....  | 49 |
| Figure 3.6 X-Ray Diffraction Patterns for GGBS .....   | 49 |
| Figure 4.1. Brookfield Viscometer DV3T .....   | 55 |
| Figure 4.2 Regression curve for water to cement ratio.....   | 58 |
| Figure 5.1 Mixing Sequence of SCC mix without fibres.....  | 76 |
| Figure 5.2 Mixing Sequence of SCC mix with fibres.....   | 77 |
| Figure 5.3 Volume of paste for SCC mixes for Case I (Plastic Viscosity 9 Pa s, water to binder ratio 0.57) and Case II (Plastic Viscosity 7 and 11 Pa s, water to binder ratio 0.57) ...                                 | 78 |
| Figure 5.4 Volume of solids for SCC mixes for Case I and Case II.....  | 79 |
| Figure 5.5 Slump flow for SCC mixes for Case I and Case II.....  | 79 |
| Figure 5.6 $T_{500}$ time for SCC mixes for Case I and Case II.....  | 80 |
| Figure 5.7 V-funnel time for SCC mixes for Case I and Case II.....   | 80 |
| Figure 5.8 J-ring spread for SCC mixes for Case I and Case II.....   | 81 |
| Figure 5.9 L-box ratio for SCC mixes for Case I and Case II .....  | 81 |
| Figure 5.10 Volume of paste for SCC mixes for Case III (Plastic Viscosity 9 Pa s, water to binder ratio 0.5, river sand as fine aggregate) and Case IV (Plastic Viscosity 9 and 13 Pa s, water to binder ratio 0.5)..... | 82 |
| Figure 5.11 Volume of solids for SCC mixes for Case III and Case IV .....  | 82 |
| Figure 5.12 Slump flow for SCC mixes for Case III and Case IV .....  | 83 |
| Figure 5.13 $T_{500}$ time for SCC mixes for Case III and Case IV.....   | 84 |
| Figure 5.14 V-funnel time for SCC mixes for Case III and Case IV.....  | 84 |
| Figure 5.15 J-ring spread for SCC mixes for Case III and Case IV .....   | 85 |
| Figure 5.16 L-box ratio for SCC mixes for Case III and Case IV .....   | 85 |
| Figure 5.17 Fresh properties of SCC mixes without fibres .....   | 87 |

|   |     |
|---|-----|
| Figure 5.18 7-days Compressive strength of SCC mixes-Case I and Case II.....  | 88  |
| Figure 5.19 28-days Compressive strength of SCC mixes-Case I and Case II.....   | 88  |
| Figure 5.20 7-days compressive strength of SCC mixes for Case III and Case IV .....                                   | 89  |
| Figure 5.21 28-days compressive strength of SCC mixes for Case III and Case IV .....                                  | 89  |
| Figure 5.22 Split tensile strength of SCC mixes for Case III and Case IV .....  | 90  |
| Figure 5.23 Flexural strength of SCC mixes for Case III and Case IV .....   | 90  |
| Figure 5.24 Pulse velocity of SCC mixes for Case III and Case IV .....  | 91  |
| Figure 5.25 Slump flow for SCC mixes with and without fibres for a plastic viscosity of 9 Pa s .....                  | 94  |
| Figure 5.26 V-funnel time for SCC mixes with and without fibres for a plastic viscosity of 9 Pa s .....               | 94  |
| Figure 5.27 J-ring spread for SCC mixes with and without fibres for a plastic viscosity of 9 Pa s .....               | 95  |
| Figure 5.28 for T <sub>500</sub> time SCC mixes with and without fibres for a plastic viscosity of 9 Pa s .....       | 95  |
| Figure 5.29 L-box ratio for SCC mixes with and without fibres for a plastic viscosity of 9 Pa s .....                 | 96  |
| Figure 5.30 Slump flow for Ternary SCC mix with fibres .....  | 97  |
| Figure 5.31 V-funnel time for Ternary SCC mix with fibres .....   | 97  |
| Figure 5.32 J-ring spread for Ternary SCC mix with fibres .....   | 98  |
| Figure 5.33 T <sub>500</sub> for Ternary SCC mix with fibres .....  | 98  |
| Figure 5.34 L-box ratio for Ternary SCC mix with fibres.....  | 99  |
| Figure 5.35 Fresh properties of SCC mixes with fibres.....  | 100 |
| Figure 5.36 J-ring blockage for ternary mix with 0.5% fibres.....   | 101 |
| Figure 5.37 L-box blockage for ternary mix with 0.5% fibres .....   | 101 |
| Figure 5.38 7-days compressive strength of SCC mixes with and without fibres for a plastic viscosity of 9 Pa s .....  | 103 |
| Figure 5.39 28-days compressive strength of SCC mixes with and without fibres for a plastic viscosity of 9 Pa s ..... | 104 |
| Figure 5.40 Split tensile strength of SCC mixes with and without fibres for a plastic viscosity of 9 Pa s.....        | 104 |
| Figure 5.41 Flexural strength of SCC mixes with and without fibres for a plastic viscosity of 9 Pa s.....             | 105 |

|   |     |
|---|-----|
| Figure 5.42 Pulse velocity of SCC mixes with and without fibres for a plastic viscosity of 9 Pa s.....        | 105 |
| Figure 5.43 7-days compressive strength of Ternary SCC mix with fibres.....                                   | 106 |
| Figure 5.44 28-days compressive strength of Ternary SCC mix with fibres.....                                  | 106 |
| Figure 5.45 Split tensile strength of Ternary SCC mix with fibres .....                                       | 107 |
| Figure 5.46 Flexural Strength of Ternary SCC mix with fibres .....  | 107 |
| Figure 5.47 Pulse velocity of Ternary SCC mix with fibres.....  | 108 |
| Figure 5.48 Testing on Hardened Concrete .....  | 108 |
| Figure 5.49 Notched beams of size $a/d = 0.1$ and $0.6$ .....   | 109 |
| Figure 5.50 Typical experimental setup for fracture .....   | 109 |
| Figure 5.51 Load carrying capacities of SCC mixes with and without notch .....                                | 112 |
| Figure 5.52 Size dependent fracture energies ( $G_f$ ) of SCC mixes .....                                     | 113 |
| Figure 5.53 Bilinear Tension Softening.....   | 114 |
| Figure 5.54 Trilinear Tension Softening.....  | 115 |
| Figure 5.55 Size independent fracture energies ( $G_F$ ) of SCC mixes .....                                   | 116 |
| Figure 5.56 Crack propagation of SCC specimen with $a/d$ ratio = $0.1$ .....                                  | 116 |
| Figure 5.57 Load-CMOD curves for $a/d = 0.1$ .....  | 117 |
| Figure 5.58 Load-CMOD curves for $a/d = 0.6$ .....  | 117 |
| Figure 6.1 Sum-Squared-Errors vs. Factor Value (for IS 456:2000).....   | 123 |
| Figure 6.2 Correction Factor vs. Characteristic Compressive Strength (for IS 456:2000).....                   | 125 |
| Figure 6.3 Saenz Curve for M40 grade concrete (Factor value = Correction Factor).....                         | 126 |
| Figure 6.4 Saenz Curve for M40 grade concrete (Factor value $\neq$ Correction Factor).....                    | 127 |
| Figure 6.5 Stress-Strain curve generated by Hsu & Hsu model .....   | 128 |
| Figure 6.6 Tensile Stress-Strain curve for M20 grade concrete .....   | 129 |
| Figure 6.7 Stress-Strain Plot considered by Birtel and Mark .....   | 130 |
| Figure 6.8 Compressive damage ( $d_c$ ) vs. Inelastic strain( $\epsilon_c^{in}$ ) for M40 grade concrete..... | 133 |
| Figure 6.9 Tensile damage ( $d_t$ ) vs. cracking strain ( $\epsilon_t^{ck}$ ) for M40 grade concrete.....     | 133 |
| Figure 6.10 Effect of Mesh Element size using Quadrilateral Elements .....                                    | 135 |
| Figure 6.11 Effect of Mesh Element size using Triangular Elements .....                                       | 136 |
| Figure 6.12 Effect of Mesh Element type using 2mm mesh element size.....                                      | 136 |
| Figure 6.13 Effect of Mesh Element type using 5mm mesh element size.....                                      | 137 |
| Figure 6.14 Effect of Mesh Element type using 10mm mesh element size.....                                     | 137 |
| Figure 6.15 Effect of Mesh Element type using 25mm mesh element size.....                                     | 138 |

|   |     |
|---|-----|
| Figure 6.16 Effect on fracture energy with variation in mesh element type and size.....   | 138 |
| Figure 6.17 Load-Displacement curves for different notch-to-depth ratios (M50 Grade Concrete).....                                  | 140 |
| Figure 6.18 Effect on peak loads with varying notch-to-depth ratios (M50 Grade Concrete) .....                                      | 140 |
| Figure 6.19 Effect on fracture energy with variation in notch-to-depth ratio (M50 Grade Concrete).....                              | 141 |
| Figure 6.20 Effect on Fracture energy with variation in $\varepsilon$ and $\psi$ ( $a/D = 0.1$ ) using M20 grade of concrete.....   | 142 |
| Figure 6.21 Effect on Fracture energy with variation in $\varepsilon$ and $\psi$ ( $a/D = 0.1$ ) using M40 grade of concrete.....   | 143 |
| Figure 6.22 Effect on Fracture energy with variation in $\varepsilon$ and $\psi$ ( $a/D = 0.6$ ) using M20 grade of concrete.....   | 143 |
| Figure 6.23 Effect on Fracture energy with variation in $\varepsilon$ and $\psi$ ( $a/D = 0.6$ ) using M40 grade of concrete.....   | 144 |
| Figure 6.24 Effect on Size Independent fracture energy with variation in $\varepsilon$ and $\psi$ using M20 grade of concrete ..... | 145 |
| Figure 6.25 Effect on Size Independent fracture energy with variation in $\varepsilon$ and $\psi$ using M40 grade of concrete.....  | 145 |
| Figure 6.26 Effect on Characteristic Length with variation in $\varepsilon$ and $\psi$ using M20 grade of concrete .....            | 146 |
| Figure 6.27 Effect on Characteristic Length with variation in $\varepsilon$ and $\psi$ using M40 grade of concrete .....            | 146 |
| Figure 6.28 Saenz Model Compression Curve (M40) - with and without modification .....   | 148 |
| Figure 6.29 Effect on fracture energy with varying grade of concrete and Compressive behaviour Design model ( $a/D = 0.1$ ) .....   | 148 |
| Figure 6.30 Effect on fracture energy with varying grade of concrete ( $a/D = 0.6$ ).....   | 149 |
| Figure 6.31 Effect on Size independent fracture energy with varying grade of concrete .....   | 150 |
| Figure 6.32 Effect on characteristic length with varying grade of concrete .....  | 151 |
| Figure 6.33 Effect on fracture energy with variation in maximum tensile damage value.....   | 152 |
| Figure 6.34 Effect on peak load with variation in maximum tensile damage value.....   | 153 |
| Figure 6.35 Tensile damage propagation path.....  | 153 |



---

## LIST OF SYMBOLS

---

|                       |   |   |
|-----------------------|---|---|
| $a$                   | = | Notch Depth   |
| $a/d$ or $a/D$        | = | Notch to Depth Ratio  |
| $a_l$                 | = | Transition Ligament Length  |
| $b, d$                | = | Width and Depth of the Prism                                      |
| $d_c$                 | = | Compression Damage  |
| $d_t$                 | = | Tensile Damage  |
| $E_{cm}$              | = | Modulus of elasticity of concrete                                 |
| $f_{ctm}$             | = | Maximum Tensile Stress  |
| $f_{cm}$              | = | Mean Compressive Strength   |
| $f_{cu}, f_{ck}$      | = | 28-day cube compressive strength of concrete in MPa               |
| $f_t$                 | = | Tensile Strength Of Concrete                                      |
| $(f_{b0}/ f_{c0})$    | = | Ratio of Compressive Strength in Bi-Axial State to Uniaxial State |
| $G_f$                 | = | Size-Dependent Fracture Energy                                    |
| $G_F$                 | = | Size Independent Fracture Energy                                  |
| $K_c$                 | = | Shape constant  |
| $L$                   | = | Length of the prism   |
| $l_{ch}$              | = | Characteristic Length of the Mix                                  |
| $P$                   | = | Maximum load  |
| $Pa \ s$              | = | Pascal Second   |
| $P-\delta$            | = | Load-Deflection   |
| $T_{500}$             | = | Slump flow time in seconds  |
| $w_c$                 | = | Crack Mouth Opening Displacement                                  |
| $w$                   | = | Water   |
| $w/b$                 | = | Water to Binder Ratio   |
| $w/cm$                | = | Water to Cementitious Ratio                                       |
| $W_F$                 | = | Work of fracture  |
| $W_{nm}$              | = | Non-Measured Work-Of-Fracture                                     |
| $\beta$               | = | Shape of Stress-Strain Curve                                      |
| $\gamma$              | = | Shear rate  |
| $\varepsilon$         | = | Eccentricity  |
| $\varepsilon_c$       | = | Total Compressive Strain  |
| $\varepsilon_{c,max}$ | = | Maximum Compressive Strain  |

|                             |   |  |
|-----------------------------|---|--|
| $\epsilon_{t,max}$          | = | Maximum Tensile Strain   |
| $\epsilon_{c1}, \epsilon_0$ | = | Strain at Maximum Compressive Stress   |
| $\epsilon_c^{el}$           | = | Elastic Compressive Strain   |
| $\epsilon_c^{in}$           | = | Inelastic Compressive Strain   |
| $\epsilon_c^{pl}$           | = | Plastic Compressive Strain   |
| $\epsilon_{cr}$             | = | Cracking Strain  |
| $\epsilon_{cu}$             | = | Ultimate Compressive Strain  |
| $\epsilon_t$                | = | Total Tensile Strain   |
| $\epsilon_t^{ck}$           | = | Tensile Inelastic Cracking Strain  |
| $\epsilon_t^{el}$           | = | Tensile Elastic Cracking Strain  |
| $\epsilon_t^{pl}$           | = | Tensile Plastic Strain   |
| $\eta$                      | = | Intrinsic Viscosity  |
| $\eta_{mix}$                | = | Plastic Viscosity of the Mix   |
| $\eta_{paste}$              | = | Plastic Viscosity of the Paste   |
| $\eta_r$                    | = | Plastic Viscosity of the Suspension of Particles   |
| $\rho_{CA}$                 | = | Density of Coarse Aggregate  |
| $\rho_{cem}$                | = | Density of Cement  |
| $\rho_{FA}$                 | = | Density of Fine Aggregate  |
| $\rho_{sp}$                 | = | Density of Superplasticizer  |
| $\rho_w$                    | = | Density of Water   |
| $\sigma_{b0}/\sigma_{c0}$   | = | Ratio of Compressive Strength in Bi-axial State to Uniaxial State                                      |
| $\sigma_c, \sigma_t$        | = | Compressive and Tensile Stress in Concrete   |
| $\tau$                      | = | Shear Stress   |
| $\phi$                      | = | Volume Fraction of Particles   |
| $\phi_{CA}, \phi_{FA}$      | = | Volume Fraction of Coarse Aggregate and Fine Aggregate   |
| $\phi_m$                    | = | Maximum Packing Fraction of the Particle   |
| $\psi$                      | = | Dilational Angle   |
| $V_{C-S-H(P)}$              | = | Volume of CSH gel of Unreacted Portland Cement   |
| $V'_{C-S-H(P)}$             | = | Volume of CSH gel of Unreacted Portland Cement with<br>Supplementary Cementitious Materials            |
| $V_{C-S-H(S)}$              | = | Volume of CSH gel of Unreacted Portland Cement with Fly ash as<br>Supplementary Cementitious Materials |
| $\mu$                       | = | Shear Viscosity of the Fluid   |

---

## ABBREVIATIONS AND ACRONYMS

---

|                                  |   |   |
|----------------------------------|---|---|
| $\text{Al}_2\text{O}_3$          | = | Aluminium Oxide   |
| ASTM                             | = | American Society for Testing and Materials  |
| BEM                              | = | Boundary Effect Method  |
| BIS                              | = | Bureau of Indian Standards  |
| $\text{C}_2\text{S}$             | = | Dicalcium Silicate  |
| $\text{C}_3\text{A}$             | = | Tricalcium Aluminate  |
| $\text{C}_3\text{H}_6\text{O}$   | = | Acetone   |
| $\text{C}_3\text{H}_6\text{O}_3$ | = | Glycerol  |
| $\text{C}_3\text{S}$             | = | Tricalcium Silicate   |
| $\text{C}_4\text{AF}$            | = | Tetracalcium Aluminoferrite   |
| CA                               | = | Coarse Aggregate  |
| CaO                              | = | Calcium Oxide   |
| CDP                              | = | Concrete Damage Plasticity  |
| Cem                              | = | Cement  |
| CMOD                             | = | Crack Mouth Opening Displacement  |
| $\text{CO}_2$                    | = | Carbon Dioxide  |
| CPS                              | = | Counts Per Second   |
| CRF                              | = | Crushed Rock Fines  |
| CSH                              | = | Calcium Silicate Hydrate  |
| EFNARC                           | = | European Federation of Producers and Contractors of Specialist<br>Products for Structures |
| FA                               | = | Fine Aggregate  |
| Fl.A                             | = | Fly Ash   |
| $\text{Fe}_2\text{O}_3$          | = | Iron Oxide  |
| FPZ                              | = | Fracture Process Zone   |
| GGBS                             | = | Ground Granulated Blast Slag  |
| $\text{H}_2\text{O}$             | = | Water   |
| $\text{K}_2\text{O}$             | = | Potassium Oxide   |
| LP                               | = | Limestone Powder  |
| OPC                              | = | Ordinary Portland Cement  |
| PV                               | = | Plastic Viscosity   |
| RHA                              | = | Rice Husk Ash   |

|                  |   |   |
|------------------|---|---|
| RMSE             | = | Root Mean Square Error  |
| SBA              | = | Sugarcane Bagasse Ash   |
| SCC              | = | Self-Compacting Concrete  |
| SCCC100          | = | Self-Compacting Concrete with 100% OPC                          |
| SCCC50F25G25     | = | Self-Compacting Concrete with 50% OPC, 25% GGBS and 25% Fly ash |
| SCCC75G25        | = | Self-Compacting Concrete with 75% OPC and 25% GGBS              |
| SCCC80F20        | = | Self-Compacting Concrete with 80% OPC and 20% Fly ash           |
| SCM              | = | Supplementary Cementitious Material                             |
| SF               | = | Silica Fume   |
| SiO <sub>2</sub> | = | Silicon Dioxide   |
| SO <sub>3</sub>  | = | Sulphur Trioxide  |
| SP               | = | Superplasticizer  |
| SSE              | = | Sum Squared Error   |
| TiO <sub>2</sub> | = | Titanium Dioxide  |
| UPV              | = | Ultrasonic Pulse Velocity                                       |
| VMA              | = | Viscosity Modifying Agent                                       |
| XRD              | = | X-Ray Diffraction   |
| XRF              | = | X-Ray Fluorescence  |

# **CHAPTER 1**

## **INTRODUCTION**

## 1.1. Background of the study

Concrete being second largest consumed material in the world needs an attention to address the issue of achieving sustainability. With the demand for high rise structures, there is a significant challenge to the designer to bring out a sustainable as well as environment-friendly concrete. Another important aspect in producing concrete is to make use of the locally available material. Majority of the construction happening in the world is of concrete. So there is a dire need to adopt innovative methodologies in making concrete more usable. Raw materials used in concrete play an important role in attaining the desired properties as per the requirements of a laboratory or a site. This brings in the usage of High-Performance Concrete (HPC) which is the combination of performance and homogeneity in concrete mixes. HPC has the characteristics which conventional concrete fails to bring in during casting, curing and placing (Mehta *et al.* 2006). A concrete can be termed as HPC if it has the high durability, strength and reliability (Golaszewski *et al.* 2004).

Self-Compacting Concrete (SCC) is one type of HPC which has good characteristics in terms of achieving desired workable mixes. Since the concept of SCC was introduced into the construction industry, the need for producing efficient mixes which satisfies both fresh and hardened properties has become a challenge for researchers as well as for construction sector. Okamura was the first person to propose the concept of SCC in 1986, followed by Ozawa in developing a prototype at the University of Tokyo in 1988. Over the last two decades, significant growth was seen in the production of SCC.

SCC has many advantages compared to conventional concrete, including

- a) Reduction of labour cost and time consumption,
- b) Capacity to fill highly congested structural members
- c) Increase the durability of structures and
- d) Improves the overall performance of structures (Caijun Shi 2015).

The production of 1 metric ton of cement releases almost 1 ton of CO<sub>2</sub> to the atmosphere (Concrete Fact Sheet 2008). SCC mixes, to achieve sustainability, there is a need for reducing the amount of cement consumption in the concrete mixes to ensure that there will be a significant reduction in CO<sub>2</sub> emission. Use of supplementary cementitious materials like Fly

Ash (Fl.A), Ground Granulated Blast Slag (GGBS) will reduce the impact of CO<sub>2</sub> emission and increase the sustainability of the mix.

The main characteristics of SCC are its stability and flowability. To obtain a good flowable and stable mix the percentage of coarse aggregate should be minimum, size of coarse aggregate should be less than 20mm and water to powder ratio should be reduced (Okamura 1998). Superplasticizer addition to the concrete mixture will result in the high amount of flow-ability.

Enhancing the viscosity of the mix will overcome segregation and bleeding during transportation and placing of SCC mix. Reduction in coarse aggregate will increase the usage of the high volume of cement which further increases cost of the mix and temperature rise during hydration (Khayat (1999) Khayat and Guizani (1997)). Proportioning the raw materials to make SCC mixes should follow the standard EFNARC guidelines for an enhanced performance of SCC mixes in terms of material compositions.

One of the challenging aspects in most of the constructions is to make use of locally available materials to reduce the overall economy of the project. In the recent past, there is a shortage of river sand in India which led to the stoppage of many of the construction works leading to overshooting of the budget for many of the construction projects. Situations like these can be avoided by utilizing the locally available materials like stone dust, manufactured sand, crushed rock fines which are obtained from quarries.

Rheology plays an important role in the construction industry to address the plastic state behaviour of concrete especially SCC. The flow of SCC is best described using Bingham Constitutive model. Two main influential properties of this model are yield stress  $\tau_y$  and plastic viscosity  $\eta$ . The yield stress has very low values of around 200 Pa for SCC mixes in comparison to thousands of Pascal for normally vibrated concrete. It is very important to accurately measure the rheological properties of SCC to assess the flow behaviour in a fresh state. Though the prediction of rheological properties of concrete may not remain the same for two different rheometers, measuring the plastic viscosity of cement pastes through rheometers or viscometers is a worth trying. Plastic viscosity is a parameter that can be directly correlated to the flow time as well as the filling and passing ability of SCC mixes. A proper SCC mix designed based on plastic viscosity can address the issues of pumping concrete to congested reinforcements reducing the overall time for pumping.

Over the last two decades, the use of SCC as a primary structural material in complex structures such as tall buildings, submerged structures, bridges, dams, liquid and gas containment structure has increased enormously. A proper understanding of the structural behaviour of SCC is absolutely necessary for designing complex concrete structures. Due to the presence of microcracks and other inherent flaws, the strength of the concrete structure decreases. Engineering fracture mechanics can deliver the methodology to compensate the inadequacies of conventional design concepts. It might be expected that SCC would exhibit more brittle behaviour than normal conventional concrete. The improved pore structure and better densification of the matrix have great influence on the fracture characteristics of SCC. It is widely agreed that the strength, elastic modulus and fracture resistance of SCC slightly decreased with increased paste content. Increasing the volume of paste tended to make SCC brittle. Due to the quasibrittle nature of concrete; various computational fracture models have been developed to study the crack characterizing parameters in concrete structures, such as fictitious crack model, crack band model, two parameter fracture model, size effect model, smeared crack model, cohesive crack band model and effective crack model. Compared to conventional vibrated concrete, SCC often has a higher susceptibility to crack due to different mix design, material properties and construction practices. Many studies have addressed the SCC fracture properties using different computational models. As mentioned above, all these studies require sophisticated experimental setup to assess the failure of SCC.

It might not be possible all the time to evaluate the fracture properties of SCC with high-end experimental setup. To compensate this and to attain reasonably better solutions, there is a need to make use of suitable failure models of concrete. These failure models in combination with the finite element analysis would lead an approximate evaluation of fracture properties of concrete. Numerical evaluation using existing failure models like Mohr-Coulomb, Drucker-Prager, Concrete Damage Plasticity (CDP), etc. are already available to predict the failure of concrete. Concrete Damage plasticity model has gained a lot of significance in the recent past because of its added advantage of being more compatible with finite element tools like ABAQUS.

ABAQUS has got an internal option of making use of CDP model especially while evaluating the non-linear response of concrete. Choosing appropriate stress-strain models will help in the numerical evaluation of the fracture properties of concrete using CDP model in combination with ABAQUS.



## 1.2. Organization of thesis

**Chapter 1**, presents the introduction about the importance of research undertaken, brief description, and organization of thesis.

**Chapter 2** presents a brief review of existing literature corresponding to the current study in

- History and origin of SCC along with relevant case studies of structures made with SCC
- Introduction to Rheology of SCC
- Proportioning the SCC mixes with supplementary cementitious materials.
- Role of superplasticizers on the behaviour of SCC mixes
- Influence of addition of fibres on fresh and hardened properties of SCC
- Experimental investigations on the fracture properties of SCC with and without fibres
- Numerical evaluation of fracture properties of concrete using various numerical models.

Further, it summarizes the gaps identified in the existing literature and it concludes by defining the objectives of the current research.

**Chapter 3** gives the summary of various raw materials used in making sustainable mixes and presents the physical and chemical properties of various raw materials chosen for the current research.

**Chapter 4** presents a brief review of the rheology of SCC along with the study undertaken to evaluate the plastic viscosity of various cement pastes. Step-by-step procedure in proportioning SCC mixes with and without the addition of fibres based on the plastic viscosity of the mix is presented. It concludes by summarizing a total of six cases of SCC mixes with their detailed mix compositions for further experimental studies.

**Chapter 5** presents experimental results of fresh and hardened properties of four types of SCC mixes made with river sand and crushed rock fines (CRF) as fine aggregates. It also presents the results for choosing ternary SCC mixes in combination with CRF as fine aggregate. Role of plastic viscosity on the fresh and hardened properties of various SCC mixes is also presented. Further, the influence of addition of fibres in varying proportions, on the fresh and hardened properties of ternary SCC mixes with CRF as a fine aggregate is also

presented. It concludes by presenting the evaluation of fracture energy and generating load-CMOD curves for ternary SCC mixes with and without fibres.

**Chapter 6** summarizes the importance of Concrete Damage Plasticity Model (CDPM) in numerical evaluation of fracture properties of concrete. It also presents the role of HSU & HSU and Saenz stress-strain models in predicting the fracture properties of concrete. Use of correction factor for Saenz model to evaluate the fracture properties is also presented. It concludes with the validation of numerical studies with existing experimental investigations.

**Chapter 7** presents the conclusions based on the research work carried out.

Contributions from the study, recommendations for the scope for future work, details of the publications, references are included in the thesis.

C++ code used for proportioning the SCC mixes, MATLAB codes for generating the compressive and tensile stress-strain values and their corresponding damage values are included in Appendices A and B.

**CHAPTER 2**  
**LITERATURE REVIEW**

This chapter is divided into three sections. In the first section, review of literature related to proportioning SCC with various supplementary cementitious materials, different methodologies of mix design is presented. In the second section literature related to numerical modelling of SCC using various plasticity models is presented. The final section deals with the gaps in the existing literature which helps in defining the objectives of the current research.

## **2.1. Introduction to Rheology of SCC**

Rheology is the branch of physics that deals with the deformation and flow behaviour of matter. It mainly deals with the non-Newtonian flow of liquids and the plastic flow of solids. It is started way back in the 1920s to describe the flow of liquids and the deformation of solids.

Rheology is an important to measure the properties of fluids, to predict the flow behaviour of liquids and also to model it. It deals with materials whose deformation is in between liquids and solids. It is important to understand the relation between structure and flow properties of materials. (Barnes *et al.*, 1989).

### **2.1.1. Newtonian and Non-Newtonian Fluids**

Rao (2010) defined any fluid that obeys Newton's law of viscosity is called a Newtonian fluid. All other fluids which do not comply with it are termed as non-Newtonian fluids.

In a Newtonian fluid, there is a single coefficient of viscosity for a given temperature. In a Newtonian fluid, the viscosity is, therefore, a function of temperature alone and is unaffected by the shear rate or strain rate.

According to Newton's law of viscosity, the relationship between viscous stress and shear rate for an incompressible, isotropic Newtonian fluid is given by

$$\tau = \mu \frac{du}{dy} \quad (2.1)$$

where

$\tau$  is the shear stress in the fluid

$\mu$  is a scalar constant of proportionality, the *shear viscosity* of the fluid

$du/dy$  is the derivative of the velocity component that is parallel to the direction of shear, relative to displacement in the perpendicular direction.(Rao, 2010)

There is no such fluid whose behaviour perfectly resembles the Newtonian fluid but many common liquids and gases such as water and air can be considered as Newtonian under ordinary conditions *Table 2.1*(Tennet, 2004).

**Table 2.1 Typical viscosities of some common materials**

| <b>Material</b>         | <b>Approximate Viscosity(Pas)</b> |
|-------------------------|-----------------------------------|
| Air                     | $10^{-5}$                         |
| Acetone( $C_3H_6O$ )    | $10^{-4}$                         |
| Water( $H_2O$ )         | $10^{-3}$                         |
| Olive oil               | $10^{-1}$                         |
| Glycerol( $C_3H_6O_3$ ) | $10^{+0}$                         |
| Molten Polymers         | $10^{+3}$                         |
| Bitumen                 | $10^{+8}$                         |

In a non-Newtonian fluid, viscosity i.e. resistance to gradual deformation is dependent on the shear rate to which the fluid is subjected to. Few examples of non-Newtonian fluids are ketchup, toothpaste, blood etc.

Flow curves which indicate the relationship between shear rate and shear stress in a material are used to find the yield stress and plastic viscosity of the material. Based on the shape of the curve, they can be classified into the following as shown in *Figure 2.1*

*Newtonian behaviour:* Viscosity remains constant. Shear stress is dependent on the shear rate that is applied.

*Shear thinning behaviour:* Viscosity decreases as the shear rate is increased. The fluids that exhibit this type of behaviour are called shear thinning fluids or pseudoplastic fluids. Blood is a good example for this behaviour

*Shear thickening behaviour:* Viscosity increases as the shear rate is increased. The fluids that exhibit this type of behaviour are called Shear thickening fluids or dilatant fluids. Cornstarch dissolved in water is a good example for this behaviour

*Bingham Plastic:* Viscosity appears to be infinite until a certain shear stress is achieved. Once this value called yield stress is achieved, they began to exhibit a linear relationship between shear stress and shear rate. These fluids are called Bingham Plastic fluids. Clay suspensions, toothpaste, chocolate etc. are a good example for this behaviour

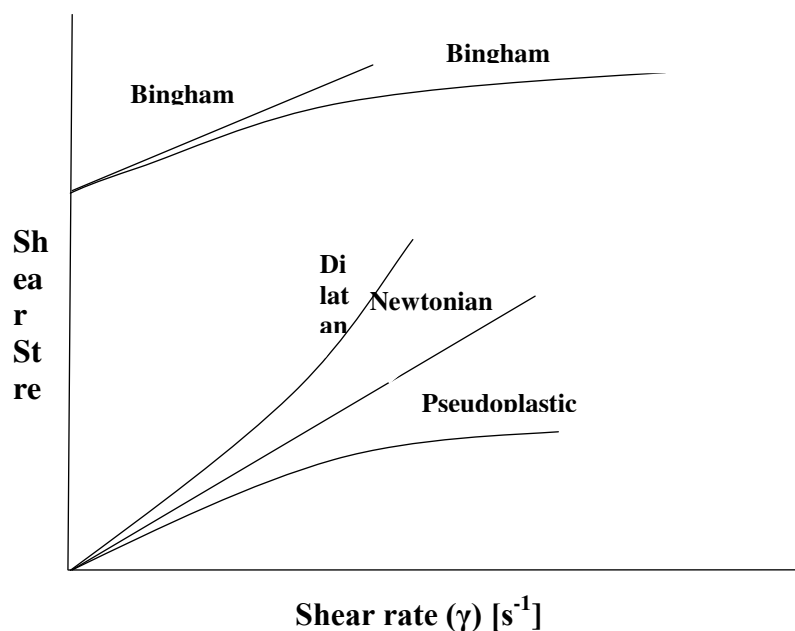


**Figure 2.1 Classification of fluids with  $\tau$  as a function of  $\gamma$  (Rao A, 2010)**

Based on the way viscosity is affected by the passage of time, two classifications can be made.

*Thixotropic behaviour:* It is a time-dependent shear thinning property. These fluids take some time to attain equilibrium viscosity when subjected to a change in shear rate. Yoghurt is one such example of this behaviour

*Rheopectic or anti-thixotropic behaviour:* It is a time-dependent shear thickening property. In these fluids, apparent viscosity increases with the duration of the stress. Examples of such a fluid are printer ink. (Rao A, 2010)

## **2.1.2. Models to Describe the Flow Behaviour**

Some of the fundamental models that are generally used to describe the flow behaviour of materials are stated here. These models hold good only for a small shear range and thus cannot be used for large shear ranges.

### **2.1.2.1. Newtonian model**

A simple relationship exists between shear rate and shear stress. Here, the viscosity of the material remains constant and does not change with the alteration of shear rate. Newtonian liquids such as water, oil etc. satisfy this model

$$\tau = \mu\gamma \quad (2.2)$$

### **2.1.2.2. Power law**

The equation presented here is used to describe the behaviour of non-Newtonian materials.

$$\tau = \mu\gamma^n \quad (2.3)$$

Here,  $n$  is referred to as the power law index of the material.

If the viscosity decreases with the increase in shear rate i.e. for a shear thinning material, the value of  $n$  will be less than one

If the viscosity increases with the increase in shear rate i.e. for a shear thickening material, the value of  $n$  will be more than one.

### **2.1.2.3. Bingham model**

The materials that require a minimum shear stress so as to start deformation and then behave as a Newtonian fluid are best described by this model.

$$\tau = \tau_0 + \mu\gamma \quad (2.4)$$

This minimum shear stress required for the material to flow is generally called as yield stress or Bingham yield stress.

### **2.1.2.4. Herschel Bulkley Model**

This model constitutes elements from all the above three models.

$$\tau = \tau_0 + k\gamma^n \quad (2.5)$$

For a pure Newtonian material, limiting stress = 0 and  $n = 1$

For a power law fluid, limiting stress = 0 and  $n =$  power law index

For a Bingham fluid, limiting stress = yield stress and  $n = 1$  (Instruments, 1999)

It is also defined as the science of deformation and flow by (Barnes *et al.*, 1989). (Tattersall, 1991) reported that the flow properties of concrete can be represented by Bingham model, which has two parameters i.e. yield stress and plastic viscosity. These parameters are evaluated by conducting experiments using a viscometer but not based on the physical properties of concrete. A study done by (Grzeszczyk and Lipowski, 1997) on the rheological behaviour of cement paste when high calcium fly ash is used as an SCM revealed that with the increase in fly ash content, yield stress and plastic viscosity of the paste increases. It is also observed that the fine fraction content was a better parameter than the specific surface area to describe the fluidity of the paste. Their study was a clear indication that the chemical composition of the materials used will be a parameter to assess the rheological behaviour of the cement paste. (Yahia *et al.*, 1999) reported that use of silica fume along with superplasticizer has reduced the viscosity of paste by 30% compared to paste containing cement and superplasticizer only. (Kurita *et al.*, 1999) observed that use of fly ash improves rheological behaviour and reduces the possibility of cracking of concrete because less amount of heat is generated during the process of hydration. For SCC, which has the ability to flow into every corner of the framework, to avoid segregation, it should possess low yield stress to achieve better flowability and sufficient plastic viscosity to maintain its stability. (Billberg, 1999) has found that using viscosity modifying agents or increasing the solid fraction of the cement paste, viscosity of the paste can be increased which will satisfy the requirements of SCC mix. (Nehdi and Rahman, 2004) in their paper highlighted that it is too difficult to compute shear stress at zero shear rate i.e. yield stress. Thus to overcome these problems, rheological models serve as a good statistical approximation. (Shienn, 2007) has concluded that the rheology of cement paste is affected by the properties of cement, SCMs, chemical admixtures, the water content in the paste and on the reaction between cement and admixtures used. (Mukhopadhyay and Jang, 2009) focused on the importance of proper compatibility between the cement and chemical admixtures used in the mix, which is a function of the rheology of the cement paste to some extent. (Cordeiro and Alvarenga, 2016) conducted studies to observe the rheological behaviour of cement paste when rice husk ash (RHA) is used as an SCM. It is observed that with the addition of RHA, there was an improvement in the rheological and mechanical properties of concrete. In the same study,



mechanical and rheological properties of concrete are also studied when a percentage of natural sand (fine aggregates) is replaced by crushed fine aggregates (CGA). It is observed that the compressive strength of the concrete mix has seen a significant increase with 50% replacement of CGA. Also, with the increase in CGA content, there is a reduction in segregation of the material.

## **2.2. Proportioning SCC with Various Supplementary Cementitious Materials**

### **2.2.1. Origin and History of SCC**

Durability is one of the major topics of interests during the early eighties of the last century in Japan. Strength and durability of concrete at its hardened state depends on the quality of concrete and quantity of vibration. Skilled workers are required to make the concrete mixes more compactable. Japan faced the scarcity of skilled labour during the early eighties, which resulted in poor quality of construction. This led to the development of SCC which was first coined in mid-eighties in Japan (Okamura and Ouchi, 2003). Underwater placement of concrete is also one of the primary reasons for the outcome of SCC (Gaimster and Dixon, 2003). Concrete which has the ability to flow and consolidate under its own weight is defined as SCC as per European guidelines (EFNARC, 2005). It is also defined as a special type of concrete which provides the good filling ability, passing ability and segregation resistance (Khayat *et al.*, 1999). The first SCC mix was proposed by Okamura in 1986 in Japan at Tokyo University. SCC was mainly introduced to reduce the noise during vibration and make the mix more reachable to congested formwork. In the end of 1990's the concept of SCC was spread to European countries (Billberg, 1999). Sweden used about 20% to 30% of SCC as an annual production of the overall concrete production in ready-mix and precast industries (Thrane *et al.*, 2004). Later the UK, France and Germany also have started developing and using SCC in their construction industry (Ouchi *et al.*, 2003).

### **2.2.2. Uses and Applications of SCC**

Some of the famous structures where SCC was used for construction are

- a) Anchorages of Akashi-Kaikyo suspension bridge, Japan
- b) Pumping of SCC for 166 stories above the ground of Burj Khalifa, Dubai
- c) Sodra Lanken project, Stockholm

d) 74 storied Yokahoma Landmark tower in Japan

e) La Maladiere Football Stadium, which was made up of 60000 cum of SCC

SCC is successfully used in many of the bridges and tunnelling projects of European countries (Ouchi *et al.*, 2003). In the recent past United States also started using SCC in the name of Self-consolidating Concrete especially in precast industries. Industry Critical Technology Committee on Self-Consolidating Concrete wanted all the ready mix concrete plants to adopt 15% of SCC by 2015 (ICT-SCC 2011).

In India, SCC has been widely used since 1990's. It is used mainly in the construction of bridges, buildings and tunnel construction. With the increasing use of Ready Mix Concrete (RMC) in India, use of SCC is also increasing. RMC used in 2012 was to the tune of 11 million cubic meters which is expected to increase 300% by 2022. Mumbai-Pune expressway, Mumbai sewage disposal project, J.J. Flyover, Bangalore International Airport, Vivekananda Bridge, Kolkata, Bandra-Worli Bridge and Delhi Metro (Fig. 2.8, 2.9, 2.10 & 2.11) are few projects where SCC has been used successfully (Kumar and Kaushik, 2003). It is also expected that there will be an increased production of SCC considering the need for large-scale construction.

### **2.2.3. Cement Replacement Materials**

The following cement replacement materials can be used in making SCC mixes.

#### **2.2.3.1. Ground Granulated Blast Slag (GGBS)**

GGBS is obtained by rapid water cooling of slag from the blast furnace in the production of pig iron (Dashet *al.*, 2016). It is used in concrete because of its cementitious properties due to the presence of lime in it. The particles of GGBS are generally flaky in nature and in the size of 0.1 to 40 microns (Avinash, 2014). GGBS is generally used as a partial replacement for OPC in concrete. The effect of adding this material on the 28-day compressive strength of concrete is very less but the workability of concrete is reduced as GGBS requires more water than OPC. The optimum % replacements of OPC with GGBS in the preparation of concrete is in the range of 25-50% (IS: CED2 (11290) \_ 30012017). It is observed that GGBS improves the resistance of concrete towards chloride and sulphates attacks which serves as a good application especially in the coastal areas where the humidity levels are high. It reduces shrinkage cracks as it reduces the heat of hydration of concrete (Babu *et al.*, 2000; Abdullah Reddy, 2017).

### **2.2.3.2. Fly Ash**

FA is a residue obtained by burning coal and collected on an electrostatic precipitator or a baghouse from a thermal power plant. FA is a pozzolanic material which contains siliceous and aluminous material that combines with calcium hydroxide to form Calcium Silicate Hydrate (CSH) gel in concrete. It is generally used for partially replacing the OPC in concrete. FA is classified into two types: Class - C Fly Ash and Class - F Fly Ash. Class - F fly ash is generally obtained by burning anthracite or bituminous coal and Class - C fly ash is produced from lignite or subbituminous coal. FA particles are generally spherical in shape and their size is approximately in the range of 1 to 150 microns depending on the source (Team WFM, 2014). The % replacements of OPC with FA in concrete is suggested to be in the range of 15-30% (IS: CED2 (11290) \_ 30012017). The 28-day compressive strength of concrete by adding this material reduces drastically but the long-term compressive strength will be the same as conventional concrete (Ahmaruzzaman, 2010; Ramezaniapour, 2014). Particles present in FA are small in size when compared with the OPC and spherical in shape which makes FA-concrete impermeable and resistance to aggressive chemical attacks. For the same reason, the workability of concrete also improves and reduces bleeding, segregation problems in concrete (Ramezaniapour, 2014). FA also requires more water for attaining the same workability as conventional concrete but the rate of hydration is very less when compared with OPC which means the strength gain process is slow when FA is used.

### **2.2.3.3. Limestone Powder**

Limestones are sedimentary rocks generally of calcium carbonate. These rocks are obtained from the remains of freshwater organisms embedded in the calcareous mud. They are soft clays but transform to hard crystalline rocks. In olden days, limestones were used as aggregates in concrete but due to their weak nature, poor grading and due to a belief that they are less resistant to heat when compared with conventional aggregates they were rejected. Later limestones are powdered and used as cement replacement materials. Although LP doesn't have pozzolanic properties, it reacts with alumina stages of cement and forms calcium monocarboaluminate hydrate which doesn't have any effect on the strength of concrete (Naiket *al.*, 2003). It is used in the partial replacement of OPC in cement concrete and shows no effects on the strengths of concrete. But the usage of LP improves the early stage strength gain properties of concrete as the rate of hydration of concrete increases by adding LP (Naiket *al.*, 2003;Ramezaniapouret *al.*, 2009). In order to obtain similar strength

and durability as conventional concrete, concrete made with LP requires more water in which case water reducing admixtures have to be used in producing concrete which makes it costly. One of the disadvantages of using LP is the development of shrinkage cracks while curing due to the high heat of hydration. Another disadvantage of using LP is that it might react with other chemicals present in the atmosphere causing the expansion of concrete. LP is even used as filler in cement concrete and mortars.

#### **2.2.3.4. Silica Fume**

SF is obtained as a by-product while producing the ferrosilicon alloys. The raw materials used for the production of ferrosilicon alloys are quartz, coal and woodchips. These materials are burnt together in an electric furnace to produce ferrosilicon alloys. The smoke generated from this process is collected and sold as SF (Silica Fume Association, 2014). SF primarily consists of amorphous silicon-di-oxide which is responsible for its pozzolanic property. The silicon-di-oxide present in SF reacts with calcium hydroxide obtained as a byproduct of cement reaction to produce CSH gel (Norchem, 2011). These particles of SF are spherical in shape and approximately of size equal to 0.1 to 0.2 nm and a surface area of 30,000 m<sup>2</sup>/kg approximately (Vivek *et al.*, 2017). Due to its fineness and high surface area, SF is highly reactive pozzolanic material and can be used as a partial replacement of cement in concrete. SF also contains carbon, sulphur and oxides of iron, sulphur etc (Vivek *et al.*, 2017). SF has variable densities ranging from 150 to 700 kg/m<sup>3</sup> and it is suited for addition to concrete when its density is approximately 550 kg/m<sup>3</sup> (The Constructor). There will be no effect on the workability of concrete up to 15% replacement of cement with SF but after that the mixture becomes sticky and the workability reduces. Preparation of concrete with SF requires more water than ordinary concrete made with OPC completely because of its higher surface area and fineness. SF also reduces the segregation and bleeding in concrete. The hardened properties of concrete (compressive, flexural and tensile strengths) made with SF as partial replacement of OPC improve as the % replacement of OPC with SF increases but higher pores in concrete make it impermeable. The impermeable nature of SF makes it resistance to the attacks of chlorides and sulphates. There might be some problems in the handling of SF and its availability is less when compared with the other cement replacement materials. Also, the cost of this material is high but this proves to be less disadvantageous as very fewer replacements of OPC with SF results in very good hardened properties of concrete. It is generally used in the construction of high rise structures (King *et al.*, 2012).

### **2.2.3.5. Sugarcane Bagasse Ash**

SBA is a by-product of manufacturing sugar from sugarcane. It is generally used as a fuel in boilers to generate steam and electricity. Approximately 26% of bagasse and 0.62% of residual ash is produced from a total of sugarcane used for manufacturing sugar (Snehith Devasani, 2015). SBA is used in the partial replacement of cement in concrete due to its pozzolanic activity (Snehith Devasani, 2015; Bahurudeen *et al.*, 2015). Bagasse is packed in airtight graphite crucible and placed in electric control furnace at 1200 degrees for 5 hours to obtain a black ash known as bagasse ash. The main reactive component of this ash is the siliceous oxide which reacts with free lime. SBA improves the workability and compressive strengths of concrete when used in selective quantities (Amin *et al.*, 2010). It is also a very light weighted material and can be used in high rise structures for construction practices. It improves the quality of construction and also reduces the cost of construction as SBA is as cheap as FA (Snehith Devasani, 2015). There is a reduction in density of concrete observed due to the addition of SBA as its specific gravity is very less. Other applications of SBA include making bricks, floor and wall tiles, lightweight concrete, fertilizers, for making ceramic products etc (Snehith Devasani, 2015).

### **2.2.3.6. Rice Husk Ash**

RHA is obtained from the protecting outer cover over rice. It contains non-crystalline silicon dioxide with high pozzolanic activity and high surface area. The chemical properties of this material are almost similar to that of silica fume. RHA is produced by burning rice husk at 600 degrees for 2 hours (Mohamad Mujtaba, 2015). The major pozzolanic activity of RHA comes from its silica content where the silicon dioxide in the material reacts with the calcium hydroxide producing CSH gel (Mohamad Mujtaba, 2015; Ambedkar *et al.*, 2017). It is used as a partial replacement of OPC in concrete and this addition improves the compressive strength of concrete, reduces efflorescence and increases the resistance of concrete towards sulphates and other chemical (Mohamad Mujtaba, 2015; Ambedkar *et al.*, 2017; Muthadhi *et al.*, 2013). RHA also showed to improve the bond strength and the permeability properties of concrete (Mohamad Mujtaba, 2015; Muthadhi *et al.*, 2013). Higher replacements of RHA (around 30%) reduce the strength of concrete (Ambedkar *et al.*, 2017; Muthadhi *et al.*, 2013). One disadvantage of using RHA is it requires heavy machinery for preparing good quality rice husk ash from rice husk.

#### **2.2.4. Crushed Rock Fines as Fine Aggregate**

CRF is obtained by crushing rocks in quarries to a size which would completely pass through 4.75mm sieve (Chow *et al.*, 2013). This material can be used as a viable partial and full replacement for natural sand in concrete (Chow *et. al.*, 2013, Mundra *et al.*, 2016, Shyam Prakash *et al.*, 2016). Natural sand generally contains organic impurities due to which the properties of concrete prepared using natural sand would decline. CRF eliminates these problems as it is free from all these impurities. The percentage of fines present in CRF, when compared with natural sand, is higher. The workability of concrete prepared using CRF for a replacement of 30% of fine aggregate declined when compared with conventional concrete (Shyam Prakash *et al.*, 2016). This reduction in workability of concrete due to CRF can be compensated by adding mineral admixtures like Fly Ash and reduce the aggregate size. The physical properties of the aggregate such as specific gravity and water absorption are almost similar to that of natural sand in the range of 2.6 - 2.7 and 0.5 - 1% respectively (Mundra *et al.*, 2016;Shyam Prakash *et al.*, 2016). The durability of concrete made with CRF is high when compared with natural sand due to a reduction in problems like bleeding, segregation etc (Chow *et al.*, 2013). The hardened properties (Compression, Flexure and Split tensile strengths) of concrete due to the addition of this material increased when compared with conventional concrete due to the fines filling the voids in the cement paste (Mundra *et al.*, 2016;Shyam Prakash *et al.*, 2016). Apart from usage in concrete, CRF can also be used for backfills, in asphaltic concrete as a fine aggregate, granular filters etc (Chow *et al.*, 2013).

#### **2.2.5. Mix design of SCC with various supplementary cementitious materials**

The technical advantages of SCC mainly comprised of the benefits like concreting in heavily reinforced sections, thin section precast units could be manufactured and also structures of any geometry could cast. Economically, SCC was preferred due to its reduced construction time and labour costs with improved safety. Because SCC had a reduced level of carbon foot-printing and had a large scope for use of waste materials, it had environmental advantages as well.

Coarse aggregate content in SCC mixes are less compared to conventional concrete and fines are in larger content. A typical mix composition of SCC and conventional concrete is shown in *Figure 2.2* for ready reference.

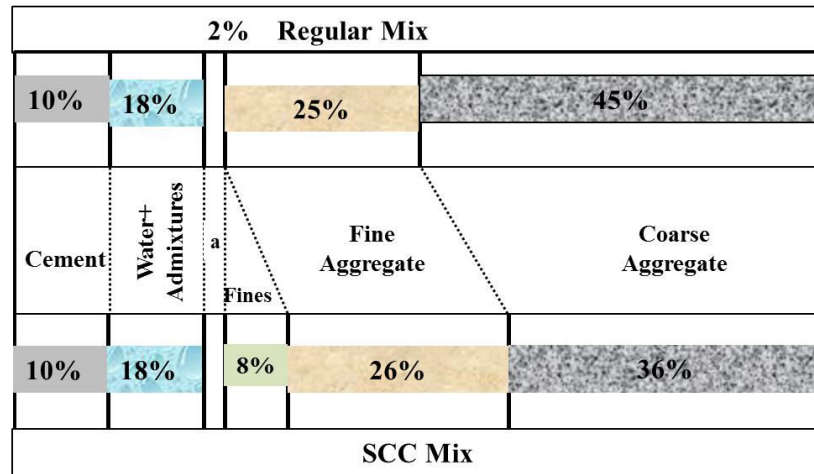


**Figure 2.2 Conventional concrete vs SCC mix (Okamura and Ouchi,2003)**

Based on several researchers contribution the mix design of SCC is classified into 3 main categories (Domone *et al.*, 1999).

- a) Powder method – Achieved by adding more powder content and by increasing fines. Supplementary Cementitious materials are also added to improve the viscosity of the mix.
- b) Viscosity Modifying Agent (VMA) method – Use of suitable VMAs as well as High Range Water Reducing admixtures to enhance the segregation resistance.
- c) Combination method – Balanced use of powder and viscosity agents based on the availability of materials, requirements of construction and limitation of concrete plants.

Sonebi (2004) aimed at developing medium strength SCC by partial replacement of cement with pulverized fly ash and reduced the usage of superplasticizer which reduces the cost of resulting SCC. A mathematical model was developed based on the major four parameters in SCC like filling ability, passing ability, compressive strength & segregation. The parameters used as an input into the mathematical model were cement content & fly ash, water to powder ratio and the dosage of SP. The outputs of the mathematical model were slump flow, fluidity loss, V-funnel time, L-box, orimet time, L-box combined with orimet, the compressive strength at 7, 28, 90 days, rheological parameters, segregation etc. A polynomial regression was fitted into the model. The results obtained showed that a 28-day compressive strength of 30 to 35 MPa was obtained with a cement content of 210 kg/m<sup>3</sup>.

(Khatib, 2006) studied the influence of fly ash on the properties of SCC. Fly ash up to a replacement of 0-80% was used and water to binder ratio of 0.36 was constantly maintained. Properties of SCC like workability, compressive strength, ultrasonic pulse velocity, absorption and shrinkage were studied. Replacing cement with 40% fly ash resulted in the maximum compressive strength of 65Mpa at 56 days. Increasing the % replacement of fly ash increased the absorption values and the same trend was observed in the case of shrinkage. Increase in admixture content increased compressive strength up to certain content and later strength got reduced. Shrinkage reduced by two-thirds at 56 days and there was a linear relationship observed between PFA content and shrinkage. Up to 1 to 2 % of absorption, strength increased and later it reduced with a slower rate.

Glesoglu *et al.* (2009) worked on the effects of binary, tertiary & quaternary blends of cementitious materials on the properties of SCC. A durability based study was also performed to achieve optimal mix proportion. Water to binder ratio of 0.44 and cementitious content of 450 kg/m<sup>3</sup> was adopted. This cementitious is a binary, ternary, quaternary blends of Fly ash, GGBS, Silica fumes. Fresh properties of SCC like slump flow, V-funnel etc. were performed and hardened properties like sorptivity, water permeability, compressive strength etc. were performed. It was observed that the ternary blend of GGBS and silica fume to be more durable when compared with other blends of mineral admixtures. By the addition of mineral admixtures, properties of SCC moderately varied and higher compressive strength obtained in the case of a ternary blend of silica fumes and GGBS. A multi-objective based optimization was performed and an optimal mix was obtained which gave certain values of the fresh properties like slump cone, V-funnel etc.

Liu(2010) worked on different levels of fly ash on SCC. A replacement level of up to 80% of fly ash was tested. Fresh and Hardened properties of concrete were studied. The maximum percentage replacement of fly ash observed was 80%. To improve the fresh properties of concrete by this replacement water to powder ratio is increased and SP dosage is decreased. Filling ability, passing ability and compressive strength values reduced by this replacement of cement with fly ash. Replacement of fly ash up to 20% did not show any significant effects on the properties of concrete. But it was observed that fly ash content may be restricted to 40% as after that the results obtained were not satisfactory.

Uysal and Yilmaz(2011) also studied the effects of marble powder, basalt powder and limestone powder on the properties of SCC as a partial replacement of cementitious used.



Water to binder ratio used in this study was 0.33. Different properties of concrete like workability (slump flow, V-funnel, L-box), compressive strength, ultrasonic pulse velocity etc. were examined. The study showed that usage of these wastes in SCC had considerable advantages with respect to fresh properties and even hardened properties. Comparing all the mixes, the ones with marble powder produced highest compressive strength and the most economical SCC mix was the one using marble powder and M30 grade of concrete.

Corinaldesi *et al.* (2011) worked on the usage of industrial by-products like fly ash, limestone powder, rubble powder (the powder obtained by rubble recycling of aggregates). The coarse recycled aggregate was also substituted in the place of aggregate in some mixes. In this study, water to binder ratio of 0.45 and an acrylic based superplasticizer up to a dosage of 1 to 2% by weight of fines (150-micron passing) were used. Rheological studies on cement pastes were also carried out and it was found out that rubble powder was most effective addition. Further, the fresh properties of concrete like slump flow, V-funnel, L- box and compressive strength test of 1, 3, 7, 28-days were also performed. Comparing the 28 day compressive strengths, fly ash had the best among all the mixes due to its pozzolanic activity. Fresh properties were best in the case of usage of rubble powder and recycled aggregate. Optimization of concrete mix is possible by simultaneous use of rubble powder and recycled coarse aggregate simultaneously.

Dinakar *et al.*(2013) developed a new mix design methodology for the usage of ground granulated blast furnace slag into SCC. This methodology was verified through experimental investigations like workability and strength properties. The results indicated that GGBS up to a replacement of 20 to 80% can only be used and concretes up to strength of 30 to 100 MPa can only be developed. The results also indicate that this design methodology can also produce good quality GGBS based SCC mixes.

Raharjo *et al.*(2013) worked on optimization of concrete mix using silica fumes, fly ash and iron slag. Some tests had been performed as trial tests on SCC for testing its properties with these admixtures. Fresh properties like slump flow, V-funnel, L-box had been evaluated. Compressive strengths at an age of 3, 7, 14, 28, 56 days had been performed. Various mixture compositions with superplasticizer dosages from 0.5 to 1.8% of cementitious had been adopted and silica fumes from 10 to 20% of fly ash weight. The main of this work was to arrive at an optimal mix which would satisfy the fresh and hardened properties of concrete and must also be cost-effective.

Chen *et al.* (2013) studied the effect of amount of paste on the properties of SCC. The mineral admixtures used in this study were fly ash and GGBS. Different water to binder ratios and paste contents were used and a densified mixture design algorithm was created and applied to SCC. The study focuses on the calculation of sufficient paste amount calculation and a dense blended aggregate which provides a less early strength and a higher long-term compressive strength. The results showed that higher the unit weight of concrete, higher the compressive strength and lesser the cement used, lesser will be the early strength and higher the long-term strength. It was also concluded that lower the paste content, higher the quality of concrete.

Nepomucenco *et al.*(2014) worked on developing a new mix design methodology for SCC using different blends of mineral additives. The main aim of the study was to evaluate the interaction between coarse aggregate and mortar phase using a two-phase diagram. In the first stage different combinations of mortars were produced and then different concretes were produced based on the above combinations of mortars. Based on these results, correlation between the fresh and hardened properties of SCC was obtained and a mix design methodology was proposed. The results showed that there is a minute correlation between v-funnel time and T50 and the L-box height ratios cannot be analyzed independently from the rheological properties of concrete. It can also be inferred that under certain conditions, the flowability of SCC depends on the fine aggregate volume fraction and the coarse aggregate volume fraction. There was even a correlation that was observed between L-box height ratios and powder volume fractions and it is also concluded that the self compactibility depends on type of cement up to a volume fraction of  $0.216\text{m}^3$  and later it depends on the paste volume fraction.

Caijun Shi *et al.*(2015) studied different mix design methods that were developed for SCC. The mix design methodologies are broadly classified into five categories: Based on statistical factorial model, rheology of paste model, compressive strength method, close aggregate packing method & empirical design method. Different mix designs were evaluated based on their advantages and limitations. Results obtained showed that the empirical design method was easy to follow, compressive strength method gives a very clear procedure to obtain at the ingredients of the mix, close aggregate packing requires less amount of binders as it considers interaction between aggregate and paste, statistical design produced an optimal mix & rheology of paste model reduces the laboratory materials used.

Okamura is the first person to propose the concept of SCC in 1986, followed by Ozawa in developing a prototype at the University of Tokyo in 1988 (Ozawa, *et al.*, 1989). Over the last two decades, a significant growth is seen in the production of SCC. SCC has many advantages compared to conventional concrete, including a) reduction of labour cost, noise pollution and time consumption; b) capacity to fill highly congested structural members; c) increase the durability of structures; d) improve the overall performance of structures. There will be a release of 1 ton of Carbon dioxide to the atmosphere in the production of 1 metric ton of cement (Concrete Fact Sheet, 2008). For SCC mixes to achieve sustainability there is a need for reduction in the amount of cement consumption in the concrete mixes to ensure that there will be a significant reduction in CO<sub>2</sub> emission. Supplementary Cementitious Materials (SCM) like Ground Granulated Blast Slag (GGBS) and Fly Ash (Fl.A) will reduce the impact of CO<sub>2</sub> emission and increase the sustainability of the mix.

Based on the desired fresh and hardened properties of concrete suitable Cement Replacement Materials (CRM) or SCMs may be used as a partial replacement of Cement (Mindess *et al.*, 2003). They can be used as binary mixes or ternary mixes in combination with OPC. Replacement levels of Fly ash can be as high as 80% (Khatib, 2008). Admixture dosage is an important factor for strength gain of SCC mixes with fly ash, the increase in the dosage reduces the strength.

Mahdikhani and Ramezani pour (2014) investigated the effect of silica fume and nano silica on the compressive strength and chloride permeability of self-consolidating mortars. They concluded that the addition of nano silica resulted in higher compressive strength and also enhanced the durability with reduced chloride permeability. Liu (2010) worked on different levels of fly ash on SCC. A replacement level of up to 80% of fly ash is tested. Replacement of fly ash up to 20% did not show any significant effects on the properties of concrete. But it is observed that fly ash content may be restricted to 40% as after that the results obtained were not satisfactory.

Hamoon Fathi and Tina Lameie (2017) studied the effect of two different types of aggregates on the behaviour of SCC subjected to varying temperatures. They found that Scoria type aggregate showed less sensitivity compared to ordinary aggregate and it has resulted in less strain too.

Khan *et al.* (2016) developed a statistical model to proportioning the high-strength SCC mixes using Response Surface Methodology. They have considered the cost to be the influential parameter for the mix proportioning. They came up with optimum combinations of cement, fine aggregate, fly ash and superplasticizer using a statistical model. The flow of a viscous non-Newtonian fluid like SCC is best described using Bingham Constitutive model Dransfield (2003). Two main influential material properties of this model are yield stress  $\tau_y$  and plastic viscosity  $\eta$ . Plastic viscosity is considered to be an important parameter which depends on the plastic viscosity of the paste and composition of the mix. The paste is a combination of Cement or Cementitious materials, water + superplasticizer. Paste being a homogeneous viscous fluid unlike SCC mix which is non-homogeneous in nature, rheological parameters can be calculated accurately using a rheometer or viscometer. But for SCC mix a hectic process is involved when tested using a viscometer.

Alireza Mohebbi *et al.* (2011) investigated the influence of various parameters on the rheological properties of self-consolidating concrete using Artificial Neural Network (ANN). They have determined optimum percentage of additives based on the analysis of the model. They concluded that the optimal percentages of silica fume, metakaolin, calcium carbonate and limestone is 15%, 15%, 20% and 20% by cement weight.

It was also proved by Lynn E Brower (2003) and Andraz Hocevar, *et al* (2013) that no two rheometers would result in similar values of plastic viscosity and yield stress for the same SCC.

Domone (2005) studied the past 11 years case studies of SCC mixes and their applications. This study tells that SCC mixes have a wide range of mix proportions which shows its diverse nature and there are many factors that govern the design of SCC mixes. All the outcomes are represented in this paper in statistical terms which would benefit the current users and researchers.

Struble *et al.* (1994) studied the viscosity of Portland cement paste and developed a relation between the plastic viscosity of cement paste and concentrations of materials in the paste. Krieger - Dougherty equation was used in this study which gives a good relation between the concentrations and plastic viscosity of the cement paste. Paste which were not dispersed in the liquid and flocculated gave higher values of plastic viscosity indicating that there were high floc particles even at high strain rates.

Nan Su *et al.*(2001) proposed a simple mix design methodology for designing SCC mixes. It is stepwise process in which first the aggregates which are required for the mix are found and followed by the paste which fills the voids in between the aggregates. Several tests are carried out by producing SCC mixes with this design procedure. Results obtained showed that the method is simpler than the one that is used by Japan RMC association and reduces cost.

Haraldsson *et al.*(2011) studied on the usage of rheology as a tool in concrete technology. The study deals with the usage of rheology of the mixes as a tool for the process of optimization. For this purpose, the authors use rheographs and workability boxes. Different applications of these instruments for designing new SCC mixes have been discussed.

Thanh Le *et al.*(2015) developed a mix design for Self Compacting high performance concrete containing various admixtures. The main principle behind this mix design is absolute volume method. The filling capacity of paste is computed based on the packing capacity of the aggregates. Factors to describe the efficiency of concrete using different admixtures are used including the compressive strengths of concrete. The results indicated that this particular mix design is applicable for proportioning of mixes which are self compactibility requirements and compressive strength from C60/75 to C90/105 with 5-20% replacement of mineral admixtures.

Dinakar *et al.*(2014) developed a mix design for high strength SCC with metakaolin in which they developed high strength high performance concrete. The main concept behind this mix design is the efficiency of the mix. These mixes have been successfully evaluated for their fresh and hardened properties. The results indicated that this mix design method can produce concretes up to 120Mpa.

Mathew *et al.*(2012) proposed a mix design for lateralized SCC and studied its behaviour at elevated temperatures. The difference between this concrete and normal SCC they have used laterite as an aggregate in producing the SCC mix. Fly ash is used as a cement replacement material. Fresh and hardened properties of this concrete are evaluated. The performance of this concrete developed is tested at elevated temperatures of 200, 400 & 600 °C. The results obtained indicated there is a decrease in crack formation and growth due to usage of fly ash and this concrete can be used as a fire resistant material.

Alyamac *et al.*(2008) developed a new preliminary mix design for SCC with marble powder. The aim of this work is to bring a relationship between fresh and hardened properties of SCC

and for this purpose; monograms developed by Monteiro are used. Concrete mixes are casted based on this new mix design procedure and various tests for evaluating the fresh and hardened properties of SCC. Results obtained show that this mix design can be used as a preliminary mix design for SCC with marble powder.

Dvorkin *et al.*(2012) used mathematical modelling technique in the design process of SCC mixes containing metakaolin as admixture. This mathematical modelling provides optimal proportions of materials (mainly admixtures) that are required for the preparation of SCC mixes with required properties. Regression equations are developed to study the influence of different parameters like water to cement ratio, compressive strength etc. on the efficiency factor of metakaolin. Results obtained indicated that this mix design can be used for optimizing the admixtures in concrete mixes which reduces the cost of the mix.

Long *et al.*(2015) worked on design of sustainable and greener SCC. It establishes relation between the mix proportions of SCC and the environmental factors associated with them. Results indicated that the addition of mineral admixtures in higher volumes is an effective method of reducing the emission of carbon-dioxide into the atmosphere. It also states that as the compressive strength of SCC increases, the e-resource and e-index values also increase.

Khaleel *et al.*(2013) proposed a mix design method for SCC by varying the properties of coarse aggregate. Work is performed in stages with investigation of paste followed by mortar and then concrete. Metakaolin is used in varying proportions as cement replacement material from 5 to 20 %. Results indicated that the optimum level of metakaolin is 10% in view of workability and strength. Mixes which contained lower volume & size of coarse aggregate produced better fresh properties.

Kanadasan *et al.*(2013) developed mix design for SCC with palm oil clinker concrete. It is a waste product from oil industry which is lightweight and can be used as an aggregate replacement material in concrete. This mix design is based on the particle packing concept which would ensure good fresh and hardened properties. The results obtained from this mix design process indicated that it produced satisfactory fresh and hardened properties and can also be used for different varieties of aggregates.

Ghanbari *et al.*(2011) developed a micro-mechanical model for the prediction of plastic viscosity of Self Compacting high performance and ultra-high performance concrete. In this model, concrete is considered as a solid particles suspended in viscous liquid phase. All the

solid particles (aggregates) are added to viscous liquid phase (cement, water & admixtures) one after the other.

Rola Deeb *et al.*(2013) found a new model which would predict the plastic viscosity of SCC mixes developed. This model needs the plastic viscosity of cement paste (cement, water & admixtures) as an input and the other proportions of mixes considered for the mixing process.

Abo Dhaheer *et al.*(2015) proposed a mix design procedure based on the target compressive strength & plastic viscosities of SCC mix. This procedure uses target compressive strength and plastic viscosity of the SCC mix as its inputs. Using this concept, a set of mixes for plastic viscosities ranging from 3 to 15 Pa s and compressive strengths of concrete varying from 30 to 80 Mpa were designed. Design charts were also prepared based on the data obtained above which would make the design process easy.

Farid *et al.*(2017) addressed the robustness involved in designing the mixes of SCC. They studied the influence of paste volume on the water to powder ratio. Results indicated that the mixtures with a low yield stress and a high plastic viscosity decreased the robustness. They also suggested that the robustness can be reduced by increasing water to powder ratio as the plastic viscosity plays a role in maintaining the stability of mixtures.

Longet *et al.*(2017) recommended a suitable mix design of SCC based on optimal packing density in order to maintain ecological sustainability. Their proposal resulted in the reduction of required binder content by 16% and CO<sub>2</sub> emissions by 33.98%. and material cost by 6.24%.

### **2.2.6. Role of superplasticizers on the fresh properties of SCC**

Since their introduction in the early 1960's, superplasticizers have become an essential component of concrete. By reducing substantially, the amount of water in concrete, superplasticizers have contributed to a significant reduction in its porosity and to a concomitant increase in its compressive strength and durability. These chemical admixtures are also at the forefront of the use of mineral admixtures such as silica fume, fly ash and blast-furnace slags in high-performance concrete. By making possible the use of these industrial by-products as partial replacement of cement, superplasticizers are also contributing in the reduction of CO<sub>2</sub>emission into the atmosphere, a keyissue in several industrialized countries Mather (1968).

Superplasticizers are linear polymers containing sulfonic acid groups attached to the polymer backbone at regular intervals Page and Spiratos (2000). Most of the commercial formulations belong to one of four families:

- Sulfonated melamine-formaldehyde condensates (SMF)
- Sulfonated naphthalene-formaldehyde condensates (SNF)
- Modified lignosulfonates (MLS)
- Polycarboxylate derivatives

Lignosulphonates are generally regarded as '1st generation' superplasticizers, while the sulfonated formaldehyde condensates are called '2nd generation', and the polycarboxylates and polyacrylates are termed as '3rd generation' superplasticizers. Currently, the most widely used superplasticizers are the sulfonated formaldehyde condensates. However, the beneficial effects of polycarboxylates are ensuring a gradual shift towards these chemicals.

#### **2.1.4.1. Cement – Superplasticizer Incompatibility**

The term incompatibility refers to the adverse effect on performance when a specific combination of cement and superplasticizer is used. Common problems include flash setting, delayed setting, rapid slump loss, improper strength gain, inordinate cracking etc. These issues, in turn, affect the hardened properties of concrete, like strength and durability. The use of superplasticizers has become very common in India. There has also been a proliferation in the number of brands of cement and in the types of cement available. It is very difficult to ensure that an admixture that produces all the desired effects with cement A would do the same with cement B. Users, who are unaware of compatibility issues, often, suffer when the supply of cement and/or admixture is changed midway through a project. Problems arising out of compatibility issues are often mistaken for problems with concrete mixture design, because of the lack of information about the subject amongst practising engineers. Admixture manufacturers try to overcome the problem by formulating project specific chemicals. Obviously, this is only a short-term solution.

The water to cement ratio of concrete seems to affect the performance of SPs. As already stated, SNF admixtures are more prone to slump loss problems at low w/b ratio, as compared to the Polycarboxylic Ether (PCE). Collepardi (1998) feels that the lower w/b in superplasticized concrete and the resulting lower inter-particle separation of the cement particles makes it more sensitive to loss of water by evaporation or reaction with cement



during transportation of the concrete. In general, most compatibility problems only exist at low w/b.

A new hybrid type superplasticizer with two different lengths of polyethylene oxide (PEO) side chains is also a new polycarboxylate derivative. The moderation of PEO amount can maximize fluidity and minimize setting retardation. This new generation superplasticizer leads to develop a stable workability of pre-cast concrete, ready mixed concrete, and high-performance concrete. It has been found that the new hybrid type superplasticizer, which is a polycarboxylate type polymer with polyethylene oxide side chains, provides both of viscosity lowering ability and flowing ability. This new superplasticizer possesses several components which adsorb to cement particle very fast, but also adsorb very slowly.

The main technological problem in the production of new generation concrete such as high performance (HPC) or Self Compacting (SCC) concrete is the conflict between low water to binder (water to powder) ratio and the required high workability. Rheological properties of SCC or HPC mixtures can be adjusted adequately to the method and conditions of concrete processing by using superplasticizers only. The main task of the superplasticizers is to deflocculate the cement paste and to increase the amount of free water in the mixture. Hence, they enable one to obtain the beneficial rheological properties of the mixture, and consequently achieve any one of the following results:

- 1) improvement in concrete strength and durability due to the reduced amount of water in the mixture, whilst preserving the established workability and

- 2) improvement in workability without alteration of the amount of water in the mixture, which simplifies the concrete production process. To assure the required workability of HPC or SCC, the following superplasticizers are usually used:

- 1) salts of naphthalene sulphonate formaldehyde polymers (SNFs)

- 2) carboxylic polymers (polymers and copolymers of carboxylic acrylic acid) (PC) and

- 3) carboxylic ethers (PEs) (Aïtcin, 1999), and (De Schutter *et al.*, 2008).

### **2.2.7. Role of fibres on fresh and hardened properties of SCC**

Ponikiewski *et al.*(2013) investigated the influence of various compositions and properties of steel fibres on the fresh and hardened properties of SCC. Results indicated that the addition

fibres had a negative impact on fresh properties of SCC. Suitable additions of superplasticizers have shown improvement of fresh properties. Results also indicated that the random distribution of fibres enhanced the mechanical properties.

Gencil *et al.*(2011) studied the influence of polypropylene fibres on fresh and hardened properties of SCC. They concluded found that mixing process is unaltered when the fibres are uniformly distributed. It was also observed that the air content increased with increase in fibre content. Densities decreased and strengths increased with the increase in fibre content.

Pajak *et al.*(2013) investigated the effect of straight and hooked end steel fibres on flexural strength of SCC with varying volume fractions. They have conducted the experiments as per RILEM TC 162-TDF recommendations. Results indicated that pre-peak and post-peak parameters of SCC increased with increase in fibre volume ratio. Hooked end steel fibres resulted in higher deflection at maximum load compared to straight fibres. Fracture energy also increased with increase in fibre content with hooked end steel fibres resulting in maximum fracture energy compared to straight fibres.

Siddique *Ret al.*(2016) evaluated the fresh and hardened properties of SCC with varying volume fractions of hooked end steel fibres. Results indicated that with 0.5% and 1% volume fraction of fibres, the fresh properties are satisfying the requirements of EFNARC. They observed the increase in compressive strength, split tensile strength, flexural strength, and a decrease in pulse velocity with the increase in volume fraction of fibres.

Madandoust *et al.*(2015) investigated the performance of steel fibres on SCFRC for two different aggregate sizes. Results indicated that there is a significant effect of fibres on the strength properties. Mixture characteristics and volume fraction of fibres adversely affected the properties of SCC. Strength increased with the increase in aggregate size. Workability decreased with the increase in fibre content.

Kamalet *et al.*(2014) explored the utilization of steel and polypropylene fibres in SCC mixes. Presence of both the categories of fibres enhanced fresh and hardened properties of SCC. SCC mixes with polypropylene fibres increased compressive strength by 13% and with steel fibres strength gain is 37% compared to SCC mixes without fibres. Impact resistance also increased by 22% and 67% for SCC mixes with polypropylene and steel fibres.

Abukhashaba *et al.*(2014) investigated the influence of polypropylene fibres on the stress-strain characteristics of SCC. Results showed that the fresh properties slightly reduced and mechanical properties enhanced with the presence of polypropylene fibres.

Pai *et al.*(2009) made an attempt to study the influence of silica fume as filler material on the performance of SCC with the addition of steel fibres. Results showed that the strength increased with the increase in fibre content.

### **2.3. Fracture properties of SCC**

The first study to explore the fracture mechanics and the parameters of SCC was carried out in 1995 (B. Bourdette, *et al.*, 1995). In this research, the ion diffusion process in different mortars has been studied. The diffusion process arises due to the presence of transition zones in the mortar paste. With the help of mercury, these transition zones were studied and it was concluded that this zone depends upon the mortar composition and degree of hydration.

Further studies carried out by (G. Prokopskia and J. Halbiniak, 2000) in 2000 demonstrated the critical values of stress intensity factors,  $K$ , and the critical values of crack tip opening displacement, CTOD as per RILEM specifications. The samples with aggregates used directly and aggregates coated with paraffin were tested. The different transition zones in both the cases showed the difference in the mechanical strengths of both the samples as well. The crack tip opening displacement dropped when the aggregates with coating were used.

Jefferson (2002) produced a model to demonstrate the formed cracks in concrete. The main aim of the model was to understand the interlocking of aggregates and crack closing behaviour. Three contact states were observed for experimental data with the help of a contact function. These states were named open, where there is no contact, interlock, for which the stresses depend upon the nearest distance to the contact surface and closed, for which the stresses depend upon the relative displacements directly. Jefferson concluded that the interlocking of aggregates plays a crucial role in the fracture behaviour of SCC. This behaviour had not been accounted for in the previous studies.

Toumi and Bascoul(2002) studied the crack propagation in concrete under fatigue. They observed the mode I crack in a notched beam specimen by carrying out a three-point bending test. Microscopic observations and FEM modelling were both used to understand the propagation of the crack. It was concluded through this study that cohesive force distribution can be assumed at various loading stages. This study was extended by (Hanson and Ingraffea,

2003) when the size-effect, two-parameter, and fictitious crack models were developed to predict crack growth in materials like concrete that experience tension softening. They studied the crack mouth opening displacement of a specimen by plotting a graph against specific loading.

Appa Rao and Raghu Prasad (2002) reported that the fracture energy, fracture toughness and characteristic length of SCC increases as the maximum size of coarse aggregates increases. The fracture energy increases as the compressive strength of concrete increases whereas the characteristic length of concrete slightly decreases as the compressive strength increases. The ductility of concrete as indicated by the extension of the tail end of the softening curve increases with the maximum size of coarse aggregates.

Rene de Borst *et al.* (2004) made an attempt to bridge the gap between discrete and smeared crack model for concrete fracture. They challenged the conventional belief of the two models being very different from each other by exploiting the partition-of-unity property of finite element shape functions. The study concluded that both approaches have their domain of application: discrete crack models are appropriate for modelling one or more dominant cracks, while smeared crack models can simulate the diffuse cracking patterns that arise due to the heterogeneity of concrete and the presence of reinforcement.

Cervera and Chiumenti (2006) carried out a study to show the difference between the discrete and smeared crack model. The paper focuses on the smeared approach, identifying as its main drawbacks the observed mesh-size and mesh-bias spurious dependence when the method is applied 'straightly'. This paper shows the application of standard finite elements with continuous displacement fields, such as linear triangles, to the solution of problems involving the propagation of tensile cracks using the classical smeared crack approach; in this case, via a local isotropic continuum damage model with strain softening regularized using the classical fracture energy regularization technique.

Zhifang Zhao *et al.* (2008) extended the study on effects of specimen size on the fracture energy and softening curve of concrete. With the help of a three-point test on a notched beam, they studied if the fracture energy changed with a variation in the size of the specimen. They concluded through their test results that the fracture energy increases with an increase in specimen size in both the beam and wedge splitting tests. They asserted that the fracture energy increases with an increase of the specimen size, especially in the wedge tests, and

asymptotic behaviour over the size is observed in some concretes. Additionally, it was shown that the fracture energy increases with an increase of the maximum aggregate size, but there was no systematic trend with the water to binder ratio and the test method. They continued their research by representing the relationship between the crack opening and the gradual stress drop after tensile strength by an inverse analysis. In this extended research work, they have discussed the fracture process zone with respect to the size effect. The fracture analysis of concrete was therefore done in two-fold stages, first being the fracture energy analysis and the second being the inverse analysis.

M. H. Seleem *et al.* (2008) observed the effect of coarse aggregate type, the crack-depth ratio ( $a/d$ ) and area of tensile steel reinforcement ( $A_s$ ) on the fracture toughness of SCC. This was an extension of the previous research work done on the size effect of aggregated on the fracture properties of SCC. This study covered the coarse aggregate type and reinforcement with steel is the main criteria of change from the previous works. At the end of this research, it was concluded that the fracture toughness SCC decreased with increasing crack –depth ratio and that the presence of steel reinforcement in the cracked section created a closing effect to the crack propagation. Another observation they made was in 2012, when they studied the fracture parameters by varying the depth of the notch and increasing the area of reinforced bars (Attwa and Shaheen, 2012) and (Eskandari *et al.*, 2010) also concluded almost similar results but they also compared the results between beam specimens with and without notches.

Cifuentes and Karihaloo (2013) analyzed the wedge splitting results obtained for normal- and high-strength SCC by comparison with the available results previously obtained under similar conditions for normal- and high strength vibrated concrete, and concluded that the specific fracture energy of SCC mixes is lower than that of vibrated mixes of the same strength and the ductility of vibrated concrete mixes as measured by their characteristic length is only marginally higher than that of SCC mixes.

Muralidharan *et al.* (2013) made an attempt to obtain size independent fracture energy from fracture energy release rate. The new method using the relationship between RILEM fracture energies and un-cracked ligament lengths seem gave size independent fracture energy comparable with other methods and the method seemed to give good results when adopted for varying depths of beam.

Morteza *et al.*(2013) researched experimentally on fracture characteristics of SCC. Three-point bending tests conducted on 154 notched beams with different water to cement (w/ c) ratios. The specimens were made from mixes with various w/b ratios from 0.7 to 0.35. For all mixes, common fracture parameters were determined using two different methods, the work-of-fracture method (WFM) and the size effect method (SEM). Investigations on mechanical properties of SCC for twelve SCC mixes with wide spectrum of different variables i.e. maximum coarse aggregate size, coarse aggregate volume and aging were performed (Nikbin *et al.*, 2014). They made various conclusions relating the size of coarse aggregate, volume of coarse aggregate , SCC age, to parameters of compressive and tensile strength of the concrete.

Nikbin *et al.*(2014) performed a series of experiments in order to determine the effect of coarse aggregate volume on fracture behaviour of SCC using three-point bending tests on 58 notched beams. SCC was prepared with coarse aggregate in varying percentages of 30%, 40%, 50% and 60% (as the percentage of the total aggregate volume). For all mixes, the fracture parameters were analyzed by the workof- fracture method (WFM) and by the size effect method (SEM) to obtain a suitable correlation between these methods which is used to calibrate fracture numerical models .On evaluating the effect of maximum aggregate size on fracture behaviour of SCC (Beygi M *et al.*, 2014)., the parameters were analyzed by the work-of-fracture method (WFM) and by the size effect method (SEM) and consequently a correlation between these methods was obtained which is used to calibrate cracking numerical models.

#### **2.4. Numerical Evaluation of Conventional and SCC Using Various Plasticity Models**

Though there are many constitutive models for the nonlinear response of concrete proposed in the literature, commonly used frameworks are plasticity models, damage mechanics models and combinations of plasticity and damage mechanics models. Stress-based plasticity models are useful for the modelling of concrete subjected to triaxial stress states since the yield surface corresponds to the strength envelope of concrete at a certain stage of hardening. Hence a constitutive model based on the combination of damage mechanics and plasticity is to be developed to analyze the failure of concrete structures. The model should describe the important characteristics of the failure process of concrete subjected to multi-axial loading. This can be achieved by combining an effective stress based plasticity model with a damage model based on plastic and elastic strain measures. Then the model response in tension and

under uniaxial, biaxial and triaxial compression can be compared with experimental results. The Concrete Damage Plasticity (CDP) model is an apt model and its modelling in the finite element software ABAQUS can help us understand the nonlinear response of concrete. However, to understand the CDP model, Knowledge on some basic failure criteria and models is a prerequisite. Initial understanding of the failure criteria of concrete under varied loading conditions and alternate state of stresses. Later, inferences from certain experimental works and the features of the concrete failure have been discussed. This is followed by a study on prominent failure criteria such as the Tresca and Von-Mises etc. which are one parameter models and a comprehensive discussion on the Drucker-Prager failure model and its application to the CDP model was also studied.

#### **2.4.1. Failure Criteria of Concrete**

Failure theory is the phenomenon of predicting the conditions which cause failure of solid materials under the action of external loads. Two of the most significant concrete failure mechanisms are cracking under tension and crushing under compression. However, concrete strength observed under uniaxial compression or tension drastically varies from the one determined in complex states of stress. For example, the same concrete under biaxial compression reaches the strength of almost twenty percent higher than in the uniaxial state and under uniform triaxial compression its strength is unlimited (theoretically). The behaviour of concrete changes radically when the nature of loading changes from compressive to tensile. Under tension, the response of concrete is same whether under uniaxial or under biaxial loads. But, the same concrete exhibits different behaviour for uniaxial and biaxial loads under compression. Hence, the nature and type of loading play a vital role in the behaviour of concrete. In order to describe strength for triaxial stress, its plane should be presented in a three-dimensional stress space (since concrete is assumed to be an isotropic material in a wide range of stress). The states of stress on this surface correspond to material failure, whereas the states of safe behaviour are inside. Also the so-called plastic potential surface is located inside this space. Once the plasticity surface is crossed, two cases may arise (Majewski, 2003):

1. Ideal Plasticity condition ( i.e. an increase in strain with no change in stress)
2. Rupture (material weakening)

To understand the actual behaviour of concrete in compression and tension, numerous analytical models have been developed. These models are formulated based on

the microscopic and macroscopic behaviour of concrete. The models based on macroscopic behaviour are essentially used in practice especially in construction field (Copper and Gerstle 1973; Kotsovos and Newman, 1977; Mills and Zimmerman, 1970; Lee *et al.*, 2004)

The deformation patterns and stress-strain curves are the two vital indicators of the behaviour of concrete. In order to define completely the deformational and stress-strain behaviour of concrete, the structure must be analyzed till failure. The deformation of the structure is linearly elastic till the yield limit, and beyond this point, plastic deformation (irreversible) occurs. A model chosen must be capable of exhibiting the above-mentioned behaviour till failure. One such way of obtaining a model is by utilizing the plasticity theory (Chen and Chen, 1975).

According to plasticity theory, yield limit is the limit below which the material property remains elastic and further loading beyond this point causes plastic flow. In the case of elastic-perfectly plastic, the initial yield surface becomes a failure/bounding surface, reflecting the increase in strain without further change in stress. However, for concrete which has an elasto-plastic behaviour, strain hardening and strain softening behaviour are to be included. Strain hardening is the region between the yield and peak stress which reflects the hardening nature of concrete with an increase in stress value. If the concrete hardens and attains the peak stress, further loading results in a decrease in stress with an increase in strain, hence enabling the softening behaviour. Thus initial loading or yield surface is allowed to expand on the application of load resulting in the strain-hardening behaviour of concrete, defining the subsequent loading surface (Muthukumar and Manoj Kumar 2014).

The Drucker–Prager hypothesis is one of the strength hypotheses which is applied to concrete more often. According to it, failure is determined by non-dilatational strain energy and the boundary surface assumes the shape of a cone. As the failure surface proposed by this model is smooth, the numerical computations will be simple compared to many other models. However, a certain drawback exists too. The failure behaviour according to this criterion is not fully consistent with the actual failure mechanism. According to the Drucker-Prager theory, the failure surface is a perfect circle, but experiments have proved that it is not a circle and is governed by a parameter  $K_c$  as shown in *Figure 2.3*



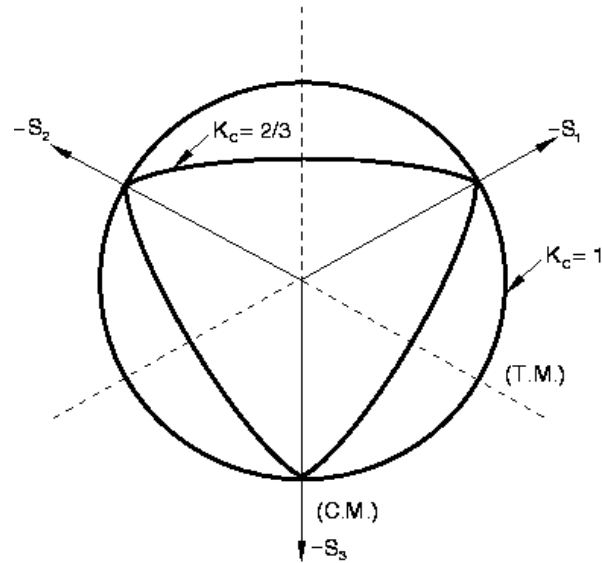


**Figure 2.3 Deviatoric cross section of failure surface as per CDP model**

Valentini and Hofstetter(2011) studied the plasticity model and a damage-plasticity model of a 3D concrete specimen with the help of finite element analysis. They observed and studied the variation between the predicted and actual material behaviour. As a result of their study, they developed an efficient stress update algorithm in a finite element program for performing large-scale 3D numerical simulations of concrete structures.

Farhad and Nejadi(2012) developed three new models for the fracture study on SCC and conventional concrete both. These models included elastic model, tensile strength model and a compressive stress-strain model. These models were also verified against the experimental results. Upon verification against experimental results, they concluded that the three models could accurately predict the branches of the stress-strain curves. The models also predicted the descending curves with a minimum range of deviation with a reasonable accuracy, which helped to study the fracture parameters.

Grégoire *et al.*(2013) compared experimental results with numerical simulations performed with reference to an integral non local model. The shortcomings of this classical formulation were also illustrated, which failed to describe size effect over the investigated range of geometries and sizes. Experimental results were also compared with the universal size effect law.

Peter Grassl and Milan Jirasek(2006) proposed a new constitutive model to enhance the analysis of failure of concrete structures. This model incorporates both strain based damage

and stress based plasticity with an aim to achieve the important characteristic of concrete structure when subjected to multi-axial loading. More realistic behaviour of concrete can be observed as two separate isotropic damage parameters for tension and compression has been defined. The above proposed model gives mesh independent load-displacement curves for tensile and compression failures.

Mitra and Lowes (2008) in their work have tried to study the influence on response of concrete in tension as it is required in case of massive concrete structures that are designed on the basis of un-cracked concrete sections. The response of concrete was observed by subjecting a beam to three-point bending test using finite element analysis software in terms of element type, size and integration rules as well as material model parameters. The constitutive modelling was thus found to be dependent on the mesh size and element type.

Jankowiak and Lodygowski(2005) presented the procedures to obtain the constitutive parameters essential for defining Concrete Damaged Plasticity (CDP) in ABAQUS. Also, they have stated the prerequisite experimentations required to extract the model parameters. Simulations of three-point single edge notched beam and four-point bending single edge notched beam has been carried out and the similarity of crack initiation and evolution between experimental and numerical simulations has been shown and studied thus striking a link between actual response of concrete structure and its numerical modelling.

Chaudhari and Chakrabarti(2012), strived on the usage of computer simulation ABAQUS so as to satisfy the increasing urge to find exact solution for a concrete fracture problem. A fair comparison has been carried out between Smeared Crack modelling and Concrete Damaged plasticity model- a model available in ABAQUS and the results has been verified with the theoretical values of stresses obtained by the equations formulated by Hognestad. Results also indicated that the concrete damaged plasticity model is mesh sensitive and thus smaller the mesh size closer would be the results to the desired values.

Lopez-Almansa *et al.*(2014) in their work have strived on the significance of Concrete Damaged Plasticity model being able to reproduce the actual geometric non-linear behaviour of concrete RC frames as compared to other computational models like distributed plasticity models or lumped plasticity models. Procedures to identify the concrete Damaged Plasticity model have been very well explained in their work. The authors have further appraised attention to be paid to CDP model parameters and mesh sensitivity of the FE model.

## **2.5. Gaps Identified in Literature**

Based on the findings from the literature review, following gaps are identified

- i. There are no reported studies in proportioning SCC mixes with crushed rock fines as fine aggregate in combination with binary and ternary combination of cementitious materials based on the plastic viscosity approach.
- ii. Though there are many investigations reported on the addition of fibres into SCC mixes, suitable mixture methodologies are not proposed in the addition of fibres into SCC mixes based on the plastic viscosity of cement paste.
- iii. Role of plastic viscosity on the fresh and hardened properties of SCC mixes made with binary and ternary mixes are not reported in existing studies.
- iv. Very limited work has been carried out to use the Concrete Damaged Plasticity model in tandem with Hsu & Hsu model and Saenz model with the final goal of predicting fracture parameters of concrete.
- v. Though there are several works reported on the numerical evaluation on the response of concrete, very few or none of them have reported the applicability of suitable damage model in evaluating the fracture properties of concrete.

## **2.6. Objectives of the Proposed Research**

The following are the objectives of the proposed research based on the gaps identified from the literature

- i. Development of plastic viscosity based mix design for Self-Compacting Concrete with and without the addition of fibres incorporating supplementary cementitious materials.
- ii. Experimental investigation on the fresh and hardened properties of SCC mixes with Crushed Rock Fines as fine aggregate incorporating supplementary cementitious materials with and without hooked end steel fibers
- iii. To develop a numerical model that predicts the fracture properties of concrete and its experimental validation.

- iv. Numerical evaluation of fracture properties of notched concrete beams using Concrete Damage Plasticity Model coupling with a suitable stress-strain model.

The next chapter presents the characterization of raw materials used for designing the SCC mixes.

**CHAPTER 3**  
**CHARACTERIZATION OF MATERIALS**

### 3.1 Introduction

Concrete being the second most consumed material after water, there is a need for enhancing the quality of construction using concrete. The demand for concrete is increasing day by day because of the rapid growth in constructions happening globally. The main challenge faced in the usage of this material is maintaining the quality of construction by balancing the overall economy of the construction. One major part of construction where the cost can be reduced is the use of cheaper raw materials than the conventional materials used. These conventional raw materials used also affect the environment due to carbon-di-oxide (CO<sub>2</sub>) emission which leads to global warming. Hence, there is a dire need for using sustainable raw materials in construction which reduces the emission of CO<sub>2</sub> into the atmosphere, enhances the overall quality and reduces the economy of construction.

Ordinary Portland Cement (OPC) used in the preparation of concrete proves to be an environmental hazard as it emits carbon-di-oxide into the atmosphere during the hydration process of OPC resulting in global warming. So, there is a need for the replacement of cement with alternate cementitious material which reduces the environmental impact. In the present study, various sustainable cementitious materials used in the construction sector in India are presented. These materials are used as a partial or full replacement of OPC in concrete and proved to be sustainable as the usage of these materials for cement replacement reduced the environmental impact and retained the quality of construction.

After cementitious materials, aggregates are the major components in the preparation of concrete. Aggregates classified into fine and coarse aggregates are used in high quantities in the production of concrete. So the availability of these materials is reducing day by day. Natural Sand, the most commonly used fine aggregate is reducing due to their unavailability from river beds. Natural sand even consists of organic impurities which reduce the workability and in turn the quality of concrete. The coarse aggregates are generally of two types: Basalt and Granite. The demand for these conventional aggregates used in concrete is increasing day by day and there is a need for alternative aggregates to meet the increasing demands. In the present study, alternative coarse and fine aggregates which can be used as a partial or full replacement of aggregates in concrete are discussed in detail. These materials are wastes from different industries and also from our day to day life. Hence using these materials, makes concrete inexpensive and is an ecological way of disposing and reutilizing waste materials.

From the list of various cement replacement materials used in concrete, GGBS and fly ash are chosen for the current study considering the needs of the construction industry. Based on the discussions with the experts from the industry it is understood that the utilization of GGBS and fly ash as binary mixes and ternary mixes along with OPC is the primary need for maintaining the sustainability in the construction.

As an alternate for river sand as fine aggregate, CRF is also used for the current study.

The following combinations are adopted for proportioning the SCC mixes based on the inputs from industry experts in the field of concrete as well as from literature review from 2.

Combination I: SCC mixes with 100% OPC

Combination II: SCC mixes with 80% OPC and 20% fly ash

Combination III: SCC mixes with 75% OPC and 25% GGBS

Combination IV: SCC mixes with 50% OPC and 25% GGBS and 25% fly ash

### 3.2 Physical and Chemical Properties of the Materials

**Cement:** Ordinary Portland Cement (OPC) of 53 grade is used for the present study. The physical and chemical composition of cement is shown in

*Table 3.1.* The compressive strength of cement after 28-days is found out to be 58.5 N/mm<sup>2</sup>. Loss of ignition is 1.6% which is within the limits as per the ASTM C114 - 15.

**Fly Ash:** Class F Fly ash with low calcium content used for the present study is obtained from National Thermal Power Coal Plant, Ramagundam, in Telangana. The physical and chemical composition of fly ash is shown in

*Table 3.1.*

**GGBS:** Ground Granulated Blast Slag is obtained from Jindal Steel Works, Vijayanagar, Karnataka. The physical and chemical composition of GGBS is shown in

*Table 3.1.* The chemical compositions of blended cement are shown in *Table 3.2*

**Fine Aggregate:** Locally available Crushed Rock Fines (CRF) is used as a fine aggregate for the present study. It is confirmed to IS 383: 2016. CRF is chosen over river sand to ensure that the organic impurities are minimized. The specific gravity used in the present study is 2.61. Fineness modulus of 2.00 is obtained and it belongs to Zone II. River sand is also used for some of the mixes in comparison with CRF. The specific gravity of river sand is 2.56.

**Coarse Aggregate:** Basalt type coarse aggregate with a maximum particle size of 20mm is used for the present investigation. All the mixes for the current study adopted a combination of 10mm and 20mm size aggregates. The specific gravity of the coarse aggregate used in the present study is 2.71 and the water absorption for 10mm size aggregates is 4.6% and for 20mm aggregates it is 1.6%. Particle size distribution of fine and coarse aggregate is shown in *Figure 3.1* and *Figure 3.2*

**Admixture:** Master Glenium Sky 8233, a light brown liquid made of a new generation based on modified polycarboxylic ether is used as a superplasticizer for the current study. The specific gravity of 1.07 at 25<sup>0</sup> C is adopted.

**Water:** Water with a pH value ranging from 7-8 is used for mixing and curing purposes based on its usual satisfactory performance.

**Fibres:** Hooked end steel fibres of length 30mm and diameter 0.5mm with an aspect ratio of 60 are used for the current study. The specific gravity of fibres is 7.8.

The raw materials used for the SCC mixes are shown in *Figure 3.3*

Particle size distribution and the grading curves for coarse and fine aggregates are shown in *Figure 3.1* and *Figure 3.2*.

### **3.3 Chemical Analysis**

Chemical properties and identification of various phases of raw materials used are characterized using X-Ray Fluorescence and X-Ray Diffraction.

#### **3.3.1 X-Ray Diffraction**

X-ray diffraction is a technique used for the characterization and identification of crystalline phases, polycrystalline phases and residual stresses. This identification of materials by this method is possible due to its unique crystalline structure. These X-rays possess a short wavelength that lies in the range of 0.01 to 10 nanometers, are high energy waves of electromagnetic radiation. It is known that constructive interference of waves occurs when two waves of same wavelength do not have a phase difference between them are combined. Destructive interference of waves occurs when the two waves are combined with a phase difference of a half wavelength ( $\lambda/2$ ). In fact, for a phase difference of  $n\lambda$  between the waves, constructive interference occurs and for a phase difference of  $n\lambda/2$ , destructive interference occurs.



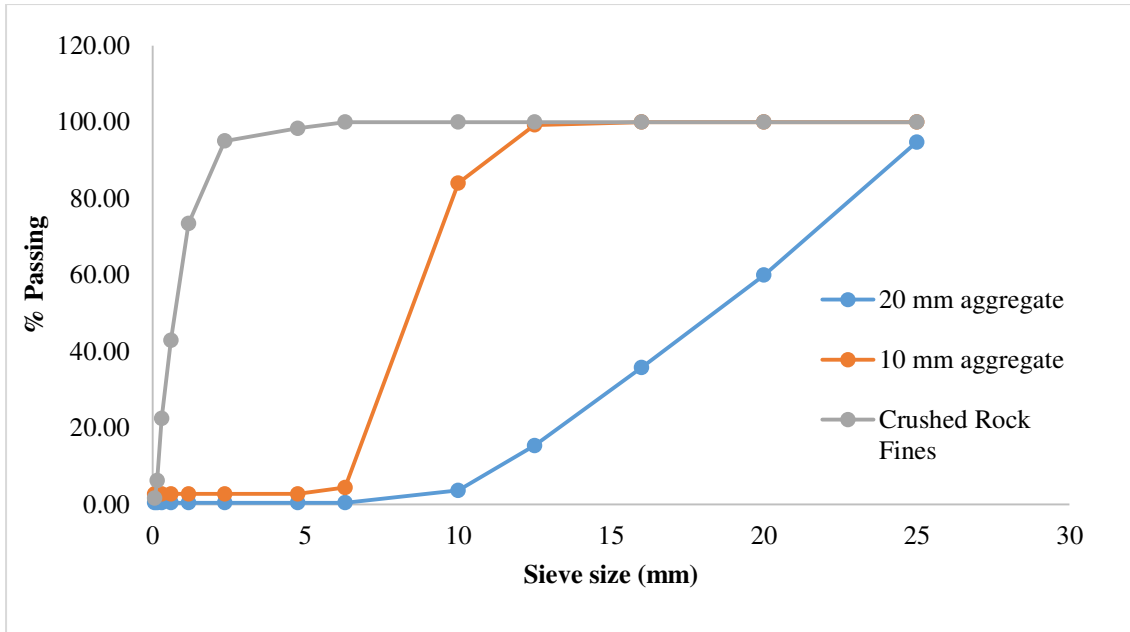


**Figure 3.1 Particle Size distribution of Aggregates**

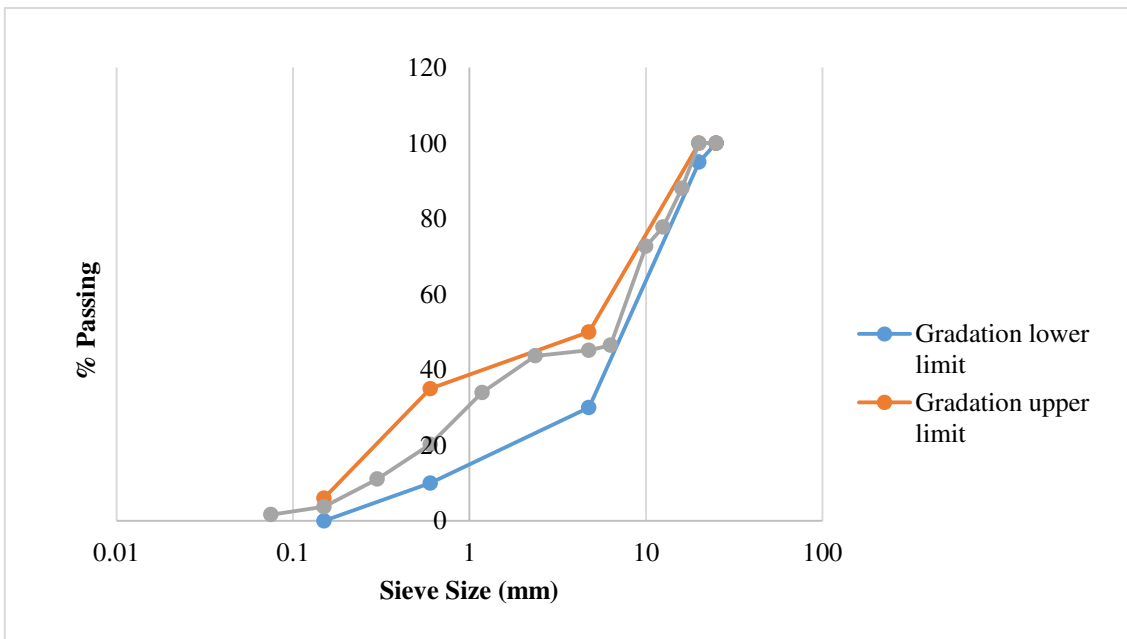


**Figure 3.2 Combined Gradation as per IS 383:2016**



**Figure 3.3 Raw Materials used for SCC mixes**

The instrument used for XRD is called X-ray diffractometer. A detector present in it measures the intensity of the diffracted beam. The incident beam on the specimen surface changes its angle continuously from  $0^\circ$  to  $90^\circ$  and thus a number of diffraction intensities are witnessed. A graph is plotted between the spectrum of diffraction intensities and the angle between the incident and diffracted beams. This diffraction spectrum is then compared with the database containing over 60,000 diffraction spectra of known crystalline substances to identify the phase composition of the given specimen. (Dodds, 2013)

X-ray diffraction and X-ray fluorescence are conducted on the four combinations mentioned below:

- 100% OPC
- 80%OPC+20%FA
- 75%OPC+25%GGBS
- 50%OPC+25%FA+25%GGBS

By observing the intensity peaks, XRD study helps us to identify the various phases present in the sample. The samples are scanned by an X-Ray diffractometer using  $\text{CuK}\alpha$  radiation at 40 kV / 20 mA, CPS = 1k, width 2.5mm, speed  $0.6^\circ$  / min and scanned with an angle of  $2\theta$

from 20-100°. The analysis is stepped in 0.02 degree increments and continued for a period of 2 seconds.

X-ray diffraction study of OPC and fly ash has identified the various phases present in them. The peak intensities of OPC show that quartz and calcite are present in it, whereas quartz, mullite and hematite are seen in fly ash *Figure 3.4, Figure 3.5 and Figure 3.6.*

### 3.3.2 X-Ray Fluorescence

XRF study provides us with the information about the elemental as well as various oxide compositions by percentage weight in the sample. The chemical compositions of individual cementitious materials, as well as blended cement, are shown in

*Table 3.1 and Table 3.2.*

For the same samples mentioned above, the volume of CSH gel formed (both primary and secondary CSH) are calculated based on the degree of hydration and silica content of OPC and SCMs. w/b ratio of 0.5 is used for finding the volume of CSH formed per 100 ml of unreacted Portland cement along with SCM. This value of 0.5 w/b is used because the SCC mixes are prepared for the same w/b ratio.

The equations used for the calculation of CSH gel volume are taken from the (Karet *al.*, 2012).

$$V_{C-S-H(P)} = \alpha(21.6n + 50.9) \text{ ml. per 100ml of unreacted Portland cement}$$

For blended cement containing SCM,

$$V'_{C-S-H(P)} = \frac{PV_{C-S-H(P)}}{100} \text{ ml. per 100ml of unreacted Portland cement with SCM}$$

$$V_{C-S-H(S)} = \frac{(s_f Q \alpha^r + s_s R \alpha^n)}{100} * \frac{(1.215n' + 2.821)}{2.2} \text{ ml per 100ml of unreacted Portland cement containing } Q\% \text{ of fly ash as SCM}$$

Using Bruker's formula, the percentage of bogue's compounds C<sub>3</sub>S, C<sub>2</sub>S, C<sub>3</sub>A & C<sub>4</sub>AF by weight in the cement sample are calculated. These calculations are done for all the four combinations mentioned above by making use of various oxides composition obtained through XRF analysis on the samples.

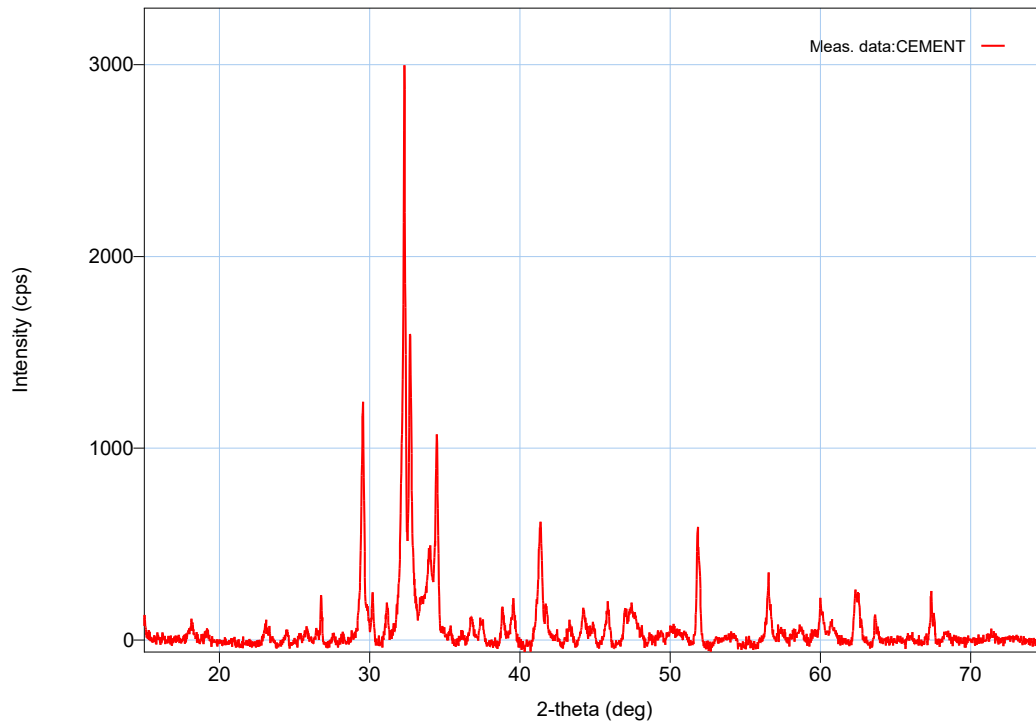


**Figure 3.4 X-Ray Diffraction Patterns for OPC**

$$C_3S = 4.07 (\text{CaO}) - 7.60 (\text{SiO}_2) - 6.72 (\text{Al}_2\text{O}_3) - 1.43 (\text{Fe}_2\text{O}_3) - 2.85 (\text{SO}_3)$$

$$C_2S = 2.87 (\text{SiO}_2) - 0.754 (3\text{CaO} \cdot \text{SiO}_2)$$

$$C_3A = 2.65 (\text{Al}_2\text{O}_3) - 1.69 (\text{Fe}_2\text{O}_3)$$

$$C_4AF = 3.04 (\text{Fe}_2\text{O}_3)$$

Percentage weights of Bogue's compounds are calculated using the Bruker's formula mentioned above. The method followed for finding the volumes of CSH gel (both primary and secondary) has also been discussed above. The volumes of CSH gel formed are for 100 ml. of unreacted ordinary Portland cement for pure OPC. In case of blended cement where SCMs are added in addition to cement, the volumes of CSH gel are for 100ml of unreacted ordinary Portland cement along with SCMs. CSH gel for blended cements is shown in *Table 3.3* and the Bogue's compounds calculated are shown in *Table 3.4*

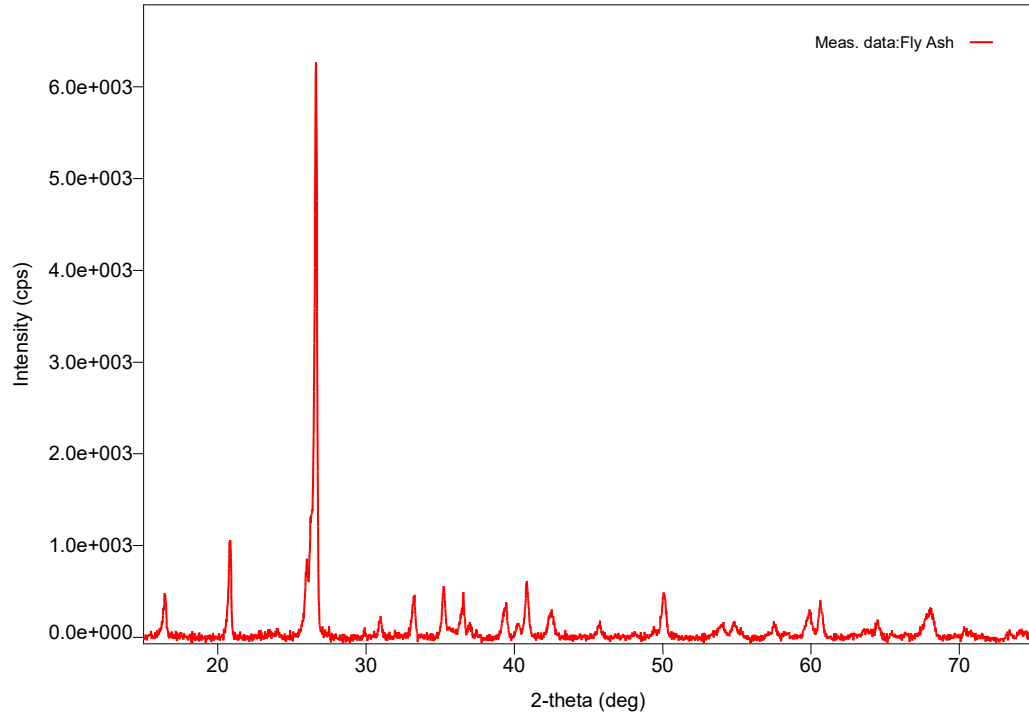


**Figure 3.5 X-Ray Diffraction Patterns for Fly ash**

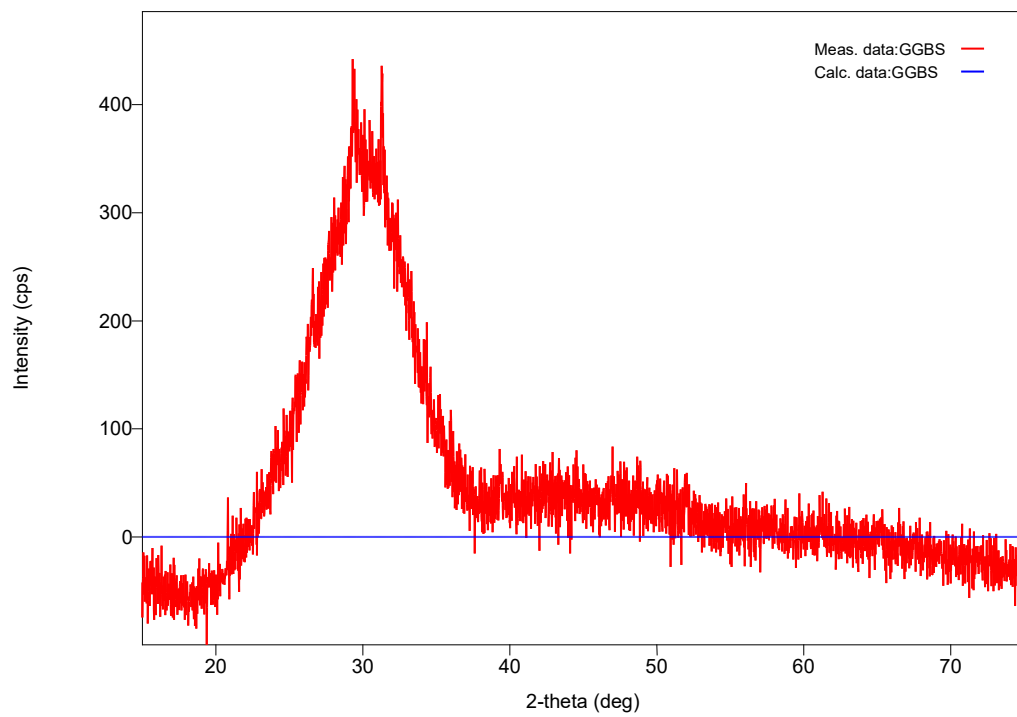


**Figure 3.6 X-Ray Diffraction Patterns for GGBS**

**Table 3.1 Chemical and physical properties of Ordinary Portland Cement, fly ash and GGBS**

| <b>Chemical Composition (%)</b>    | <b>OPC</b> | <b>Fly Ash</b> | <b>GGBS</b> |
|------------------------------------|------------|----------------|-------------|
| <b>CaO</b>                         | 65.23      | 1.78           | 40.64       |
| <b>SiO<sub>2</sub></b>             | 18.64      | 60.13          | 35.15       |
| <b>Al<sub>2</sub>O<sub>3</sub></b> | 5.72       | 28.37          | 19.60       |
| <b>Fe<sub>2</sub>O<sub>3</sub></b> | 4.54       | 5.10           | 0.53        |
| <b>SO<sub>3</sub></b>              | 4.32       | 0.11           | 1.89        |
| <b>K<sub>2</sub>O</b>              | 0.59       | 2.16           | 0.40        |
| <b>TiO<sub>2</sub></b>             | 0.50       | 1.42           | 0.92        |
| <b>Physical Properties</b>         |            |                |             |
| <b>Specific Gravity</b>            | 3.15       | 2.16           | 2.85        |

**Table 3.2 Chemical composition of blended cements**

| <b>Chemical Composition</b>    | <b>80% OPC+20% FA</b> | <b>75% OPC+25% GGBS</b> | <b>50% OPC+25% GGBS+25% FA</b> |
|--------------------------------|-----------------------|-------------------------|--------------------------------|
| CaO                            | 43.79                 | 49.75                   | 39.37                          |
| SiO <sub>2</sub>               | 30.88                 | 28.01                   | 34.51                          |
| Al <sub>2</sub> O <sub>3</sub> | 14.60                 | 13.46                   | 16.60                          |
| Fe <sub>2</sub> O <sub>3</sub> | 5.04                  | 3.78                    | 4.15                           |
| SO <sub>3</sub>                | 2.45                  | 2.17                    | 2.10                           |
| K <sub>2</sub> O               | 1.35                  | 1.05                    | 1.24                           |
| TiO <sub>2</sub>               | 1.21                  | 1.08                    | 1.22                           |

**Table 3.3 CSH gel volumes for various combinations of blended cements**

|             | CSH Gel Volume |            | TOTAL VCSH(MI) |
|-------------|----------------|------------|----------------|
|             | VCSHI(MI)      | VCSHII(MI) |                |
| OPC         | 57.99          | 0          | 57.99          |
| OPC+GGBS    | 43.49          | 12.58      | 56.07          |
| OPC+FA      | 46.39          | 4.20       | 50.59          |
| OPC+FA+GGBS | 28.99          | 17.94      | 46.93          |

\*Volumes of C-S-H are calculated per 100ml of unreacted Portland cement with SCM

**Table 3.4 Bogue's Compounds Content (By % Wt) for Various Combinations**

|                                    | OPC   | OPC+FA | OPC+GGBS | OPC+FA+GGBS |
|------------------------------------|-------|--------|----------|-------------|
| <b>CaO</b>                         | 65.23 | 43.79  | 49.75    | 39.37       |
| <b>Al<sub>2</sub>O<sub>3</sub></b> | 5.72  | 14.60  | 13.46    | 16.60       |
| <b>SiO<sub>2</sub></b>             | 18.63 | 30.88  | 28.01    | 34.51       |
| <b>Fe<sub>2</sub>O<sub>3</sub></b> | 4.54  | 5.04   | 3.79     | 4.15        |
| <b>SO<sub>3</sub></b>              | 4.32  | 2.50   | 2.17     | 2.10        |
| <b>K<sub>2</sub>O</b>              | 0.59  | 1.35   | 1.06     | 1.24        |
| <b>TiO<sub>2</sub></b>             | 0.50  | 1.21   | 1.08     | 1.22        |
| <b>C<sub>3</sub>S</b>              | 66.81 | 53.45  | 50.11    | 33.40       |
| <b>C<sub>2</sub>S</b>              | 3.05  | 2.44   | 2.28     | 1.52        |
| <b>C<sub>3</sub>A</b>              | 7.47  | 5.97   | 5.60     | 3.73        |
| <b>C<sub>4</sub>AF</b>             | 13.80 | 11.04  | 10.35    | 6.90        |

This chapter concludes with the physical and chemical characterization of all the raw materials used to make SCC mixes. The next chapter presents proportioning of SCC mixes with and without fibres.



**CHAPTER 4**  
**DEVELOPMENT OF SCC MIXES BASED ON**  
**PLASTIC VISCOSITY OF CEMENT PASTE**

## 4.1. Introduction

It is important for the current research because of the scope it offers for characterizing fresh cement paste, grout, mortar and concrete, and for understanding how they perform in practical applications. Without satisfactory fresh properties, it is unlikely that the desirable properties of the hardened materials can be achieved. Hence, to describe the flow behaviour of concrete, a rheological parameter plastic viscosity is much better than workability which is calculated by conducting slump flow test, compaction factor tests etc.

## 4.2. Measuring Plastic Viscosity for Various Cement Paste Compositions

Rheological studies are done to measure the yield stress and most importantly plastic viscosity of cement paste with different compositions.

During the initial part of the study, a water to binder ratio varying from 0.35 to 0.55 is chosen with superplasticizer to cementitious ratio of 0.0075 to study the influence of water to binder ratio on the yield stress and plastic viscosity of the cement pastes. The compositions are given in *Table 4.1*.

**Table 4.1 Mix combinations**

| Mix combination              | Water to binder ratio       |
|------------------------------|-----------------------------|
| 100% OPC                     |                             |
| 75% OPC+25% GGBS             |                             |
| 80% OPC+20% Fly Ash          | 0.35, 0.4, 0.45, 0.5 & 0.55 |
| 50% OPC+25% Fly Ash+25% GGBS |                             |

In continuation to the initial study, four different cases are chosen with varying water to binder ratio and superplasticizer to the cementitious ratio as given below.

*Case I:* Water to binder ratio-0.57 and Superplasticizer to cementitious ratio-0.0065

*Case II:* Water to binder ratio-0.57 and Superplasticizer to cementitious ratio-0.0075

*Case III:* Water to binder ratio-0.5 and Superplasticizer to cementitious ratio-0.01

*Case IV:* Water to binder ratio-0.5 and Superplasticizer to cementitious ratio-0.0125

The following step by step procedure is adopted for conducting the experiment:

1. Required weights of cement and other supplementary cementitious materials are taken into a glass beaker
2. Based on the water to binder content ratio, required amount of water is added using a burette
3. Based on the superplasticizer to cementitious content ratio, required amount of superplasticizer is added using a burette
4. The contents of the beaker are stirred thoroughly and allowed to settle for about 10 minutes
5. The sample paste is subjected to viscosity test in a Brookfield Rotational Viscometer DV3T at a room temperature for a chosen shear rate. The spindle used for testing is SC4-21
6. A graph is then plotted between shear stress and shear rate for different shear rates at different times of the test. From the graph, yield stress and plastic viscosity values are obtained.

Brookfield rotational viscometer DV3T as shown in *Figure 4.1* is used for the entire testing sequence. The viscometer was equipped with a Vane geometry spindle of 2.53 mm height and 0.64 radii. The rheological properties of cement pastes are measured with varying shear rates for different intervals of time at a constant room temperature.



**Figure 4.1. Brookfield Viscometer DV3T**

For the initial study with varying water to binder ratios, the plastic viscosity of the cement pastes as shown in *Table 4.2* followed a decreasing trend with the increase in w/b ratio due to

the reaction between cementitious molecules and water. The full hydration process will happen at a w/b of 0.38 to 0.42 for a pure OPC paste which directly indicates that there will be a sudden decrease in plastic viscosity till 0.4 followed by a gradual decrease. But in the case of paste with 25% GGBS as a replacement, due to the flaky nature of particles, paste with GGBS required more water resulting in a gradual decrease of plastic viscosity. For 20% fly ash as replacement, reaction of water with fly ash required more time resulting in a gradual decrease of plastic viscosity. For ternary mix as, the total contribution of fly ash and GGBS are 25% and with the increase in water to cement ratio a decreasing trend of plastic viscosity was observed.

**Table 4.2: Plastic Viscosity values in Pa s for various combinations of cement paste**

| W/b                                 | 0.35 | 0.4  | 0.45 | 0.5  | 0.55 |
|-------------------------------------|------|------|------|------|------|
| <b>100% OPC</b>                     | 0.39 | 0.35 | 0.32 | 0.30 | 0.22 |
| <b>75% OPC+25% GGBS</b>             | 0.41 | 0.37 | 0.33 | 0.32 | 0.23 |
| <b>80% OPC+20% Fly ash</b>          | 0.34 | 0.30 | 0.28 | 0.24 | 0.19 |
| <b>50% OPC+25% GGBS+25% Fly ash</b> | 0.43 | 0.39 | 0.35 | 0.33 | 0.24 |

Similarly, the values of plastic viscosity for Cases I to IV are shown in *Table 4.3*.

**Table 4.3 Measured plastic viscosity of cement pastes for Case I to Case IV**

| Cementitious material combinations | Paste plastic viscosity (Pa s) |         |          |         |
|------------------------------------|--------------------------------|---------|----------|---------|
|                                    | Case I                         | Case II | Case III | Case IV |
| <b>100 % OPC</b>                   | 0.17                           | 0.165   | 0.25     | 0.24    |
| <b>75 % OPC + 25 % GGBS</b>        | 0.18                           | 0.174   | 0.26     | 0.25    |
| <b>80 % OPC + 20 % Fly ash</b>     | 0.16                           | 0.15    | 0.235    | 0.22    |

|  |      |      |       |      |
|--|------|------|-------|------|
| <b>50 % OPC + 25 %<br/>GGBS + 25 % Fly ash</b> | 0.20 | 0.19 | 0.275 | 0.26 |
|--|------|------|-------|------|

From *Table 4.3*, it is inferred that with the increase in water to cement ratio and superplasticizer dosage, the plastic viscosity decreases.

### 4.3. Role of Water to Cement Ratio on Compressive Strength of Concrete

According to Abram's law of water to cement ratio, the compressive strength of concrete depends on the water-cement ratio adopted and the strength is inversely proportional to water to cement ratio (in terms of mass). Based on this law it is clear that the strength of SCC also depends on the water to binder ratio. In order to establish a relation between the strength of concrete and the water to cement ratio, a set of values for water to cement ratio and the resulting 28 day-compressive strength using various mineral admixtures are adopted from (Boukendakdji *et al.*, 2012; Douma *et al.*, 2016, 2014; Uysal *et al.*, 2012; Uysal and Tanyildizi, 2012; Uysal and Sumer, 2011; Gesoglu *et al.*, 2009; Siddique *et al.*, 2011; Alqadi *et al.*, 2013; Raheman and Modani, 2013; Aggarwal and Aggarwal, 2011; Pathak *et al.*, 2012; Guneyisi *et al.*, 2010; Beycioğlu *et al.*, 2014) Using this data, regression analysis is performed to obtain the best fit curve as shown in *Figure 4.2* which is Abram's type power curve with  $R^2 = 0.941$ . The expression for compressive strength in terms of w/b ratio is given by

$$f_{cu} = \frac{132.77}{11^{(w/cm)}} \quad (4.1)$$

Where,

$f_{cu}$  is the 28-day cube compressive strength of concrete in MPa.

$\frac{w}{cm}$  represents the adopted water to cement ratio of the concrete mixture.

### 4.4. Development of Plastic Viscosity Based Mix Design for SCC

SCC is generally modelled as rigid solid particles (aggregates) suspended in a viscous liquid medium (cement paste). Based on this principle, many theories have been proposed:

#### 4.4.1. For low concentrations

At low concentrations, the particles are assumed to be far apart from each other and the interactions between them can be neglected. Einstein (Struble and Sun, 1994) proposed an equation to find the relative viscosity of one phase with respect to other which leads to increase in plastic viscosity of the suspension of particles.

$$\eta_r = 1 + [\eta]\phi \quad (4.2)$$

where,

$[\eta]$  represents the intrinsic viscosity which is the viscosity of individual particles.

$\phi$  represents the volume fraction of particles.

The intrinsic viscosity of particles can be calculated from relative viscosity of the suspension as

$$[\eta] = \lim_{\phi \rightarrow 0} \frac{\eta_r - 1}{\phi} \quad (4.3)$$

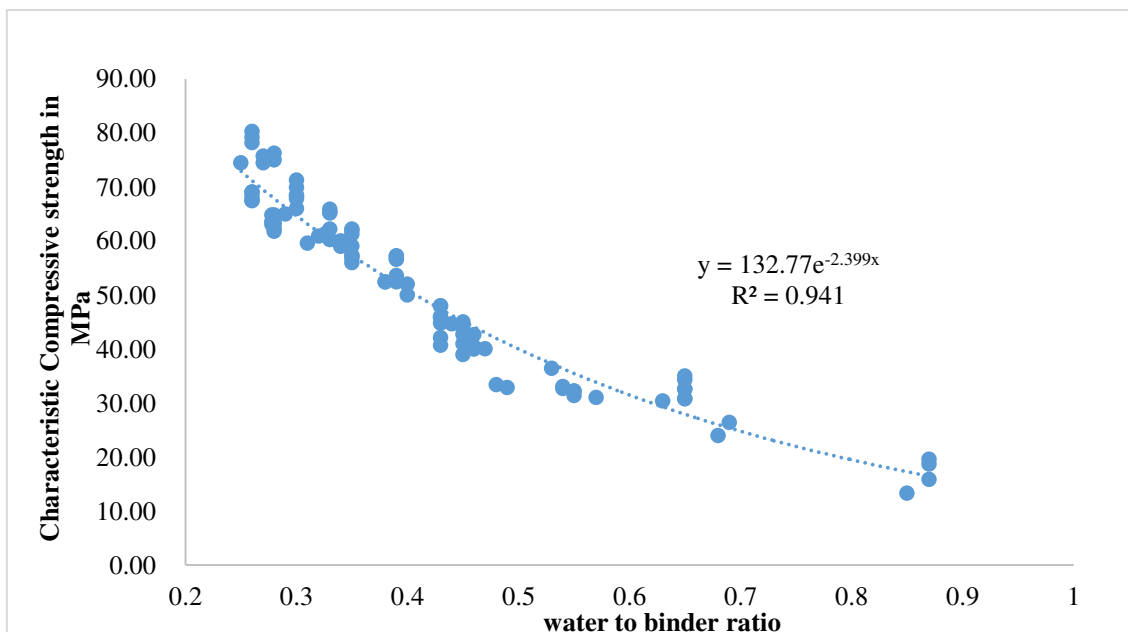


Figure 4.2 Regression curve for water to cement ratio

Shenoy (2013) proposed an equation based on Einstein's Eq. (4.2) and named it as modified Einstein's Eq. in the binomial form as

$$\eta_r = (1 - [\eta]\phi)^{-1} \quad (4.4)$$

(Utracki and Wilkie, 2002) modeled the solid particles as rigid spheres having radius 'a' and the particles are enclosed in a closed domain of radius b. Generally  $[\eta] = 2.5$ , when the particles are rigid and have a hexagonal random packing. (Neglecting the particle interaction effects) It is also assumed that the movement of the particles is very slow and their kinetic energy can be neglected. Simplifying the above Eq. (4.3) using these assumptions leads to

$$\eta_r = 1 + 2.5\phi \left[ 1 + \frac{25}{32} \left( \frac{\phi}{\phi_m} \right) - \frac{21}{64} \left( \frac{\phi}{\phi_m} \right)^3 + \frac{625}{128} \left( \frac{\phi}{\phi_m} \right)^2 + \dots \right] \quad (4.5)$$

where,

$\phi_m$  represents the maximum packing fraction of the particle.

Shenoy (2013) based on the above Eq. (4.5) derived an expression for dilute suspensions as

$$\eta_r = 1 + 2.5\phi \left( 1 + \frac{25\phi}{4a_1^3} \right) \quad (4.6)$$

For low concentrations of particles generally,  $a_1 = 1.111$

#### 4.4.2. For high concentrations

As the concentration of suspension increases, the viscosity of the suspension not only depends on the concentration of particles but also on the size and shape i.e. packing of the particles. Based on this concept, the plastic viscosity of the suspension is given as

$$\eta_r = 1 + [\eta]\phi + B\phi^2 + C\phi^3 + \dots \quad (4.7)$$

Where, the values of these constants B & C depend on the size, shape and distribution of particles in the suspension i.e. on the nature of the suspension. These values are available in the literature (Shenoy, 2013; Batchelor, 1977; Vand, 1948; Saito, 1950).

Thomas Kumar (1999) proposed an exponential replacement for the constant term C in Eq.(4.7) as

$$\eta_r = 1 + 2.5\phi + 10.05\phi^2 + 0.00273e^{16.6\phi} \quad (4.8)$$

This expression is derived from experimental data by performing a regression analysis and finding out the best fit curve. The range of values  $\phi$  suggested for this expression is 0.15 to 0.6.

From the Eq. (4.7) and Eq. (4.8), it is clear that there is a limitation in using the constants B and C as they are restricted to a particular range of volume fraction of particles. So, in view of these restrictions, Krieger and Dougherty (1959) came up with expression to calculate the viscosity of suspensions based on their maximum packing fraction concept. It is assumed that in the maximum packing fraction state, the particles are bound to have minimum voids in them and maximum possible viscosity. These values are shown in *Table 4.4*

**Table 4.4 Packing fractions for different types of packing of particles**

| Packing type     | Maximum packing fraction |
|------------------|--------------------------|
| Cubic            | 0.524                    |
| Random Hexagonal | 0.637                    |
| Hexagonal        | 0.74                     |

From the above values, they came up with a generalized equation for calculation of plastic viscosity based on the maximum packing fraction of particles and the viscosity of individual particles expressed as

$$\eta_r = \left(1 - \frac{\phi}{\phi_m}\right)^{-[\eta]\phi_m} \quad (4.9)$$

Where  $\phi_m$  is the maximum packing fraction of particles and is dependent on the distribution of particles and  $[\eta]$  is the intrinsic viscosity of particles in the suspension. These values also depend on the shear rate applied to the suspension.



The value of  $[\eta]$  decreases with increase in shear rate and  $\phi_m$  increases with increase in shear rate indicating that both are inversely proportional to each other. But practically, the products of both the parameters remain constant and the value is approximately equal to 1.9.

Frankel *et al.* (1967) proposed an expression for high concentration suspensions when the volume fraction of particles almost equal to the maximum volume packing fraction of particles i.e. when  $\phi \rightarrow \phi_m$  as

$$\eta_r = \frac{9}{8} \left( \frac{(\phi / \phi_m)^{\frac{1}{3}}}{1 - (\phi / \phi_m)^{\frac{1}{3}}} \right) \quad (4.10)$$

Chong *et al.* (1971) developed an expression for a complete range of volume fraction of particles i.e. from  $\phi \rightarrow 0$  to  $\phi \rightarrow \phi_m$  by applying the Brownian random distribution of particles based on the regression analysis of experimental data. It is given as

$$\eta_r = \left( 1 + \frac{[\eta]\phi_m}{2} \left[ \frac{(\phi / \phi_m)}{1 - (\phi / \phi_m)} \right] \right)^2 \quad (4.11)$$

This Brownian distribution contributes to a slight increase in viscosity of the suspension and the range of values of concentrations considered for  $\frac{\phi}{\phi_m}$  is from 0 to 0.7.

#### 4.4.3. Methodology for proportioning SCC mixes

SCC mix is considered as a suspension of particles in which the rigid solid spheres (aggregates) are suspended in a viscous fluid (cement paste). Firstly, to the suspension of cement paste, fine aggregate is added and then to this mixture coarse aggregate is added and then the process continues. Now, following this procedure, a standard expression is developed as

$$\eta_{mix} = \eta_{paste} * f_1(\phi_1) * f_2(\phi_2) \dots * f_n(\phi_n) \quad (4.12)$$

Where,

$\eta_{paste}$  represents the plastic viscosity of cement paste.

$\phi_1, \phi_2, \dots, \phi_n$ , are the volume fractions of the particles (phases) to be added to the suspension of cement paste.

Applying the Krieger and Dougherty Eq. (4.8) to calculate the contribution of individual particle to the plastic viscosity of the mix is given as

$$f_i(\phi_i) = \left(1 - \frac{\phi_i}{\phi_m}\right)^{-1.9\phi_m} \quad (4.13)$$

From the Eq.s (4.12 and 4.13), the plastic viscosity of the SCC mix is given as

$$\eta_{mix} = \eta_{paste} * \left(1 - \frac{\phi_{FA}}{\phi_m}\right)^{-1.9} * \left(1 - \frac{\phi_{CA}}{\phi_m}\right)^{-1.9} \quad (4.14)$$

By adding fine aggregate to the suspension of cement paste, first the packing fraction of the suspension or the mixture is assumed to be random hexagonal packing and then after the addition of coarse aggregate the packing becomes dense and then the packing is assumed to be hexagonal packing. Based on these assumptions, the plastic viscosity of SCC mix is given as

$$\eta_{mix} = \eta_{paste} * \left(1 - \frac{\phi_{FA}}{0.63}\right)^{-1.9} * \left(1 - \frac{\phi_{CA}}{0.74}\right)^{-1.9} \quad (4.15)$$

Based on the literature available as well as the gaps identified, the following cases are chosen to study the effect of plastic viscosity on the workability and strength characteristics of SCC using Crushed Rock Fines as a fine aggregate with varying water to binder ratio.

*Case I:* A trial plastic viscosity of 9 Pa s is chosen for water to binder ratio of 0.57 (adopted from Abo Daheer, 2016 without filler and with CRF as a fine aggregate).

*Case II:* Influence of plastic viscosities 7 Pa s and 11 Pa s on the fresh and hardened properties for water to binder ratio of 0.57.

*Case III:* Influence of plastic viscosities 9 Pa s on the fresh and hardened properties for water to binder ratio of 0.5 with river sand as a fine aggregate.

*Case IV:* Influence of plastic viscosities 9 Pa s and 13 Pa s on the fresh and hardened properties for water to binder ratio of 0.5.

Specific gravities of materials used for proportioning the materials required for SCC mix with the proposed mix design methodology are given in section 1:

Another input required for the proposed mix design methodology is the plastic viscosity of the cement paste. So, for the given grade of SCC to be proportioned, the water to cement ratio adopted is 0.5 as per Eq. (4.1). Corresponding to 0.5 water to cement ratio, the plastic viscosity of cement pastes for different cementitious materials are measured using Brookfield viscometer as explained in section 4.3. The plastic viscosities of pastes with different cementitious materials are given in *Table 4.3* for cases I, II and III.

Based on these plastic viscosities and considering the target plastic viscosity of the SCC to be proportioned as 7, 9 and 11 Pa-s for water to binder ratio of 0.57 and 9 and 13 for water to binder ratio of 0.5. The proportions of different materials used to prepare an SCC mix with a grade equal to M 40 are calculated with the help of a computer program. Different values of parameters  $t_1$  &  $t_2$  are considered as an input starting from 0 to the maximum value with a condition that the volume fractions of coarse and fine aggregates do not exceed 1. The output of this code generated several combinations of SCC mix proportions and some of the best mixes from many combinations generated are chosen based on the satisfactory requirements of EFNARC guidelines.

**Case I:** A trial plastic viscosity of 9 Pa s is chosen for water to binder ratio of 0.57 (adopted from Abo Daheer *et al.*, 2016 without filler and with CRF as a fine aggregate).

The following is the step-by-step process for proportioning the SCC mixes:

1. First, a trial plastic viscosity value is chosen considering that slump cone  $T_{50}$  increases with the increase in plastic viscosity.
2. Water to cement ratio is calculated using equation given by (Abo Daheer *et al.*, 2015).

$$f_{cu} = \frac{195}{12.65^{(w/cm)}} \quad (4.16)$$

Where,  $f_{cu}$  = 28-days characteristic compressive strength of concrete

3. Choose the water content following EFNARC guidelines in the range of 150 to 210 kg/m<sup>3</sup>.
4. The percentage replacement of cement with GGBS and Fly ash is assumed to be 25% (Abo Daheer *et al.*, 2015) and 20% (Abhijeet S *et al.*, 2015). Based on one to one interaction with industry experts, for ternary combination mixes, the amount of GGBS and Fly Ash is assumed to be 25%+25%. A trial superplasticizer dosage of 0.45% to 1.25% of the cementitious material is adopted. Glenium Sky 8233 is used as superplasticizer in the present study.
5. Plastic viscosity of the paste ( $\eta_{\text{paste}}$ ) for 75% OPC+25% GGBS, 80% OPC + 20% Fly ash and 50% OPC+25% GGBS+25% Fly ash are measured using Brookfield viscometer. The corresponding values are tabulated in *Table 4.3*.
6. Mass of fine aggregate and coarse aggregate are calculated based on their volume fractions using Eq. (4.6) and (4.7). Volume fractions of fine and coarse aggregate are estimated using a randomization computer code such that the amount of fine and coarse aggregate does not exceed the limits as per EFNARC guidelines (The European Guidelines for SCC – EFNARC, 2005).

$$\phi_{FA} = \frac{\frac{FA}{\rho_{FA}}}{\left( \frac{cem}{\rho_{cem}} + \frac{w}{\rho_w} + \frac{SP}{\rho_{SP}} + 0.02 \right) + \frac{FA}{\rho_{FA}}} \quad (4.17)$$

$$\phi_{CA} = \frac{\frac{CA}{\rho_{CA}}}{\left( \frac{cem}{\rho_{cem}} + \frac{w}{\rho_w} + \frac{SP}{\rho_{SP}} + \frac{FA}{\rho_{FA}} + 0.02 \right) + \frac{CA}{\rho_{CA}}} \quad (4.18)$$

Where,

|                       |   |                                |
|-----------------------|---|--------------------------------|
| Cem                   | = | Cementitious material          |
| FA                    | = | Fine Aggregate                 |
| CA                    | = | Coarse Aggregate               |
| SP                    | = | Superplasticizer               |
| w                     | = | Water                          |
| $\eta_{\text{mix}}$   | = | Plastic Viscosity of the Mix   |
| $\eta_{\text{paste}}$ | = | Plastic Viscosity of the Paste |

|                        |   |  |
|------------------------|---|--|
| $\eta_r$               | = | Plastic Viscosity of the Suspension of Particles       |
| $\rho_{CA}$            | = | Density of Coarse Aggregate                            |
| $\rho_{cem}$           | = | Density of Cement                                      |
| $\rho_{FA}$            | = | Density of Fine Aggregate                              |
| $\rho_{sp}$            | = | Density of Superplasticizer                            |
| $\rho_w$               | = | Density of Water                                       |
| $\phi_{CA}, \phi_{FA}$ | = | Volume Fraction of Coarse Aggregate and Fine Aggregate |

7. The total volume of the mix should be equal to  $1 \text{ m}^3$ . If not, suitable corrections are to be applied to the raw materials to attain a total volume of  $1 \text{ m}^3$ .
8. The measured plastic viscosity of the mix is compared with the assumed plastic viscosity (step 1). The assumed value of plastic viscosity mix is in good agreement with the estimated value if the difference between the two is within  $\pm 5\%$ . If not, choose different volume fractions of solid phase ingredients i.e. fine and coarse aggregates and repeat the steps 7 and 8.

One of the best proportions of SCC mix among several combinations generated for Case-I is given in *Table 4.5*

**Table 4.5 Mix proportions of SCC mixes-PV:9 w/b:0.57**

| Mix Composition | PV of Paste | OPC (kg/m <sup>3</sup> ) | Fly Ash (kg/m <sup>3</sup> ) | GGBS (kg/m <sup>3</sup> ) | Water (kg/m <sup>3</sup> ) | CRF (kg/m <sup>3</sup> ) | Coarse Aggregate (kg/m <sup>3</sup> ) | SP (kg/m <sup>3</sup> ) | SP/CM (kg/m <sup>3</sup> ) |
|-----------------|-------------|--------------------------|------------------------------|---------------------------|----------------------------|--------------------------|---------------------------------------|-------------------------|----------------------------|
| SCCC100         | 0.17        | 364                      | 0                            | 0                         | 209                        | 895                      | 838                                   | 2.35                    | 0.0065                     |
| SCCC80F20       | 0.16        | 285                      | 71                           | 0                         | 204                        | 940                      | 784                                   | 2.3                     | 0.0065                     |
| SCCC75G25       | 0.18        | 272                      | 0                            | 91                        | 209                        | 895                      | 829                                   | 2.34                    | 0.0064                     |
| SCCC50F25G25    | 0.2         | 179                      | 90                           | 90                        | 206                        | 896                      | 806                                   | 2.32                    | 0.0065                     |

Similarly, based on the step-by-step procedure, the proportions of SCC mixes for various mix compositions with varying plastic viscosities of 7 Pa s, and 11 Pa s are given in *Table 4.6*

**Case II:** Influence of plastic viscosities 7 Pa s and 11 Pa s on the fresh and hardened properties for water to binder ratio of 0.57. Similar to Case I based on the step-by-step procedure, the proportions of SCC mixes for various mix compositions with varying plastic viscosities of 7 Pa s, and 11 Pa s are given in *Table 4.6*.

**Table 4.6 Mix proportions of SCC mixes-PV: 7 and 11 w/b: 0.57**

| Mix Composition | PV of mix | PV of Paste | OPC (kg/m <sup>3</sup> ) | Fly Ash (kg/m <sup>3</sup> ) | GGBS (kg/m <sup>3</sup> ) | Water (kg/m <sup>3</sup> ) | CRF (kg/m <sup>3</sup> ) | Coarse Aggregate (kg/m <sup>3</sup> ) | SP (kg/m <sup>3</sup> ) | SP/CM (kg/m <sup>3</sup> ) |
|-----------------|-----------|-------------|--------------------------|------------------------------|---------------------------|----------------------------|--------------------------|---------------------------------------|-------------------------|----------------------------|
| SCCC100         | 7         | 0.17        | 379                      | 0                            | 0                         | 217                        | 870                      | 823                                   | 2.46                    | 0.0065                     |
| SCCC80F20       |           | 0.16        | 296                      | 74                           | 0                         | 212                        | 915                      | 770                                   | 2.4                     | 0.0065                     |
| SCCC75G25       |           | 0.18        | 285                      | 0                            | 95                        | 218                        | 871                      | 811                                   | 2.47                    | 0.0065                     |
| SCCC50F25G25    |           | 0.2         | 187                      | 94                           | 94                        | 215                        | 869                      | 790                                   | 2.43                    | 0.0065                     |
| SCCC100         | 11        | 0.17        | 352                      | 0                            | 0                         | 202                        | 909                      | 852                                   | 2.28                    | 0.0065                     |
| SCCC80F20       |           | 0.16        | 276                      | 69                           | 0                         | 198                        | 951                      | 799                                   | 2.24                    | 0.0065                     |
| SCCC75G25       |           | 0.18        | 264                      | 0                            | 88                        | 202                        | 907                      | 845                                   | 2.29                    | 0.0065                     |
| SCCC50F25G25    |           | 0.2         | 174                      | 87                           | 87                        | 200                        | 913                      | 817                                   | 2.25                    | 0.0065                     |

**Case III:** Influence of plastic viscosities 9 Pa s on the fresh and hardened properties for water to binder ratio of 0.5 with river sand as fine aggregate

Similar to earlier cases the proportions for different combinations of SCC mixes with river sand as fine aggregate is given in *Table 4.7*

**Table 4.7 Mix proportions for SCC mixes with river sand as fine aggregate**

| Mix ID                                       | SCCC100 | SCCC75G25 | SCCC80F20 | SCCC50G25F25 |
|--|---------|-----------|-----------|--------------|
| Cement<br>(kg/m <sup>3</sup> )               | 428     | 320       | 327       | 206          |
| GGBS (kg/m <sup>3</sup> )                    | 0       | 107       | 0         | 103          |
| Fly Ash<br>(kg/m <sup>3</sup> )              | 0       | 0         | 82        | 103          |
| Water (kg/m <sup>3</sup> )                   | 214     | 204       | 204       | 206          |
| Coarse<br>Aggregate<br>(kg/m <sup>3</sup> )  | 755     | 753       | 753       | 752          |
| River Sand<br>(kg/m <sup>3</sup> )           | 886     | 882       | 900       | 877          |
| Super<br>plasticizer<br>(kg/m <sup>3</sup> ) | 4.28    | 4.27      | 4.09      | 4.12         |

**Case IV:** Influence of plastic viscosities 9 Pa s and 13 Pa s on the fresh and hardened properties for water to binder ratio of 0.5.

The water to binder ratio is adopted from *Figure 4.2* based on the literature review and the plastic viscosities of cement paste are adopted from *Table 4.3*.

The following step-by-step process is followed

1. The first step is to choose a corresponding grade of concrete and accordingly water to cement ratio is calculated from Eq. (4.1).
2. Plastic viscosity of the paste is to be adopted based on the water to cement ratio obtained from step (1). The values of plastic viscosity of the paste are obtained either by measuring using Brookfield Viscometer or from standard literature available. For the current study, these values are obtained using Brookfield Viscometer.
3. Based on the required workability of the mix, a trial plastic viscosity of the mix has to be chosen. With the increase in plastic viscosity of the mix,  $T_{50}$  time increases



accordingly. With the addition of fibres, the plastic viscosity of the mix will be on the higher side.

4. Adopt suitable water content as per the standard EFNARC guidelines ranging from 150 to 210 kg/m<sup>3</sup> based on the overall workability of the mix.
5. With the known water to cement ratio and water content, total cementitious content is to be calculated. Total cementitious content is a combination of OPC, fly ash and GGBS depending on the type of additions i.e. binary or ternary.
6. The % replacement of OPC with GGBS and Fly ash with OPC for binary blends is suggested as 25 % for GGBS and 20 % for Fly ash for good strength gain properties by ACC limited. By consulting the industry experts, a replacement of 25% of GGBS and 25% of Fly ash is suggested for ternary mixes (Abhijeet *et al*).
7. A trial super-plasticizer dosage as a % of the cementitious material is adopted which satisfies the required workability of the SCC mix.
8. Individual quantities of ingredients i.e. amounts of coarse and fine aggregate to be added can be found from the volume fractions of materials obtained from Eq. (4.6 and 4.7).  $t_1$  and  $t_2$  are arbitrarily chosen such that  $t_1 \times t_2 = 1$ . Each of them corresponding to the factor representing the volume fraction of fine and coarse aggregate.
9. The total volume of the mix should be equal to 1 m<sup>3</sup>. Suitable adjustments have to be made to ensure that the total volume equals 1 m<sup>3</sup>.
10. Eq. (4.15) is being used to estimate the plastic viscosity of the mix with the obtained proportions of raw materials. The percentage difference between the assumed plastic viscosity from step (3) and the estimated plastic viscosity should be within  $\pm 5\%$ . If the difference is more, then different sets of volume fractions for solid phase ingredients i.e. fine and coarse aggregates are to be chosen and steps 9 and 10 are to be repeated. The proportions for different combinations of SCC mixes are given in *Table 4.8*

**Table 4.8 Mix proportions of SCC mixes-PV: 9 and 13 w/b: 0.5**

| Mix Composition | PV of mix | PV of Paste | OPC (kg/m <sup>3</sup> ) | Fly Ash (kg/m <sup>3</sup> ) | GGBS (kg/m <sup>3</sup> ) | Water (kg/m <sup>3</sup> ) | CRF (kg/m <sup>3</sup> ) | Coarse Aggregate (kg/m <sup>3</sup> ) | SP (kg/m <sup>3</sup> ) | SP/CM % |
|-----------------|-----------|-------------|--------------------------|------------------------------|---------------------------|----------------------------|--------------------------|---------------------------------------|-------------------------|---------|
| SCCC100         | 9         | 0.245       | 426                      | 0                            | 0                         | 213                        | 904                      | 755                                   | 4.27                    | 0.01    |
| SCCC80F20       |           | 0.256       | 326                      | 82                           | 0                         | 204                        | 918                      | 753                                   | 4.08                    | 0.01    |
| SCCC75G25       |           | 0.23        | 319                      | 0                            | 106                       | 213                        | 900                      | 753                                   | 4.25                    | 0.01    |
| SCCC50F25G25    |           | 0.27        | 206                      | 103                          | 103                       | 206                        | 894                      | 752                                   | 4.11                    | 0.01    |
| SCCC100         | 13        | 0.24        | 400                      | 0                            | 0                         | 200                        | 937                      | 772                                   | 5.011                   | 0.0125  |
| SCCC80F20       |           | 0.22        | 309                      | 77                           | 0                         | 193                        | 964                      | 754                                   | 4.833                   | 0.0125  |
| SCCC75G25       |           | 0.25        | 300                      | 0                            | 100                       | 200                        | 937                      | 772                                   | 5.009                   | 0.0125  |
| SCCC50F25G25    |           | 0.26        | 194                      | 97                           | 97                        | 194                        | 943                      | 756                                   | 4.855                   | 0.0125  |

With the help of a computer program, the quantities of raw materials required for SCC mix are obtained based on the plastic viscosities of cement pastes from *Table 4.3*, target plastic viscosity of the SCC mix, and target compressive strength for a grade of concrete equal to M40. Different values of parameters  $t_1$  &  $t_2$  are considered as an input starting from 0 to the maximum value with a condition that the volume fractions of coarse and fine aggregates do not exceed 1. The output of this code generated several combinations of SCC mix proportions and some of the best mixes from many combinations generated are chosen based on the satisfactory requirements of EFNARC guidelines.

#### 4.4.4. Effect of addition of fibres

Due to the addition of fibres, the plastic viscosity of the SCC mix increases as these fibres offer some resistance to the flow of the mixture. If fibres are assumed to be acting as slender bodies in dilute suspension, the effect of dilute concentration of steel fibres is estimated by applying Russel's slender body approximation Phan-Thien *et al.* (1994). It is assumed that the fibres are considered as rigid bodies and their motion is restricted due to the resistance that is offered by the surrounding medium of materials which are highly viscous in nature. After applying all these approximations, the resulting plastic viscosity of SCC mix is obtained as

$$\eta_{mix} = \eta_{paste} * \left(1 - \frac{\phi_{FA}}{0.63}\right)^{-1.9} * \left(1 - \frac{\phi_{CA}}{0.74}\right)^{-1.9} * (1 + K_{fib}\phi_{fib}) \quad (4.19)$$

Where,

$\phi_{fib}$  is the volume fraction of fibres in the mix.

$K_{fib}$  is termed as the fibre contribution factor.

$$K_{fib} = \frac{\pi l_d^2}{3 \ln(2l_d)} - 1 \quad (4.20)$$

$l_d$  is the aspect ratio of fibres being used in the mix design.

With the change in the aspect ratio of fibres, the fibre contribution factor changes which in turn alters the plastic viscosity of the mix. Aspect ratio is also one of the most important parameter in addressing the overall performance of SCC mixes especially the fresh properties.

If the mix design is with the addition of fibres, then the initial trial of plastic viscosity is assumed based on the aspect ratio, volume fraction, compressive strength of concrete and water to cement ratio. For the current study, the following cases are chosen

**Case V:** Volume Fraction of fibres: 0.35, Aspect ratio: 60, Type of fibres: Steel Hooked End, Plastic Viscosity of mix with fibres given in *Table 4.9*

**Case VI:** Volume Fraction of fibres: 0.1 to 0.5 with an incremental interval of 0.1, Aspect ratio: 60, Type of fibres: Steel Hooked End, Plastic Viscosity of mix with fibres given in Table 4.9

**Table 4.9 Plastic Viscosity of mix with fibres**

| Mix Composition | Cases   | Computed Plastic Viscosity (Pa s) (based on Eq.(4.19)) | Fibre % |
|-----------------|---------|--|---------|
| SCCC100         |         |  |         |
| SCCC80F20       | Case V  | 33.77  | 0.35    |
| SCCC75G25       |         |  |         |
| SCCC50F25G25    |         |  |         |
| SCCC50F25G25    |         | 23.22  | 0.1     |
| SCCC50F25G25    |         | 33.44  | 0.2     |
| SCCC50F25G25    | Case VI | 43.66  | 0.3     |
| SCCC50F25G25    |         |  |         |
| SCCC50F25G25    |         |  |         |
| SCCC50F25G25    |         |  |         |
| SCCC50F25G25    |         | 64.09  | 0.5     |

#### 4.5.4.1. Step by step mix design procedure

If the mix design is with the addition of fibres, then the initial trial of plastic viscosity is assumed based on the aspect ratio, volume fraction, compressive strength of concrete and water to cement ratio.

1. Choose a corresponding grade of concrete and accordingly water to cement ratio is calculated from Eq. (4.1).
2. Plastic viscosity of the paste is to be adopted based on the water to cement ratio obtained from step (1). The values of plastic viscosity of the paste are obtained either by measuring using Brookfield Viscometer or from standard literature available.
3. Based on the required workability of the mix, a trial plastic viscosity of the mix has to be chosen. With the increase in plastic viscosity of the mix,  $T_{50}$  time increases accordingly. With the addition of fibres, the plastic viscosity of the mix will be on the higher side.

4. Adopt suitable water content as per the standard EFNARC guidelines ranging from 150 to 210 kg/m<sup>3</sup> based on the overall workability of the mix.
5. With the known water to cement ratio and water content, total cementitious content is to be calculated. Total cementitious content is a combination of OPC, fly ash and GGBS depending on the type of additions i.e. binary or ternary.
6. The % replacement of GGBS and Fly ash with OPC for binary blends is suggested as 25 % for GGBS and 20 % for Fly ash for good strength gain properties by ACC limited. By consulting the industry experts, a replacement of 25% of GGBS and 25% of Fly ash is suggested for ternary mixes.
7. A trial super-plasticizer dosage as a % of the cementitious material is adopted which satisfies the required workability of the SCC mix.
8. As the volume fraction of fibres to be added and their aspect ratio will be known initially, the corresponding fibre contribution factor from Eq. (4.20) and volume fraction have to be substituted in Eq. (4.19) and the steps have to be repeated to calculate the aggregate quantities.
9. Individual amount of ingredients i.e. amounts of coarse and fine aggregate to be added can be found from the volume fractions of materials obtained from Eq. (4.15) and if fibres are added use Eq. (4.19).  $t_1$  and  $t_2$  are arbitrarily chosen such that  $t_1 \times t_2 = 1$ . Each of them corresponding to the factor representing the volume fraction of fine and coarse aggregate.
10. The total volume of the mix should be equal to 1 m<sup>3</sup>. Suitable adjustments have to be made to ensure that the total volume equals 1 m<sup>3</sup>.
11. Eq. (4.15) and (4.19) are to be used to estimate the plastic viscosity of the mix with the obtained proportions of raw materials. The percentage difference between the assumed plastic viscosity from step (3) and the estimated plastic viscosity should be within  $\pm 5\%$ . If the difference is more, then volume fractions of solid phase ingredients i.e. fine and coarse aggregates are to be chosen and steps 10 and 11 are to be repeated.

Similar to the Case V, the volume fraction of fibres is varied from 0.1% to 0.5% of total mix and the same procedure is adopted for proportioning the mixes for Case VI. The final mix proportions for Case V and Case VI are given in *Table 4.10*

**Table 4.10 Mix proportions of SCC mixes with the addition of fibres for w/b = 0.5**

| Mix Composition | PV of mix | PV of Paste | Fibre % | OPC (kg/m <sup>3</sup> ) | Fly Ash (kg/m <sup>3</sup> ) | GGBS (kg/m <sup>3</sup> ) | Water (kg/m <sup>3</sup> ) | CRF (kg/m <sup>3</sup> ) | Coarse Aggregate (kg/m <sup>3</sup> ) | SP (kg/m <sup>3</sup> ) | Fibres (kg/m <sup>3</sup> ) | SP/CM % |
|-----------------|-----------|-------------|---------|--------------------------|------------------------------|---------------------------|----------------------------|--------------------------|---------------------------------------|-------------------------|-----------------------------|---------|
| SCCC100         | 33.77     | 0.24        | 0.35    | 426                      | 0                            | 0                         | 213                        | 904                      | 755                                   | 4.27                    | 25                          | 0.01    |
| SCCC80F20       | 33.77     | 0.22        |         | 326                      | 82                           | 0                         | 204                        | 918                      | 753                                   | 4.08                    | 25                          | 0.01    |
| SCCC75G25       | 33.77     | 0.25        |         | 316                      | 0                            | 106                       | 213                        | 900                      | 753                                   | 4.25                    | 25                          | 0.01    |
| SCCC50F25G25    | 33.77     | 0.26        |         | 206                      | 103                          | 103                       | 206                        | 894                      | 752                                   | 4.11                    | 25                          | 0.01    |
| SCCC50F25G25    | 23.22     | 0.24        | 0.1     | 400                      | 0                            | 0                         | 200                        | 937                      | 772                                   | 5.011                   | 7                           | 0.0125  |
| SCCC50F25G25    | 33.44     | 0.22        | 0.2     | 309                      | 77                           | 0                         | 193                        | 964                      | 754                                   | 4.833                   | 14                          | 0.0125  |
| SCCC50F25G25    | 43.66     | 0.25        | 0.3     | 300                      | 0                            | 100                       | 200                        | 937                      | 772                                   | 5.009                   | 21                          | 0.0125  |
| SCCC50F25G25    | 53.87     | 0.26        | 0.4     | 194                      | 97                           | 97                        | 194                        | 943                      | 756                                   | 4.855                   | 28                          | 0.0125  |
| SCCC50F25G25    | 64.09     | 0.26        | 0.5     | 194                      | 97                           | 97                        | 194                        | 943                      | 756                                   | 4.855                   | 35                          | 0.0125  |

This chapter concludes with successful proportioning of the SCC mixes based on the plastic viscosity of the cement pastes with and without fibres.

In the next chapter experimental investigations and the observations on the fresh and hardened properties of SCC mixes from the proportions obtained for all the six cases, four for SCC mixes without fibres and two for SCC mixes with hooked end steel fibres will be addressed.

**CHAPTER 5**  
**EXPERIMENTAL INVESTIGATION ON SCC**  
**WITH AND WITHOUT FIBRES**

This chapter presents the mixing sequence adopted for the experimental investigations on SCC mixes. Fresh and hardened properties are evaluated for all the SCC mixes with and without fibers. Fracture energy is also evaluated for the SCC mixes with fibers.

### 5.1. Mixing Sequence of SCC Mixes with and without Fibres

Forced type pan mixer is used for mixing the raw materials in required proportions. The entire mixing sequence is finished within 10 min for all the mixes. Raw materials are added as per the following sequence shown in *Figure 5.1* and *Figure 5.2*.

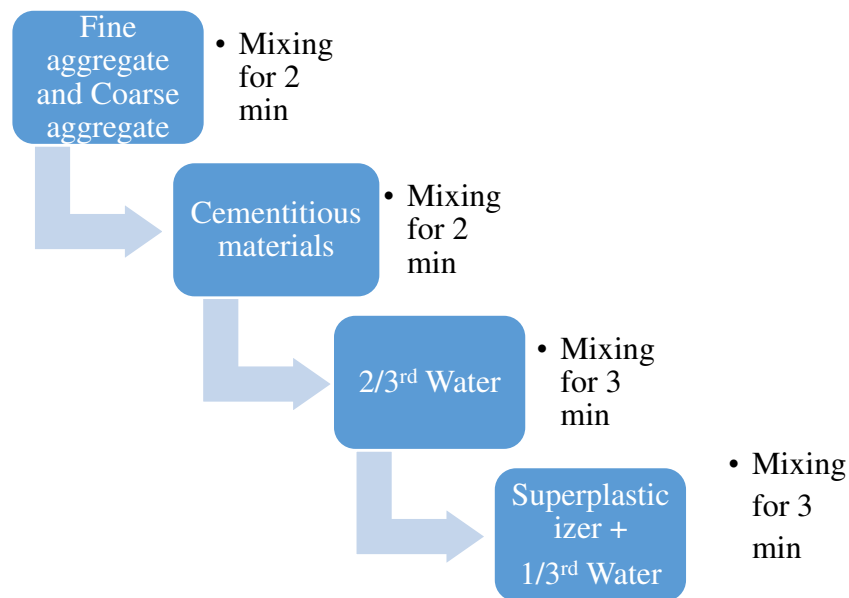


**Figure 5.1** Mixing Sequence of SCC mix without fibres

### 5.2. Test methods for fresh and hardened properties of SCC

Due to its fluid nature, SCC requires modified fresh property testing methods compared to conventional concrete. One of the most challenging aspects of satisfying the fresh properties of SCC is the composition of raw materials used for mixing. SCC with satisfied strength characteristics with un-satisfied fresh properties is not suggested for the application. Fresh properties of SCC include Slump flow which characterizes the flowable nature of the mix,  $T_{500}$  –slump flow time and V-funnel characterizes the viscous nature of the mixes based on the rate of flow, J-ring and L-box test methods characterize the passing ability of SCC mixes.

The following tests are conducted to assess the performance of SCC mixes in its hardened state.



- 7-days and 28-days compressive strength tests for cube specimen of size 150X150X150 mm and a cylindrical specimen of size 150X300mm cylinders

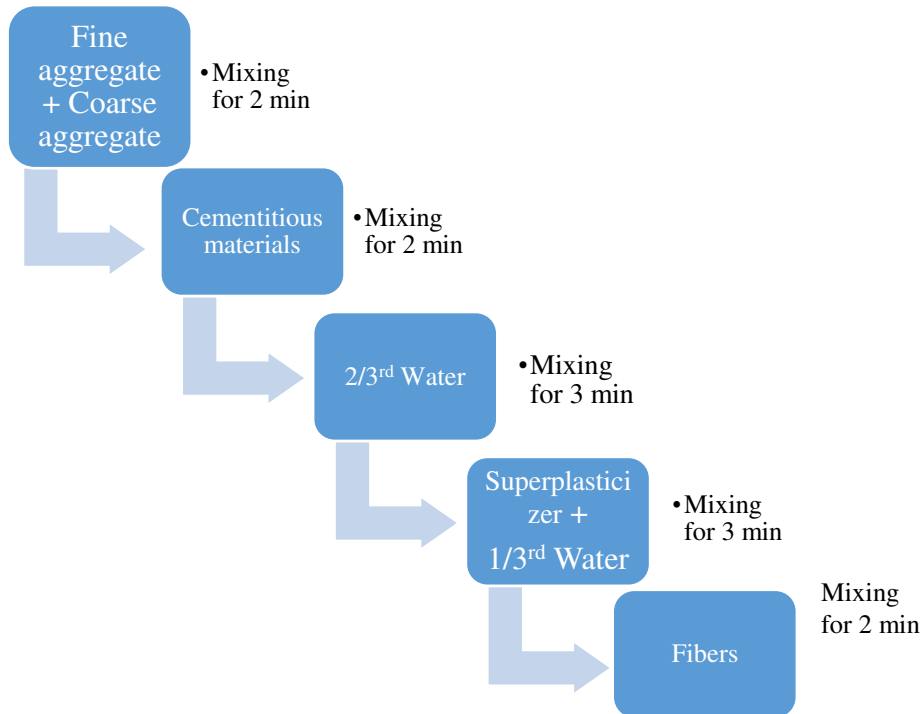


**Figure 5.2 Mixing Sequence of SCC mix with fibres**

- 28 day split tensile strength of cylindrical specimen of size 150mm diameter and 300mm height.
- 28 day flexural strength tests for prisms of size length 500mm, width 100mm and depth 100mm.
- Ultrasonic Pulse Velocity test is conducted to evaluate the non-destructive nature of SCC mixes in terms of its quality.
- Three Point Bending (TPB) tests are conducted to evaluate the fracture energy and to generate load-CMOD curves based on the TPB tests.
- A total of 3 batches i.e. 3 cube+3 cylinder specimen for compressive strength, 3 cylinder specimen for split tensile strength and 3-prism specimen for flexural strength obtained from the test result of each batch is reported.

The initial set of experimentation is carried out for SCC mixes with CRF as fine aggregate for the four combinations of mixes with water to binder ratio of 0.57. The proportions are given

in *Table 4.7*. The volume fractions of solid and paste are shown in *Figure 5.3* and *Figure 5.4* and the fresh properties of the mixes are shown in *Figure 5.5* to *Figure 5.9*.

Considering the needs of the construction industry and as per the suggestions given by experts from industry, the water to binder ratio is reduced to 0.5. The plastic viscosities of the cement paste for various combinations corresponding to a water to binder ratio of 0.5 are addressed in CHAPTER 4. Initial analysis and experimentation are conducted for a plastic viscosity of 9 Pa s which resulted in the surplus quantities of raw materials as well as strengths for a chosen M40 grade and 0.5 water to binder ratio. Plastic viscosity value is increased to 13 Pa s to ensure that the mix proportions generated will lead to desired fresh and hardened properties. The proportions are given in *Table 4.8*

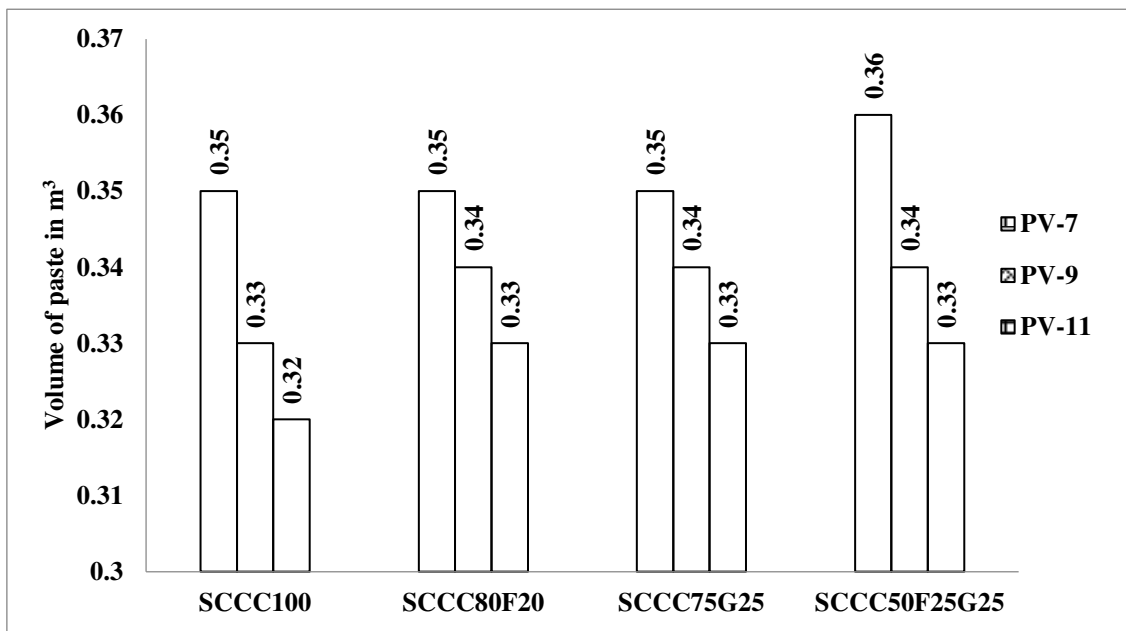


**Figure 5.3 Volume of paste for SCC mixes for Case I (Plastic Viscosity 9 Pa s, water to binder ratio 0.57) and Case II (Plastic Viscosity 7 and 11 Pa s, water to binder ratio 0.57)**

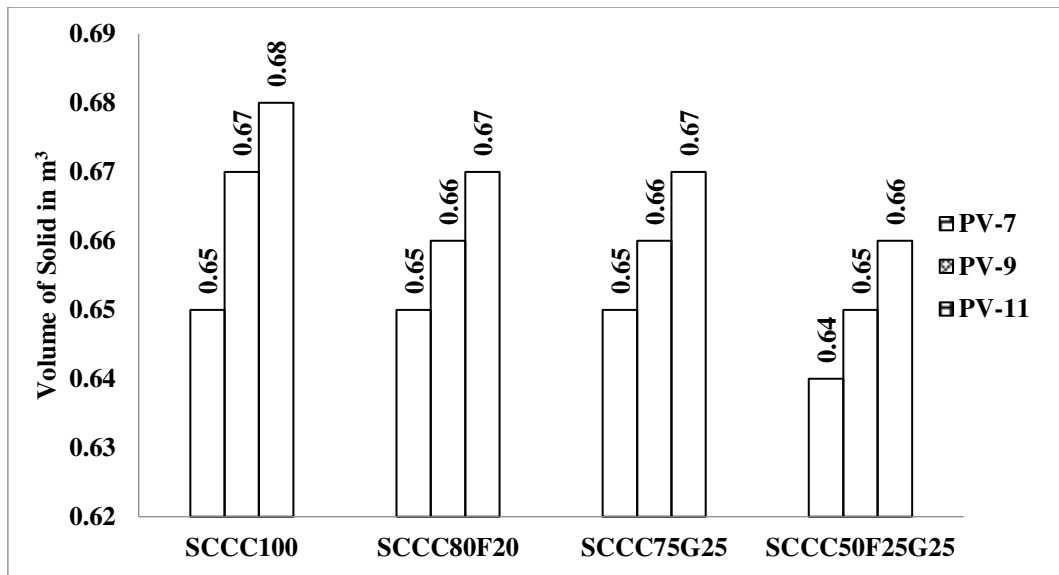


**Figure 5.4 Volume of solids for SCC mixes for Case I and Case II**

### 5.3. Fresh Properties of SCC Mix without Fibres

For SCC mixes with water to binder ratio of 0.5 superplasticizer (SP) dosage is altered for both the plastic viscosities. A dosage of 1% by weight of the binder is adopted for SCC mix with a plastic viscosity of 9 Pa s, and a dosage of 1.25% is adopted for the plastic viscosity of 13 Pa s.

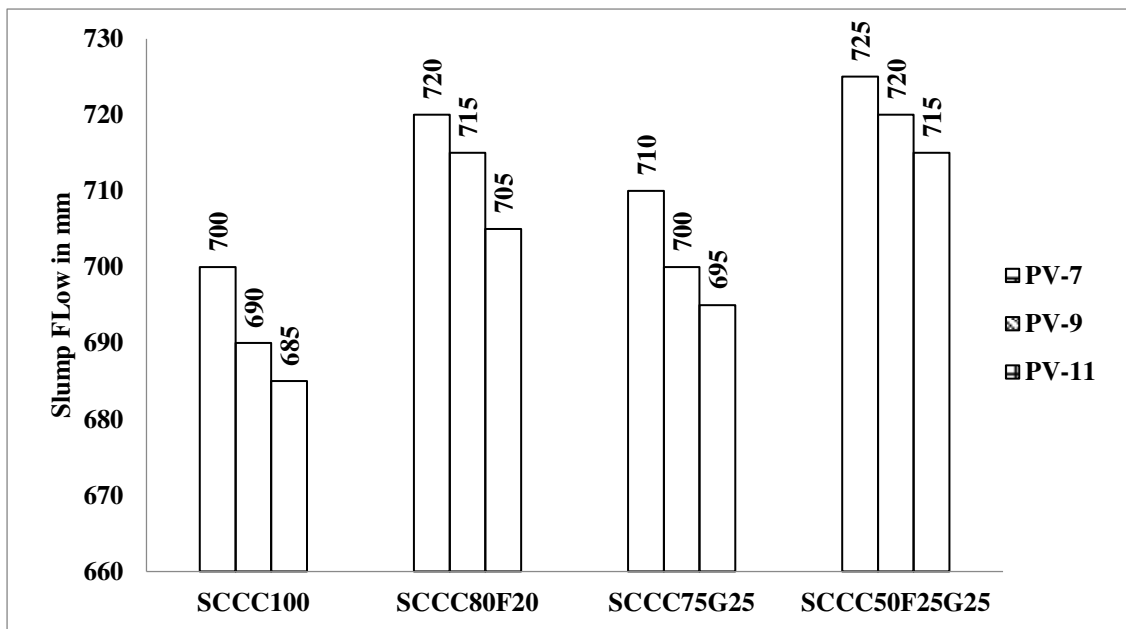


**Figure 5.5 Slump flow for SCC mixes for Case I and Case II**

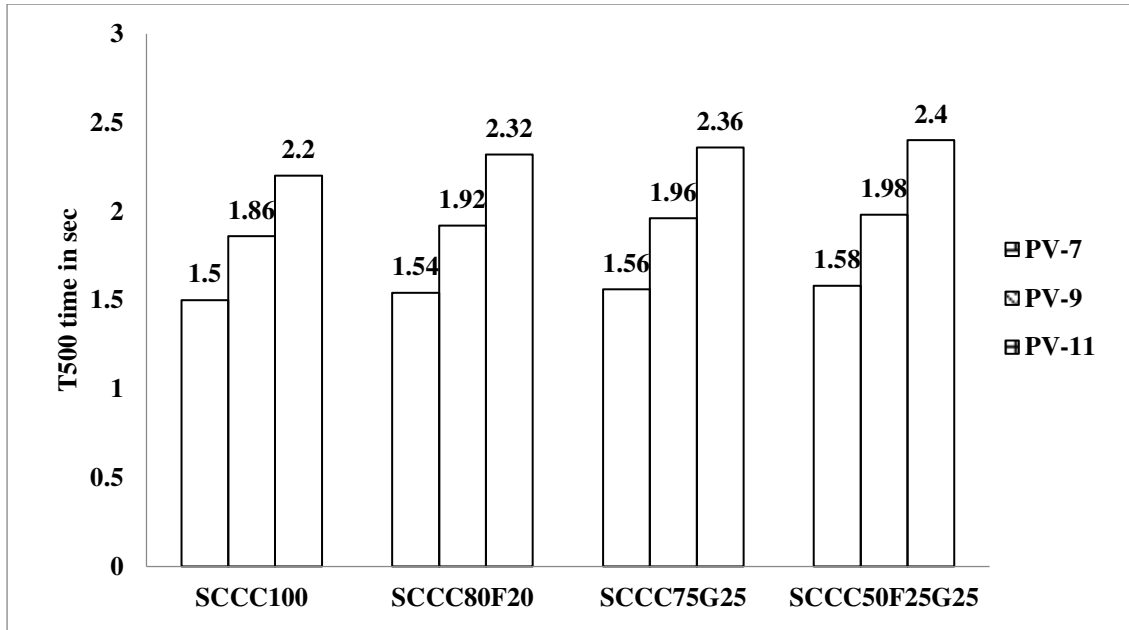


Figure 5.6 T<sub>500</sub> time for SCC mixes for Case I and Case II

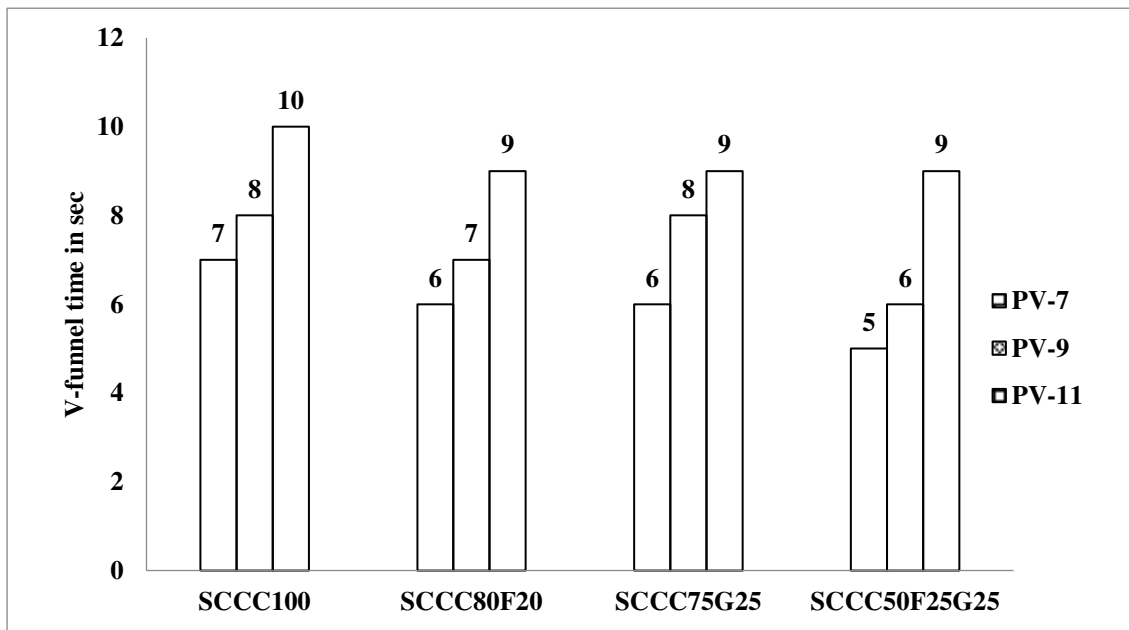


Figure 5.7 V-funnel time for SCC mixes for Case I and Case II

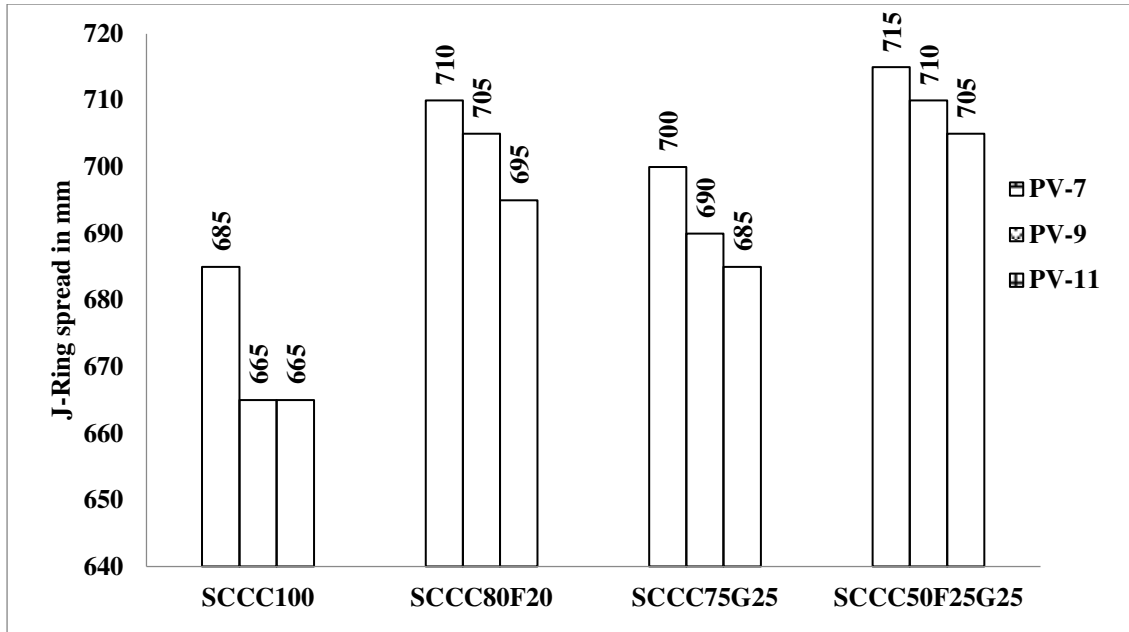


Figure 5.8 J-ring spread for SCC mixes for Case I and Case II

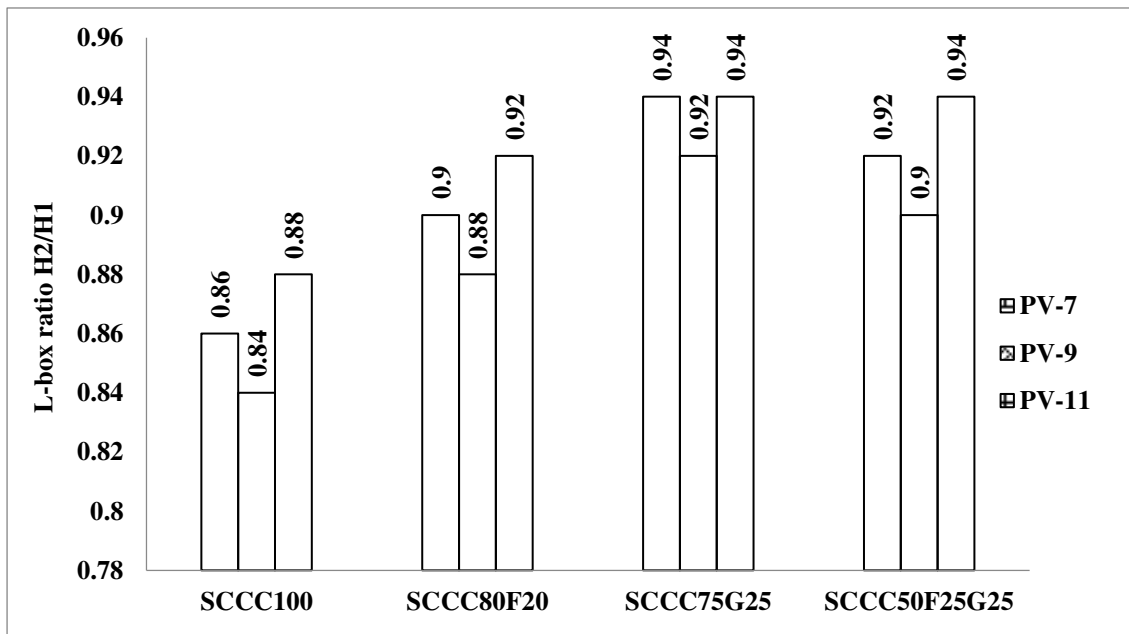
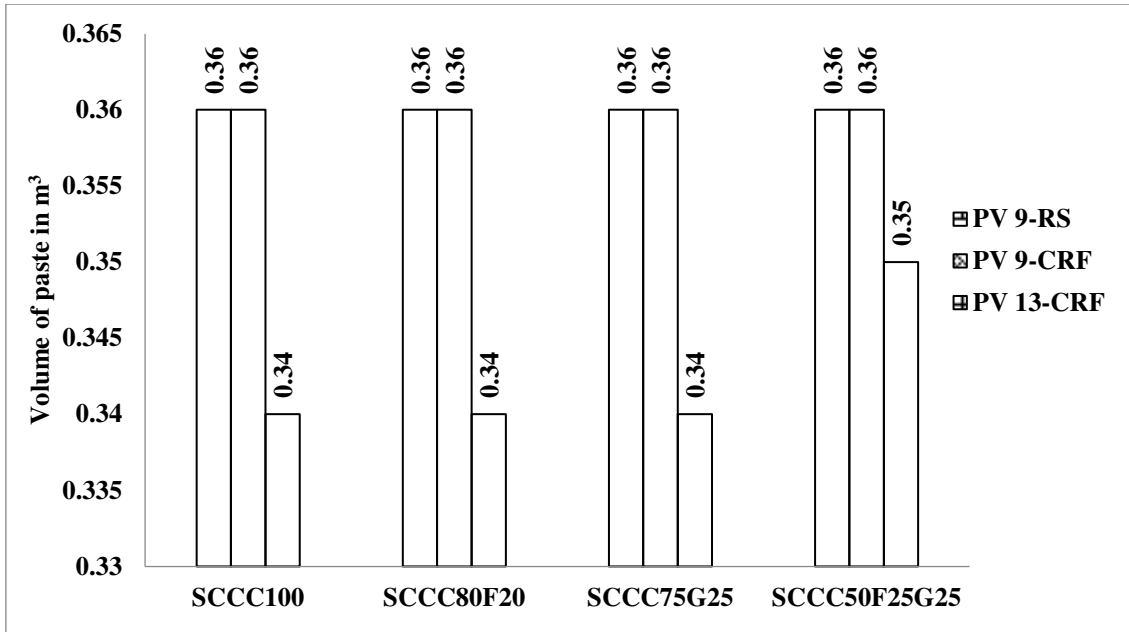
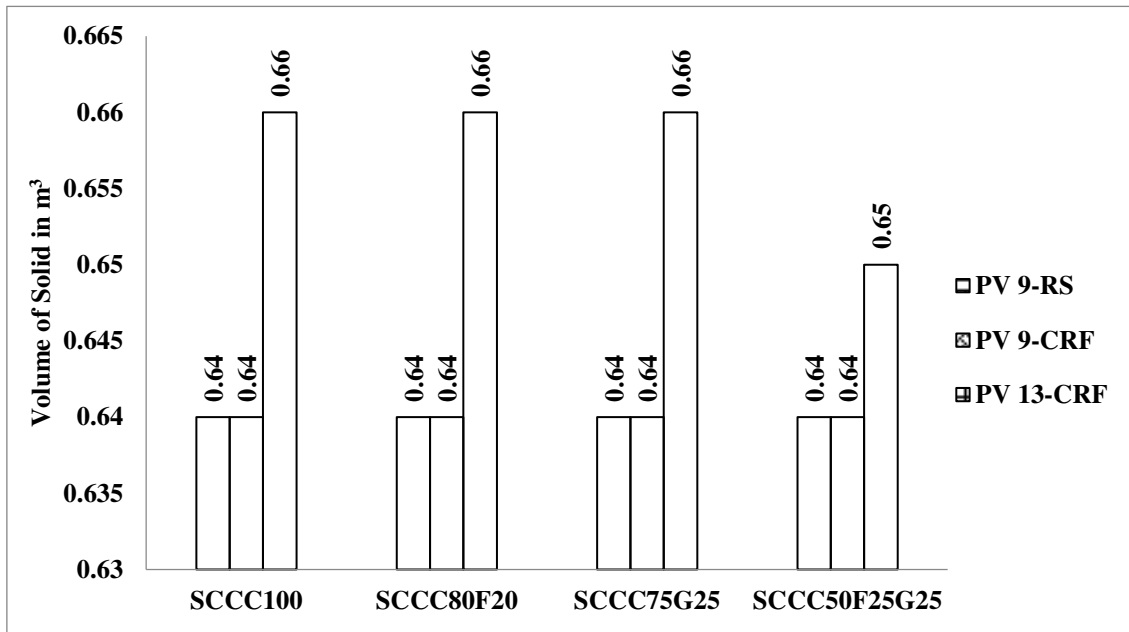


Figure 5.9 L-box ratio for SCC mixes for Case I and Case II



**Figure 5.10** Volume of paste for SCC mixes for Case III (Plastic Viscosity 9 Pa s, water to binder ratio 0.5, river sand as fine aggregate) and Case IV (Plastic Viscosity 9 and 13 Pa s, water to binder ratio 0.5)



**Figure 5.11** Volume of solids for SCC mixes for Case III and Case IV

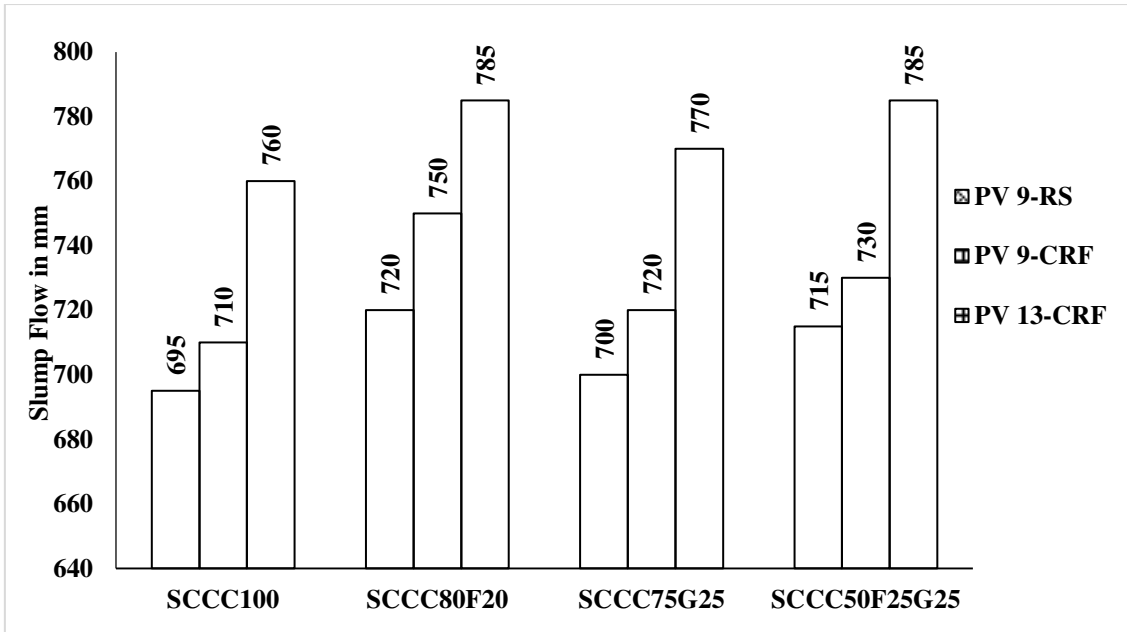


**Figure 5.12 Slump flow for SCC mixes for Case III and Case IV**

From the *Figure 5.3, Figure 5.4, and Figure 5.10, Figure 5.11* with the increase in the plastic viscosity of the mix there is a reduction in the volume of paste due to a decrease in cement content and an increase in the volume of solids due to the increase in aggregate content. When river sand is used the volume of paste and solid almost remained the same as that of CRF.

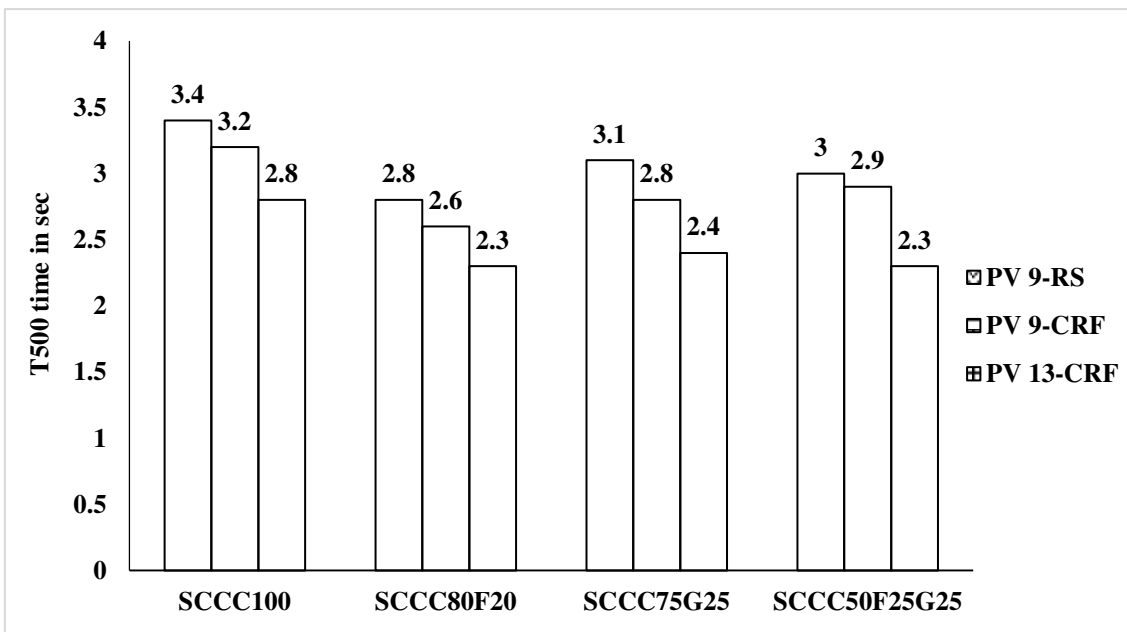


**Figure 5.13 T<sub>500</sub> time for SCC mixes for Case III and Case IV**

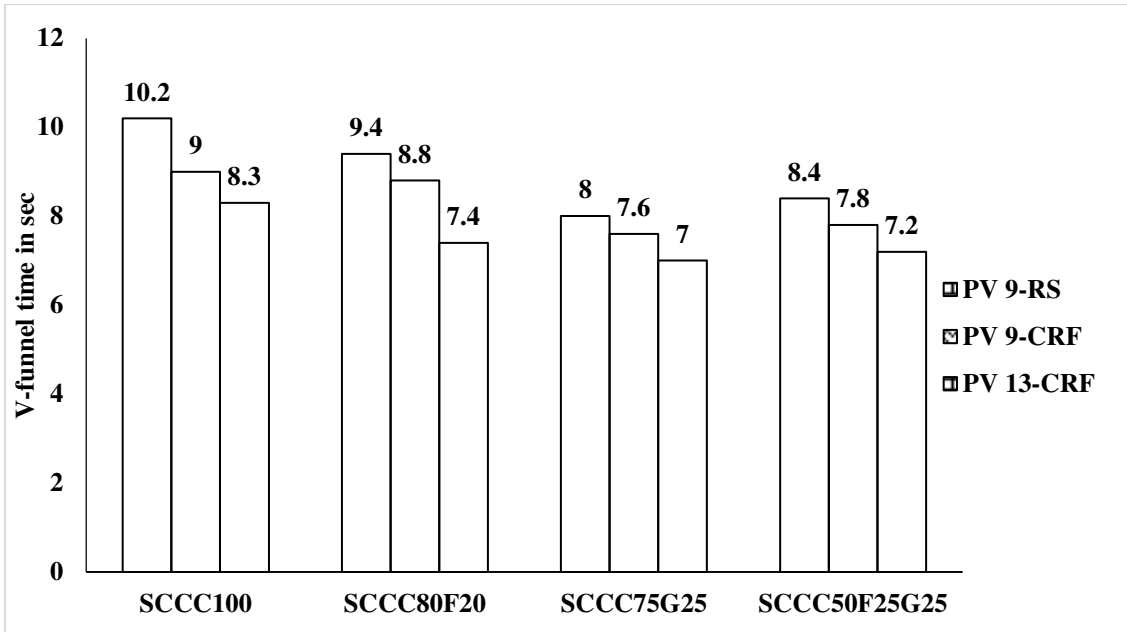


Figure 5.14 V-funnel time for SCC mixes for Case III and Case IV

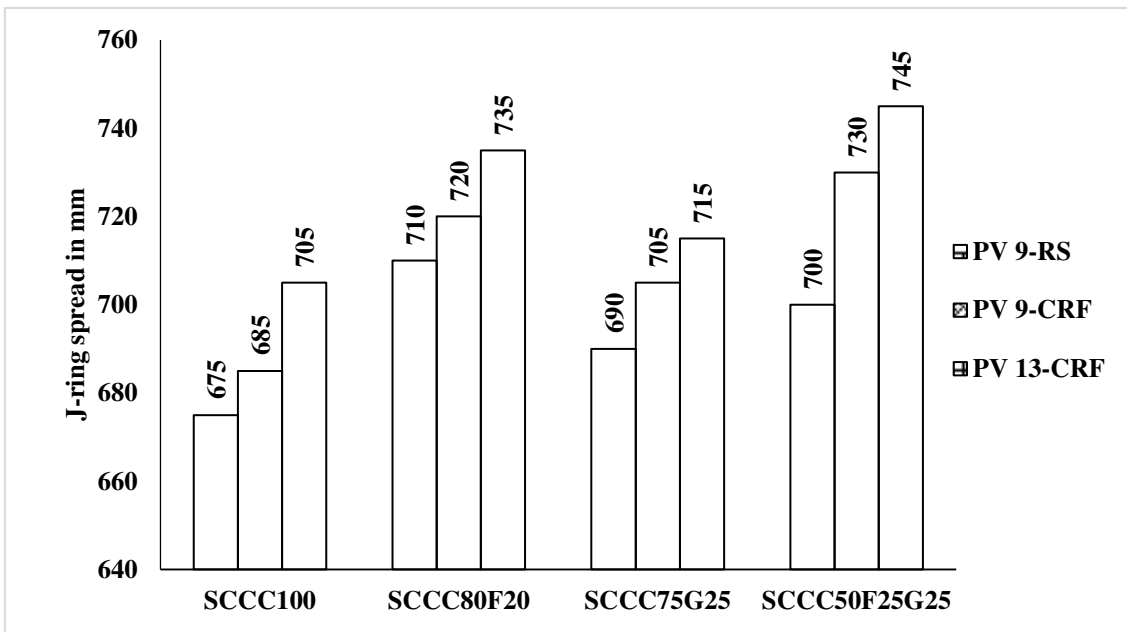
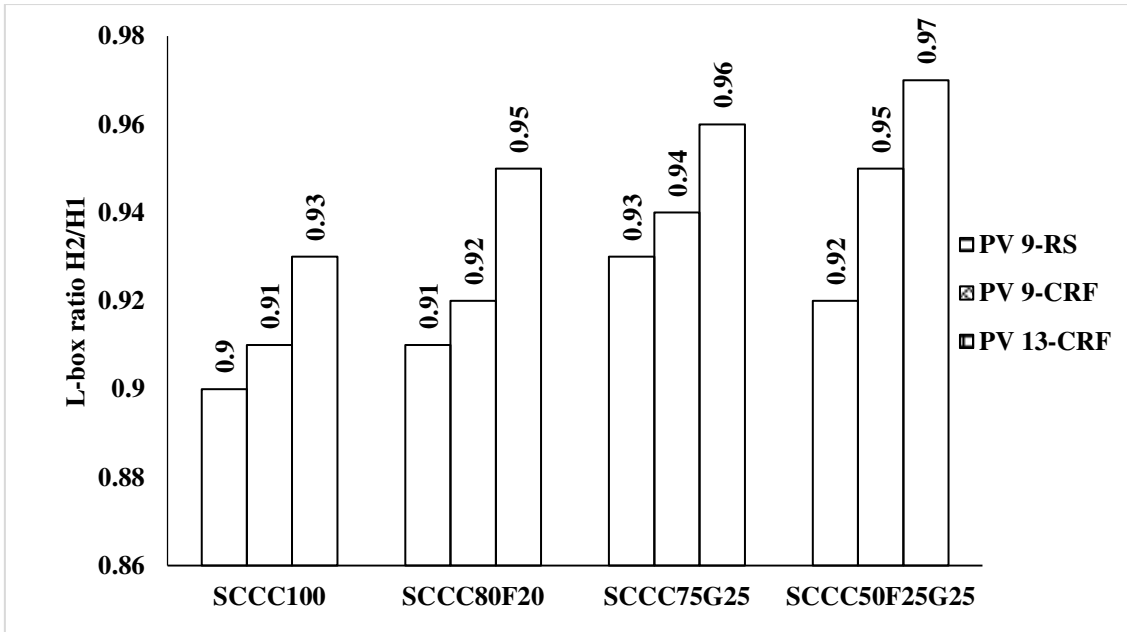


Figure 5.15 J-ring spread for SCC mixes for Case III and Case IV





**Figure 5.16 L-box ratio for SCC mixes for Case III and Case IV**

All the SCC mixes have shown satisfactory flow values ranging from 685mm to 725mm for a water to binder ratio of 0.57 *Figure 5.5* and 695mm to 760mm for a water to binder ratio of 0.5 *Figure 5.12*. Mixes with fly ash resulted in good deformability due to its own weight compared to mixes with GGBS. As the fly ash particles are spherical in shape, a partial replacement of cement with fly ash and GGBS will increase the paste content which in turn increases the cohesiveness and workability of the mix. With the increase in the plastic viscosity of the mix slump flow decreased. Reduction of paste content with increase in solid content for an increasing plastic viscosity will decrease the slump flow. The mixes with CRF resulted in better deformability compared to river sand as the fines in CRF are more compared to river sand. Also the fact that the river sand has more silt content compared to CRF, the flow of SCC mixes will be less for river sand and the flow is reduced by 2.11% for SCC mix with 100% OPC, 2.04% for the binary mix with fly ash, 2.78% for the binary mix GGBS and 4.67% for the ternary mix.





For all the SCC mixes, the slump flow time recorded (i.e.,  $T_{500}$ ) is ranging from 1.5 to 2.4 seconds for a water to binder ratio of 0.57 *Figure 5.6* and 2.3 to 3.4 seconds for a water to binder ratio of 0.5 *Figure 5.13*.  $T_{500}$  is an indicative measure of the viscosity of the mix. It increased with increase in the plastic viscosity of the mix. This property is an indicative tool when there is a requirement for the good surface finishing. As the proposed mix design is based on the plastic viscosity of the mix, the obtained values for  $T_{500}$  are in good agreement

with the viscous behaviour of SCC mixes. It is also observed that mixes with river sand resulted in higher time periods compared to CRF.

As the major portion of the size of aggregate used is less than 20mm, blocking is minimal and the mix has got a good spread passing through the obstacles in the form of reinforcement. To assess the passing ability of SCC mixes, J-Ring in combination with slump cone mold is used to find the distance of lateral flow of concrete. The difference between slump flow and J-Ring flow for all the mixes is less than 25mm which is in good agreement with [ASTM C 1621/C 1621M] indicating a good passing ability of the concrete. The rate of flow reduction with the introduction of J-ring is low for SCC mix with river sand compared to SCC mixes with CRF for a plastic viscosity of 9 *Figure 5.15*. Spread for J-Ring is measured and the values are ranging from 665mm to 710mm for water to binder ratio of 0.57 *Figure 5.8* and 675mm to 745mm for water to binder ratio of 0.5 *Figure 5.15*.

Viscosity and filling ability in terms of duration of flow of mix is investigated using V-funnel test. V-funnel time measured for SCC mixes ranged from 6 to 10 seconds *Figure 5.7* for water to binder ratio of 0.57 and 7 to 10.2 seconds *Figure 5.14* for water to binder ratio of 0.5 which are in good agreement with EFNARC guidelines. V-funnel time for SCC mixes is also an indication that the proposed mix design based on plastic viscosity is reliable and compatible with the existing standard guidelines. Mixes with increasing plastic viscosity because of the decreasing paste content increased the flow time. The usage of 100% CRF as a fine aggregate is also an influencing factor for the better performance of the mix compared to the usage of river sand as a fine aggregate.

To assess the filling and passing ability of SCC, L-Box test is performed. The ratio of heights at the two edges of L-box ( $H_2/H_1$ ) is recorded. If the ratio is less than 0.8, then this test is more sensitive to blocking. All the SCC mixes are within the range of 0.8 to 1.0 *Figure 5.9* and *Figure 5.16* as per EFNARC standards. Because of the presence of CRF in the mix, it enhanced the overall performance of flowing and passing ability of the mix. The fines present in CRF acted as an inert material thus increasing the powder content without reacting with water making the mix more cohesive. The use of CRF in combination with SCMs will result in energy efficient SCC mixes which will be practically feasible and economically viable. It also encourages the utility of locally available materials for the construction. Working images for fresh properties are shown in *Figure 5.17*

|   |   |  |   |
|---|---|--|---|
|  |  |  |  |
| Slump flow  | J-Ring  | V-Funnel   | L-box   |

**Figure 5.17 Fresh properties of SCC mixes without fibres**

From the fresh properties, it is evident that the SCC mixes have got enhanced performance with the suitable additions of ternary mixes in combination with CRF as fine aggregate. Further investigations have been carried out to address the hardened properties.

#### **5.4. Hardened Properties of SCC Mix without Fibres**

A 300 Ton capacity Compressive Testing Machine is used to estimate the characteristic compressive strength of concrete. Compressive strength depends on many parameters such as water to cement ratio, type of cement replacement materials, the percentage of coarse aggregate, the plastic viscosity of the paste and assumed plastic viscosity of mix.

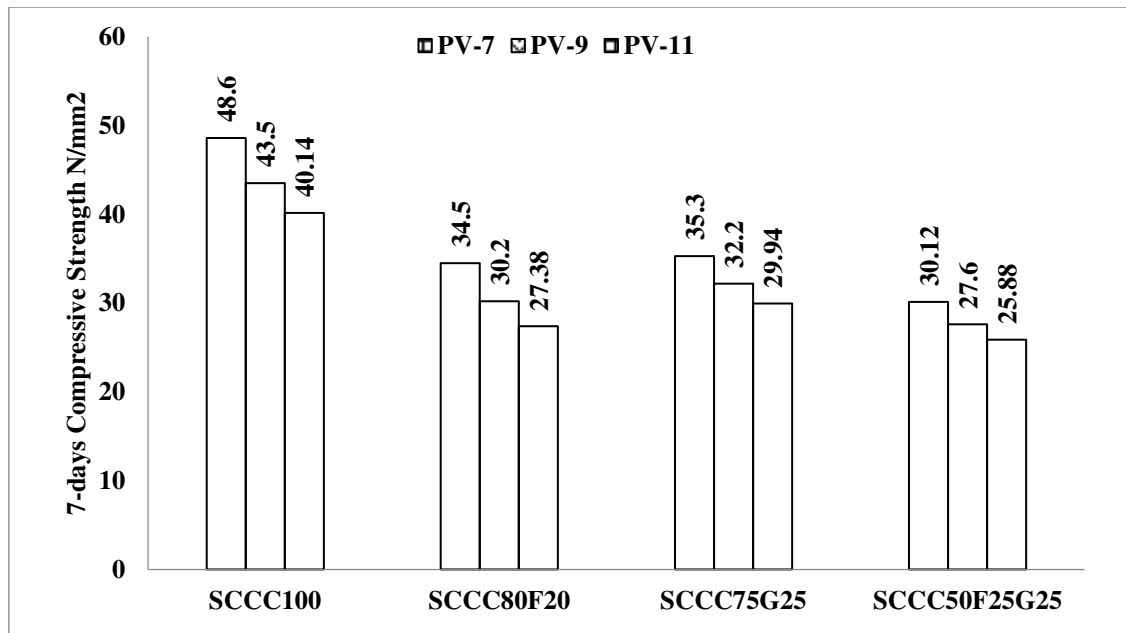


Figure 5.187-days Compressive strength of SCC mixes-Case I and Case II

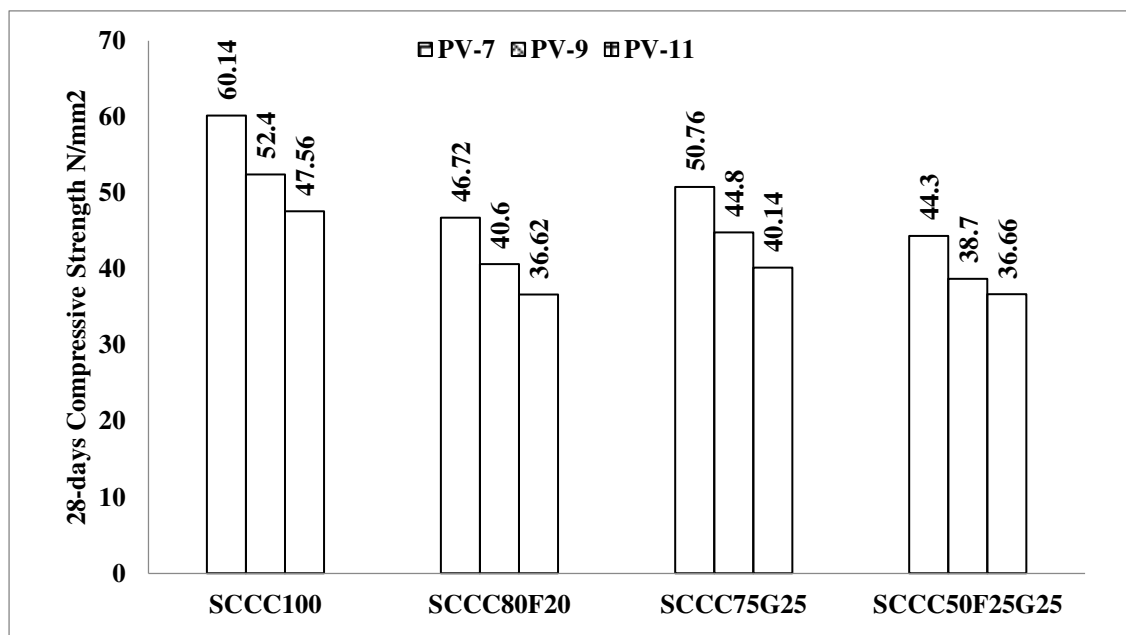
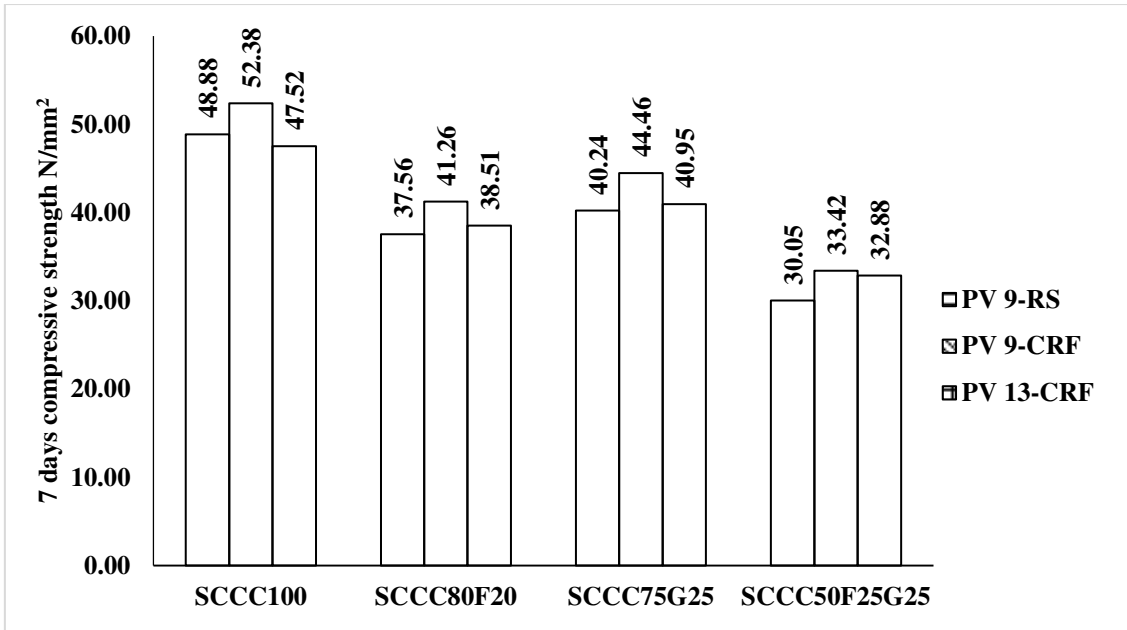
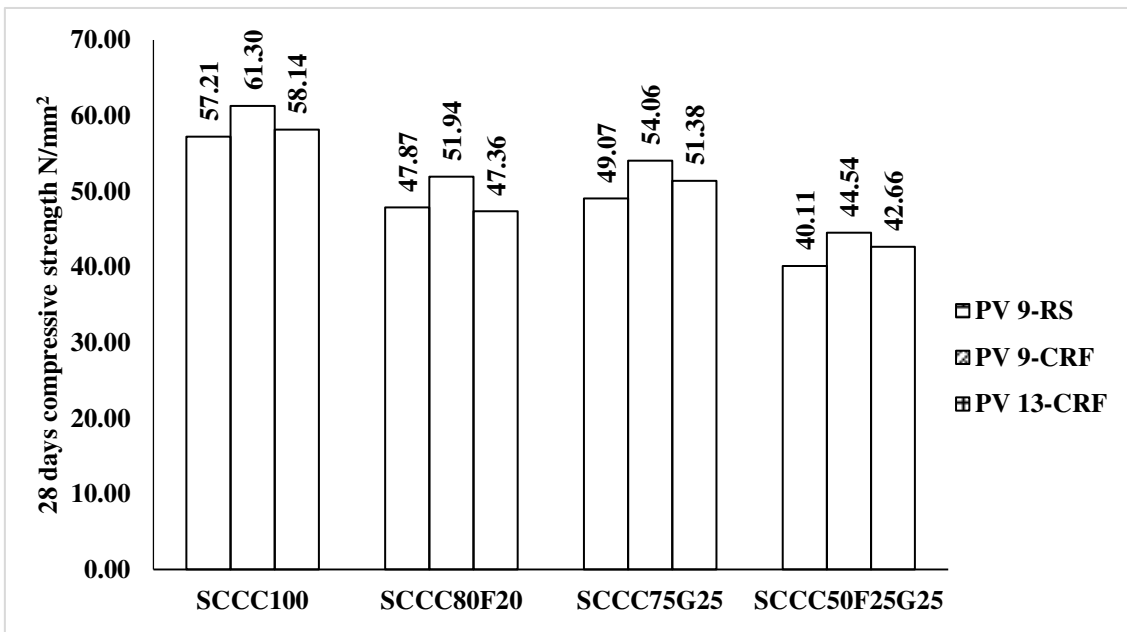


Figure 5.1928-days Compressive strength of SCC mixes-Case I and Case II

From Figure 5.18 and Figure 5.19 the following observations are made for different combinations of SCC mixes with water to binder ratio of 0.57. SCC mix with 100% OPC resulted in the maximum compressive strength of 48.16 MPa, 43.5 and 40.14 MPa for 7-days and 60.14, 52.4 and 47.56 MPa for 28-days for plastic viscosities of 7, 9 and 11 because of the dominant presence of calcium.



**Figure 5.20** 7-days compressive strength of SCC mixes for Case III and Case IV



**Figure 5.21** 28-days compressive strength of SCC mixes for Case III and Case IV

SCC mixes with 25% replacement of GGBS resulted in a compressive strength of 35.3, 32.2, and 29.94 MPa for 7-days and 50.76, 44.8, and 40.14 MPa for 28-days for plastic viscosities of 7, 9 and 11. There is a decrease of 27.36%, 25.97%, and 25.41% in the 7-days compressive strength and 15.6%, 14.5% and 15.6% decrease in 28-days compressive strength of SCC mixes with 25% GGBS replacement.

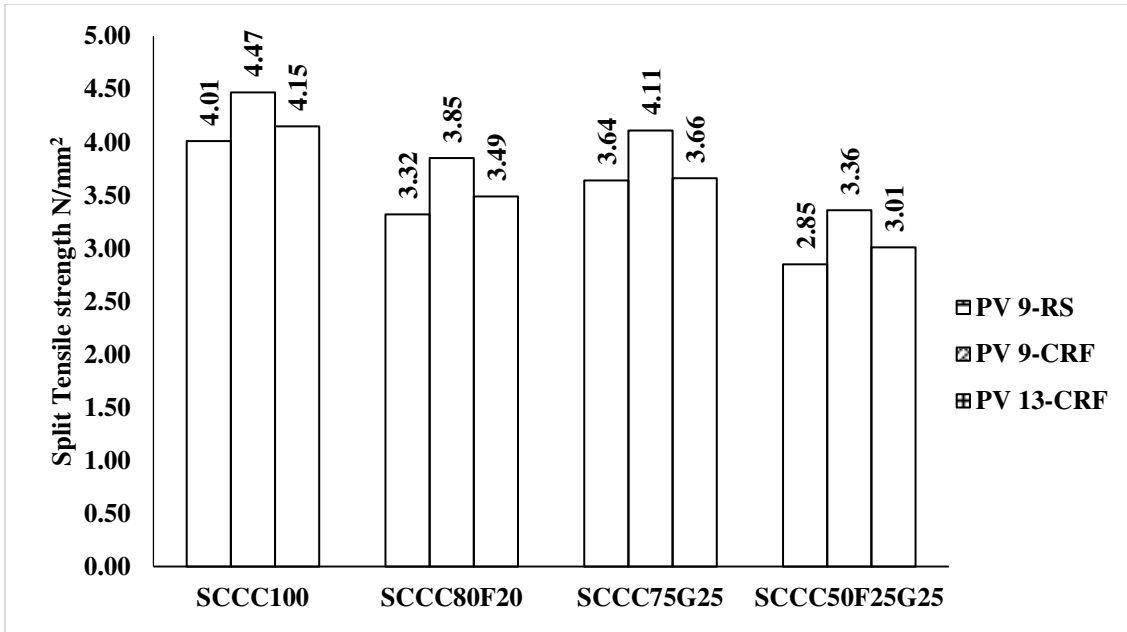


Figure 5.22 Split tensile strength of SCC mixes for Case III and Case IV

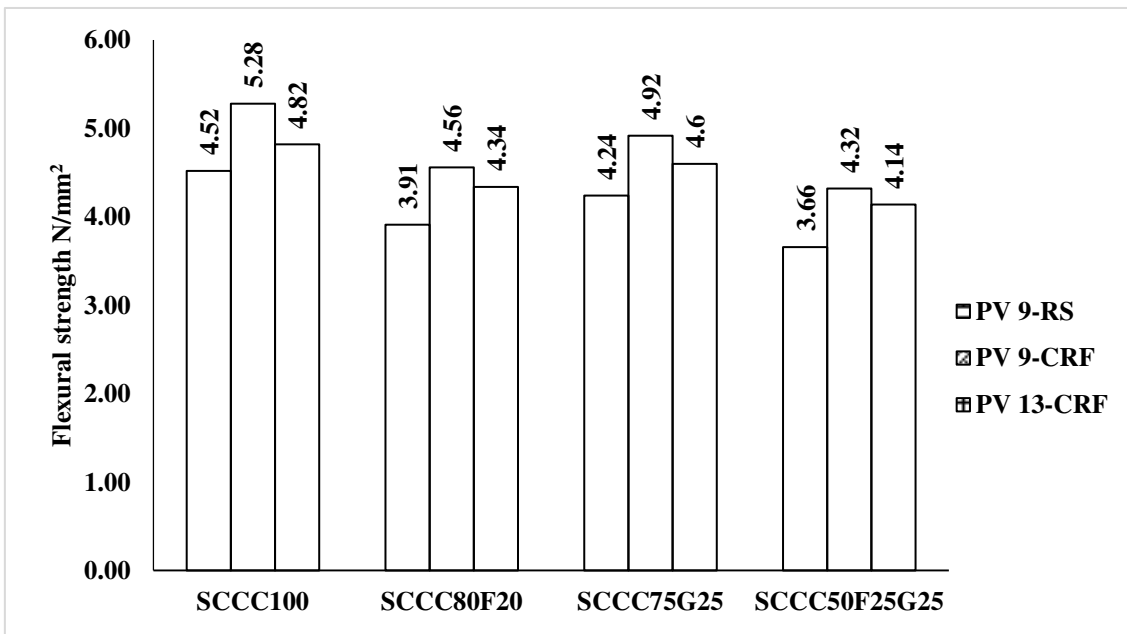
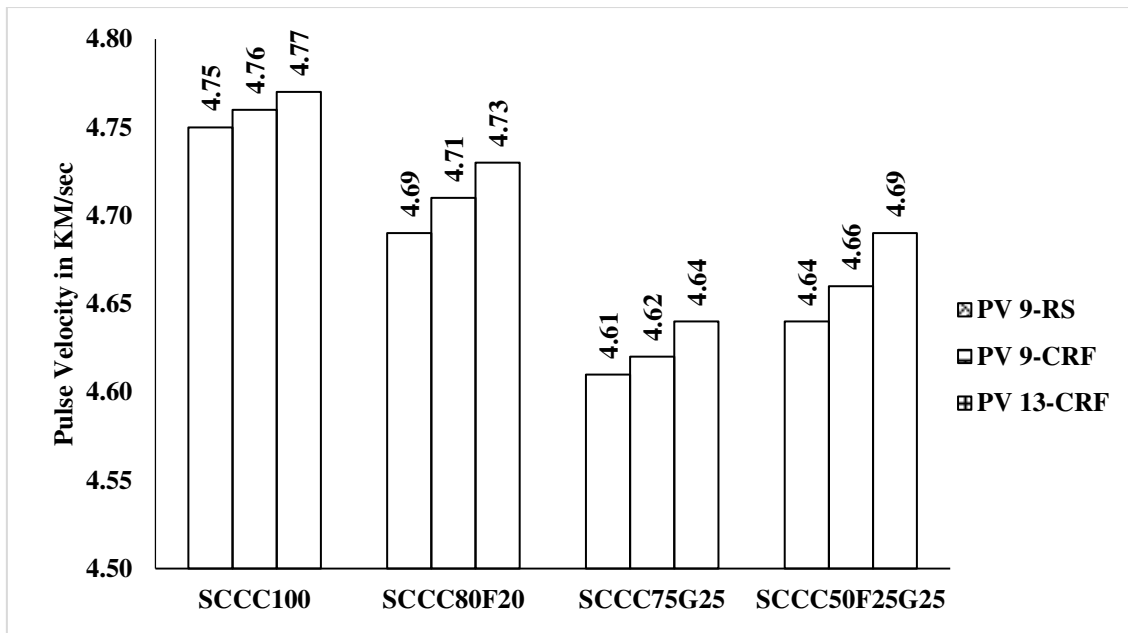


Figure 5.23 Flexural strength of SCC mixes for Case III and Case IV



**Figure 5.24 Pulse velocity of SCC mixes for Case III and Case IV**

SCC mix with 20% Fly ash resulted in the strength of 35.3, 30.2, and 27.38 MPa for 7-days and 46.72, 40.6 and 36.62 MPa for 28-days for plastic viscosities of 7, 9 and 11. There is a decrease of 29.01%, 30.57% and 31.78% in the 7-days compressive strength and 22.31%, 22.51% and 23% decrease in 28-days compressive strength of SCC mixes with 20% fly ash replacement. Due to the presence of pozzolanic reactions in GGBS and fly ash the strength decreases because of its high  $C_2S$  content. SCC mixes with ternary combinations resulted in a strength equal to 30.12, 27.6 and 25.88 MPa for 7-days and 44.3, 38.7 and 36.66 MPa for 28-days for plastic viscosities of 7, 9 and 11. There is a decrease of 38.02%, 36.55% and 35.52% in the 7-days compressive strength and 26.33%, 26.14% and 22.91% decrease in 28-days compressive strength of SCC mixes with 25% replacements of both fly ash and GGBS.

Following observations are made for the SCC mixes with water to binder ratio of 0.5 *Figure 5.20 and Figure 5.21*. SCC mix with 100% OPC resulted in the maximum compressive strength of 48.88, 52.38 and 47.52 for days and 57.21, 61.3 and 58.14 MPa for 28-days for plastic viscosities of 9 with river sand and CRF and 13 with CRF. SCC mixes with 25% replacement of GGBS resulted in a compressive strength of 40.24, 44.46 and 40.95 for 7-days and 49.07, 54.06 and 51.38 for 28-days for plastic viscosities of 9 with river sand and CRF and 13 with CRF. There is a decrease of 17.68%, 15.12%, and 13.83% in the 7-days compressive strength and 14.23%, 11.81% and 11.63% decrease in 28-days compressive strength of SCC mixes with 25% GGBS replacement. SCC mix with 20% Fly ash resulted

in the strength of 37.56, 41.26 and 38.51 MPa for 7-days and 47.87, 51.94 and 47.36 MPa for 28-days for plastic viscosities of 9 with river sand and CRF and 13 with CRF. There is a decrease of 23.16%, 221.23% and 18.96% in the 7-days compressive strength and 16.33%, 15.27% and 18.54% decrease in 28-days compressive strength of SCC mixes with 20% fly ash replacement. SCC mixes with ternary combinations resulted in a strength equal to 30.05, 33.42 and 30.18 MPa for 7-days and 40.11, 44.54 and 42.66 MPa for 28-days for plastic viscosities of 9 with river sand and CRF and 13 with CRF. There is a decrease of 38.52, 36.2% and 36.49% in the 7-days compressive strength and 29.89%, 27.34% and 26.63% decrease in 28-days compressive strength of SCC mixes with 25% replacements of both fly ash and GGBS. It is also observed that the compressive strengths of SCC mix with CRF are more than that of SCC mixes with river sand. For SCC mix with 100% OPC, there is a reduction of 6.68% and 6.67% at 7-days and 28-days' strengths with river sand as fine aggregate. For binary mix with fly ash replacement, there is a reduction of 8.97% and 7.84% at 7-days and 28-days' strengths. For binary mix with GGBS replacement, there is a reduction of 9.49% and 9.23% at 7-days and 28-days compressive strengths. For the ternary mix, there is a reduction of 10.08% and 9.95% at 7-days and 28-days compressive strengths.

An indirect method to test the tensile strength of SCC mixes is carried out using splitting tensile strength. A cylindrical specimen of diameter 150mm and height 300mm with an aspect ratio of 2 is adopted for the test. SCC mix with 100% OPC resulted in a maximum tensile strength followed by binary mix with 25% GGBS for both the plastic viscosities of 9 Pa s and 13 Pa s. There is a reduction in tensile strength of SCC mixes with river sand compared to mixes with CRF for a plastic viscosity of 9 Pa s *Figure 5.22*. There is a reduction of 10.29% for SCC mix 100% OPC, 13.77% reduction for binary mix with fly ash, 11.44% reduction for binary mix with GGBS and 15.18% reduction for the ternary mix.

A 100 Ton Universal testing machine is used to estimate the flexural strength of SCC mixes. A prism of size 500 X 100 X 100 mm is used for the test. Three-point bend test is adopted for the conducting the test. SCC mix with 100% OPC resulted in the maximum flexural strength followed by binary mix with GGBS. Flexural strength decreased for SCC mixes with river sand compared to mixes with CRF for a plastic viscosity of 9 Pa s *Figure 5.23*. There is a reduction of 14.39% for SCC mix 100% OPC, 14.25% reduction for binary mix with fly ash, 13.82% reduction for binary mix with GGBS and 15.28% reduction for the ternary mix.



There is a significant reduction in strength of ternary mixes compared to binary mixes. The reduction is mainly influenced by the 25% of fly ash present in the mix. There is a significant percentage reduction in 28-days' strength of mix with 20% fly ash replacement when compared to mix with 100% OPC. Replacement of cement with fly ash will reduce the heat of hydration which sacrifices the early strength. Sometimes the process of hydration for mixes with fly ash will be prolonged from 90 days to 365 days depending upon the reactive particles in fly ash. It is also observed that the strength loss in fly ash mixes is mainly due to its slow pozzolanic reaction and the dilution effect (Wongkeoet *et al.*, 2014).

With the increase in plastic viscosity of the mixes, the compressive strengths decreased as the cementitious content decreased. An assumed plastic viscosity of 9 Pa s is found to be suitable with 0.57 water to binder ratio and plastic viscosity of 13 Pa s with CRF is found to be suitable with 0.5 water to binder ratio for the adopted M40 grade of concrete based on the requirements of the construction.

In general, mixes with CRF performed better compared to river sand in terms of compressive, split tensile and flexural strengths.

To determine the homogeneity of concrete, the presence of cracks, voids and deficiencies UPV test is performed for all SCC mixes as per IS 13311 (Part I):1992. The test results indicated that for the plastic viscosity of 9 Pa s with river sand and CRF, for 13 Pa s with CRF the values are relatively comparable. All the test values satisfied requirements and termed as good quality as per IS 13311 (Part I) *Figure 5.24*.

### **5.5. Fresh Properties of SCC Mixes with the Addition of Hooked End Steel Fibres**

Influence of addition of hooked end steel fibres on the overall performance of SCC mixes is investigated with a trial fibre volume fraction of 0.35. The length, diameter and aspect ratio of fibre are 30mm, 0.5mm and 60 respectively as discussed in section 4.4.4. This study is carried out to enhance the SCC mixes in terms of their flexural strength. For a chosen plastic viscosity of the mix of 9 Pa s, the addition of fibres increased the plastic viscosity to 33.77 Pa s (Karihaloo *et al.*, 2009; Ghanbari *et al.*, 2013; and Abo Dhaheer *et al.*, 2015).

Workability tests are conducted to assess the fresh properties of SCC mixes with the addition of fibres and the results are compared with the SCC mixes without fibres. *Figure 5.25 to Figure 5.29* depict the comparison of fresh properties of SCC mixes with and without the the addition of fibres.

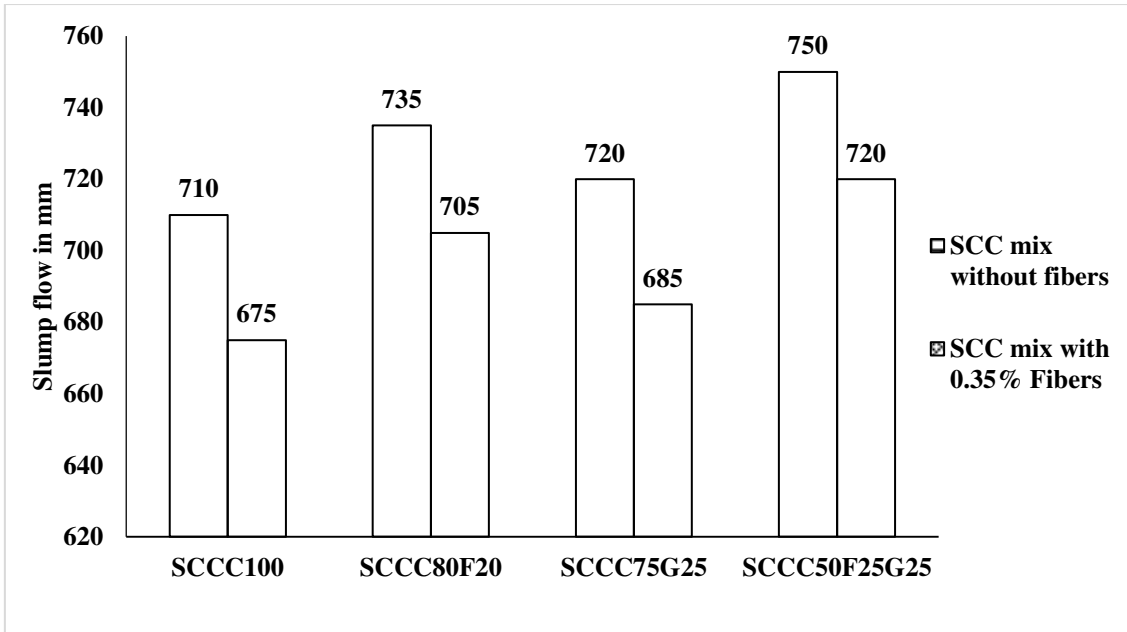


**Figure 5.25 Slump flow for SCC mixes with and without fibres for a plastic viscosity of 9 Pa s**

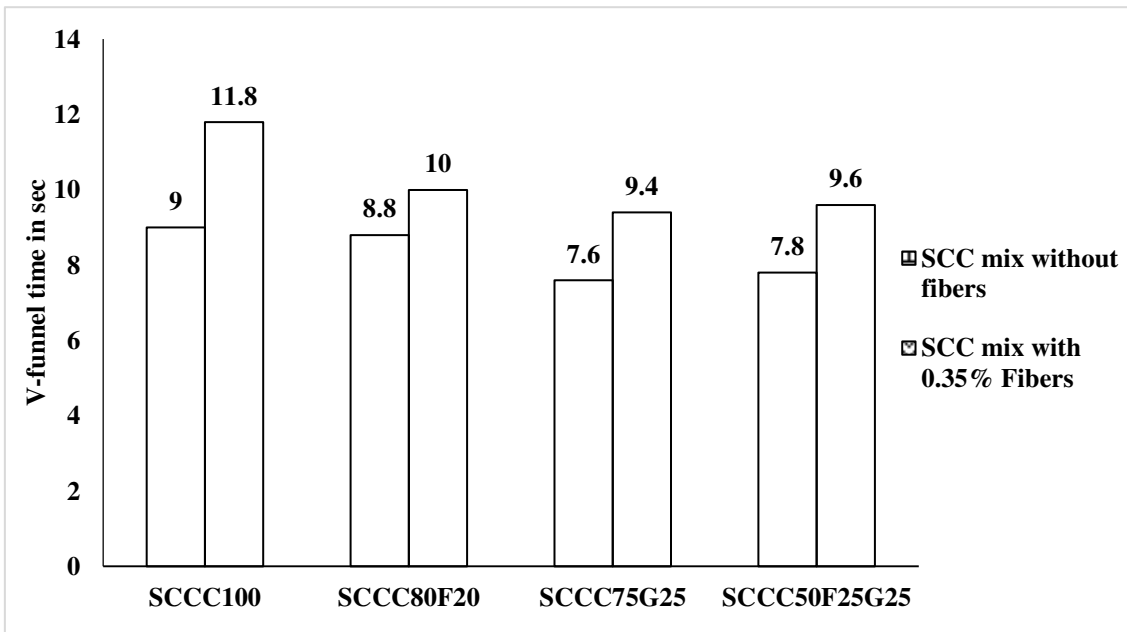


**Figure 5.26 V-funnel time for SCC mixes with and without fibres for a plastic viscosity of 9 Pa s**

Slump flow results indicated that there is a significant reduction in the flow due to the presence of fibres and flow ranged from 675mm to 720 mm *Figure 5.25*. Even though the values of slump flow satisfied the requirements of EFNARC, the presence of fibres led to the poor deformability of the mixes. Due to the presence of fibres, there is a reduction of

4.93%, 4.08%, 4.86% and 4% in slump flow for SCC mixes with 100% OPC, binary mix with fly ash, binary mix with GGBS and ternary mix.

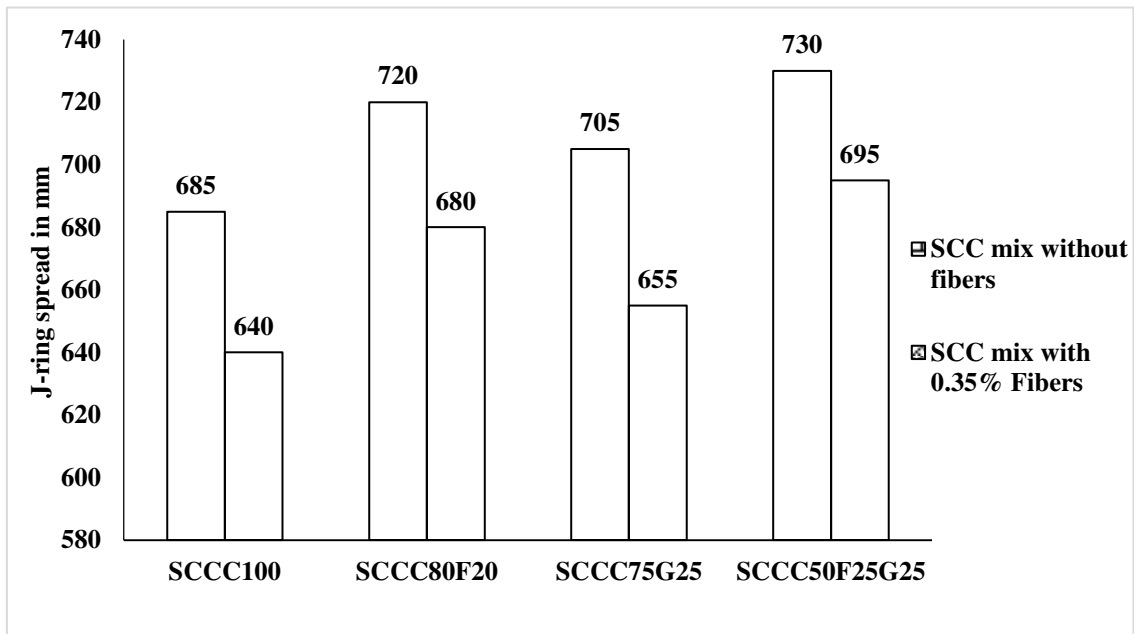


**Figure 5.27 J-ring spread for SCC mixes with and without fibres for a plastic viscosity of 9 Pa s**

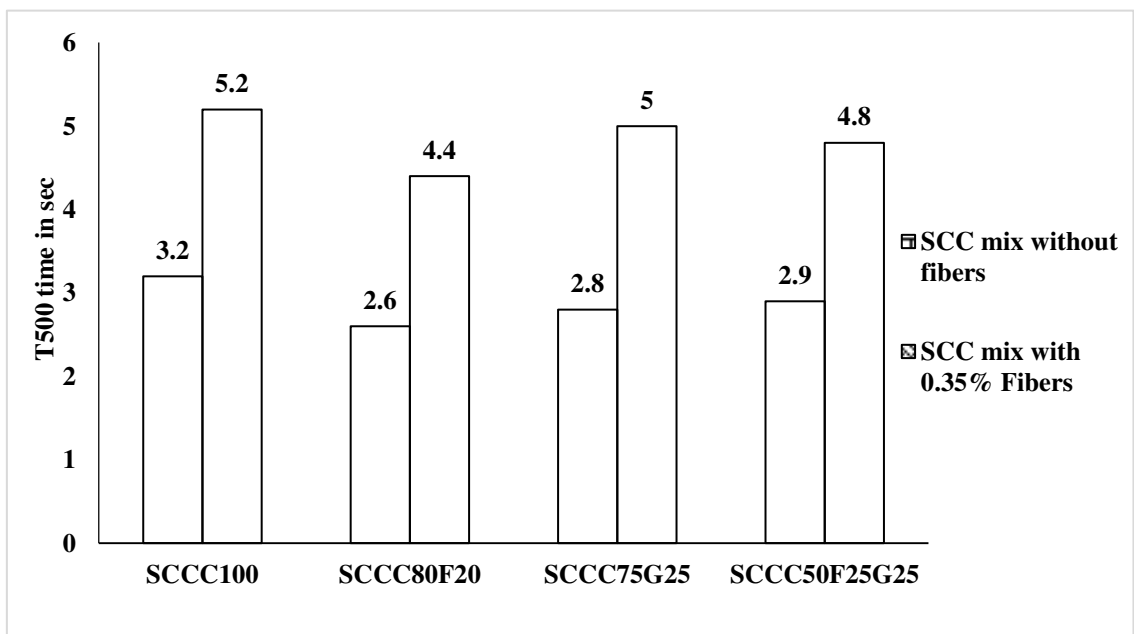


**Figure 5.28 for  $T_{500}$  time SCC mixes with and without fibres for a plastic viscosity of 9 Pa s**

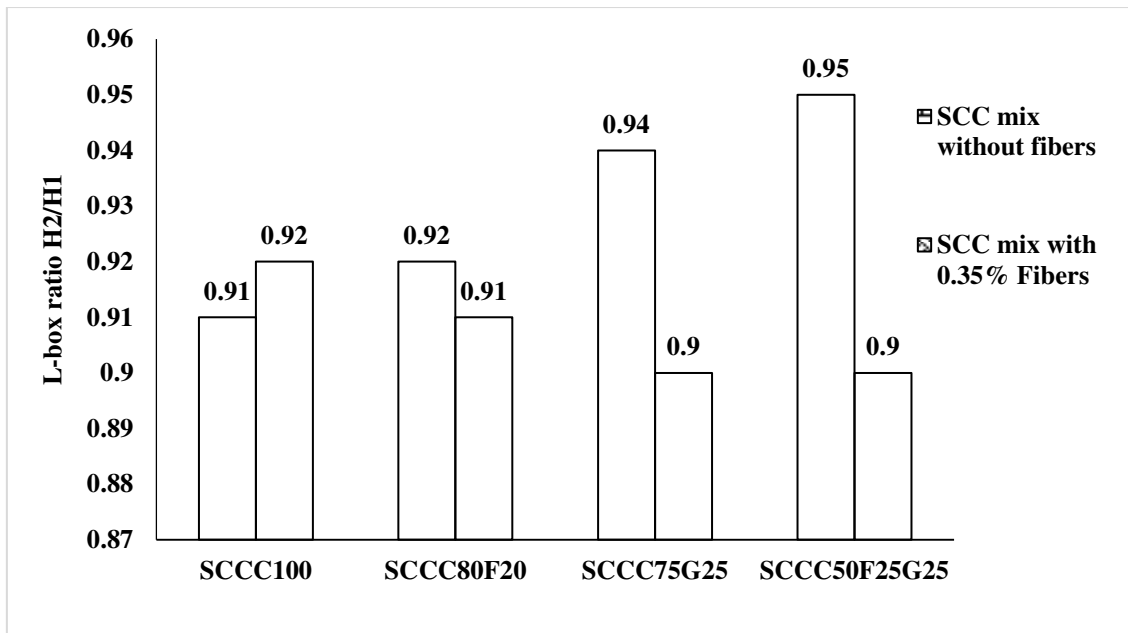


**Figure 5.29 L-box ratio for SCC mixes with and without fibres for a plastic viscosity of 9 Pa s**

V-funnel time measured for SCC mixes with the fibres ranged from 9.4 to 11.8 seconds *Figure 5.26* which are in good agreement with EFNARC guidelines. V-funnel time for SCC mixes is also an indication that the proposed mix design based on plastic viscosity is reliable and compatible with the existing standard guidelines. Due to the addition of fibres mixes, flow time increased indicating that the presence of fibres created a friction between mortar and aggregate.

For all the SCC mixes with fibres, suitable blocking is observed and the spread is not uniform through the obstacles. The difference between slump flow and J-Ring flow for all the mixes is greater than or equal to 25mm which exceeds the limit as per ASTM C 1621/C 1621M indicating a poor passing ability of the concrete. The rate of flow reduction with the introduction of J-ring is low for SCC mix with the addition of fibres *Figure 5.27*. Spread for J-Ring is measured and the values are ranging 640mm to 695mm with the addition of fibres.

SCC mixes with fibres recorded a flow time of 4.4 to 5.2 seconds, indicating that the presence of fibres delayed the flow time *Figure 5.28*. For the SCC mix with 100% OPC and fibres, the flow time exceeded the limit as per EFNARC guidelines. This is associated with the random distribution of fibre particles and their interaction with cement particles

L-box test is used to investigate the blocking of SCC mixes. All the SCC mixes with the presence of fibres are within the range of 0.85 to 1.0 *Figure 5.29* as per EFNARC standards.

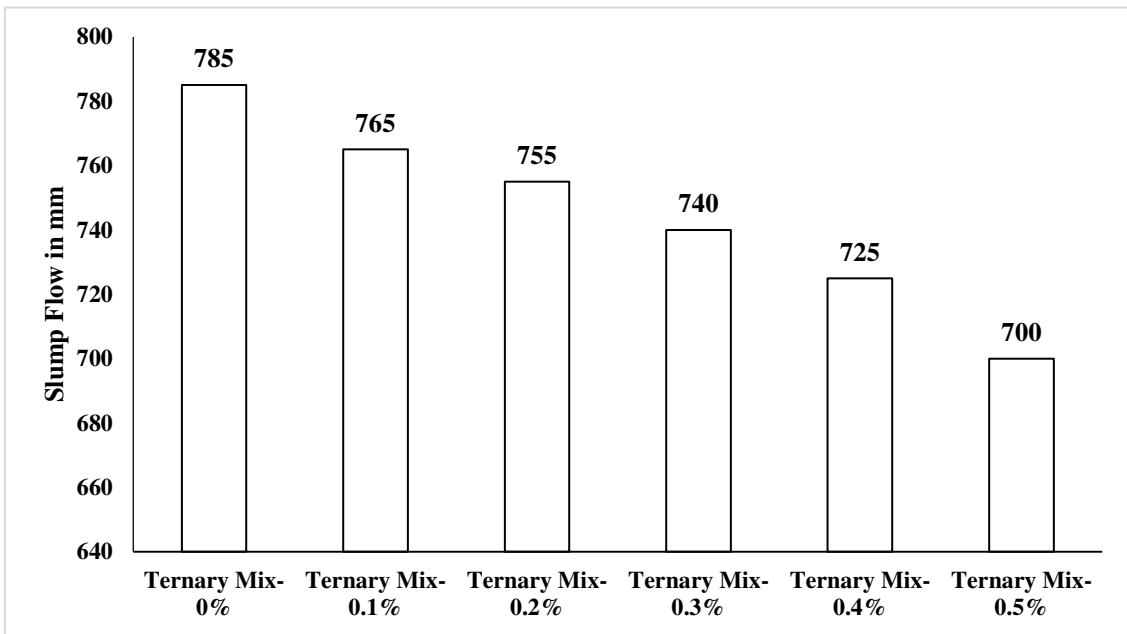


**Figure 5.30 Slump flow for Ternary SCC mix with fibres**

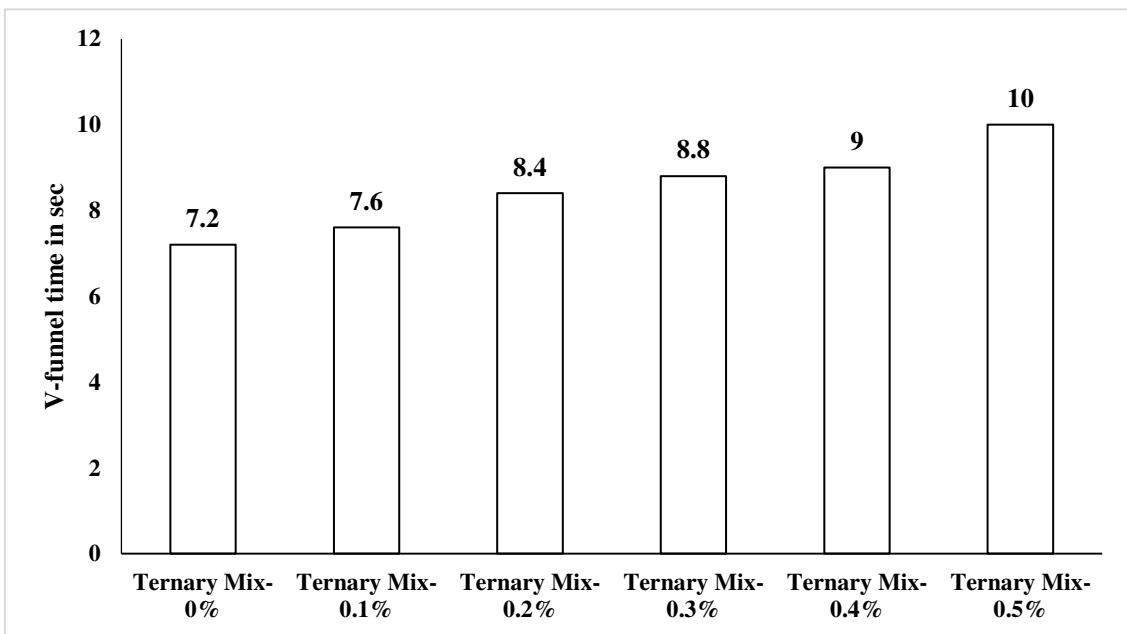


**Figure 5.31 V-funnel time for Ternary SCC mix with fibres**

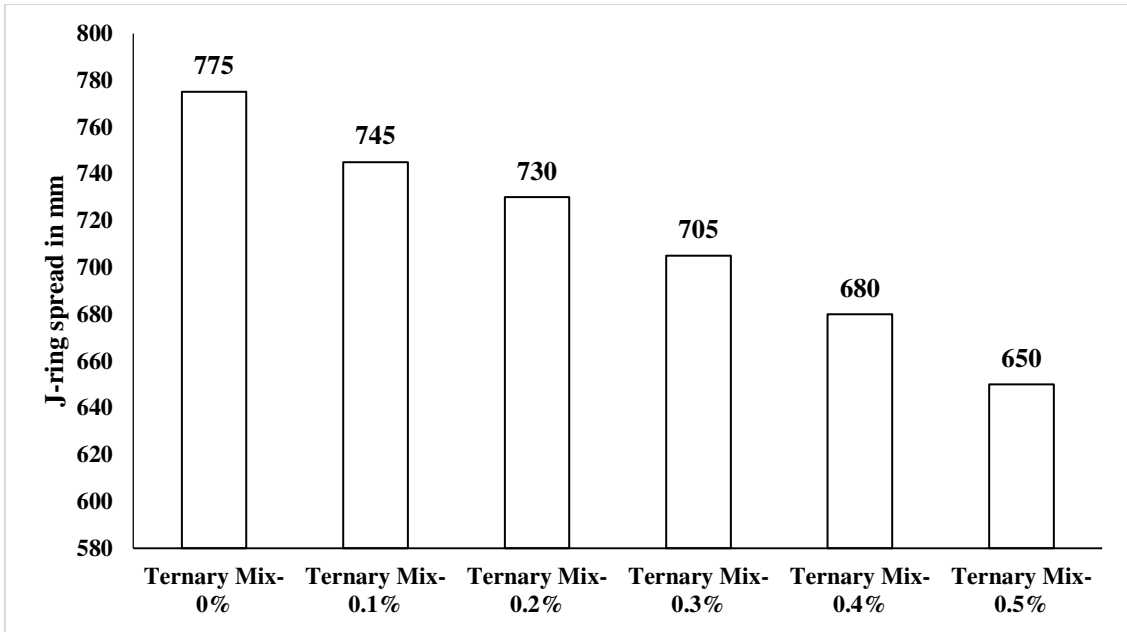


**Figure 5.32 J-ring spread for Ternary SCC mix with fibres**

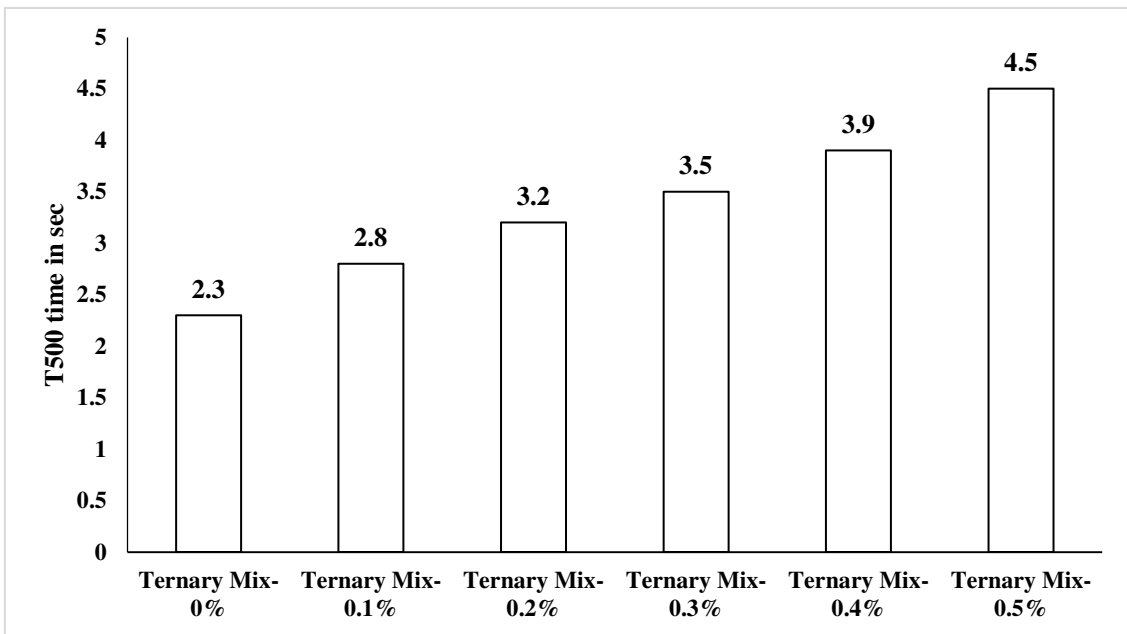


**Figure 5.33 T<sub>500</sub> for Ternary SCC mix with fibres**

From the above experimental investigations with the plastic viscosity of 9 Pa s, with the need for sustainability and reducing the amount of global warming ternary SCC mix is found to be more suitable. For a plastic viscosity of 13 Pa s fibres are added into ternary SCC mixes with varying volume fraction ranging from 0.1% to 0.5%. Performance of Ternary SCC mixes with fibres is investigated based on its fresh and hardened properties. The plastic viscosities of ternary SCC mixes with varying volume fractions are given in *Table 4.10*.

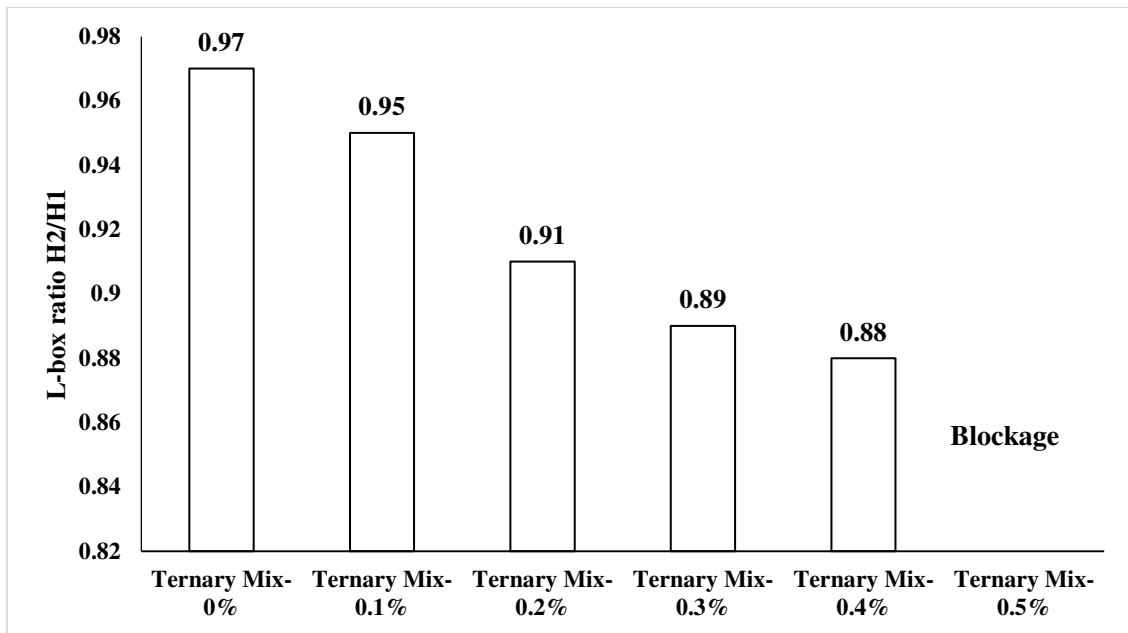


**Figure 5.34 L-box ratio for Ternary SCC mix with fibres**

Figure 5.30 to Figure 5.34 depicts the fresh properties of Ternary SCC mix with the various volume fraction of fibres. In case of slump flow, all the mixes shown flow values in the range of 700mm to 785mm which are within the limits set by EFNARC (650mm to 800mm). Fibres with the hooked end generally cause jamming of concrete particles. This, in turn, depends on the fibre content in the concrete mix. It is observed that slump flow decreased with the increase in fibre content Figure 5.30. No segregation is observed in any of the mixes.




To verify the flexibility of the mixes V-funnel test is used. All the mixes exhibited flow time ranging from 7.2 to 10 sec Figure 5.31. Presence of fibres resulted in blockage of particles during flow. With the increase in fibre content, the friction between fibre and aggregates increases, and friction of fibres with each other also increases. This increase in friction, in turn, increases the emptying time of V-funnel.

The reduction in the spread with the presence of J-ring also is significant for the mixes with increasing fibre content Figure 5.32. This reduction is maximum for ternary mix with 0.5% fibres. It is also observed that for the mixes with fibre volume fractions 0.3, 0.4 and 0.5, the difference between slump flow and J-ring flow is more than 25mm which exceeded the limit as per ASTM C 1621/C 1621M. This directly indicates that the mixes have the poor passing ability when there is congestion during concreting in the practical scenario.

The flow time ( $T_{500}$ ) also increased with increase in fibre content. It is as high as 4.5 seconds for the mix with 0.5% fibres *Figure 5.33*. The random distribution of fibres is one of the main reasons for the increase in flow time.

The blocking ratio of mix increased with increase in fibre content. The L-box ratio for all SCC mixes is between 0.88-0.97 *Figure 5.34*. The blocking is a result of the presence of fibres which would alter the smooth flow of the mix through the reinforcement. Complete blocking is observed for ternary mix 0.5% fibres as there is a complete obstruction while passing through the reinforcement.

The fresh property tests on SCC mix with steel fibres are shown in *Figure 5.35*. The blockage of SCC mixes with 0.5% volume of fibres for J-ring and L-box tests are shown in *Figure 5.36 and Figure 5.37*. Further addition of fibres is not considered as there is a significant blockage seen at 0.5% volume fraction of fibres.

|   |   |  |  |
|---|---|--|--|
|  |  |  |  |
| Slump flow  | J-Ring  | V-Funnel   |  |

**Figure 5.35 Fresh properties of SCC mixes with fibres**



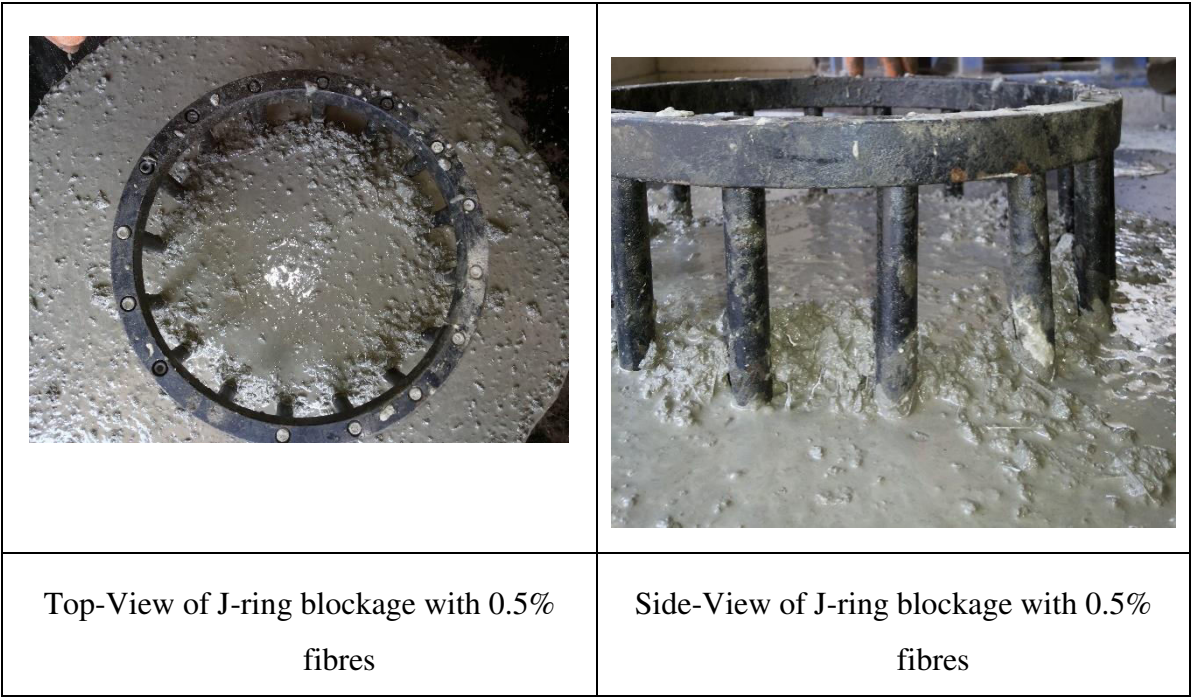


**Figure 5.36 J-ring blockage for ternary mix with 0.5% fibres**



**Figure 5.37 L-box blockage for ternary mix with 0.5% fibres**

## 5.6. Hardened Properties of SCC Mixes with the Addition of Hooked End Steel Fibres

SCC mixes with a plastic viscosity of 9 Pa s with and without fibres are tested for its compressive, split tensile and flexural strength. The increase in 7-days and 28-days compressive strength of SCC mixes with fibres for 100% OPC mix, binary mix with fly ash, binary mix with GGBS, and ternary mix is 3.61%, 3.69%, 3.93 and 4.05% and 2.36%, 2.11%, 3.33%, 3.01% compared to that of SCC mixes without fibres *Figure 5.38 and Figure 5.39*.

The increase in 28-days split tensile strength of SCC mixes with fibres for 100% OPC mix, binary mix with fly ash, binary mix with GGBS, and the ternary mix is 1.76%, 1.79%, 3.75% and 4.27% *Figure 5.40*. But there is a significant increase in flexural strength with the addition of fibres. An increase of 20.48% for mix with 100% OPC, 22.45% for binary mix fly ash, 22.64% for binary mix with GGBS, and 27.27% for the ternary mix is observed with the addition of fibres *Figure 5.41*. As the plain SCC mix is quasi-brittle in nature, there is a high risk of cracking under third point loading. With the addition of fibres, the load carrying capacity of SCC mixes will increase, increasing the flexural strength.

Pulse velocity values for all the SCC mixes with and without fibres have shown excellent performance as per ASTM C597 *Figure 5.42*. A concrete can be considered to be excellent if the pulse velocity is more than 4.5 km/s.

For ternary SCC mixes with varying fibre volume fraction, the compressive strength increased marginally with the increase in fibre content. The increase in compressive strength with 0.1%, 0.2%, 0.3%, 0.4% and 0.5% fibres content is 3.18%, 5.14%, 6.59%, 8.87%, and 10.99% compared to ternary mix without fibres *Figure 5.43 and Figure 5.44*. The maximum increment is observed for ternary mix with 0.5% fibre content. An increment of 10.99% for 7-days compressive strength and 8.45% for 28-days compressive strength is recorded. The enhancement in the strength is observed because of the uniform dispersion of fibres through SCC. Crack formations will be closed with the presence of fibres which is one more reason for the increase in strength. Care should be taken in increasing the fibre content too. Higher fibre content will lead to increased porosity which will reduce the compressive strength.

Split tensile strength increased with increase in the fibre content. The maximum split tensile strength of 3.8KN/mm<sup>2</sup> is observed for ternary mix with 0.5% fibre content. The increase in split tensile strength with 0.1%, 0.2%, 0.3%, 0.4% and 0.5% fibres content is 2.34%, 5.38%,

7.73%, 9.24% and 12.11% compared to ternary mix without fibres *Figure 5.45*. The presence of steel fibres will control the crack propagation especially in restraining the development of micro-cracks. This process will increase the split tensile strength of SCC.

There is an enhancement in the flexural strength with the increase in the percentage of steel fibre content. The increase in flexural strength with 0.1%, 0.2%, 0.3%, 0.4% and 0.5% fibres content is 5.05%, 10.20%, 15.34%, 20.08% and 28.25% compared to ternary mix without fibres *Figure 5.46*. The reason for this significant increase in flexural strength is the aspect ratio ( $l/d$ ) and the volume of fibres. With the use of hooked end steel fibres, there will be an improved performance of specimen due to the fibre-matrix bond. The random distribution of fibres also controls the crack formations and will act as a barrier to further crack growth. This enhances the load carrying capacity of the prism specimen.

Ultrasonic pulse velocity test indicated that there is a decrease in pulse velocity with the increase in the percentage of fibres *Figure 5.47*. Fibres in the mix create more accessibility of voids resulting in the decrease of pulse velocity. Maximum pulse velocity of 4.7 km/sec is observed in the mix with 0.1% fibres and a minimum value of 4.41 km/sec is observed for mix with 0.5% fibres. The presence of fibres also reduced the time required for ultrasonic waves to pass through the concrete specimen. As the fibres are oriented randomly the waves passing through the fibres may deflect back to other directions instead of forming a straight line path. Tests on hardened concrete of SCC mixes are shown in *Figure 5.48*.

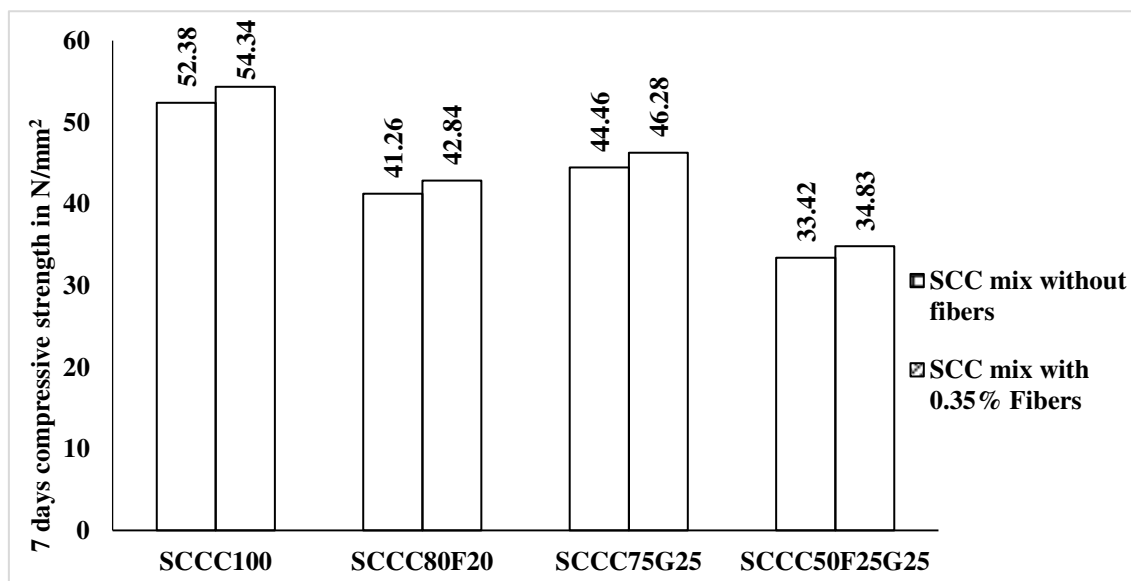


**Figure 5.38 7-days compressive strength of SCC mixes with and without fibres for a plastic viscosity of 9 Pa s**

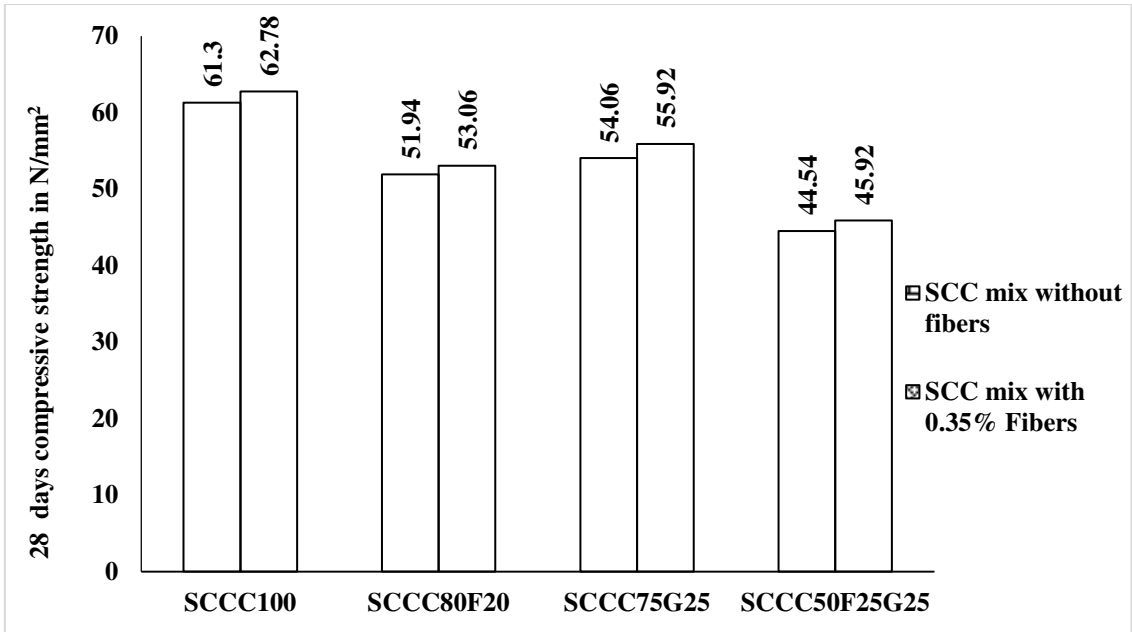


Figure 5.39 28-days compressive strength of SCC mixes with and without fibres for a plastic viscosity of 9 Pa s

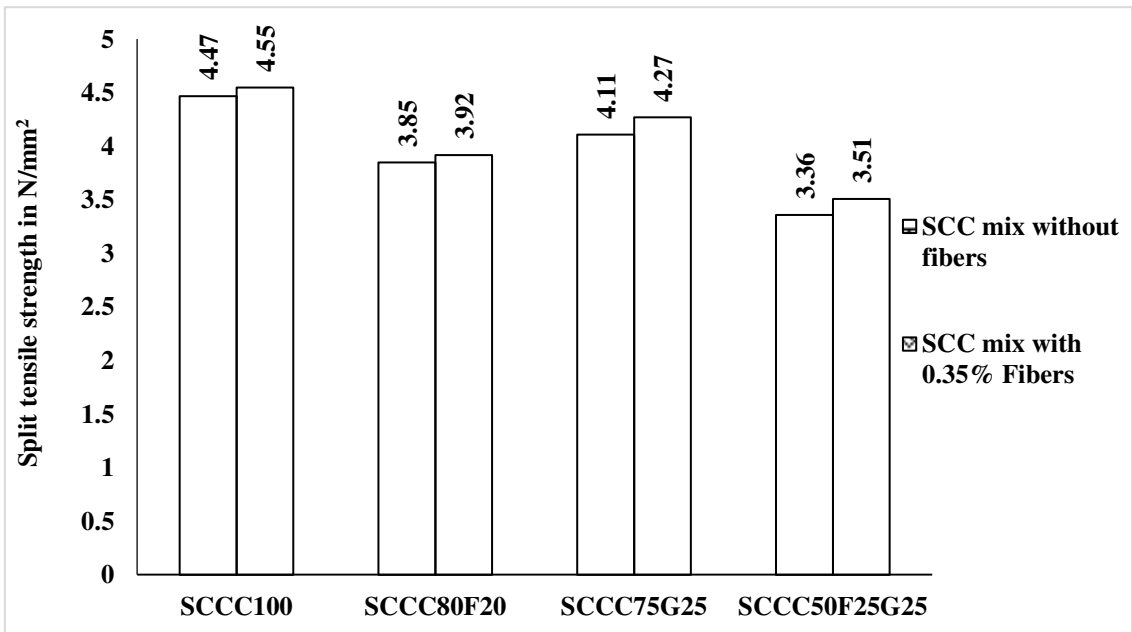


Figure 5.40 Split tensile strength of SCC mixes with and without fibres for a plastic viscosity of 9 Pa s

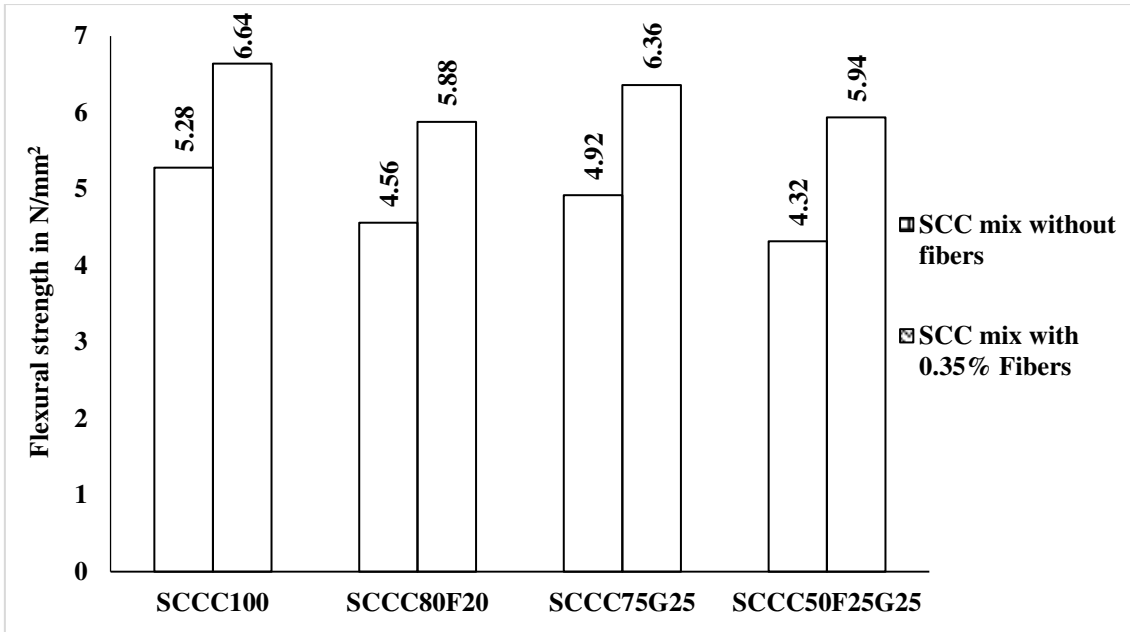


Figure 5.41 Flexural strength of SCC mixes with and without fibres for a plastic viscosity of 9 Pa s

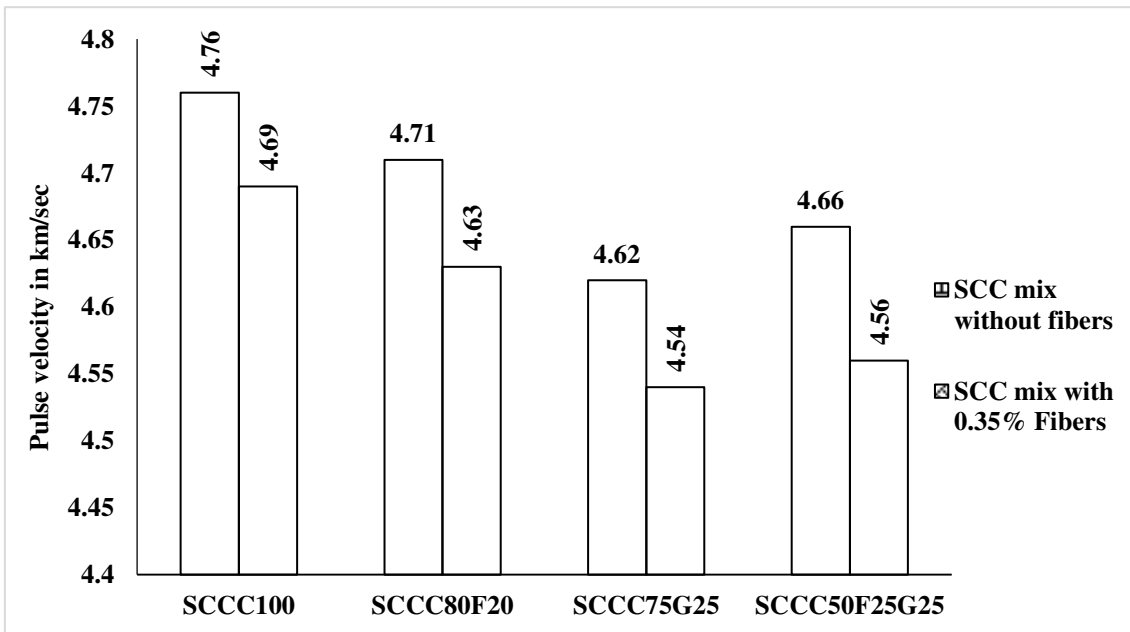
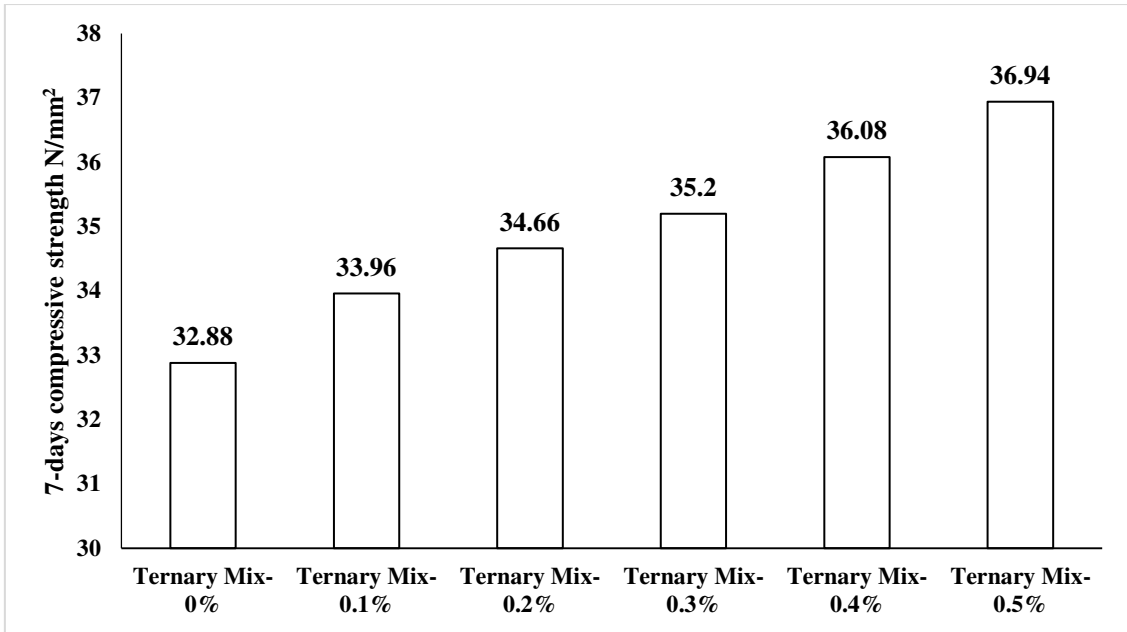
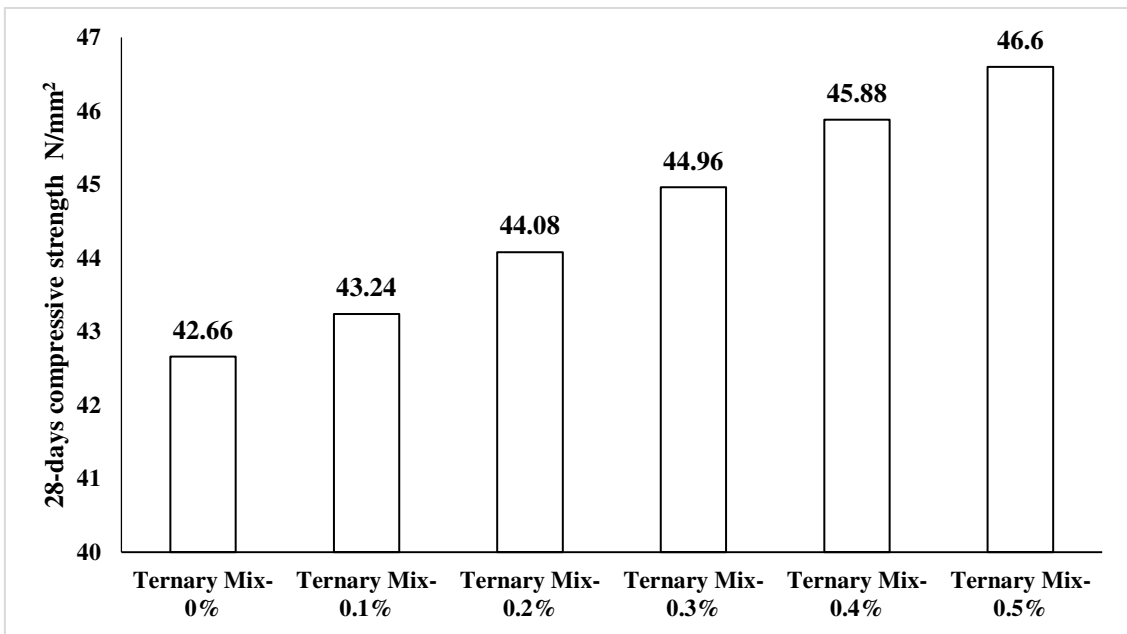


Figure 5.42 Pulse velocity of SCC mixes with and without fibres for a plastic viscosity of 9 Pa s



**Figure 5.43** 7-days compressive strength of Ternary SCC mix with fibres



**Figure 5.44** 28-days compressive strength of Ternary SCC mix with fibres

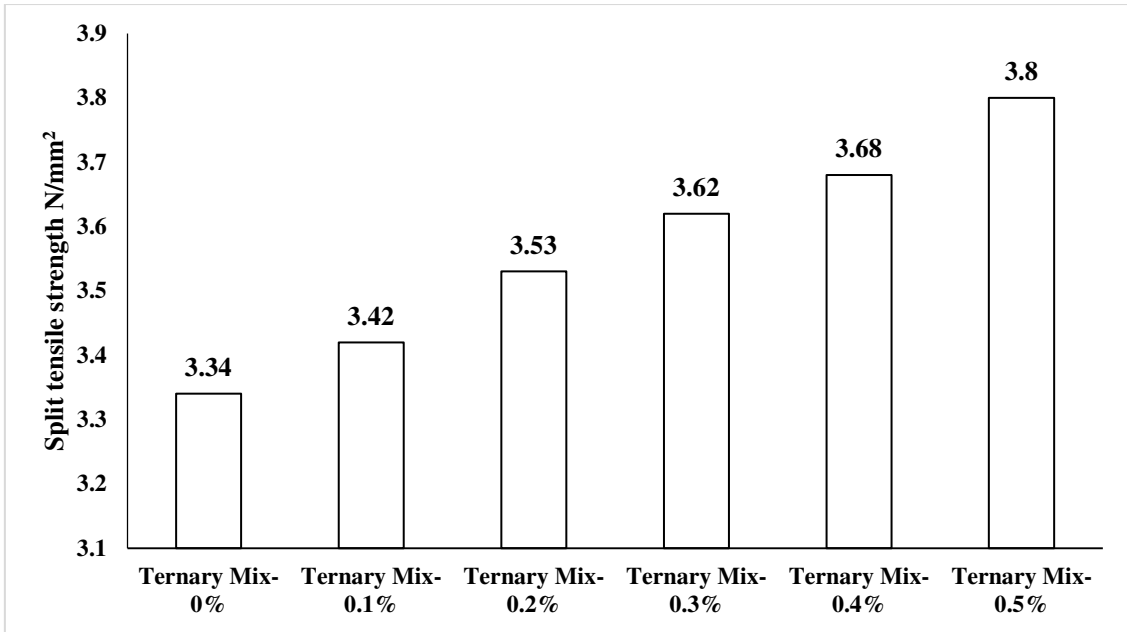


**Figure 5.45 Split tensile strength of Ternary SCC mix with fibres**

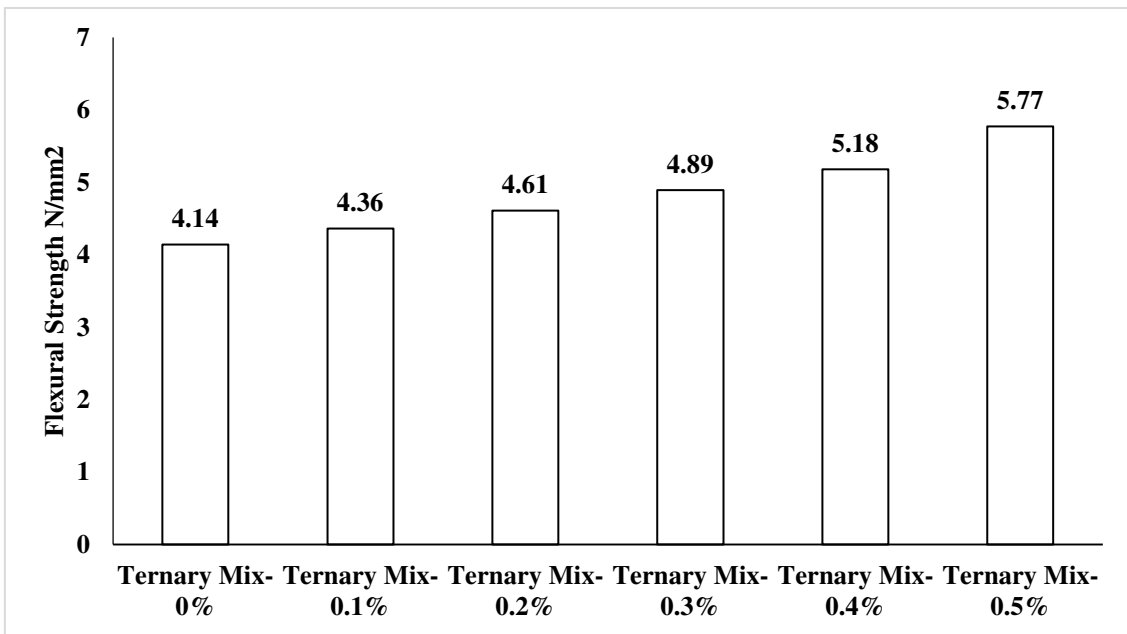


**Figure 5.46 Flexural Strength of Ternary SCC mix with fibres**

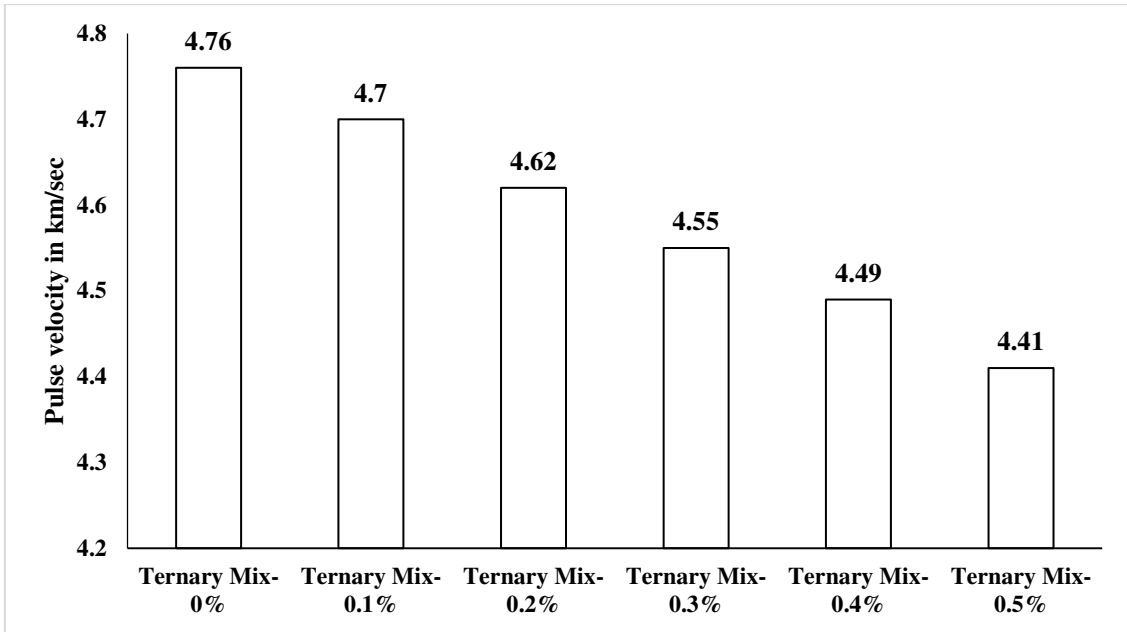


**Figure 5.47 Pulse velocity of Ternary SCC mix with fibres**

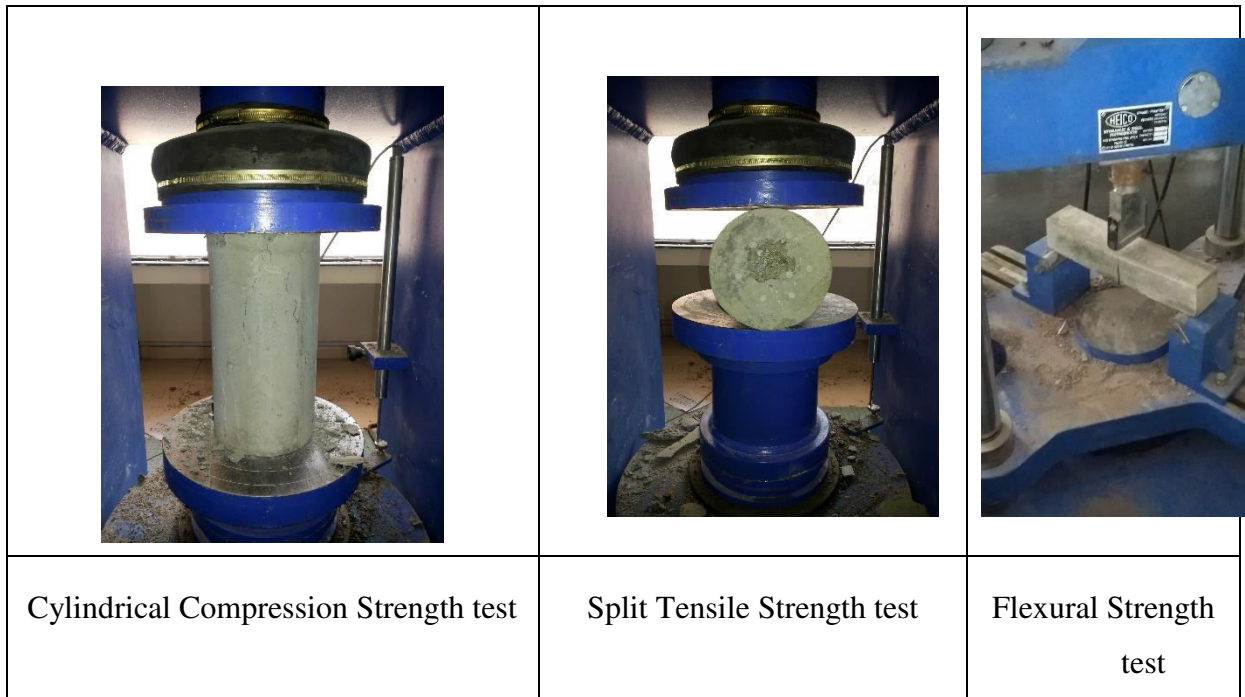


**Figure 5.48 Testing on Hardened Concrete**

### **5.7. Evaluating Fracture Properties of SCC Mixes Using Three Point Bend Tests**

Three point bend tests are conducted on seven SCC mixes consisting of one SCC mix with 100% OPC, one ternary SCC mix, and five ternary mixes with varying fibre content (0.1% to 0.5%) with a plastic viscosity of 13 Pa s. A specimen size of 500 X 100 X 100 is used for the



entire experimental program. Notches of various depths have been cut using a notch cutter. The ratio of the notch to depth ( $a/d$ ) is chosen as 0.1 and 0.6 (Karihaloo *et al.* 2003). Span to depth ratio ( $l/d$ ) is chosen as 4. Notched beams of  $a/d$  ratio 0.1 and 0.6 are shown in *Figure 5.49*

The experimental setup consists of 250 KN capacity servo hydraulic UTM with online data acquisition system (DAQ). The loading frame used is of 2000 KN capacity. All the specimens are tested under Crack Mouth Opening Displacement (CMOD) control at a rate of 0.02 mm per minute. The mid span downward displacement is measured at the center of the specimen. Epsilon clip gauge of gauge length 10mm is used to measure the CMOD and DAQ will record the loads, mid span displacement, CMOD and time. Typical experimental setup is shown in *Figure 5.50*.



**Figure 5.49 Notched beams of size  $a/d = 0.1$  and  $0.6$**



**Figure 5.50 Typical experimental setup for fracture**

### 5.7.1. Fracture Energy

Concrete structures being quasi-brittle in nature are more vulnerable to cracking due to the presence of voids and flaws. The presence of these flaws with the application of load will grow and start propagating. The fracture energy ( $G_F$ ) is one of the important parameters in the analysis of cracked concrete structures. It describes the resisting properties of concrete. This can also be used to measure the ductility of concrete being a material parameter. It is defined as the amount of energy required to create a crack of the unit surface area projected in a plane parallel to the crack direction (RILEM FMT-89; RILEM FMC-50).

Work of Fracture ( $W_F$ ) is another important parameter which is defined as the area under load-deflection curve and it is expressed as

$$W_F(w) = \int_0^{w_c} P dw \quad (5.1)$$

where ' $w_c$ ' is crack mouth opening displacement,  $W_F$  is the work of fracture and  $P$  is applied load

According to RILEM method of Hillerborg (1978), the fracture energy is the average energy given by dividing the total work of fracture by the projected fracture area (RILEM 1985; Karihaloo, 1995). In case of a specimen of depth  $d$  and initial crack length  $a$ , the fracture energy is given by

$$G_f = \frac{W_F}{b(d-a)} \quad (5.2)$$

where

$W_F$  is area under load-deflection curve

$b$  is the width of the prism

$d$  is the depth of the prism

$a$  is the notch depth

The above calculated fracture energy is also termed as RILEM fracture energy or size dependent fracture energy. This varies with the varying  $a/d$  ratio and span to depth ratio.

From *Figure 5.51* it is observed that the presence of fibres increased the load carrying capacity of the concrete specimen with and without notch. Presence of guided notch decreased the load carrying capacity of all the SCC mixes. A decrease of 44.73% and 50.86% is observed for the SCC mix with 100% OPC and ternary combinations for a/d ratio of 0.1. For the a/d ratio of 0.6, this reduction is 79.83% and 84.6%. With the presence of fibres the decrease is 45.36%, 41.43%, 35.82%, 28.88%, and 19.2% for a/d ratio of 0.1 and 82.93%, 79.04%, 75.7%, 73.35% and 70.36% for a/d ratio of 0.6. The percentage reduction reduced the increase in fibre volume fraction. It is also observed that there is a decrease in maximum load with the increase in a/d ratio. Crack propagation will be delayed with the presence of fibres. This indicates that the random distribution of fibres will not allow the micro cracks to easily propagate ahead of the notch tip.

Based on the experiments conducted on the seven SCC mixes, peaks load and corresponding size dependent fracture energy are calculated for  $a/d$  ratios of 0.1 and 0.6.

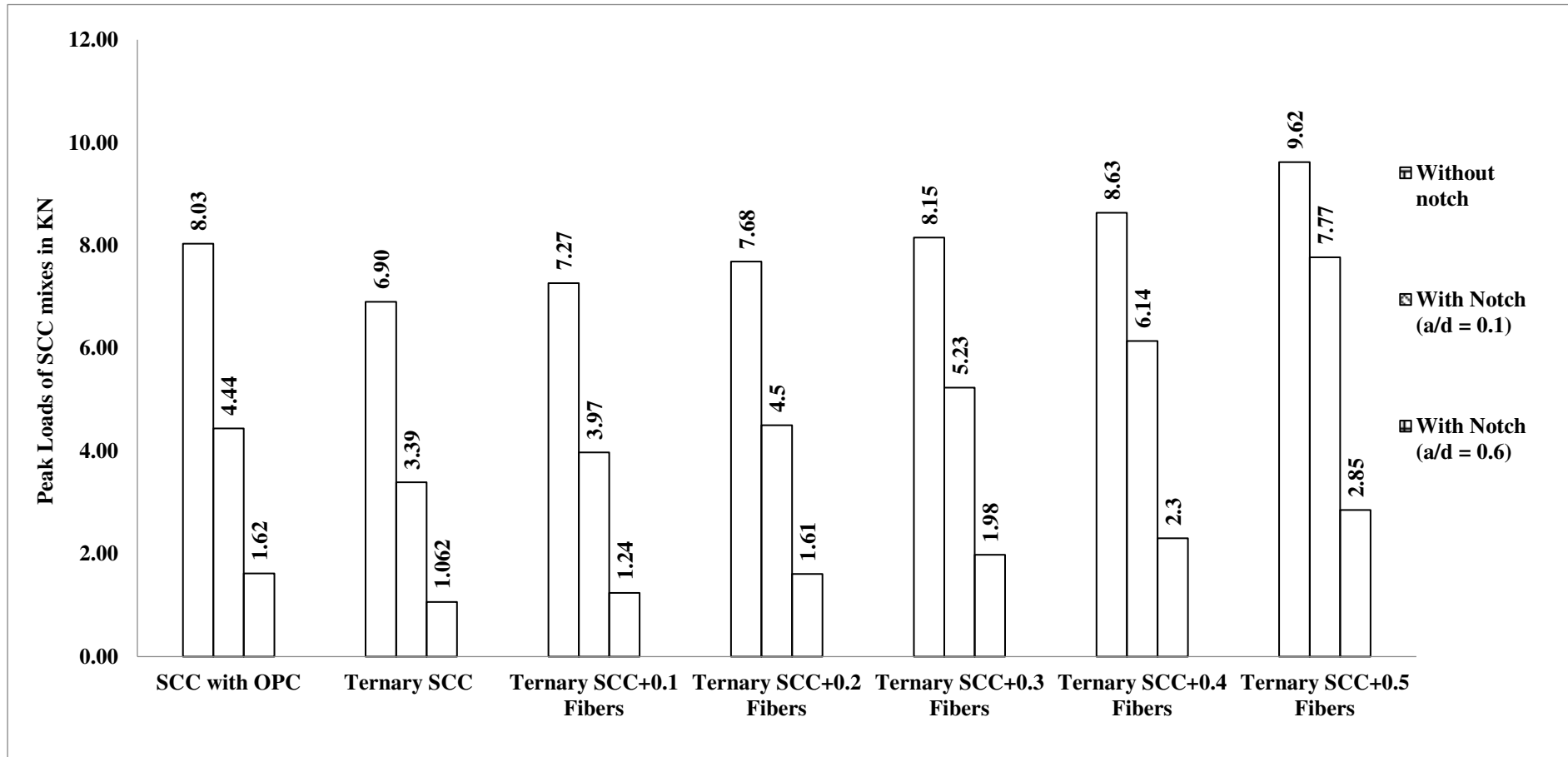
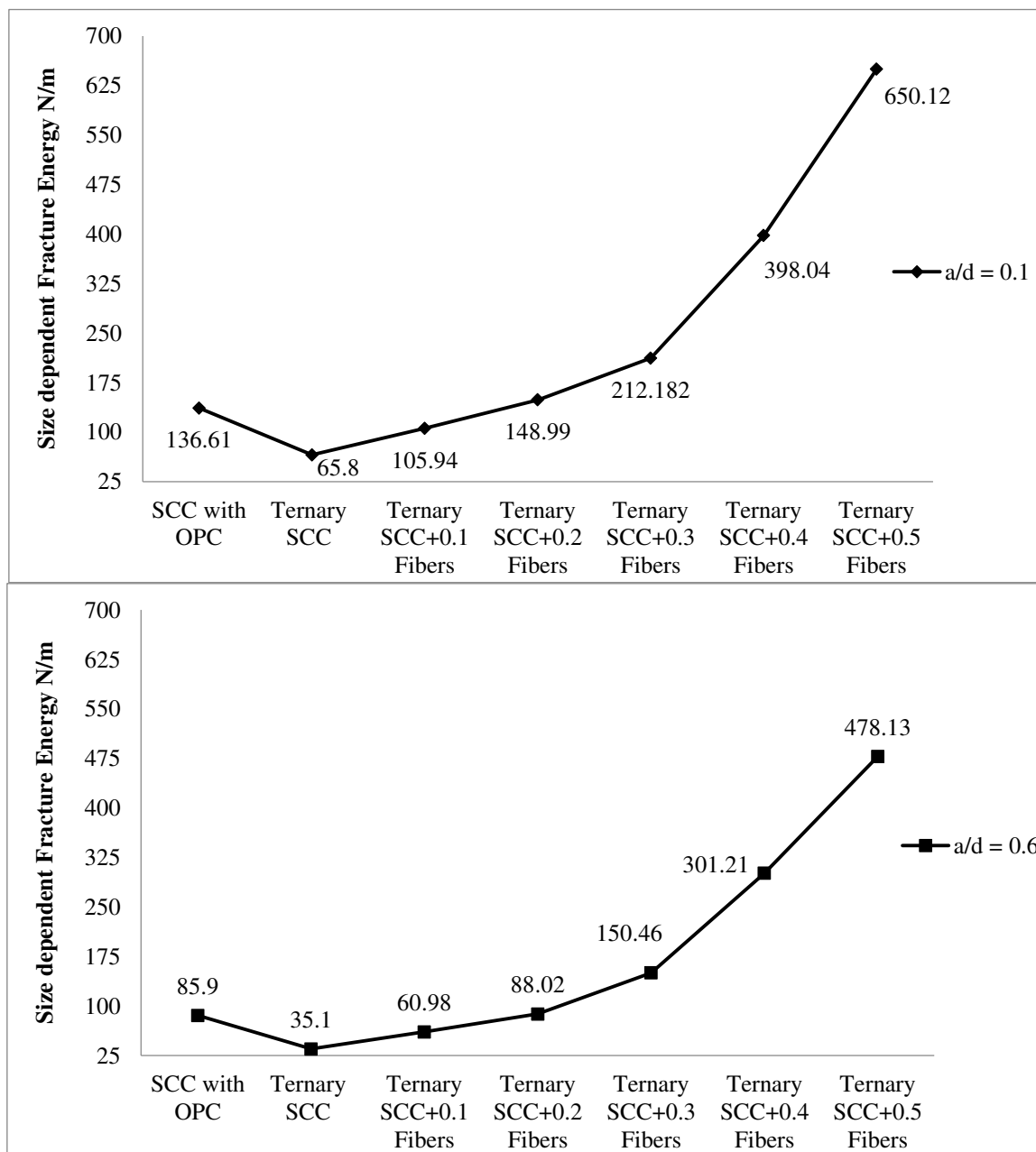


Figure 5.51 Load carrying capacities of SCC mixes with and without notch

Using the methodology given in section 5.7.1 size dependent fracture energy ( $G_f$ ) is calculated based on the load deflection curves.



**Figure 5.52 Size dependent fracture energies ( $G_f$ ) of SCC mixes**

The  $G_f$  values of the seven SCC mixes for 0.1 and 0.6  $a/d$  ratios are shown in *Figure 5.52*. SCC mix with 100% OPC achieved  $G_f$  values equal to 136.61 N/m and 85.9 N/m for 0.1 and 0.6  $a/d$  ratios. SCC mixes with ternary combination resulted in 65.8 N/m and 35.1 N/m for 0.1 and 0.6  $a/d$  ratios.  $G_f$  increased with the increase in fibre volume fraction. Fracture energy being material parameter should not be influenced by the varying notch to depth ratios. To

address the same, size independent fracture energy is evaluated based on the boundary effect method.

### 5.7.1.1. Boundary Effect Method (BEM)

It is found that the local fracture energy varies with the width of the fracture process zone (FPZ). The FPZ becomes more and more restricted as reaches the stress-free back face of the specimen. As a result, the local specific fracture energy reduces as the crack reaches the back end. Hu and Wittmann (Duan, *et al.* 2003) are the first to observe this phenomenon. They observed that initially when the crack starts to grow from a pre-existing notch, the rate of decrease is negligible, but it accelerates as it reaches the stress free back. They modelled this behaviour bilinear, after performing extensive tests *Figure 5.53*.

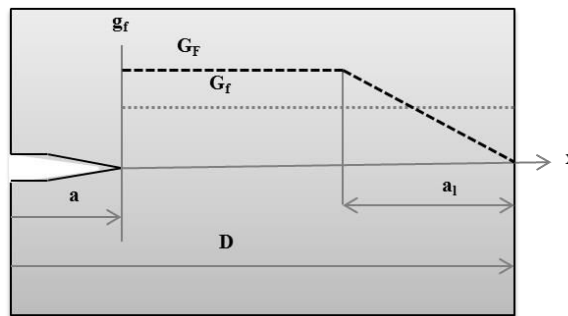


**Figure 5.53 Bilinear Tension Softening**

They also came up with the relationship:

$$G_f(a, D) = \frac{\int_0^{D-a} g_f(x) dx}{D-a} = \begin{cases} G_F \left[ 1 - \frac{a_l/D}{2(1-a/D)} \right] & ; 1-a/D > a_l/D \\ G_F \cdot \frac{(1-a/D)}{2a_l/D} & ; 1-a/D \leq a_l/D \end{cases} \quad (5.3)$$

Where,

$G_f$  represents size dependent fracture energy calculated by RILEM work-of-fracture method.

$G_F$  represents size independent specific fracture energy.

$a_l$  represents transition ligament length.

$a/D$  represents initial crack to depth ratio.

After, testing a lot of specimens, it is observed that there are come up with the over determined set of equations to determine  $G_f$  and  $a_l$  which is solved by using the method of least squares.

(Karihaloo, *et al.* 2003) found out that this lengthy procedure need not be applied. They proposed that a specimen of the same size and separate the crack-to-depth ratio by large amount say 0.05 & 0.5 or 0.1 & 0.6, and a restriction on aggregate size depending on span-to-depth ratio, which will provide us with an exact solution which is very close to the solution proposed by Hu and Wittmann.

In extension (Karihaloo, *et al.* 2013), the proposed a tri-linear model, based upon the investigations using acoustic emission techniques *Figure 5.54*.

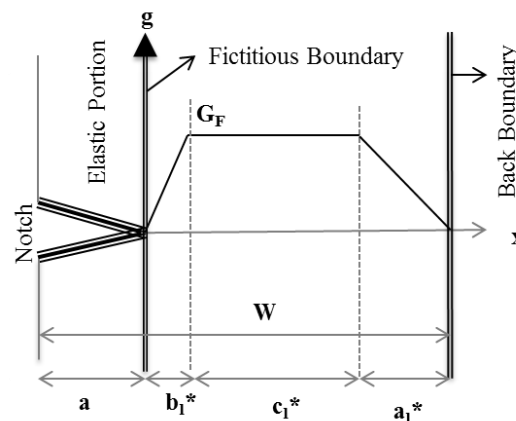


**Figure 5.54 Trilinear Tension Softening**

According to theory, at the start of load application on the notched specimen, the size of FPZ increases, then remains approximately constant for a certain range and then decreases as the crack reaches the stress-free back boundary of the specimen. This procedure gives better accuracy but is a time consuming process requiring acoustic emission setup. Hence, the bilinear approximation is generally adopted.

Size independent fracture energy ( $G_F$ ) is evaluated using Eq. (5.3). From *Figure 5.55*, size independent fracture energy increased with the increase in fibre volume fraction similar to  $G_f$ . It is also observed that  $G_F$  is more for SCC mix with 100% OPC compared to ternary SCC mix. Supplementary cementitious materials like fly ash and GGBS will slow down the

hydration process which in turn will decrease its compressive strength. With the decrease in compressive strength  $G_F$  decreases.

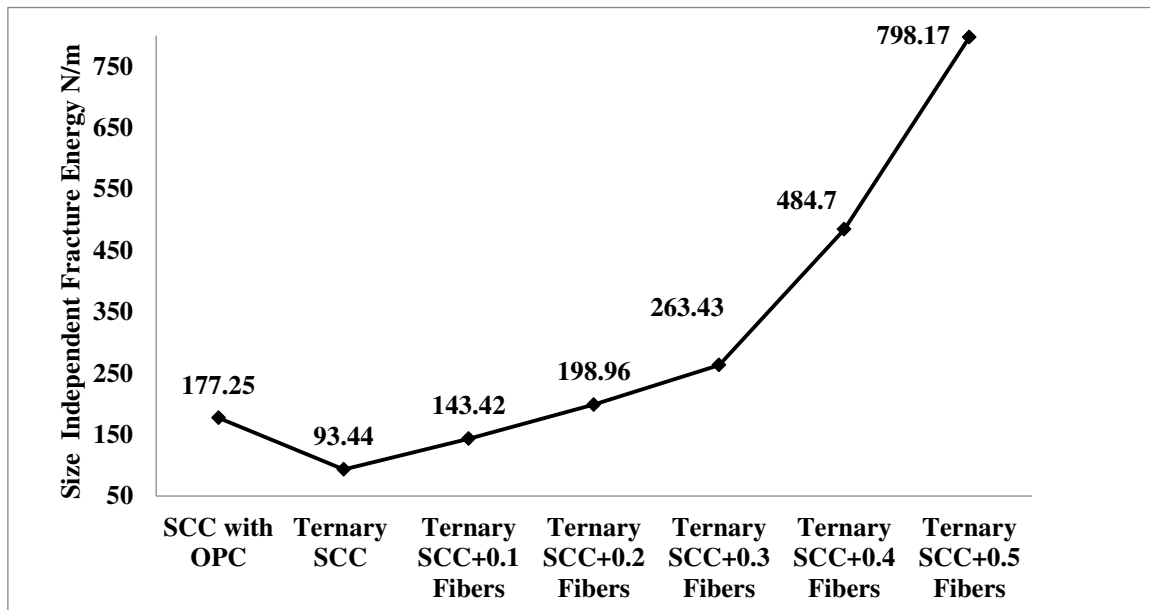


**Figure 5.55** Size independent fracture energies ( $G_F$ ) of SCC mixes

### 5.7.1.2. Load-CMOD curves

Typical Load-CMOD diagrams for 0.1 and 0.6 a/d ratios are shown in *Figure 5.57 and Figure 5.58*. The maximum displacement of 2.37mm and 1.2mm is observed for the SCC mix 0.5% fibres for 0.1 and 0.6 a/d ratio. Due to the brittle nature of SCC, capturing post peak for plain mixes has found to be very difficult. With the presence of fibres in the mixes, perfect post peak response is observed compared to the mixes without fibres. This also is an indication of delay in crack propagation of concrete due to the obstruction caused by fibres ahead of every crack tip. Sometimes the concrete can withstand higher loads with maximum utilization of maximum fibre content. Crack propagation of an SCC specimen is shown in *Figure 5.56*



**Figure 5.56** Crack propagation of SCC specimen with a/d ratio = 0.1



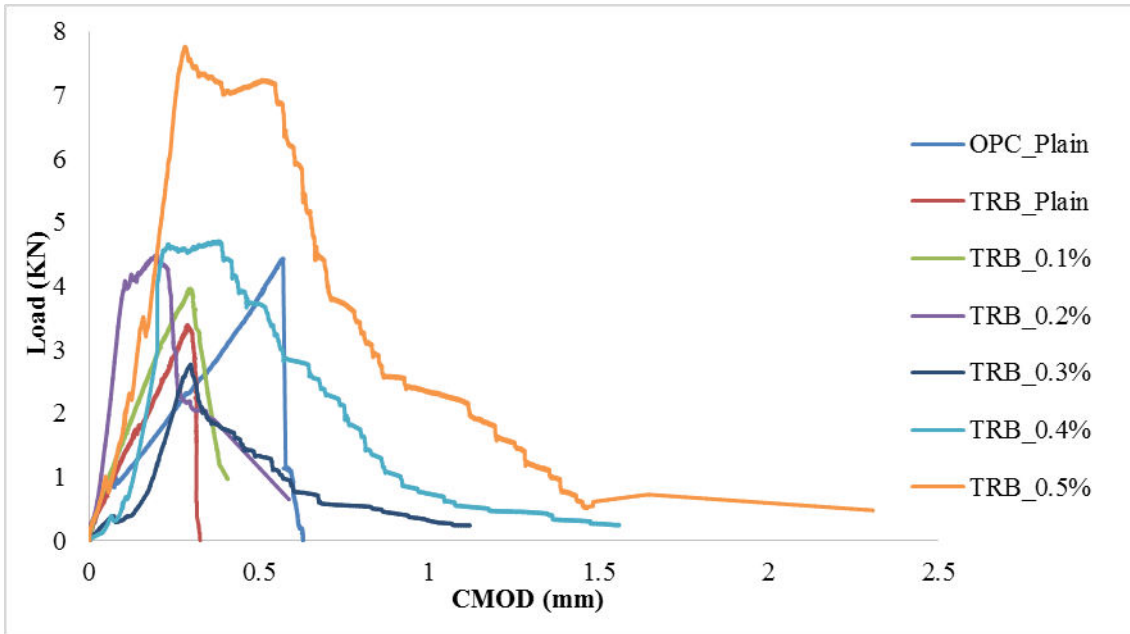


**Figure 5.57 Load-CMOD curves for  $a/d = 0.1$**

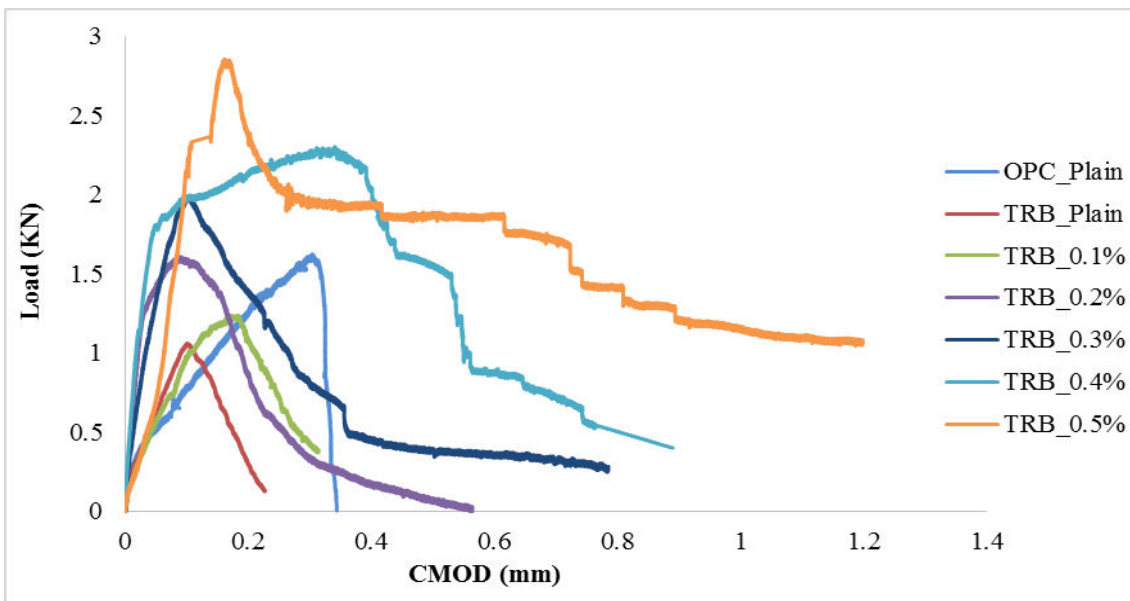


**Figure 5.58 Load-CMOD curves for  $a/d = 0.6$**

This chapter concludes with the presenting the fresh and hardened properties of SCC mixes for different plastic viscosities and the influence of fibres on fresh, hardened and fracture properties of SCC. The next chapter deals with the numerical evaluation of fracture properties of concrete.

**CHAPTER 6**  
**NUMERICAL STUDIES ON FRACTURE**  
**PROPERTIES OF SCC USING CDP MODEL**

## **6.1. INTRODUCTION**

### **6.1. Introduction**

This chapter mainly deals with the evaluation of fracture properties, namely Size dependent fracture energy, Size Independent Fracture Energy ( $G_F$ ) and Characteristic Length ( $l_{ch}$ ), for various grades of concrete.

Fracture Mechanics is a branch of Mechanics which is concerned with the study of crack propagation in materials. A crack is defined as a material deflection or discontinuity. It uses the theories of elasticity and plasticity on infinitesimally small units, to predict the macroscopic failure of bodies.

Concrete is an interesting material. It is made up of different components, primarily of cement, fine aggregate and coarse aggregates, bound by water. This mixture gives concrete good compressive strength, but is susceptible to failure under tensile stress, even in small magnitudes. This can be explained as follows; during compressive loading, the aggregates take the compressive stresses. But, in tension, the cement particles, binding the aggregates, are separated by the cracks formed under the loading. This causes the concrete specimen to fail as the crack propagates. Concrete was conventionally considered a brittle material, as its failure was not ductile. But, concrete undergoes subcritical failure prior to its ultimate load, thus exhibiting non linearity in its stress-strain behaviour and hence is considered a quasi-brittle material in modern fracture mechanics (Anderson and Anderson, 2005)

The cracking of concrete in tension and crushing of concrete in compression are the two prime mechanisms of failure (Kmieciak and Kaminski, 2011). These can be modelled using the CDP model, available as an Abaqus/CAE module, for determining the fracture behaviour of concrete.

### **6.2. Concrete Damaged Plasticity Model**

The Druker-Prager Strength Hypothesis is often used for determining the failure behaviour of concrete. The failure, according to the hypothesis, is determined by the non-dilatational strain energy (the difference between total strain energy and the strain energy resulting from volume change) and the boundary surface itself, in the stress space, assumes the shape of a cone. The advantages of this theory are the surface smoothness and no complications in computing. But, the theory is inconsistent with the actual behaviour of concrete.

The CDP model is modified from the Drucker-Prager Strength Hypothesis. In CDP model the failure cross-section in the deviatoric plane need not be a circle (as in Drucker-Prager Hypothesis) but can be any shape, which is determined by the parameter  $K_c$  (Lee and Fenves, 1998) (Lubliner, *et al.* 1989).  $K_c$  is interpreted as the ratio of distances between the hydrostatic axis and compression and tension meridians, respectively, in the deviatoric cross-section.  $K_c = 1$  implies it's a circle. The ABAQUS Users' Manual recommends a value of  $2/3$ .

$\frac{\sigma_{b_0}}{\sigma_{c_0}}$  ( $\frac{f_{b_0}}{f_{c_0}}$ ) is defined as the ratio of compressive strength in the bi-axial state to that in the uni-axial state. The value comes out to 1.16248. The ABAQUS Users' Manual recommends the value of  $\frac{\sigma_{b_0}}{\sigma_{c_0}}$  as 1.16.

Dilation Angle,  $\psi$ , is the angle of inclination of the failure surface towards the hydrostatic axis, measured in the meridional plane. Physically, it can be understood as the angle of internal friction of concrete. It generally takes values between  $36^\circ$  and  $40^\circ$ .

In CDP, the plastic potential surface takes the shape of a hyperbola. The shape of the hyperbola can be adjusted through the parameter eccentricity. It is a small positive value which expresses the rate of approach of the hyperbola to its asymptote. Eccentricity Parameter can be calculated as the ratio of tensile strength to compressive strength (Jankowiak, 2005). The CDP model recommends the value of eccentricity,  $\varepsilon$ , as 0.1. When,  $\varepsilon = 0$ , the meridional plane becomes a straight line as in classic Drucker-Prager hypothesis.

The viscosity parameter slightly helps in reduction in the step size, in order to regularize the constitutive equations. Viscoplastic adjustment consists in choosing viscosity parameter,  $\mu$ , to be greater than zero such that the ratio of problem's time step to  $\mu$  tends to infinity. Hence, the value of viscosity parameter for viscoelastic materials should be as small as possible. For non-viscoelastic materials, the value is recommended to be 0 (Kmieciak and Kaminski, 2011).

These five factors, namely  $K_c$ ,  $\frac{\sigma_{b_0}}{\sigma_{c_0}}$ ,  $\psi$ ,  $\varepsilon$  and  $\mu$ , along with the stress-strain behaviours in compression and tension and variation of damage with inelastic strain (in compression) and with cracking strain (in tension) are the input parameters for the CDP model, in Abaqus/CAE.

A summary of the above is tabulated in *Table 6.1*

**Table 6.1 Summary of CDP Parameters**

| Parameter                           | Recommended Value |
|-------------------------------------|-------------------|
| $K_c$                               | 23                |
| $\frac{\sigma_{b_0}}{\sigma_{c_0}}$ | 1.16              |
| Dilation Angle, $\psi$              | 36° – 40°         |
| Eccectricity, $\varepsilon$         | 0.1               |
| Viscosity Parameter, $\mu$          | 0                 |

### 6.3. Modeling Stress-Strain Curves

The stress-strain plots for various grades of concrete are modelled in MATLAB using Saenz Formula (Kmiecik and Kaminski, 2011), and Hsu & Hsu Formula (Hsu and Hsu, 1994) for concrete in compression and Wang & Hsu Model (Wang and Hsu, 2001) for concrete in tension.

#### 6.3.1. Formulation of Stress-Strain Curves in Compression

The characteristic compressive strength,  $f_{ck}$ , is considered the base parameter. It is used to calculate mean compressive strength,  $f_{cm}$ , as per IS 456:2000, as follows:

$$f_{cm} = f_{ck} + 1.65\sigma \quad (6.1)$$

where,  $\sigma$ , the standard deviation, is given as:

$$\begin{aligned}
\sigma &= 3.5\text{MPa}; \text{if } f_{ck} = 10,15\text{MPa} \\
\sigma &= 4.0\text{MPa}; \text{if } f_{ck} = 20,25\text{MPa} \\
\sigma &= 5.0\text{MPa}; \text{if } f_{ck} \geq 30\text{MPa}
\end{aligned} \tag{6.2}$$

The moduli of elasticity as per European (EUROCODE2), and Indian (IS456:2000) standard code of practices are given as:

$$\begin{aligned}
E_{cm} &= 22000(0.1 \cdot f_{cm})^{0.3}; \text{EUROCODE2} \\
E_{cm} &= 5000\sqrt{f_{ck}}; \text{IS456:2000}
\end{aligned} \tag{6.3}$$

where,  $E_{cm}$ ,  $f_{cm}$ , and  $f_{ck}$  are in  $MPa$ .

### 6.3.1.1.Saenz Formula

Saenz Formulation (L. Saenz, *et al.* 1964) consists of a Rational Function whose denominator is 3<sup>rd</sup> degree polynomial and numerator is 1<sup>st</sup> degree polynomial. The refined formulation of Saenz model, as per (Kmiecik and Kaminski, 2011), is given as follows:

$$\sigma_c = \frac{\varepsilon_c}{A + B\varepsilon_c + C\varepsilon_c^2 + D\varepsilon_c^3} \tag{6.4}$$

where the parameters are given as:

$$\begin{aligned}
A &= \frac{1}{E_{cm}}; B = \frac{P_3 + P_4 - 2}{P_3 f_{cm}}; C = -\frac{2P_4 - 1}{P_3 f_{cm} \varepsilon_{c1}}; D = \frac{P_4 - 1}{P_3 f_{cm} \varepsilon_{c1}} \\
P_1 &= \frac{\varepsilon_{cu}}{\varepsilon_{c1}}; P_2 = \frac{f_{cm}}{f_{cu}}; P_3 = \frac{E_{cm} \varepsilon_{c1}}{f_{cm}}; P_4 = \frac{P_3(P_2 - 1)}{(P_1 - 1)^2} - \frac{1}{P_2}
\end{aligned} \tag{6.5}$$

The parameters  $\varepsilon_{c1}$  and  $\varepsilon_{cu}$  are defined as strain at maximum compressive stress and ultimate compressive strain, respectively. Accurate quantification of these parameters was given by (Majewski, 2003), as follows:

$$\begin{aligned}
\varepsilon_{c1} &= 0.0014[2 - \exp(-0.024f_{cm}) - \exp(-0.140f_{cm})] \\
\varepsilon_{cu} &= 0.004 - 0.0011[1 - \exp(-0.0215f_{cm})]
\end{aligned} \tag{6.6}$$

The parameter  $f_{cu}$ , in the Eq. (6.5), is the stress at ultimate compressive strain,  $\epsilon_{cu}$ . This means the plot generated by Saenz model should pass through 2 points i.e.  $(f_{cm}, \epsilon_{c1})$  and  $(f_{cu}, \epsilon_{cu})$ . But, for any random value of  $P_2$ , the generated stress-strain plot will not pass through the above mentioned 2 points. A new parameter, correction factor, is, therefore, introduced. It is defined as the ratio of  $f_{cu}$  to  $f_{cm}$ , (i.e., the reciprocal of  $P_2$ ) for which the curve will pass through  $(f_{cm}, \epsilon_{c1})$  and  $(f_{cu}, \epsilon_{cu})$  for a particular grade of concrete. This correction factor is calculated by minimising the sum-squared-errors at these two points. But, finding sum-square-errors every time to find the correction factor can be tedious as well as inconvenient sometimes. So, to save time and effort, a small modification to the Saenz model is suggested, which will relate the correction factor to the characteristic strength of concrete,  $f_{ck}$ .

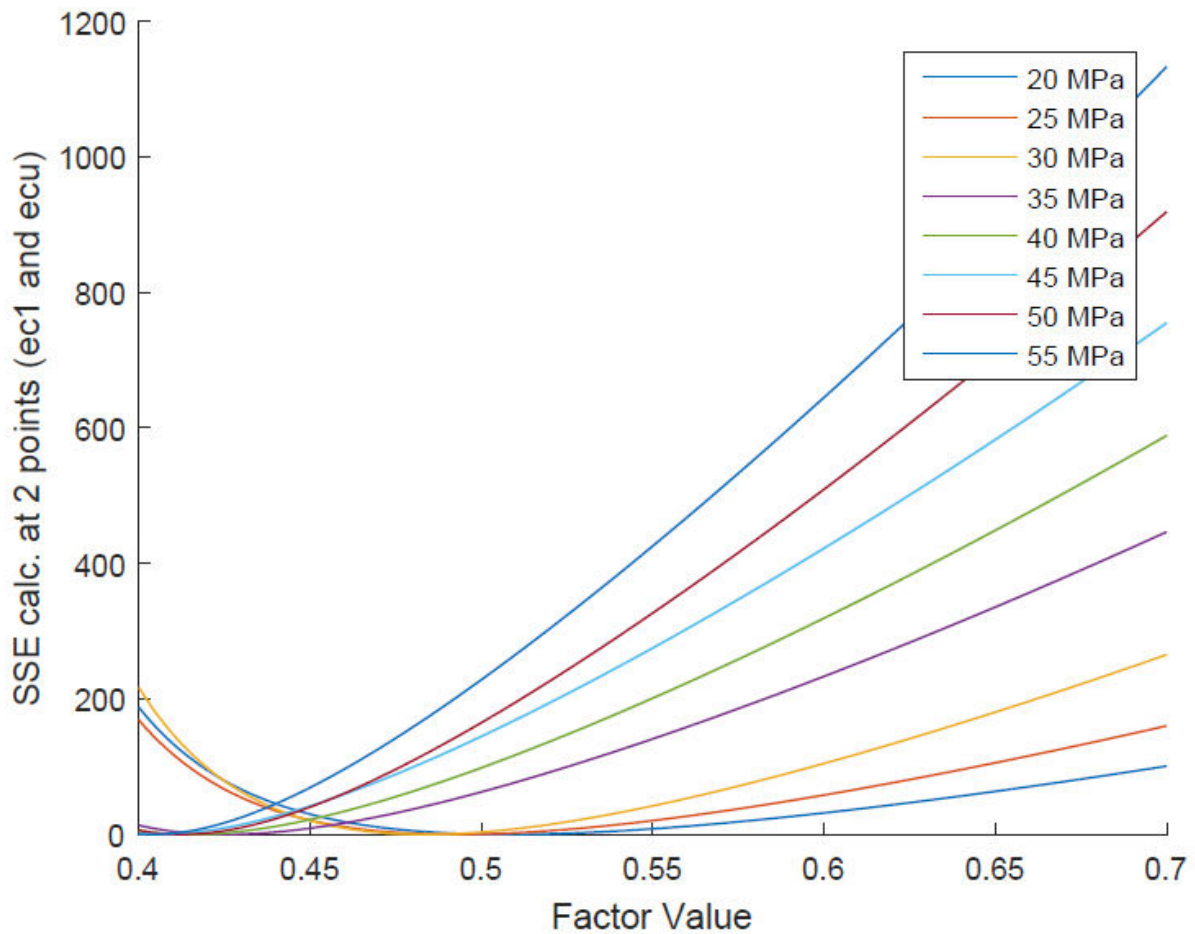


**Figure 6.1 Sum-Squared-Errors vs. Factor Value (for IS 456:2000)**

**Table 6.2 Correction Factor Values**

| Characteristic<br>Compressive<br>Strength (MPa) | Correction Factor |            |
|---|-------------------|------------|
|   | IS 456:2000       | EUROCODE 2 |
| 20  | 0.5077            | 0.5764     |
| 25  | 0.4926            | 0.5468     |
| 30  | 0.4836            | 0.5294     |
| 35  | 0.4252            | 0.4605     |
| 40  | 0.4148            | 0.4416     |
| 45  | 0.4052            | 0.4246     |
| 50  | 0.4124            | 0.4256     |
| 55  | 0.4040            | 0.4115     |

The correction factor values are obtained using  $E_{cm}$  value as per IS 456:2000

*Table 6.2.* The abscissa, from *Figure 6.1*, at minimum Sum-Squared-Errors is the correction factor. The obtained correction factors are regressed against  $f_{ck}$  to obtain a trendline, which is given as:

$$\text{Correction Factor} = 0.1043 \cdot \exp\left(-\left(\frac{f_{ck} - 22}{11.94}\right)^2\right) + 0.4035; \text{ for IS 456: 2000}$$

$$\text{Correction Factor} = 0.1887 \cdot \exp\left(-\left(\frac{f_{ck} - 14.75}{21.27}\right)^2\right) + 0.4; \text{ for EUROCODE 2} \quad (6.7)$$



The goodness parameters of the fit Eq. (6.7) are:  $R^2 = 0.9965$  and  $0.9731$ ,  $RMSE = 0.0080$  and  $0.0105$ , and  $SSE = 4.45 \times 10^{-4}$  and  $7.7183 \times 10^{-4}$  for IS 456:2000 and EUROCODE 2 respectively. The fit can be visualised in *Figure 6.2*. By substituting the value of correction factor in Saenz Eq.(6.4), the compressive stress-strain curve can be modelled. A typical stress-strain curve generated by Saenz Model is shown in *Figure 6.3*.

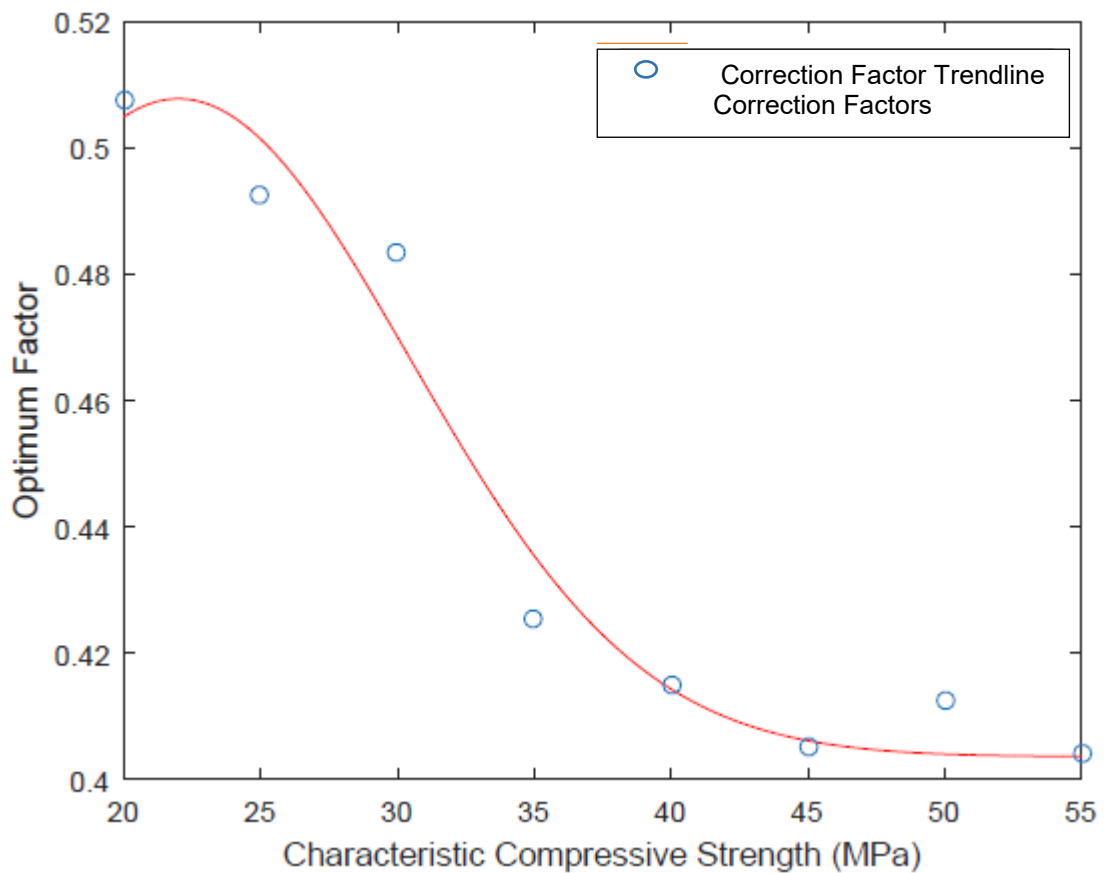


**Figure 6.2** CorrectionFactor vs. Characteristic Compressive Srength (for IS 456:2000)

The reference points are  $(f_{cm}, \epsilon_{cl})$  and  $(f_{cu}, \epsilon_{cu})$  where  $f_{cu} = f_{cm} \times \text{Factor value}$ . Factor Value can be any ratio of  $f_{cu}$  to  $f_{cm}$ . If FactorValue = Correction Factor, the plot will pass through both the points *Figure 6.3*, otherwise it will not. An example of such case is shown in *Figure 6.4*, where the CorrectionFactor is 0.4148 (*M40*), but adopt FactorValue as 0.5 while modelling. It can be observed that the plot fails to pass to through the reference points.

### 6.3.1.2. Hsu and Hsu Formula

The numerical model proposed by Hsu & Hsu in 1994, has the capacity to develop compressive stress-strain relation till  $0.3\sigma_{cu}$  in the descending portion of the stress-strain curve. This model is appropriate for both normal, and high strength concretes with minor modifications. The input parameters required for the model are  $\sigma_{cu}$  (also,  $f_{cm}$ ) and  $E_{cm}$ . No modifications are necessary for normal concretes upto 62 MPa ( $\approx$  M55 grade). Modifications for high strength concretes are detailed in Hsu and Hsu (1994).

The model for normal strength concrete is described below:

$$\begin{aligned} \sigma_c &= E_{cm} \cdot \varepsilon_c \quad ; \text{if } \sigma_c \leq 0.5\sigma_{cu} \\ \sigma_c &= \left( \frac{\beta \cdot \varepsilon_c \varepsilon_o}{\beta - 1 + (\varepsilon_c \varepsilon_o)^\beta} \right) \sigma_{cu} \quad ; \text{till } \sigma_c = 0.3\sigma_{cu} \end{aligned} \quad (6.8)$$

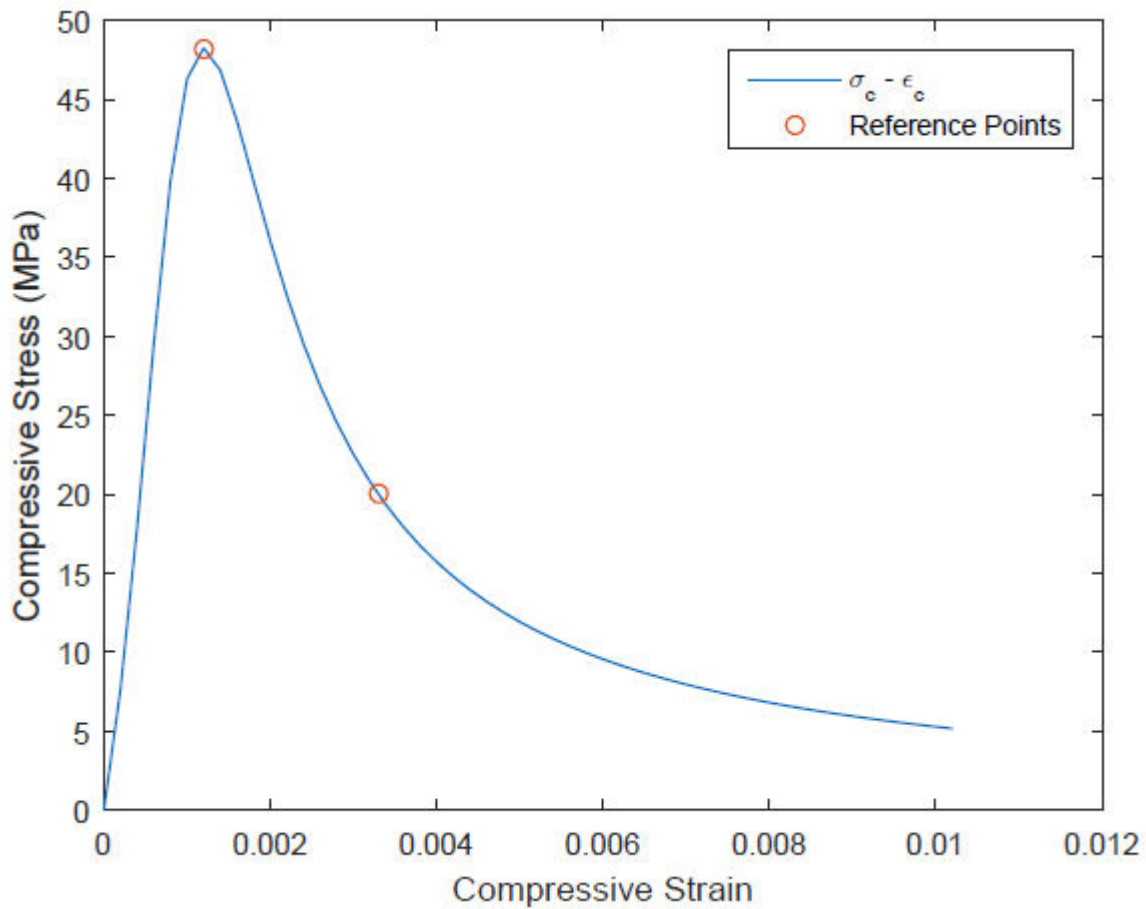


Figure 6.3 Saez Curve for M40 grade concrete (Factor value = Correction Factor)

The parameter  $\varepsilon_o$  is the strain at maximum stress ( $\sigma_{cu}$ ) and the parameter  $\beta$ , which depends on the shaped of the stress-strain curve, is given as:

$$\varepsilon_o = 8.9 \times 10^{-5} \sigma_{cu} + 2.114 \times 10^{-3} \quad (6.9)$$

$$\beta = \frac{1}{1 - \sigma_{cu} (\varepsilon_o E_{cm})} \quad (6.10)$$

Note: For the above equations, the parameters  $\sigma_c$ ,  $\sigma_{cu}$ , and  $E_{cm}$  are in  $kip/in^2$ . (1 MPa = 0.1450377  $kip/in^2$ ).

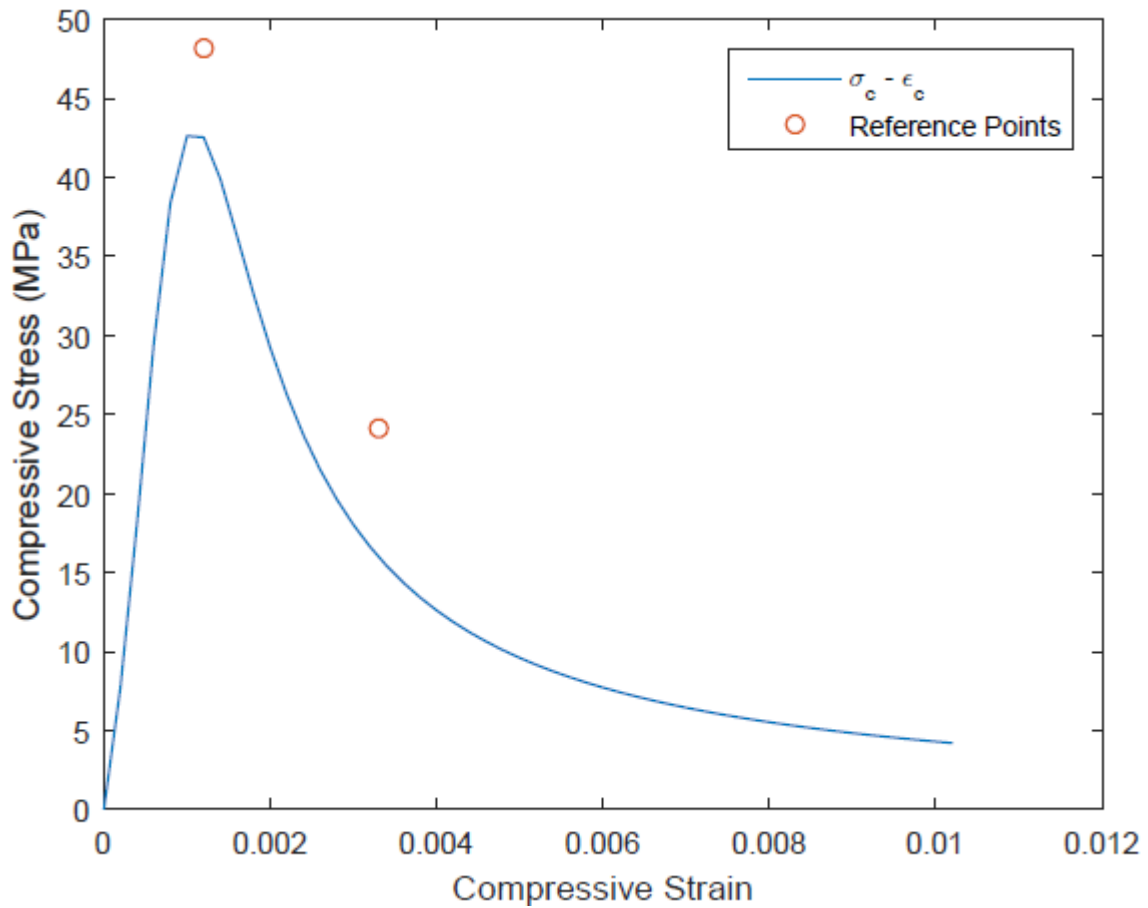


**Figure 6.4 Saenz Curve for M40 grade concrete (Factor value  $\neq$  Correction Factor)**

The inelastic compressive strain ( $\varepsilon_c^{in}$ ) is defined as the difference between total compressive strain ( $\varepsilon_c$ ) and elastic compressive strain ( $\varepsilon_c^{el}$ ). The stress strain curve generated using Hsu and Hsu model is shown in *Figure 6.5*.

### 6.3.2. Formulation of Stress-Strain Curves in Tension

The mean tensile stress governs the peak of the tensile stress-strain plot. It is given as:

$$f_{ctm} = 0.3 \cdot f_{ck}^{2/3} \quad (6.11)$$

Where,  $f_{ctm}$  is the maximum tensile stress, as per EUROCODE 2. The formulation, given by Wang and Hsu (Wang and Hsu, 2011), for modelling tensile stress-strain curve is as follows:

$$\begin{aligned} \sigma_t &= E_c \varepsilon_t \quad ; \text{if } \varepsilon_t \leq \varepsilon_{cr} \\ \sigma_t &= f_{cm} \left( \frac{\varepsilon_{cr}}{\varepsilon_t} \right)^{0.4} \quad ; \text{if } \varepsilon_t > \varepsilon_{cr} \end{aligned} \quad (6.12)$$

Where,  $\varepsilon_{cr}$  is a strain at concrete cracking which is, here, assumed to be equal to  $f_{ctm}/E_c$  and  $E_c = 1.05E_{cm}$ .

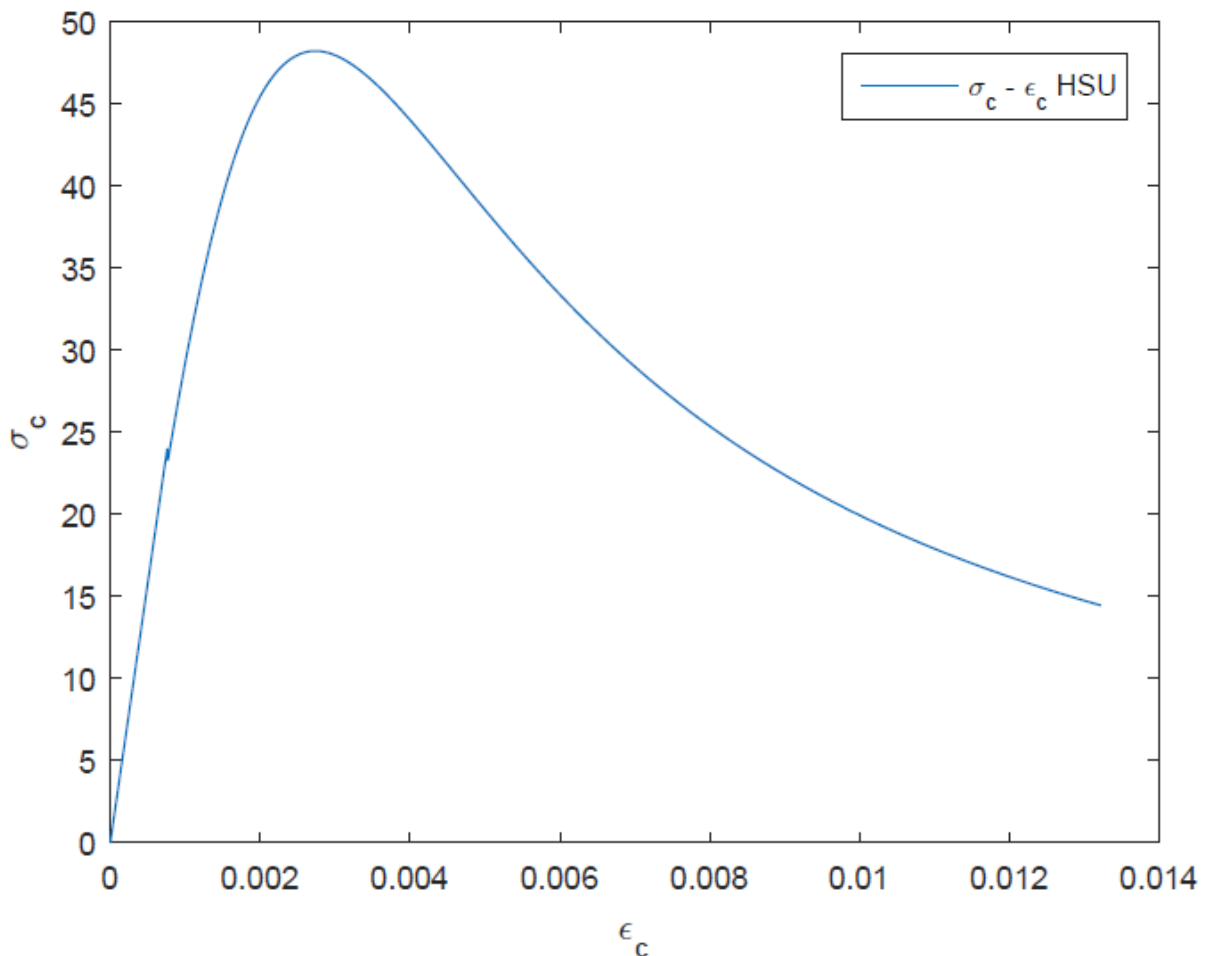


Figure 6.5 Stress-Strain curve generated by Hsu & Hsu model

The cracking strain ( $\epsilon_i^{ck}$ ), like compressive inelastic strain, is defined as the difference between total tensile strain ( $\epsilon_i$ ) and elastic tensile strain ( $\epsilon_i^{el}$ ). A typical plot generated using Wang and Hsu model is shown in *Figure 6.6*:

Here, for all simulated cases, only two values, one at maximum tensile stress and another at zero tensile stress, are adopted while modelling *Table 6.3*.

**Table 6.3 Tensile stress-strain data for CDP Model**

| Tensile Stress | Cracking Strain |
|----------------|-----------------|
| X              | 0               |
| 0              | 0.01            |

where " X " is the tensile strength of concrete in  $N / mm^2$

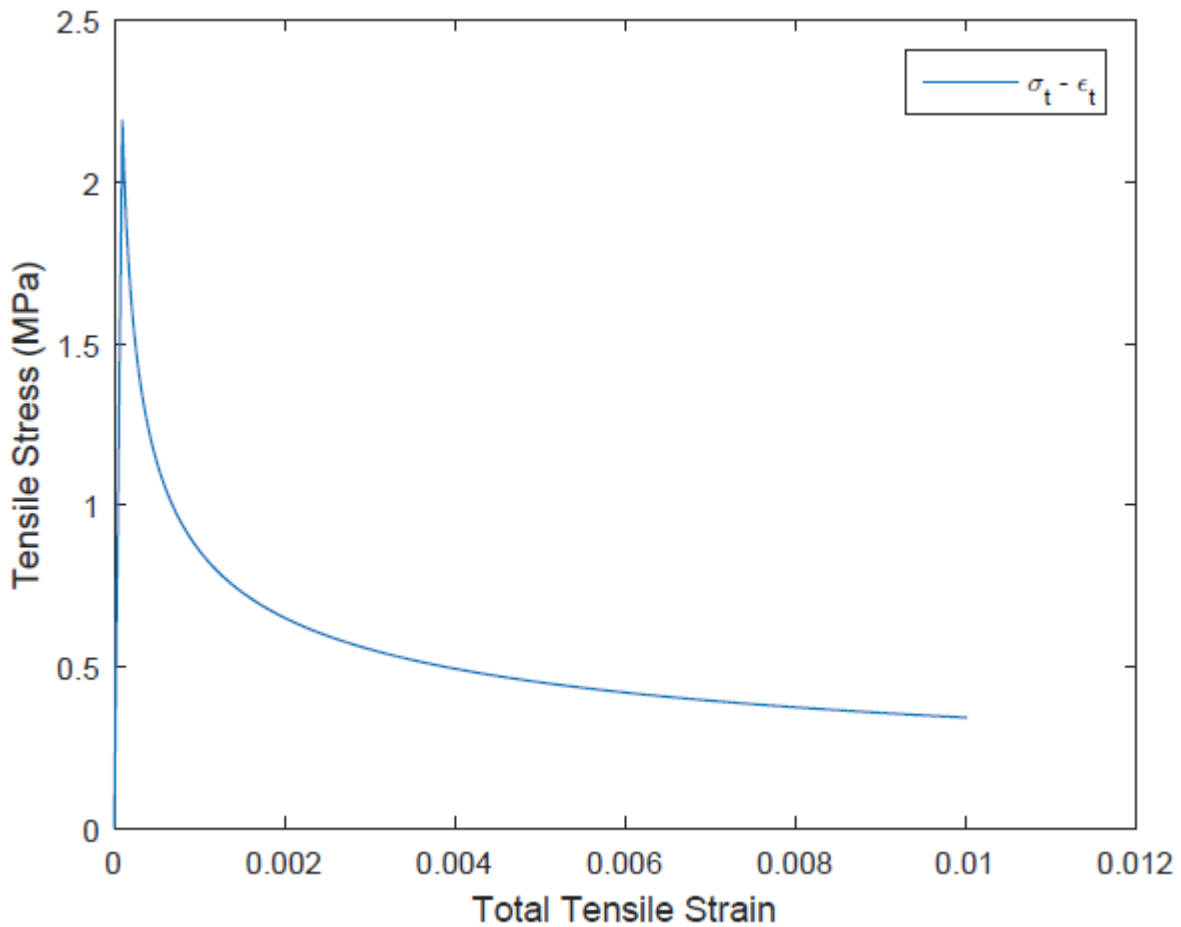


**Figure 6.6 Tensile Stress-Strain curve for M20 grade concrete**

## 6.4. DAMAGE PLASTICITY MODELS

Damage plasticity model is a linear-constitutive model which is based on the combination of damage mechanics and plasticity. This model is developed to evaluate the failure of concrete structures and in assessing the non-linear behaviour of concrete. The following are the two main damage plasticity models developed to predict the non-linear response of concrete.

### 6.4.1. Birtel and Mark

The variation of damage parameter in compression,  $d_c$ , is linked to the plastic strain of the concrete using the compressive inelastic strain and a factor  $b_c$  ( $0 < b_c \leq 1$ ) (Birtel and Mark, 2006); Typical stress-strain plot is shown in *Figure 6.7*.

$$d_c = 1 - \frac{\varepsilon_c E_{cm}^{-1}}{\varepsilon_c^{pl} \left( \frac{1}{b_c} - 1 \right) + \varepsilon_c E_{cm}^{-1}} \quad (6.13)$$

The value of  $b_c = 0.7$  is found to fit well with the experimental tests.

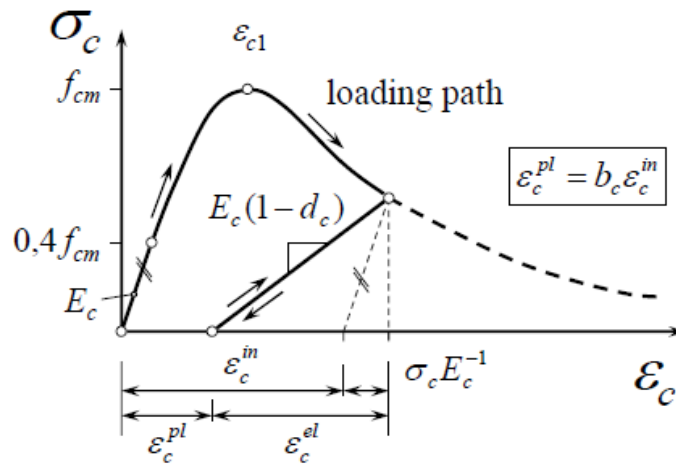


**Figure 6.7** Stress-Strain Plot considered by Birtel and Mark

Similar to  $d_c$ ,  $d_t$  is modelled based on plastic strains calculated using the cracking strain and experimentally determined parameter,  $b_t$  which is equal to 0.1. And  $d_t$ , similar to  $d_c$ , is given as:

$$d_t = 1 - \frac{\varepsilon_t E_{cm}^{-1}}{\varepsilon_t^{pl} \left( \frac{1}{b_t} - 1 \right) + \varepsilon_t E_{cm}^{-1}} \quad (6.14)$$

Seeing the formulations of  $d_c$  and  $d_t$ , it can be understood that, essentially  $d_c$  and  $d_t$  are the ratio of inelastic strain to total strain, in compression and tension respectively.

#### 6.4.2. Lopez-Almansa *et al.*

The damage variables, both in compression and tension, are modelled as exponentially dependent on the inelastic strains with parametric constants,  $a_c$  and  $a_t$ , respectively (Lopez-almansa *et al.*, 2014). The formulations are given as:

$$d_c = 1 - \exp(-a_c \varepsilon_c^{in}) \quad (6.15)$$

$$d_t = 1 - \exp(-a_t \varepsilon_t^{ck}) \quad (6.16)$$

The values of parameters  $a_c$  and  $a_t$  can be determined by subjecting them to the following boundary conditions:

$$\begin{aligned} \varepsilon_c^{in} = 0 &\Rightarrow d_c = 0 & \& \quad \varepsilon_c^{in} = \varepsilon_{c_{max}}^{in} &\Rightarrow d_c = 1 \\ \varepsilon_t^{ck} = 0 &\Rightarrow d_t = 0 & \& \quad \varepsilon_t^{ck} = \varepsilon_{t_{max}}^{ck} &\Rightarrow d_t = 1 \end{aligned} \quad (6.17)$$

The values adopted by (Lopez-Almansa *et al.*, 2014) for  $a_c$  and  $a_t$  are 2800 and 380 respectively.

The above model allows ease of computation of the damage variables but at the same time is unreliable as there can't be distinct values of parameters  $a_c$  and  $a_t$  by imposing the above boundary conditions only. Also, it is very difficult to determine the maximum inelastic strain of concrete. The changes in the parameters with respect to a change in grade of concrete is also not discussed. This model poses many unanswered questions, thus, rendering it impractical.

Here, for all simulated cases (except, when using values from literature), the damage in compression ( $d_c$ ) is modelled as the ratio of inelastic strain at that point to the total compressive strain (Wahalathantri, 2012), i.e.

$$d_c = \frac{\varepsilon_c^{in}}{\varepsilon_{c_{max}}} \quad (6.18)$$

The tensile damage is always taken as:

**Table 6.4 Tensile damage data for CDP model**

| Tensile Damage | Cracking Strain |
|----------------|-----------------|
| 0              | 0               |
| 0.9            | 0.01            |

The tension and compression damage values both the models are shown in *Figure 6.8 and Figure 6.9*

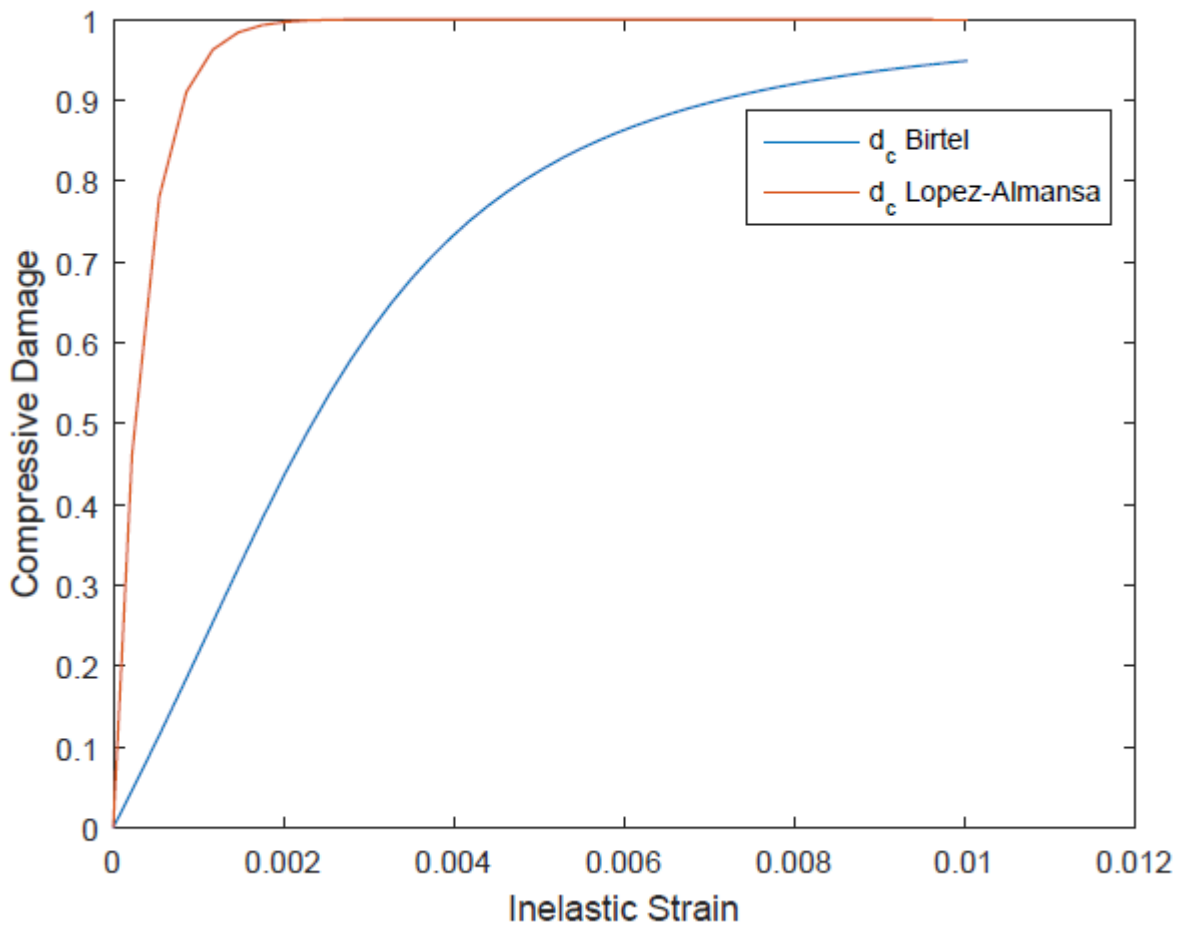




**Figure 6.8** Compressive damage ( $d_c$ ) vs. Inelastic strain ( $\varepsilon_c^{in}$ ) for M40 grade concrete

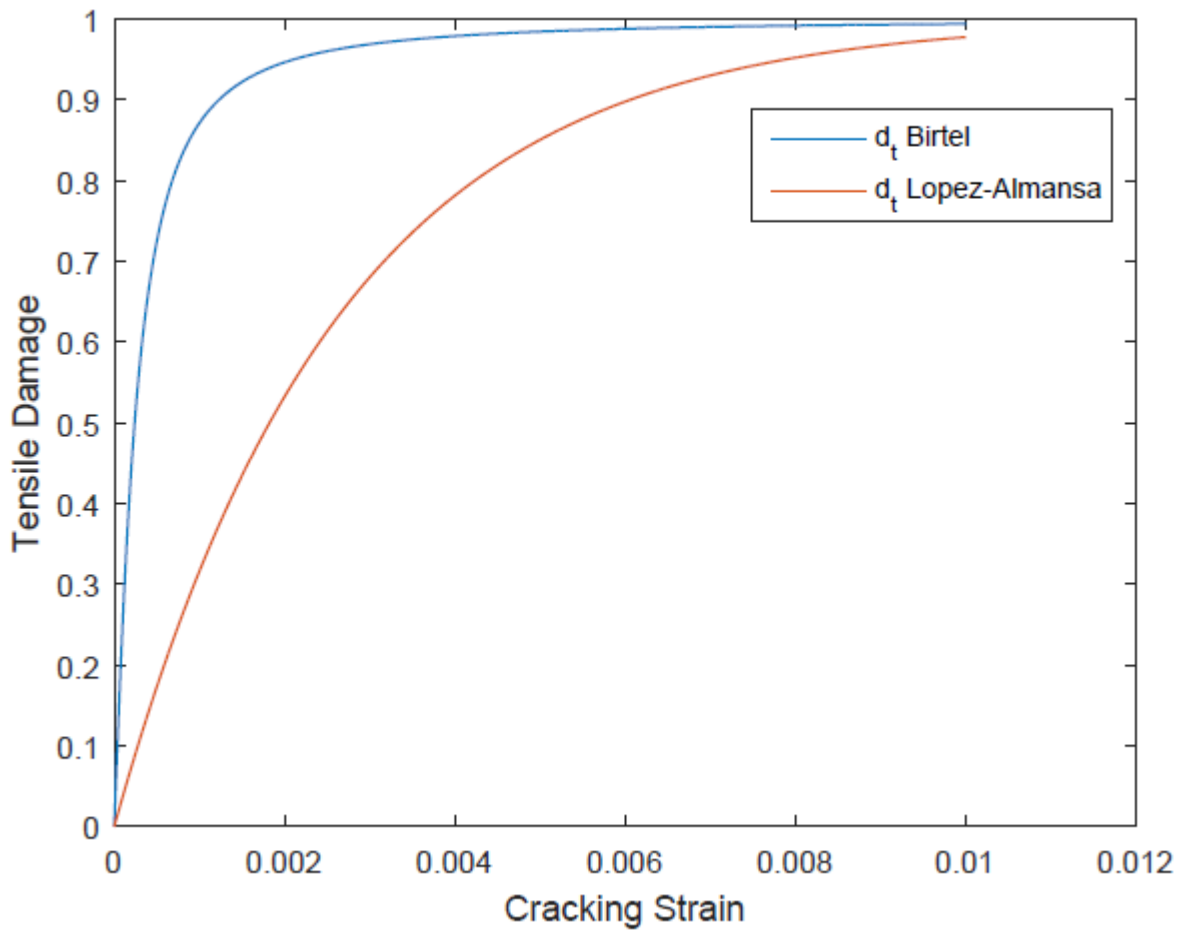


**Figure 6.9** Tensile damage ( $d_t$ ) vs. cracking strain ( $\varepsilon_t^{ck}$ ) for M40 grade concrete

## 6.5. Evaluation of Fracture Properties

To assess the failure of SCC mixes with and without fibers, fracture properties especially fracture energy is to be evaluated. Load-CMOD curves are also plotted for various SCC mixes considered for the study. The fracture energy is evaluated as per the methodology given in 5.7.1.

### 6.5.1. Characteristic length

Hillerborget *et al.*, (1976) proposed the Fictitious crack model in 1976, which assumes that the crack propagation occurs when principal tensile stress reached the tensile strength of the material ( $f_t$ ) and that the energy required to create new surfaces is negligible when compared to that required to separate them. The model introduces a material parameter,

namely, characteristic length ( $l_{ch}$ ), which depends on three other material parameters: Size independent fracture energy ( $G_F$ ), the tensile strength of the material ( $f_t$ ) and modulus of elasticity ( $E$ ).

$$l_{ch} = \frac{E \cdot G_F}{f_t^2} \quad (6.19)$$

This parameter is proportional to the length of the fracture process zone.

## 6.6. METHODOLOGY AND RESULTS

Abaqus/CAE 6.14 software package is used for analysing the behaviour of the beam under TPB test. A prism of size adopted is  $500mm \times 100mm \times 100mm$ . The notch width is adopted as  $2mm$  for all the simulated cases. Plasticity of concrete is modelled using Concrete Damaged Plasticity module available in Abaqus/CAE. The load-displacement curves are generated as output. Using these load-displacement curves, fracture energy ( $G_f$ ) for each simulation is obtained using RILEM work-of-fracture method. The size independent fracture energy ( $G_F$ ) is obtained using the modified boundary effect model (Murthy *et al.*, 2013; Karihaloo *et al.*, 2003) simple. The characteristic length is obtained from expression proposed by Hillerborg (Hillerborg *et al.*, 1976)

The study of the effect on the variation of mesh element type, mesh element size, grade of concrete, the model used for calculation of compressive behaviour, final tensile damage value, dilation angle, eccentricity, and notch-to-depth ratio on fracture parameters is done. The results of the same are summarized further in this section.

### 6.6.1. Mesh convergence studies

The mesh element type is varied among quadrilateral or triangular elements. The mesh element sizes adopted for mesh dependency are  $2mm$ ,  $5mm$ ,  $10mm$ , and  $25mm$ . This study is done by modelling beam as per the available data with  $a/D = 0.1$ . The summary of elements and nodes corresponding to element type and size is shown in *Table 6.5*.

From *Figure 6.10* and *Figure 6.11*, Quad and Tri 2, 5, 10, and 25 represents quadrilateral, triangular elements of varying mesh sizes. The average peak load for quadrilateral elements is  $5200\text{ N}$  and that for triangular elements is  $5500\text{ N}$ .

**Table 6.5 Summary of FE modelling for various mesh element types and sizes**

| Mesh element type | Mesh element size | No. of elements | No. of nodes |
|-------------------|-------------------|-----------------|--------------|
| Quadrilateral     | 2                 | 15286           | 15362        |
|                   | 5                 | 2417            | 2501         |
|                   | 10                | 596             | 651          |
|                   | 25                | 108             | 133          |
| Triangular        | 2                 | 25761           | 13187        |
|                   | 5                 | 4259            | 2253         |
|                   | 10                | 1091            | 608          |
|                   | 25                | 205             | 129          |

The maximum deviation, from mean, in case of quadrilateral elements is 10.78% and in case of triangular elements is 22.53%. The average final displacement in case of quadrilateral elements is 0.2533 mm and that for triangular elements it is 0.3168 mm, which is 25.06% higher than quadrilateral elements.

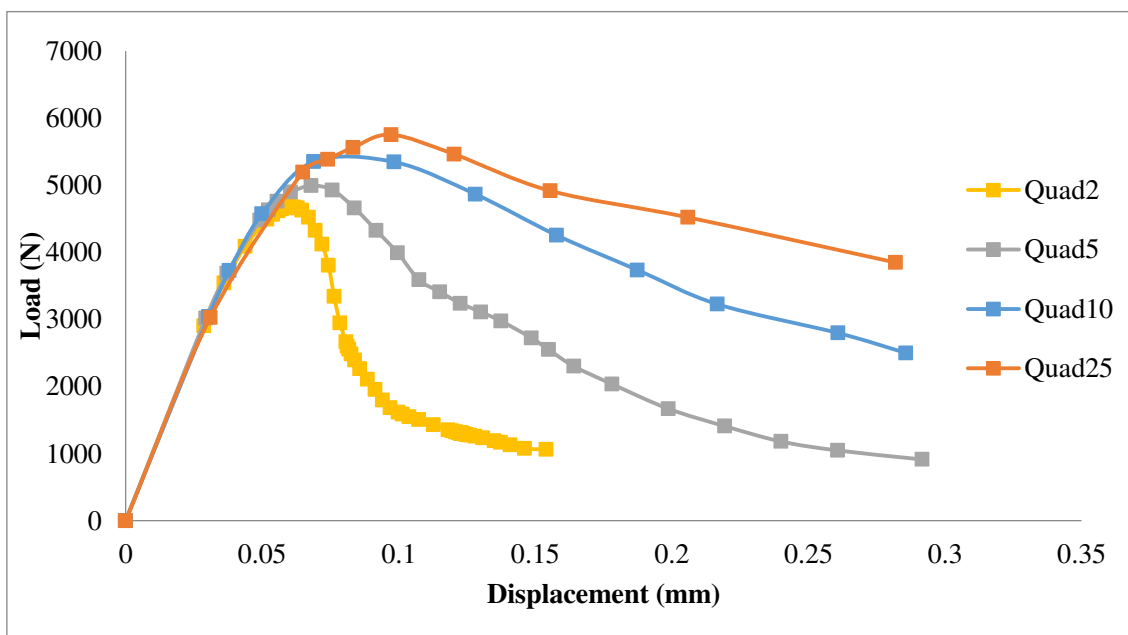


**Figure 6.10 Effect of Mesh Element size using Quadrilateral Elements**

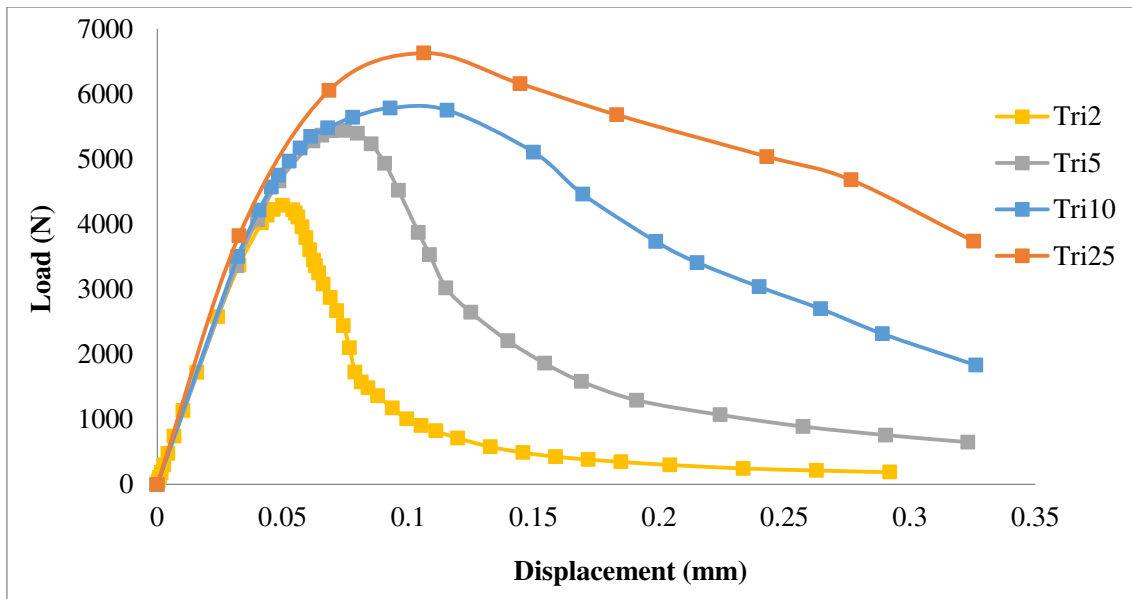


**Figure 6.11** Effect of Mesh Element size using Triangular Elements

From *Figure 6.12* to *Figure 6.15*, the residual loads for 2mm mesh size are 188 N and 1061 N, 5mm mesh size are 650 N and 914 N, 10mm mesh size are 1831 N and 2501 N and for 25mm mesh size are 3738 N and 3849 N for triangular and quadrilateral meshing, respectively. There is an increase in the ratio of residual load to peak load observed with increase in mesh size, except for the increase from 2mm quadrilateral mesh to 5mm quadrilateral mesh. This implies that the strain softening nature is diminished with increase in mesh size.

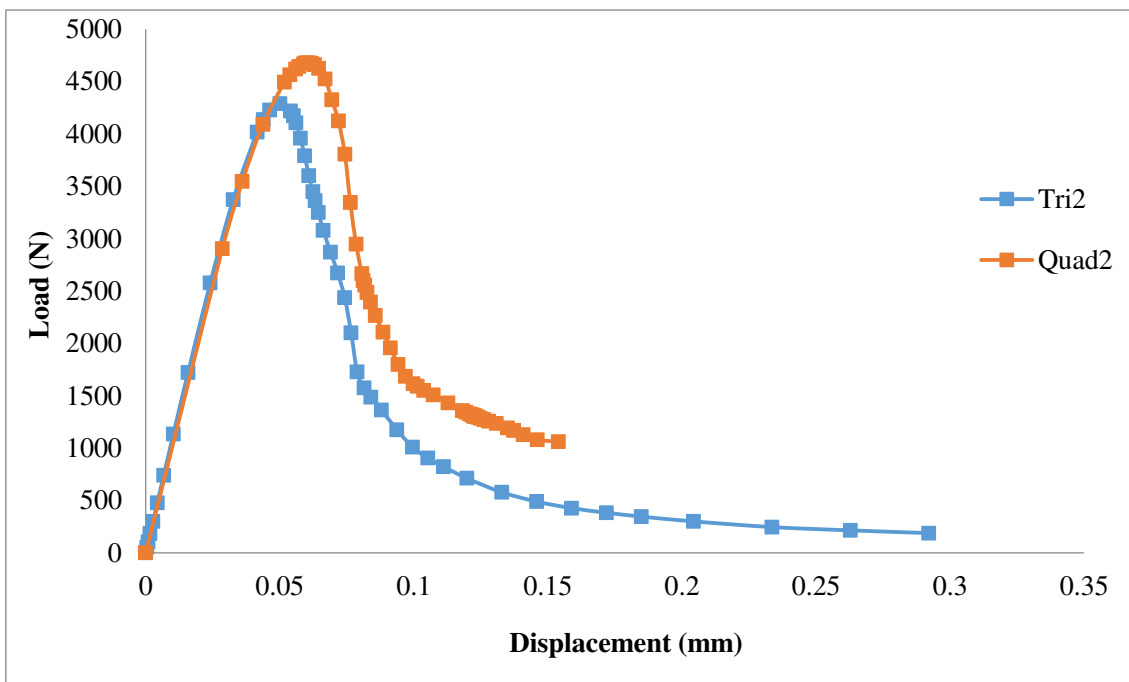


**Figure 6.12** Effect of Mesh Element type using 2mm mesh element size

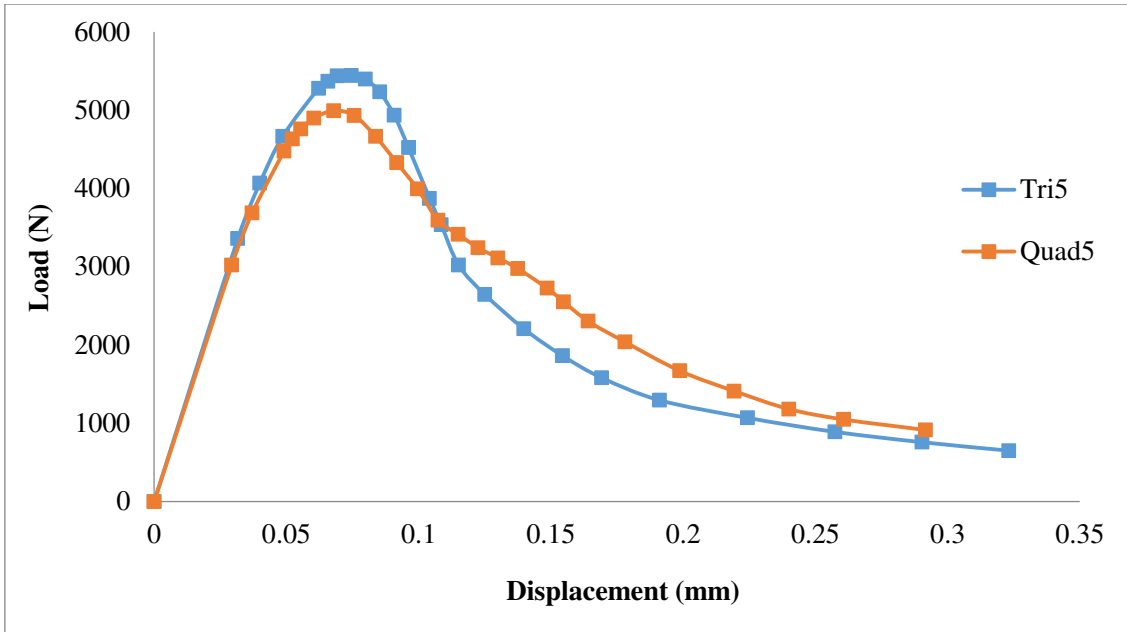


**Figure 6.13**Effect of Mesh Element type using 5mm mesh element size

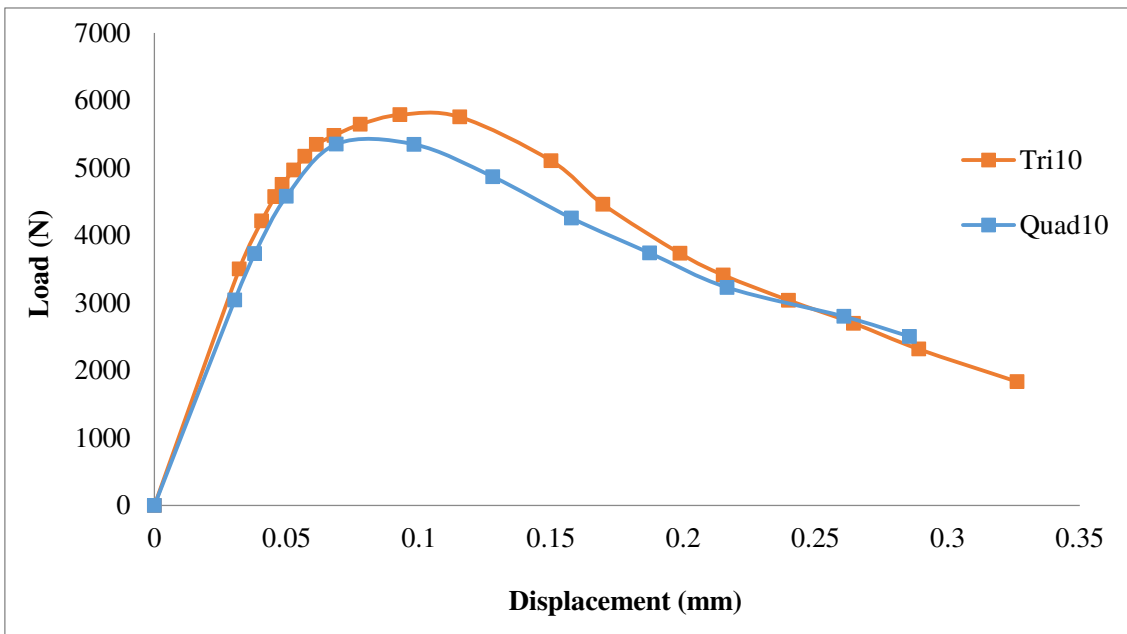


**Figure 6.14**Effect of Mesh Element type using 10mm mesh element size

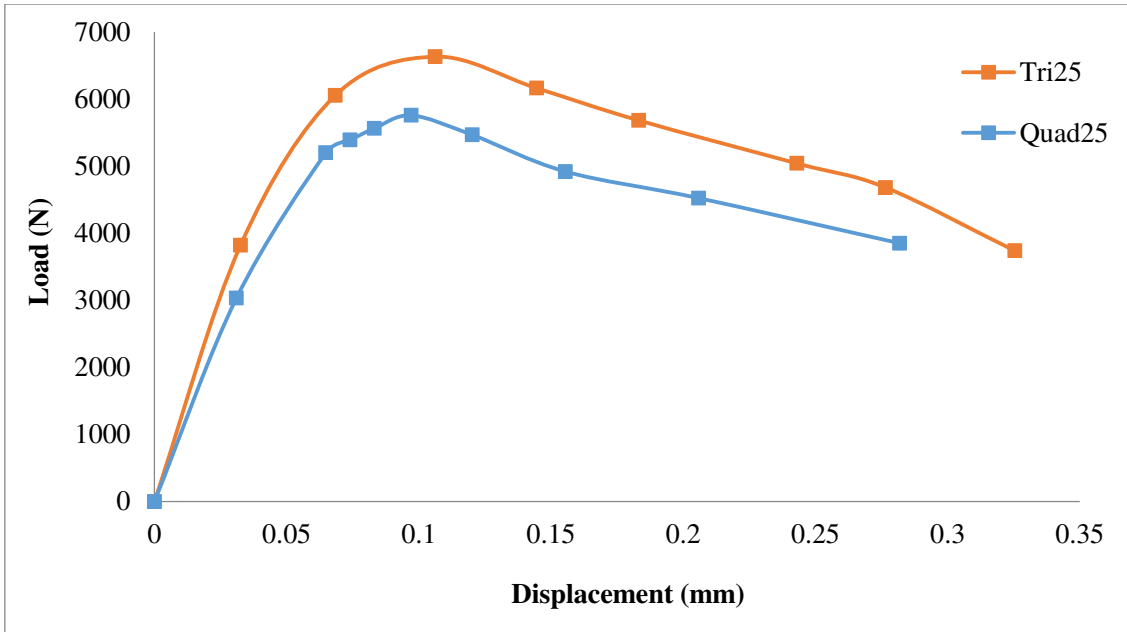


**Figure 6.15** Effect of Mesh Element type using 25mm mesh element size

From *Figure 6.16*, the difference between fracture energies of 25mm and 2mm mesh element sizes are 146.7 *N/m* and 97.0 *N/m* for triangular and quadrilateral meshing, respectively. For 2mm and 5mm mesh element sizes the fracture energies for quadrilateral and triangular elements are almost equal.

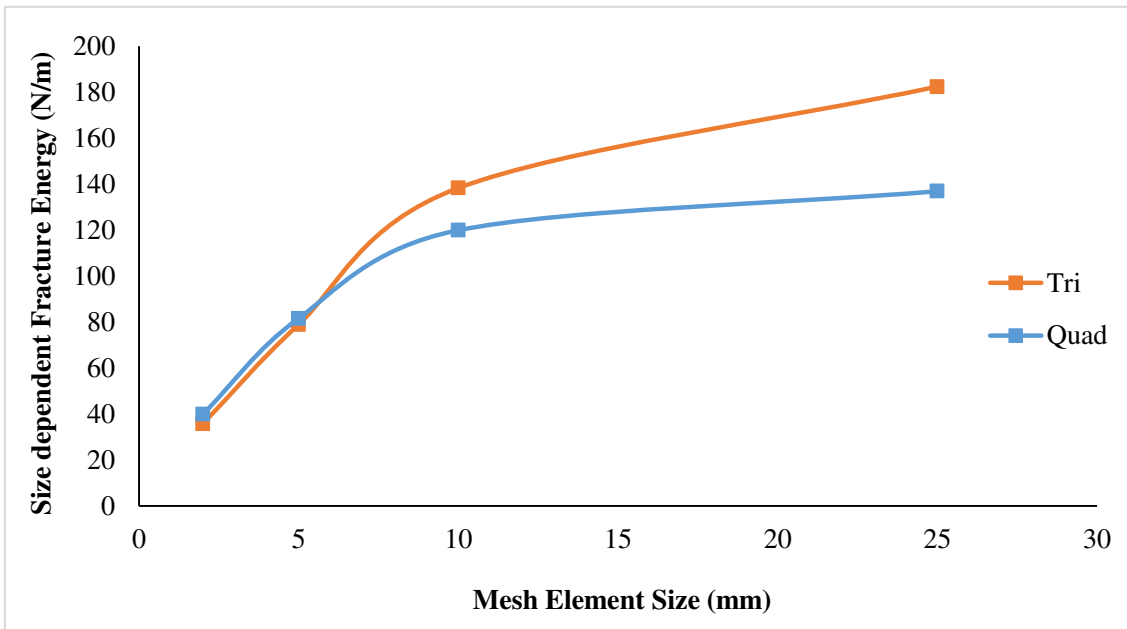


**Figure 6.16** Effect on fracture energy with variation in mesh element type and size

### 6.6.2. Influence of Notch-to-depth ratio ( $a/D$ ) on fracture properties

The notch-to-depth ratio is varied from 0.1 to 0.6 with intervals of 0.1. This study is done for M50 grade of concrete with Eccentricity ( $\varepsilon$ ) 0.01, Dilation Angle ( $\psi$ )  $34^\circ$ , Youngs Modulus ( $E_{cm}$ ) value as per IS 456:2000, and compression behaviour modelled as per Hsu and Hsu model. The summary of elements and nodes is given in *Table 6.6*.

**Table 6.6** Summary of FE modelling for various notch-to depth- ratios

|     | Mesh element size | no. of elements | no. of nodes |
|-----|-------------------|-----------------|--------------|
| 0.1 | 5                 | 2417            | 2501         |
| 0.2 | 4.44              | 3036            | 3158         |
| 0.3 | 3.89              | 3996            | 4097         |
| 0.4 | 3.33              | 5396            | 5522         |
| 0.5 | 2.78              | 7764            | 7893         |
| 0.6 | 2.22              | 12356           | 12478        |

The mesh size varies for each  $a/D$  such that each uncracked ligament length ( $D-a$ ) is divided into 18 parts.

From *Figure 6.17* and *Figure 6.18*, the peak loads for each notch-to-depth ratio from 0.1 to 0.6, in the same order, are: 7961 N, 6094 N, 4846 N, 3518 N, 2455 N, and 1615 N. The residual loads for each notch-to-depth ratios, from 0.1 to 0.6, are: 1397 N, 873 N, 856 N, 248 N, 450 N, and 141 N respectively. The average ratio of residual load to peak load is 13.9% , with a standard deviation of 2.2% .

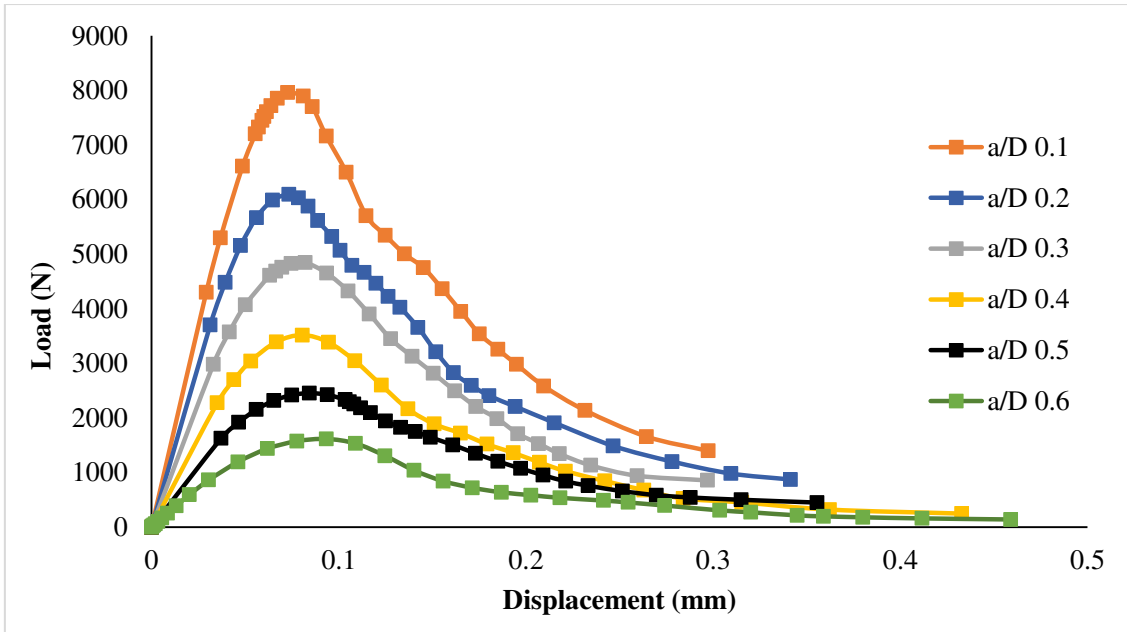


**Figure 6.17** Load-Displacement curves for different notch-to-depth ratios (M50 Grade Concrete)

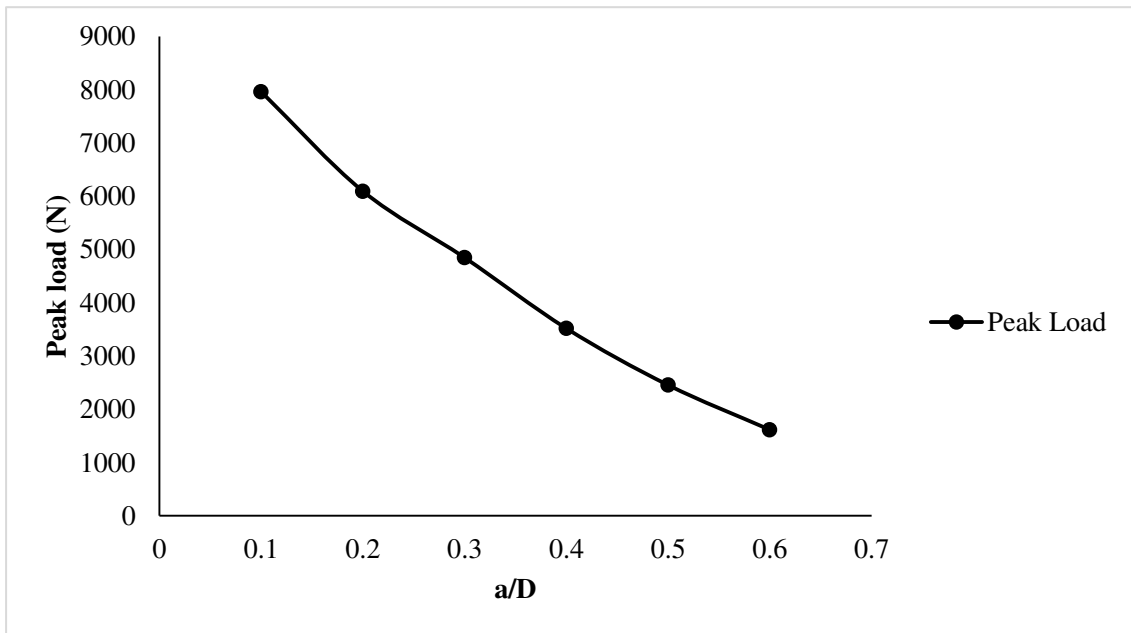


**Figure 6.18** Effect on peak loads with varying notch-to-depth ratios (M50 Grade Concrete)



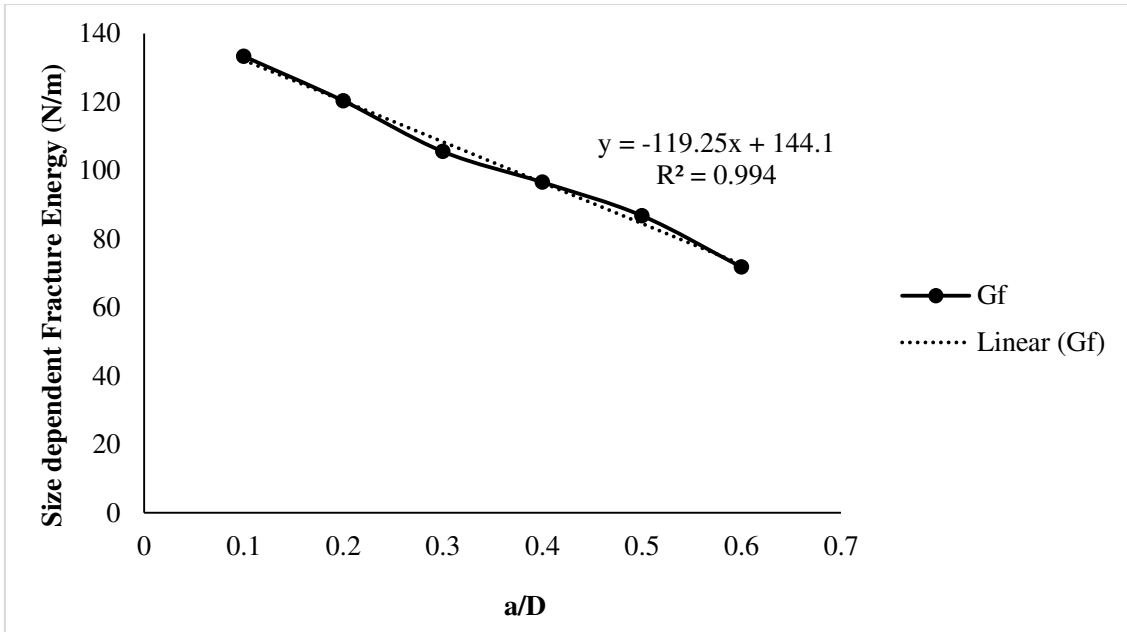


**Figure 6.19** Effect on fracture energy with variation in notch-to-depth ratio (M50 Grade Concrete)

From *Figure 6.19*, the fracture energies at each notch-to-depth ratio from 0.1 to 0.6, in order, are: 133.3 N/m, 120.3 N/m, 105.5 N/m, 96.5 N, 86.8 N/m, and 71.8 N/m, respectively. These values a linear trend with  $R^2$  value of 0.994 and  $RMSE$  value of 1.59 N/m.

**Table 6.7** Validation of numerical work - 1

| Notch-to-depth Ratio             | Size Dependent Fracture Energy Value (N/m) |                             |
|----------------------------------|--|-----------------------------|
|                                  | Numerical Model                            | Murthy <i>et.al.</i> (2013) |
|                                  | M50 ( $f_{cm} = 58.18MPa$ )                | NSC ( $f_{cm} = 57.1MPa$ )  |
| 0.1                              | 133.3                                      | 135.3                       |
| 0.2                              | 120.3                                      | 107.5                       |
| 0.3                              | 105.5                                      | 95.5                        |
| Size independent Fracture Energy | as per Modified BEM<br>188.1               | as per BEM<br>190.3         |

From Table 6.7, the % difference between numerical values from the experimental values for notch-to-depth ratios 0.1, 0.2, and 0.3 are 1.48%, -11.91%, and -10.47% respectively. The % difference in the numerically obtained Size independent fracture energy (using modified boundary effect) and the experimentally obtained Size independent fracture energy is 1.16%

### 6.6.3. Influence of Eccentricity and Dilation Angle on fracture properties

The CDP parameters, Eccentricity ( $\epsilon$ ) and Dilation Angle ( $\psi$ ), are varied to investigate their effect on fracture energy and characteristic length. The beams are modelled for  $E_{cm}$  values as per IS 456:2000 and compressive behaviour as per Hsu and Hsu, 1994 model. This study has been done for M20 and M40 grades of concrete.

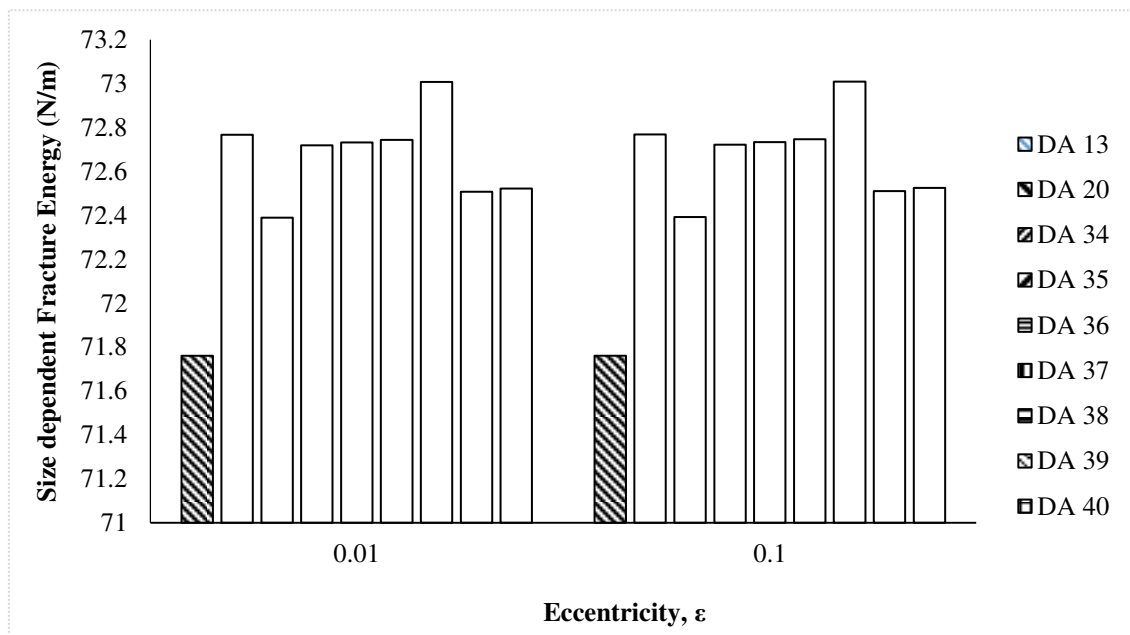


Figure 6.20 Effect on Fracture energy with variation in  $\epsilon$  and  $\psi$  ( $a/D = 0.1$ ) using M20 grade of concrete

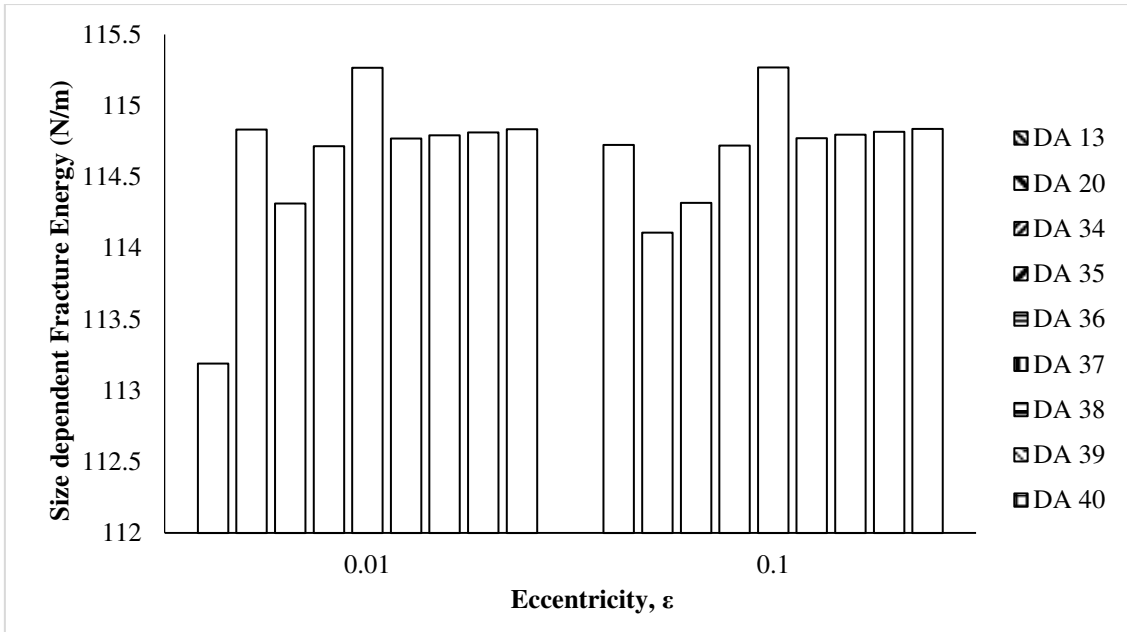


Figure 6.21 Effect on Fracture energy with variation in  $\epsilon$  and  $\psi$  ( $a/D = 0.1$ ) using M40 grade of concrete

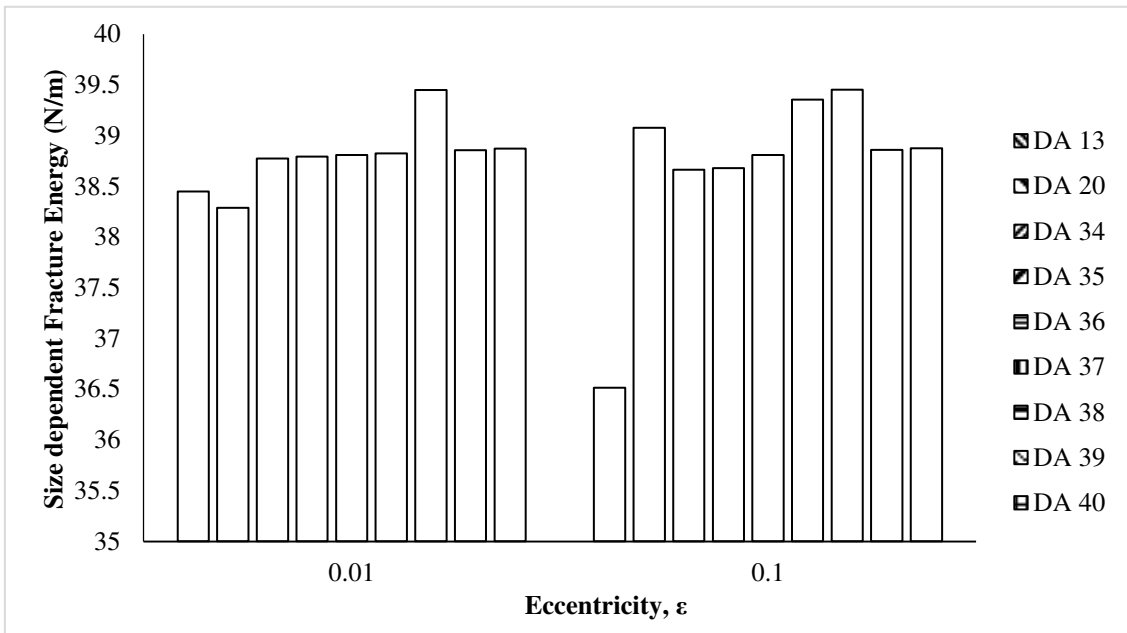
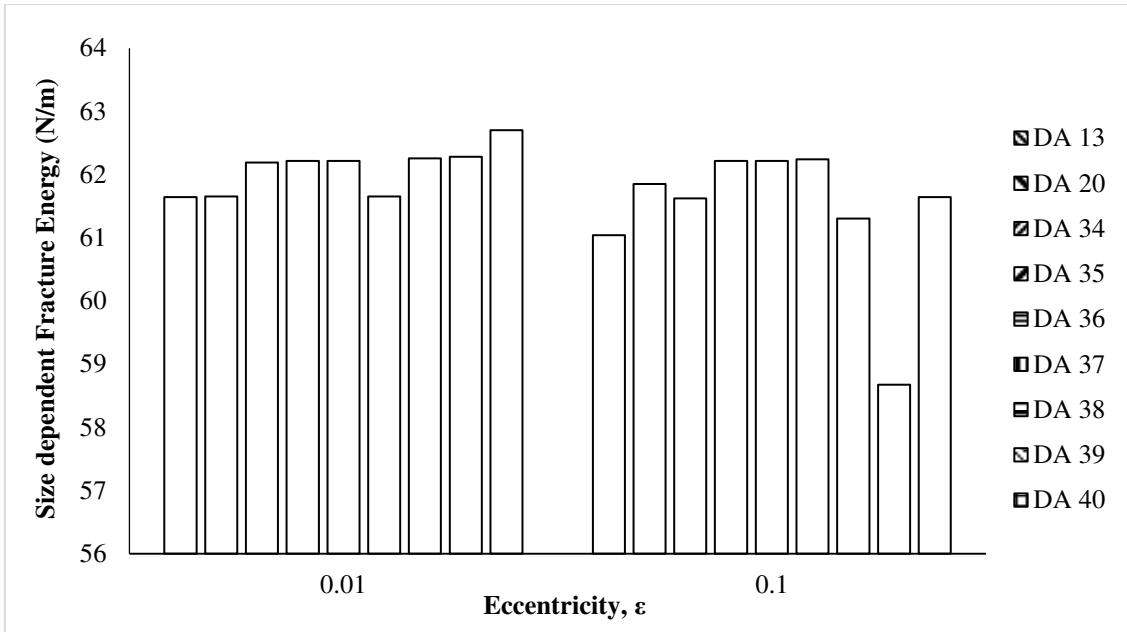
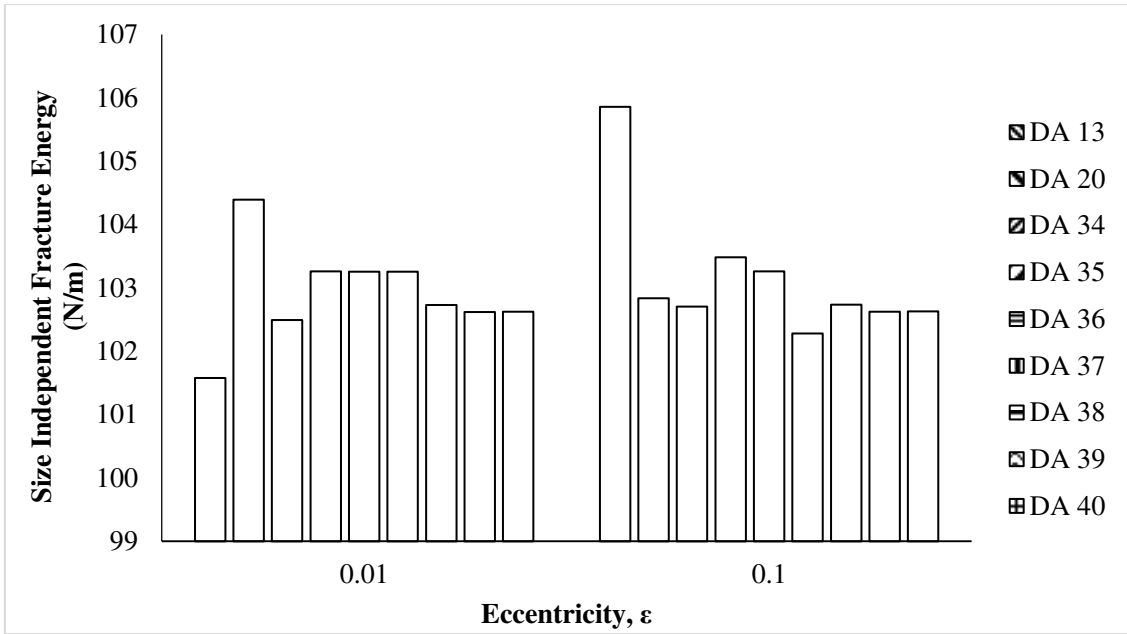


Figure 6.22 Effect on Fracture energy with variation in  $\epsilon$  and  $\psi$  ( $a/D = 0.6$ ) using M20 grade of concrete



**Figure 6.23** Effect on Fracture energy with variation in  $\varepsilon$  and  $\psi$  ( $a/D = 0.6$ ) using M40 grade of concrete

From *Figure 6.20* and *Figure 6.21*, the average fracture energy for M20 and M40 grade of concrete with notch-to-depth ratio 0.1 are 72.6 N/m and 114.6 N/m for eccentricity 0.01, and 72.6 N/m and 114.7 N/m for eccentricity 0.1, respectively. The maximum % deviations from the average values, in the same order as above, are 1.12%, 1.24%, 1.12% and 0.52%. Similarly, from *Figure 6.22* and *Figure 6.23*, the average fracture energy for M20 and M40 grade of concrete with notch-to-depth ratio 0.6 are 38.8 N/m and 62.1 N/m for eccentricity 0.01, and 38.7 N/m and 61.4 N/m for eccentricity 0.1, respectively. The maximum % deviations from the average values, in the same order as above, are 1.70%, 0.99%, 5.64% and 4.48%.



**Figure 6.24** Effect on Size Independent fracture energy with variation in  $\epsilon$  and  $\psi$  using M20 grade of concrete

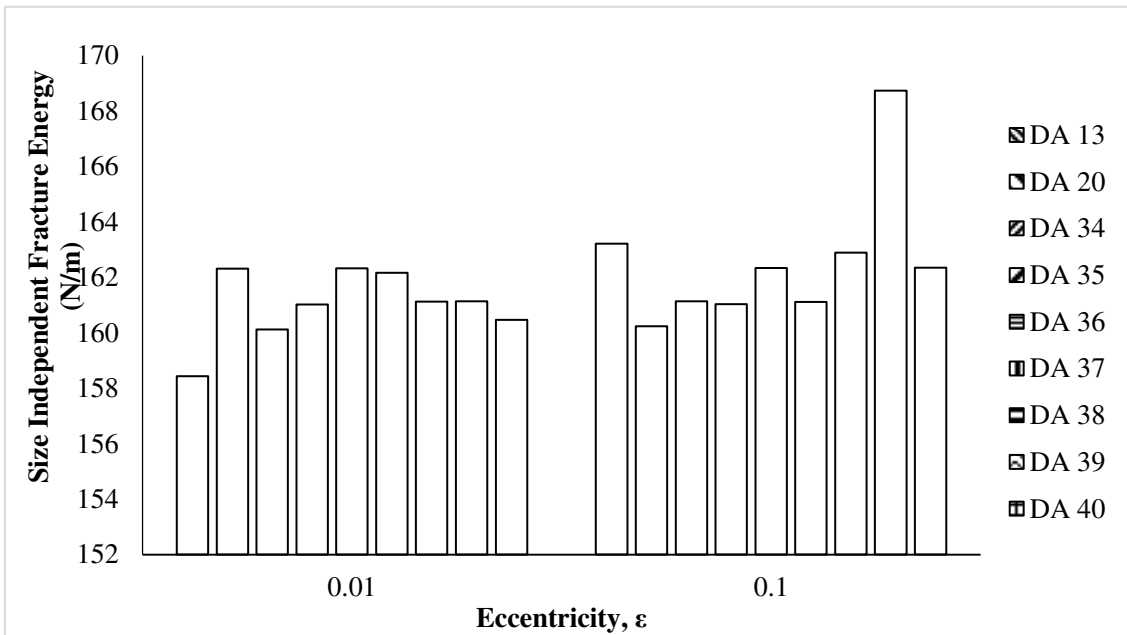


**Figure 6.25** Effect on Size Independent fracture energy with variation in  $\epsilon$  and  $\psi$  using M40 grade of concrete

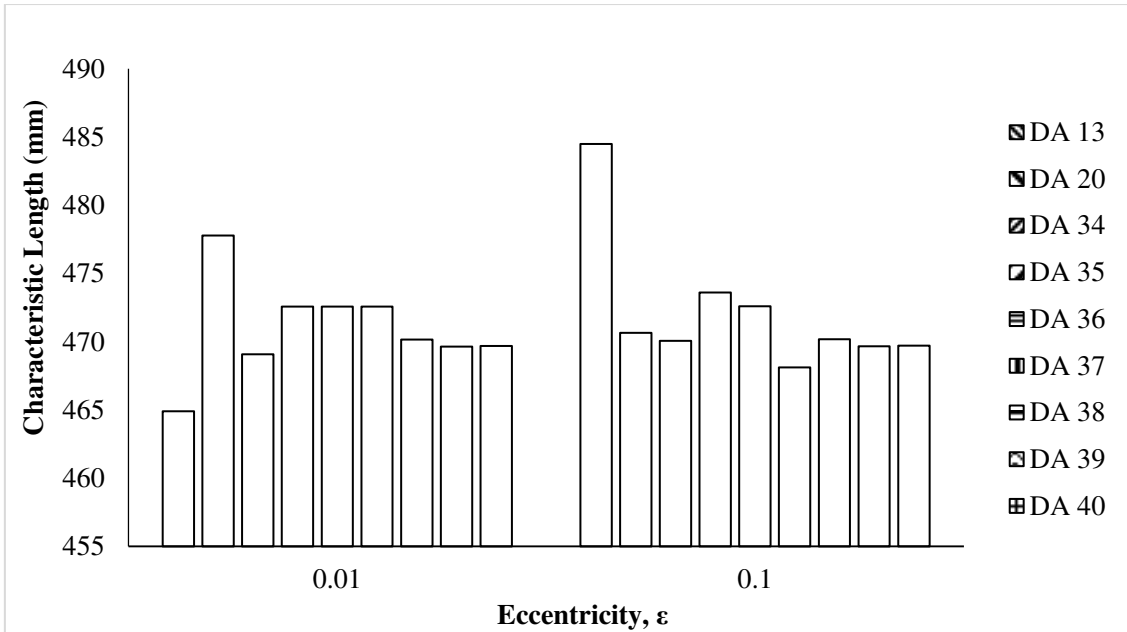


**Figure 6.26** Effect on Characteristic Length with variation in  $\epsilon$  and  $\psi$  using M20 grade of concrete

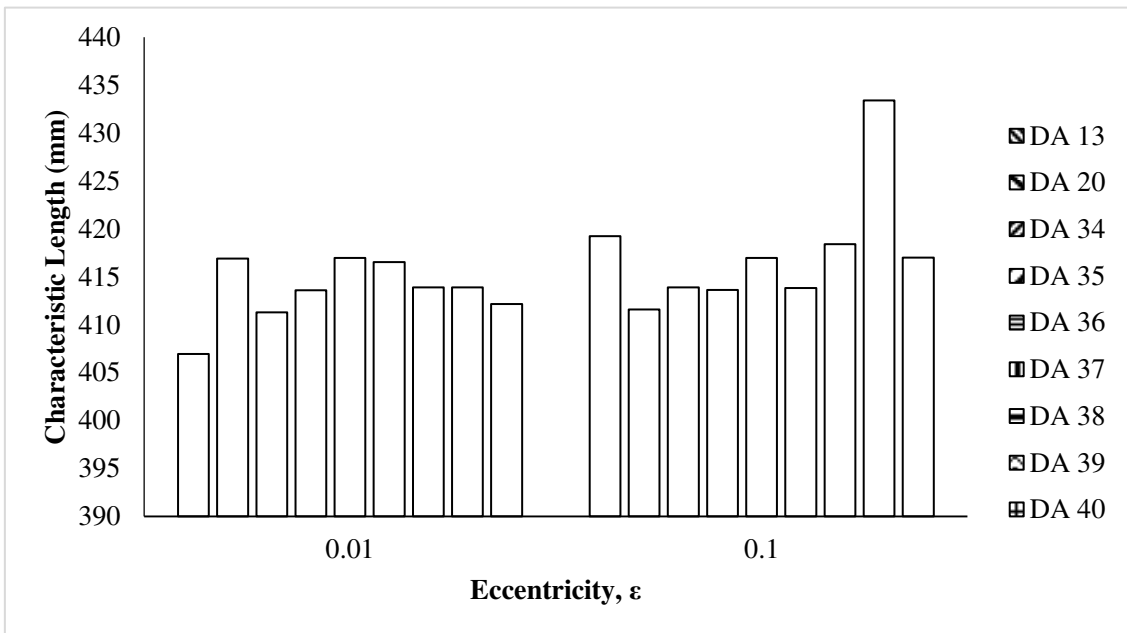


**Figure 6.27** Effect on Characteristic Length with variation in  $\epsilon$  and  $\psi$  using M40 grade of concrete

From *Figure 6.24* and *Figure 6.25*, the average Size independent fracture energy for M20 and M40 grade of concrete are 102.9 N/m and 161.0 N/m for eccentricity 0.01, and 103.2

N/m and 162.6 N/m for eccentricity 0.1, respectively. The maximum % deviations from the average values, in the same order as above, are 1.44%, 1.60%, 2.62% and 3.80%.

From *Figure 6.26 and Figure 6.27*, the average characteristic length for M20 and M40 grade of concrete are 471.0mm and 413.6mm for eccentricity 0.01, and 472.1mm and 417.5mm for eccentricity 0.1, respectively. The maximum % deviations from the average values, in the same order as above, are 1.44%, 1.60%, 2.62% and 3.80%.

#### **6.6.4. Comparative analysis of Hsu & Hsu and Saenz model on fracture properties for various grades of concrete**

As discussed in section 6.3.1, compression behaviour is modelled in two different ways. It was found that the initial tangent modulus while modelling compressive stress-strain curve using Saenz model was more than the input value of  $E_{cm}$ . Thus, one more refinement is suggested for Saenz Model. The initial part of the Saenz model is substituted with a straight line passing through origin and slope  $E_{cm}$  until the line intersects the Saenz Curve as explained in section 6.3.1.1. *Figure 6.28* shows the described modification.

The above described modification leads to a decrease in the peak stress for grades of concrete above M25 but is necessary to refrain it from generating negative inelastic and plastic strain values.

A comparative analysis is done by adopting the two chosen models with varying a/d ratios for a chosen dilation angle and eccentricity. The value of eccentricity for this study is adopted to be 0.01, Dilation angle is  $34^\circ$ , and  $E_{cm}$  values are adopted as per IS 456:2000. The effect of adopting both Hsu & Hsu and Saenz model on size dependent fracture energy and the characteristic length is discussed below.

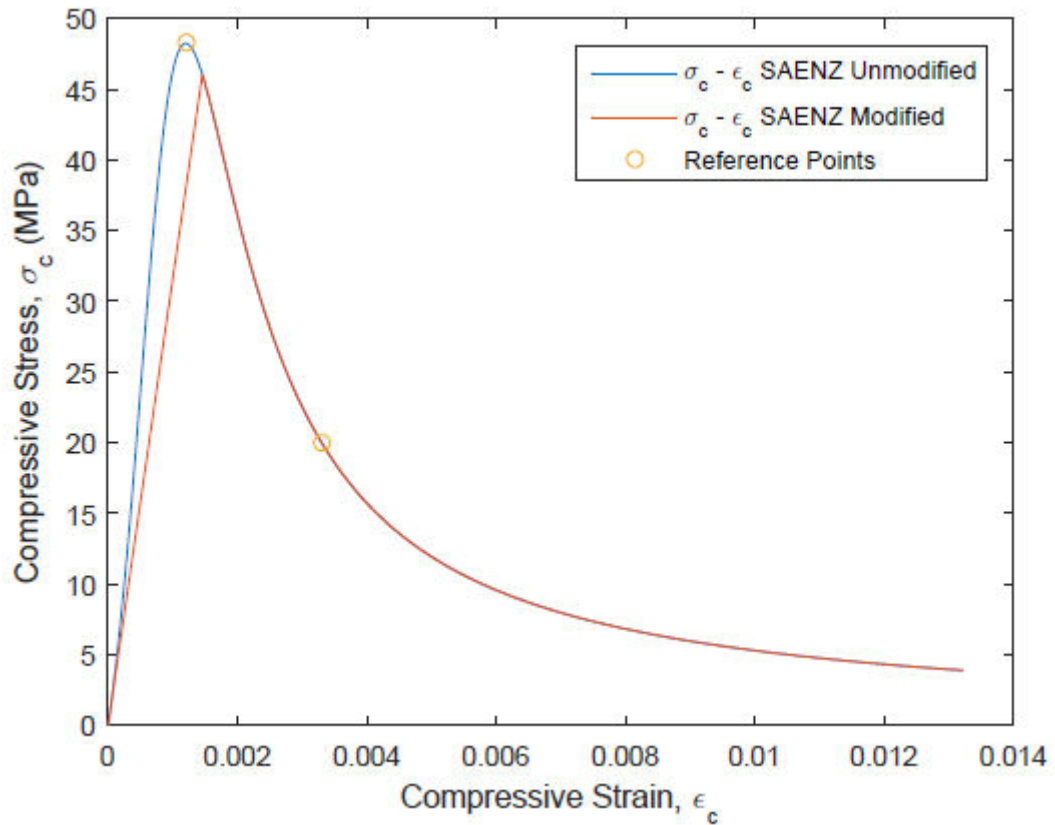


Figure 6.28 Saenz Model Compression Curve (M40) - with and without modification

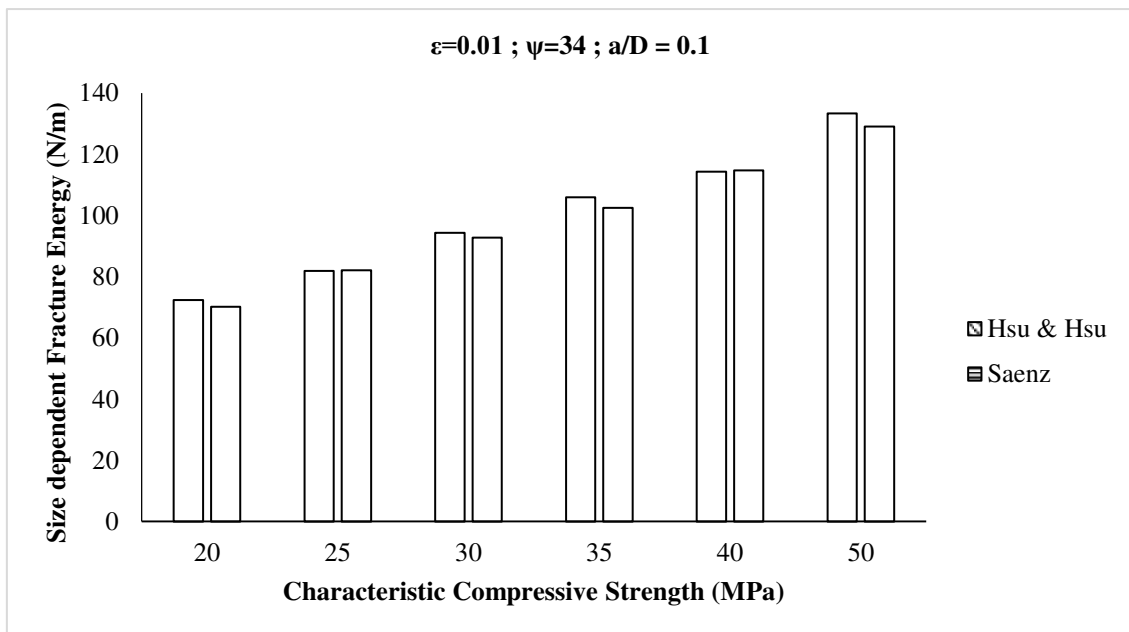
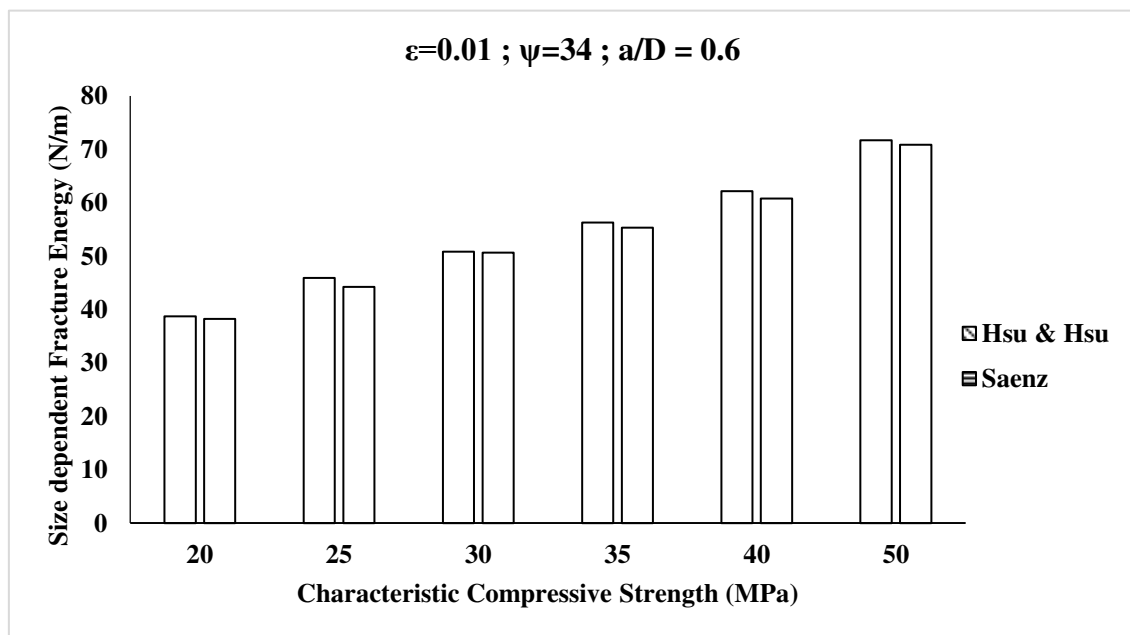


Figure 6.29 Effect on fracture energy with varying grade of concrete and Compressive behaviour Design model ( $a/D = 0.1$ )



From

**Figure 6.29**, the fracture energy for notch-to-depth ratio 0.1 increases at an average of 10.5 N/m (standard deviation = 1.1 N/m) for each subsequent grade of concrete starting from M20 to M40 for Hsu & Hsu Model. The average for Saenz Model is 11.1 N/m (standard deviation = 0.7 N/m). The fracture energy values, for notch-to-depth ratio 0.1, obtained using Saenz model are, at an average, 1.8 N/m (standard deviation = 0.9 N/m) less than those obtained using Hsu & Hsu model.



**Figure 6.30** Effect on fracture energy with varying grade of concrete ( $a/D = 0.6$ )

From *Figure 6.30*, the fracture energy for notch-to-depth ratio 0.6 increases at an average of 5.9 N/m (standard deviation = 0.5 N/m) for each subsequent grade of concrete starting from M20 to M40 for Hsu & Hsu Model. The average for Saenz Model is 5.6 N/m (standard deviation = 0.4 N/m). The fracture energy values, for notch-to-depth ratio 0.6, obtained using Saenz model are, at an average, 0.9 N/m (standard deviation = 0.2 N/m) less than those obtained using Hsu & Hsu model.

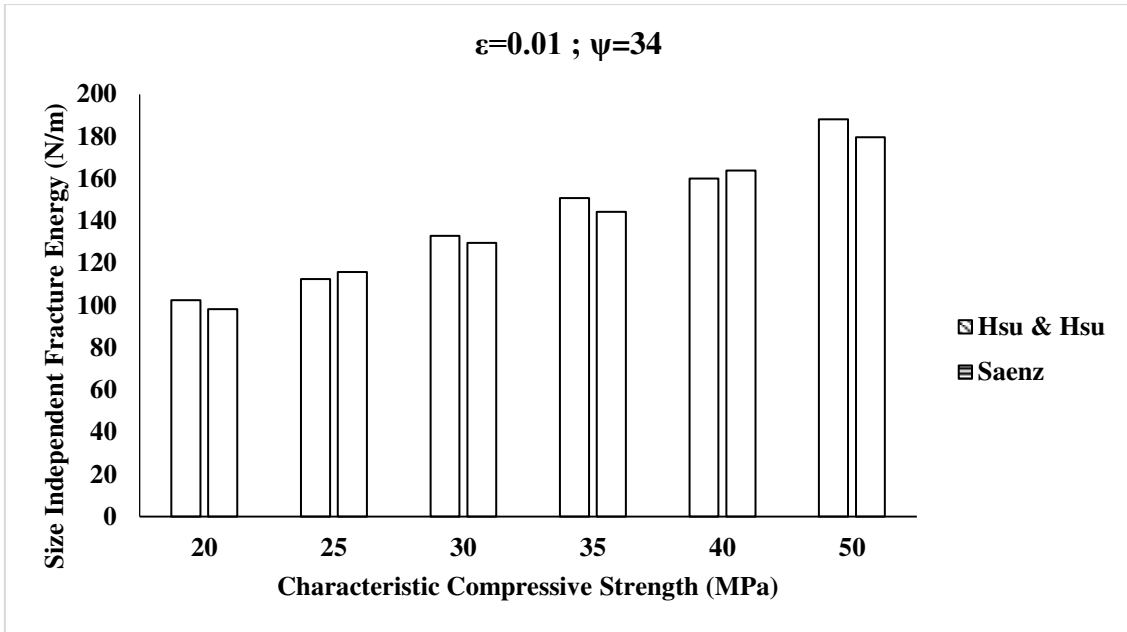


**Figure 6.31** Effect on Size independent fracture energy with varying grade of concrete

From *Figure 6.31*, the size independent fracture energy increases at an average of 14.4 N/m (standard deviation = 3.2 N/m) for each subsequent grade of concrete starting from M20 to M40 for Hsu & Hsu Model. The average for Saenz Model is 16.4 N/m (standard deviation = 1.5 N/m). The Size independent fracture energy values, obtained using Saenz model are, at an average, 2.6 N/m (standard deviation = 2.2 N/m) less than those obtained using Hsu & Hsu model.

From *Figure 6.32*, the characteristic length decreases at an average of 14.4mm (standard deviation = 12.4mm) for each subsequent grade of concrete starting from M20 to M40 for Hsu & Hsu Model. The average for Saenz Model is 7.2mm (standard deviation = 5.7mm). The characteristic length values obtained using Saenz model are, at an average, 7.6mm (standard deviation = 6.6mm) less than those obtained using Hsu & Hsu model.

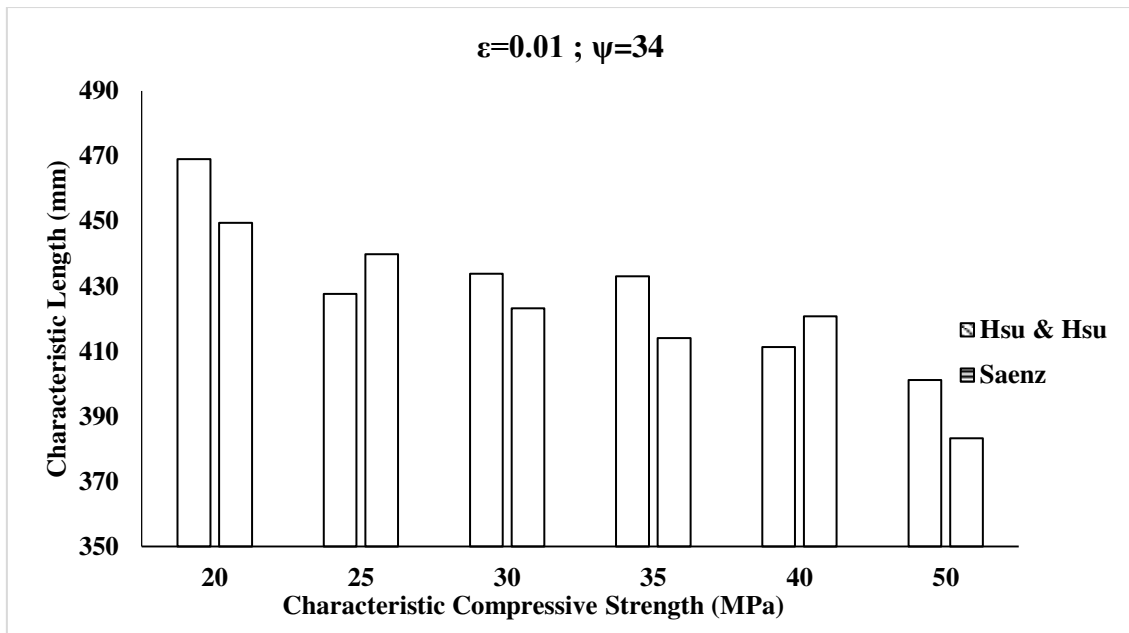


Figure 6.32 Effect on characteristic length with varying grade of concrete

Table 6.8 Validation of numerical work - 2

| Notch-to-depth Ratio             | Size dependent Fracture Energy Value ( Nm ) |                                      |                                   |
|----------------------------------|---|--------------------------------------|-----------------------------------|
|                                  | Numerical Model                             | Alyhya <i>et al.</i> , (2016)        |                                   |
|                                  | Hsu and Hsu M30<br>( $f_{cm} = 38.20MPa$ )  | Saenz M30<br>( $f_{cm} = 37.49MPa$ ) | Mix 30A<br>( $f_{cm} = 35.4MPa$ ) |
| 0.1                              | 94.3  | 92.8                                 | 96.2                              |
| 0.6                              | 50.9  | 50.7                                 | 53.5                              |
| Size independent fracture energy | as per Modified BEM                         |                                      |                                   |
|                                  | 132.9                                       | 129.7                                | 132.8                             |

From Table 6.8, the % difference between numerical fracture energy values from the experimental fracture energy value for notch-to-depth ratio 0.1 are 1.98% and, 3.53% for Hsu & Hsu model, and Modified Saenz Model, respectively. The percentage difference valued for notch-to-depth ratio 0.6 is 4.86% and 5.23%, for Hsu & Hsu model, and Modified Saenz

Model respectively. The % differences in the numerically obtained Size independent fracture energies (using modified BEM) and the experimentally obtained Size independent fracture energy are -0.08% and 2.33%, for Hsu & Hsu, and Saenz model respectively.

### 6.6.5. Influence of varying tensile damage value on fracture energy

The final tensile damage value, previously considered as 0.9 for all cases, is increased to determine its impact on fracture energy. This variation is done for M40 grade of concrete beam designed for  $E_{cm}$  as per EUROCODE2, Compression behaviour as per Hsu and Hsu model, Eccentricity 0.01, Dilation Angle  $34^\circ$  and  $a/D$  0.1.

From *Figure 6.33*, the fracture energy remains constant when the  $d_t$  value is increased from 0.9 to 0.97 at 110.0 N/m, then  $G_f$  decreases by 2.6 N/m when  $d_t$  is increased from 0.97 to 0.98 and finally  $G_f$  decreases by 1.5N/m when  $d_t$  is increased from 0.98 to 0.995. The corresponding decreases in the peak loads are 0.1 N, 2.4 N, and 38 N respectively *Figure 6.34*.

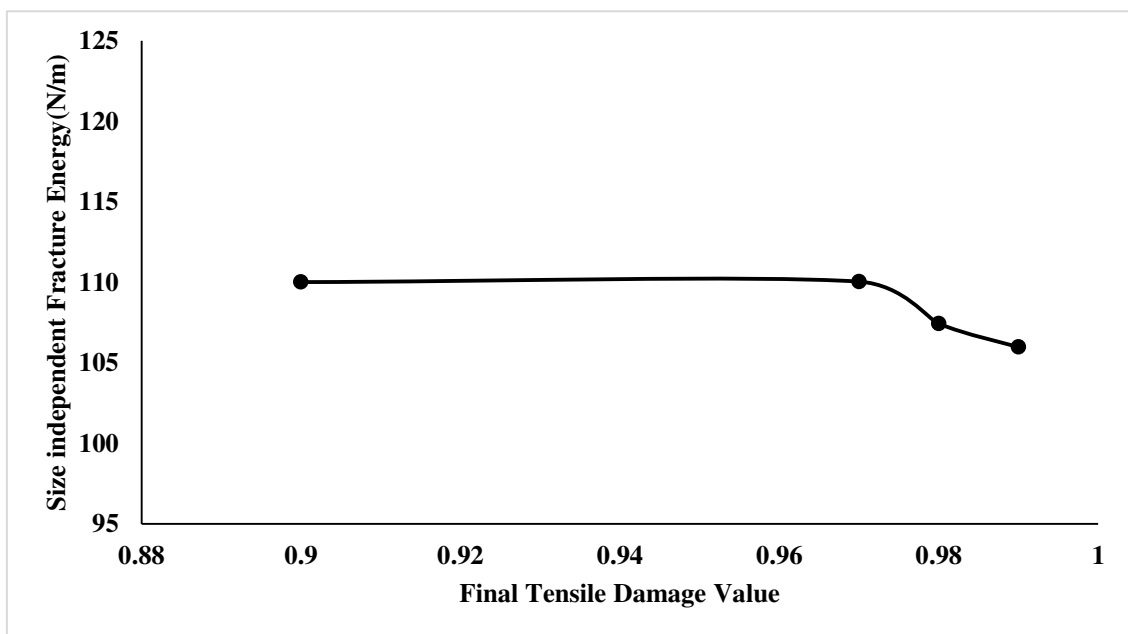


**Figure 6.33**Effect on fracture energy with variation in maximum tensile damage value

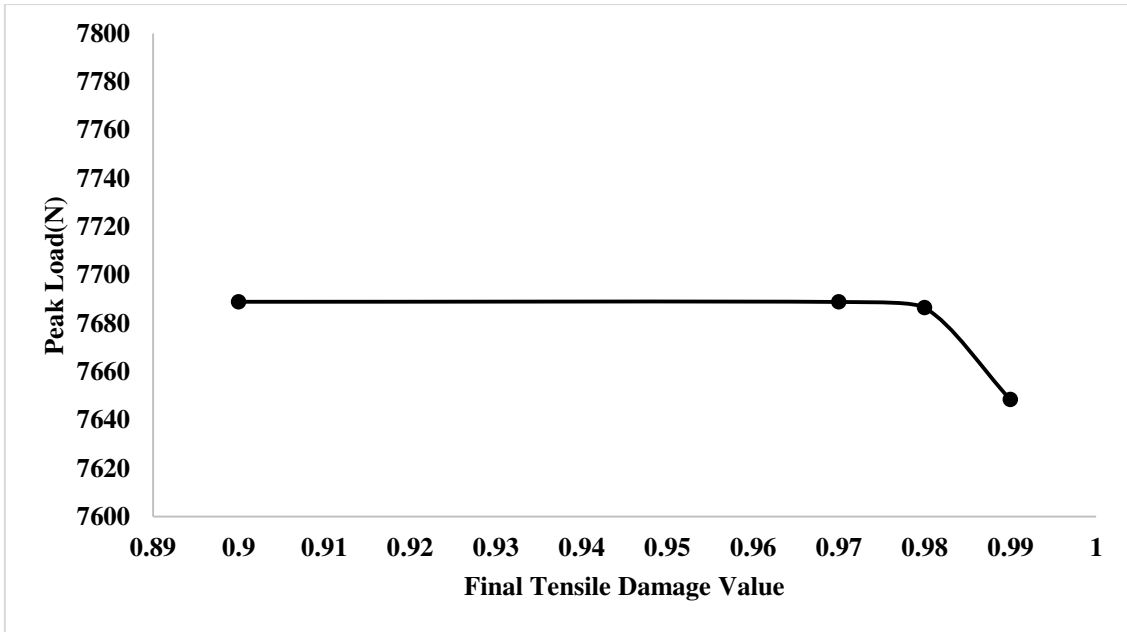


**Figure 6.34** Effect on peak load with variation in maximum tensile damage value

Figure 6.35 shows the contours of tensile damage crack propagation for a/d ratios 0.1 and 0.6.

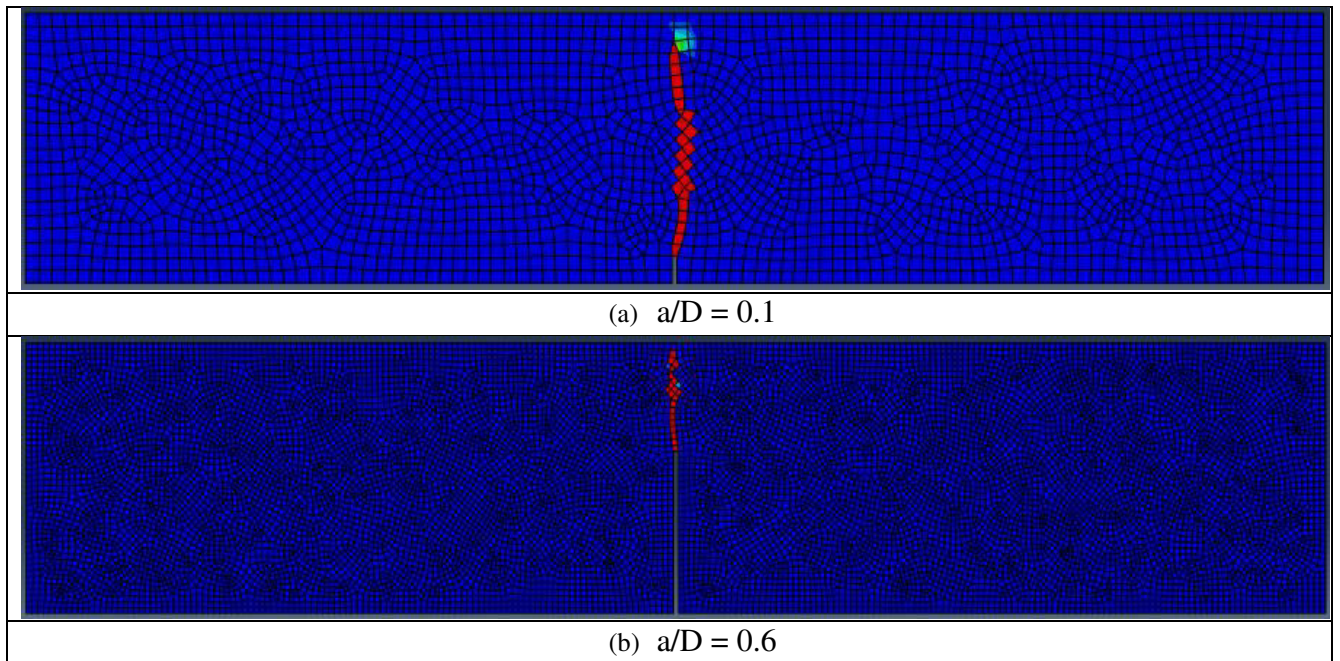


**Figure 6.35** Tensile damage propagation path

This chapter concludes with the evaluation of fracture properties of concrete using CDP model and same has been validated with the existing experimental work. Next chapter summarizes the conclusions of research work.

# CHAPTER 7

## CONCLUSIONS

The present investigation dealt with the proportioning SCC mixes with and without fibers based on the plastic viscosity of the cement paste and mix. Experimental investigations are performed to assess the fresh and hardened properties of SCC mixes. Fracture properties of ternary based SCC mixes with and without fibers are also investigated.

Numerical studies using Damage plasticity model incorporating modified Saenz model and Hsu model are adopted to evaluate the fracture properties of concrete.

Based on the experimental investigation and numerical analysis and the results obtained the following conclusions are drawn.

1. Plastic viscosity of cement pastes decreased with the increase in water to binder ratio and superplasticizer dosage
2. A new methodology to proportion SCC mixes with one of the rheological parameters is successfully achieved for all the combinations of SCC mixes with and without fibres.
3. The volume of paste decreases and volume of solids increases with an increase in plastic viscosity of the mix, which is an indication of an increase in aggregate content and decrease in cement content.
4. Slump flow,  $T_{500}$ , and J-ring spread increased while V-funnel time and L-box blocking ratio decreased with the increase in plastic viscosity of the mix.
5. SCC mixes with CRF resulted in better deformability compared to mixes with river sand. The maximum reduction in slump flow of 4.67% is observed for ternary SCC mix with CRF.
6. Filling and passing abilities of SCC mixes from various tests indicated that the mixes with CRF have shown better performance compared to the mixes with river sand. This is attributed to the presence of a larger amount of fines in CRF and silt content in river sand.
7. Compressive strength, split tensile strength and flexural strength decreased with the increase in plastic viscosity of the mix due to the reduction of the volume of paste and increase in the volume of solids. Maximum strength is observed for SCC mix with 100% OPC for all the chosen plastic viscosities.

8. For a given plastic viscosity of the mix, compressive strength, split tensile strength and flexural strength decreased for SCC mixes with river sand compared to SCC mixes with CRF.
9. For M40 grade concrete, an assumed plastic viscosity of 9 Pa s with water to binder ratio of 0.57 and a plastic viscosity of 13 Pa s with water to binder ratio of 0.5 is found to be suitable for proportioning SCC mixes to satisfy the fresh and hardened properties in making the mixes practically feasible.
10. Ternary SCC mixes with hooked end steel fibres with increasing fibre dosage resulted in poor workability. Especially at a volume fraction of 0.5%, the blockage is observed for L-box and J-ring spread. This is mainly because of non-uniform and random distribution of fibres in the fresh state of concrete mixes.
11. Compressive strength, split tensile strength and flexural strength increased with the increase in fibre content for ternary SCC mixes. The strength increment is more in the case of flexure compared to compression or split tension. Strength gain of 8.45%, 12.11% and 28.25% is observed to be the maximum in compression, split tensile and flexure for mix with 0.5% fibres compared to the mix without fibres.
12. Fracture energy increased with the increase in fibre content indicating that the crack growth rate is reduced with the presence of fibres.
13. The Saenz Model is successfully modified to the needs of Concrete Damaged Plasticity model, such that it doesn't generate negative inelastic strain values.
14. Due to high deviations in peak loads in triangular elements with an increase in mesh size, quadrilateral elements should be preferred for numerical analysis.
15. A reduction in peak loads and fracture energy is observed with increasing notch-to-depth ratio. The strain-softening behaviour is negligibly affected by an increase in the notch-to-depth ratio.
16. The change in eccentricity and dilation angle has a negligible impact on both, fracture energy and characteristic length.
17. Fracture energy increases and characteristic length decreases with increase in characteristic compressive strength of concrete, using both, Hsu & Hsu, and Saenz, models.
18. The fracture energy and peak load carrying capacity are found to be reduced with an increase in final tensile damage value.
19. The proposed CDP model is able to predict fracture properties of concrete which are at par with the experimentally obtained values.

---

## CONTRIBUTIONS FROM THE STUDY

---

1. Brookfield Viscometer is used to measure the plastic viscosity of cement pastes with binary and ternary combinations.
2. Proportioning of binary and ternary SCC mixes with crushed rock fines as fine aggregate and hooked end steel fibres is done based on the plastic viscosity of the mix for the first time.
3. This study suggests the use of crushed rock fines as fine aggregate compared to river sand which will enhance the fresh and hardened properties of SCC mixes.
4. Modified version of Saenz model is proposed for the first time to evaluate the fracture properties of concrete.
5. Concrete Damage Plasticity model is used for the first time in combination with Hsu and Hsu model to evaluate the fracture properties of concrete and validated the same with the published work.



---

## SCOPE FOR FUTURE WORK

---

1. In the present study, two water to binder ratios are adopted to proportion the SCC mixes. To make this methodology more application oriented, the same can be extended for proportioning SCC mixes with different water to binder ratios.
2. Role of Viscosity Modifying Agent (VMA) on the plastic viscosity of the mix has not been addressed in the present study. VMA will make the mixes more viscous and proposed methodology can be extended for higher plastic viscosities.
3. In the present study, a constant superplasticizer dosage of 1.25% is maintained for all ternary combination of SCC mixes with varying fibre content. In a practical scenario, sometimes there is a need of using fibres more than 0.5%. So there is a need to explore the influence of SP dosage on fresh and hardened properties of SCC mixes with increasing fibre content.
4. In the present study, only fresh and hardened properties of SCC mixes with and without fibres are investigated. The study can be extended to assess the durability aspects of the SCC mixes.
5. The present study can also be extended to the influence of different types of fibres for different aspect ratios on the fresh and hardened properties of SCC
6. Two stress-strain models i.e. Hsu & Hsu model and Saenz model are adopted to numerically evaluate the fracture properties of concrete. The accuracy of other stress-strain models in evaluating the fracture properties can be explored with and without fibres.
7. Tensile stress-strain data and tensile damage are adopted from existing models in the present study. Stress versus crack width relations can be formulated using inverse analysis for generating bi-linear tension softening curves.
8. The proposed numerical analysis can be extended to size effect related studies.

## REFERENCES

- Abhijeet, G. and VinayakRam V. (2014). "Role of supplementary cementitious materials in Self Compacting Concrete: A review." *The Indian Concrete Journal*. 88(6), 42-59.
- Abo Dhaheer, M.S., Al-Rubaye, M.M., Alyhya, W.S., Karihaloo, B.L. and Kulasegaram, S., (2016). "Proportioning of self-compacting concrete mixes based on target plastic viscosity and compressive strength: Part I-mix design procedure." *Journal of Sustainable Cement-Based Materials*, 5(4), pp.199-216.
- Abo Dhaheer, M.S., Al-Rubaye, M.M., Alyhya, W.S., Karihaloo, B.L. and Kulasegaram, S., (2016). "Proportioning of Self Compacting Concrete mixes based on target plastic viscosity and compressive strength: Part II-experimental validation." *Journal of Sustainable Cement-Based Materials*, 5(4), pp.217-232.
- Abukhashaba, M. I., Mostafa, M. A., & Adam, I. A. (2014). The behaviour of Self Compacting fibre reinforced concrete containing cement kiln dust. *Alexandria Engineering Journal*, 53(2), 341-354.
- Abutaha, F., Razak, H.A. and Kanadasan, J. (2016). "Effect of palm oil clinker (POC) aggregates on fresh and hardened properties of concrete." *Construction and Building Materials*, 112, pp.416-423.
- Aggarwal, P., & Aggarwal, Y. (2011). "Prediction of compressive strength of SELF COMPACTING CONCRETE with fuzzy logic." *World Academy of Science, Engineering and Technology*, 77, 847-854.
- Aggarwal, Y., & Aggarwal, P. (2011). "Prediction of Compressive Strength of Self Compacting Concrete Containing Bottom Ash using Artificial Neural Networks." *World Academy of Science, Engineering and Technology*, 53, 1-6.
- Ahmaruzzaman, M. (2010). "A review on the utilization of fly ash." *Progress in energy and combustion science*, 36(3), pp.327-363.
- Ahmed, S.F.U. (2012). "Properties of concrete containing construction and demolition wastes and fly ash." *Journal of Materials in Civil Engineering*, 25(12), pp.1864-1870.

- Allam, M.E., Bakhoun, E.S. and Garas, G.L. (2014). "Re-use of granite sludge in producing green concrete." *ARPJ. Eng. Appl. Sci*, 9(12), pp.2731-2737.
- Alqadi, A. N., Mustapha, K. N. B., Naganathan, S., & Al-Kadi, Q. N. (2013). "Development of Self Compacting Concrete using contrast constant factorial design." *Journal of King Saud University-Engineering Sciences*, 25(2), pp.105-112.
- Alyamaç, K.E. and Ince, R., (2009). "A preliminary concrete mix design for Self Compacting Concrete with marble powders." *Construction and Building Materials*, 23(3), pp.1201-1210.
- Alyhya, W., Dhaheer, M.A., Al-Rubaye, M. and Karihaloo, B. (2016), "Influence of mix composition and strength on the fracture properties of Self Compacting Concrete", *Construction and Building Materials*, 110, pp.312 – 322.
- Ambedkar, B., Alex, J. and Dhanalakshmi, J. (2017). "Enhancement of mechanical properties and durability of the cement concrete by RHA as cement replacement: Experiments and modeling." *Construction and Building Materials*, 148, pp.167-175.
- Amin, N.U. (2010). "Use of bagasse ash in concrete and its impact on the strength and chloride resistivity." *Journal of materials in civil engineering*, 23(5), pp.717-720.
- Aslani, F., & Nejadi, S. (2012). Mechanical properties of conventional and Self Compacting Concrete: An analytical study. *Construction and Building Materials*, 36, pp.330-347.
- ASTM (American Society for Testing and Materials) C 1621/C 1621M: Standard Test Method for Passing Ability of Self-Consolidating Concrete by J-Ring.
- Attwa, A. T., & Shaheen, Y. B. (2012). "Behaviour and analysis of cracked self-compacted reinforced concrete beams." *Concrete Research Letters*, 3(1), pp.373-385.
- Babu, K.G. and Kumar, V.S.R. (2000). "Efficiency of GGBS in concrete." *Cement and Concrete Research*, 30(7), pp.1031-1036.
- Bahurudeen, A., Kanraj, D., Dev, V.G. and Santhanam, M. (2015). "Performance evaluation of sugarcane bagasse ash blended cement in concrete." *Cement and Concrete Composites*, 59, pp.77-88.

- Barnes, H. A., Hutton, J. F., & Walters, K. (1989). "An introduction to rheology" (Vol. 3). *Elsevier*.
- Batchelor, G.K., (1977). "The effect of Brownian motion on the bulk stress in a suspension of spherical particles." *Journal of fluid mechanics*, 83(1), pp.97-117.
- Bentz, D.P., Garboczi, E.J., Haecker, C.J. and Jensen, O.M., (1999). "Effects of cement particle size distribution on performance properties of Portland cement-based materials." *Cement and Concrete Research*, 29(10), pp.1663-1671.
- Beycioğlu, A., & Aruntaş, H. Y. (2014). "Workability and mechanical properties of Self Compacting Concretes containing LLFA, GBFS and MC." *Construction and Building Materials*, 73, pp. 626-635.
- Beygi, M. H., Kazemi, M. T., Amiri, J. V., Nikbin, I. M., Rabbanifar, S., & Rahmani, E. (2014). "Evaluation of the effect of maximum aggregate size on fracture behaviour of Self Compacting Concrete." *Construction and Building Materials*, 55, pp. 202-211.
- Beygi, M. H., Kazemi, M. T., Nikbin, I. M., & Amiri, J. V. (2013). "The effect of water to cement ratio on fracture parameters and brittleness of Self Compacting Concrete." *Materials & Design*, 50, pp. 267-276.
- Bibm, C., & Ermco, E. (2005). EFNARC. *The European Guidelines for Self Compacting Concrete: Specification, Production and Use, The Self Compacting Concrete European Project Group*.
- Billberg, P. (1999). "Fine mortar rheology in mix design of Self Compacting Concrete" In. *1st International RILEM Symposium on Self Compacting Concrete* pp. 47-58.
- Billberg, P. (1999). "Self Compacting Concrete for civil engineering structures: The Swedish experience", *Report no 2:99. Swedish Cement and Concrete Research Institute, Stockholm*.
- Birtel, V. and Mark, P. (2006), "Parameterised Finite Element Modelling of RC Beam Shear Failure", *ABAQUS Users Conference*, pp. 95–108.

- BIS:383 (Bureau of Indian Standards) (2016): Specification for Coarse and Fine Aggregates from Natural Sources for Concrete, India.
- Borst, R. D., Remmers, J. J., Needleman, A., & Abellan, M. A. (2004). “Discrete vs smeared crack models for concrete fracture: bridging the gap.” *International Journal for Numerical and Analytical Methods in Geomechanics*, 28(7-8), pp.583-607.
- Boukendakdji, O., Kadri, E. H., & Kenai, S. (2012). “Effects of granulated blast furnace slag and superplasticizer type on the fresh properties and compressive strength of Self Compacting Concrete.” *Cement and concrete composites*, 34(4), pp.583-590.
- Bourdette B., Ringot E. and Ollivier J.P., “Modelling Of the Transition Zone Porosity”, *Cement and Concrete Research*, 1995, Vol. 25. No. 4, pp. 741-751
- Brestler, B. and Pister, K.S. (1958a), “, Behaviour of concrete under triaxle compressive-compressive-tensile stresses”, *ACI Materials Journal*, 8(2), 181–185.
- Brestler, B. and Pister, K.S. (1958b), “Strength of concrete under combined stresses”, in “*Proceedings of ACI Journal*”, volume 55, pages 321–345.
- Carreira, D.J. and Chu, K.H. (1985), “Stress-strain relationship for plain concrete in compression”, in “*Proceedings of ACI Journal*”, volume 82, pages 797–804.
- Cement and Concrete Sectional Committee, CED 2 (2000), *Indian Standard Plain and reinforced concrete—code of practice (IS 456: 2000)*, Bureau of Indian Standards.
- CEWEP. “Environmental sound use of Bottom Ash”, <[http://www.cewep.eu/information/publicationsandstudies/statements/ceweppublications/m\\_722](http://www.cewep.eu/information/publicationsandstudies/statements/ceweppublications/m_722) (Accessed on 20th August, 2017)
- Chavhan, P.J. and Bhole, S.D. (2014). “To Study the Behaviour of Marble Powder as Supplementary Cementitious Material in Concrete.” *Int. Journal of Engineering Research and Applications*, 4(4), pp.377-381.
- Chen, A.C. and Chen, W.F. (1975), “Constitutive relations for concrete”, *Journal of Engineering Mechanics*, 101(4), 465–481.

- Chen, Y.Y., Tuan, B.L.A. and Hwang, C.L., (2013). “Effect of paste amount on the properties of self-consolidating concrete containing fly ash and slag.” *Construction and Building Materials*, 47, pp.340-346.
- China Microsilica Union (2011). “Silica Fume In Various Applications”, <<http://www.chinamicrosilica.com/tech/84.html>> (Mar 21, 2011).
- Chong, J.S., Christiansen, E.B. and Baer, A.D., (1971). “Rheology of concentrated suspensions.” *Journal of applied polymer science*, 15(8), pp.2007-2021.
- Chow, R.K., Yip, S.W. and Kwan, A.K. (2013). “Processing crushed rock fine to produce manufactured sand for improving overall performance of concrete.” *HKIE Transactions*, 20(4), pp.240-249.
- Chuan-Zhi, W., Zhen-Hai, G. and Xiu-Qin, Z. (1987), “Experimental investigation of biaxial and triaxle compressive concrete strength”, *ACI Materials Journal*, 84(2), pp.92–100.
- Cifuentes, H., & Karihaloo, B. L. (2013). “Determination of Size independent specific fracture energy of normal-and high-strength Self Compacting Concrete from wedge splitting tests.” *Construction and Building Materials*, 48, pp.548-553.
- Concrete fact sheet, [www.nrmca.org](http://www.nrmca.org). (Browsed on 27/10/2016).
- Cordeiro, G. C., de Alvarenga, L. M. S. C., & Rocha, C. A. A. (2016). “Rheological and mechanical properties of concrete containing crushed granite fine aggregate.” *Construction and Building Materials*, 111, pp.766-773.
- Cupper, H. and Gerstle. (1973), “Behaviour of concrete under biaxial stresses”, *ASCE, J. Eng. Mech. Div.*, 99(4), pp.853-866
- Dash, M.K., Patro, S.K. and Rath, A.K. (2016). “Sustainable use of industrial-waste as partial replacement of fine aggregate for preparation of concrete—a review.” *International Journal of Sustainable Built Environment*, 5(2), pp.484-516.
- Dinakar, P. and Manu, S.N., (2014). “Concrete mix design for high strength Self Compacting Concrete using metakaolin.” *Materials & Design*, 60, pp.661-668.

- Dinakar, P., Sethy, K.P. and Sahoo, U.C., (2013). “Design of Self Compacting Concrete with ground granulated blast furnace slag.” *Materials & Design*, 43, pp.161-169.
- Dodds, L. H. (2013). “Microstructure Characterisation of Ordinary Portland Cement Composites for the Immobilisation of Nuclear Waste.”
- Domone, P. L., Jin, J., & Chai, H. W. (1999). “Optimum mix proportioning of Self Compacting Concrete.” In *Innovation in Concrete Structures: Design and Construction* (pp. 277-285). Thomas Telford Publishing.
- Domone, P.L., (2006). Self Compacting Concrete: “An analysis of 11 years of case studies.” *Cement and Concrete Composites*, 28(2), pp.197-208.
- Douma, O. B., Boukhatem, B., & Ghrici, M., (2014). “Prediction Compressive Strength of Self Compacting Concrete Containing Fly Ash Using Fuzzy Logic Inference System.” World Academy of Science, Engineering and Technology, *International Journal of Civil, Environmental, Structural, Construction and Architectural Engineering*, 8(12), pp.1336-1340.
- Douma, O. B., Boukhatem, B., Ghrici, M., & Tagnit-Hamou, A. (2016). “Prediction of properties of Self Compacting Concrete containing fly ash using artificial neural network.” *Neural Computing and Applications*, pp.1-12.
- Dransfield, J., 2003. “Mortar and grout.” *Advanced Concrete Technology Set*, p.69
- Dvorkin, L., Bezusyak, A., Lushnikova, N. and Ribakov, Y., (2012). “Using mathematical modeling for design of Self Compacting high strength concrete with metakaolin admixture.” *Construction and Building Materials*, 37, pp.851-864.
- EFNARC, S., (2002). Guidelines for Self Compacting Concrete. EFNARC, UK (www.efnarc.org), pp.1-32.
- Elices, M., Guinea, G. and Planas, J.(1992), “Measurement of the fracture energy using three-point bend tests: Part 3-influence of cutting the P- tail”, *Materials and Structures*, 25(6), pp.327–334.

- Eskandari, H., Muralidhara, S., Raghuprasad, B. K., & Reddy, B. V. (2010). "Size effect in self-consolidating concrete beams with and without notches." *Sadhana*, 35(3), pp.303-317.
- European Committee for Standards, E.C. (2008), *BS EN 1992-1-1 - Design of concrete structures. General rules and rules for buildings*, CEN, Brussels.
- Fathi, H., and Lameie, T., (2017). "Effect of aggregate type on heated Self Compacting Concrete." *Computers & Concrete*, 19(5), pp.033-039.
- Ferraris, C.F., Brower, L.E. and Banfill, P., (2001). Comparison of Concrete Rheometers: International Test at LCPC (Nantes, France) in October, 2000. Gaithersburg, MD, USA: *National Institute of Standards and Technology*.
- Francisco Lopez-Almansa, Bashar Alfarah and Sergio Oller "Numerical Simulation of RC Frame testing with Damaged Plasticity model. Comparison with simplified models." *Second European conference on Earthquake Engineering and Seismology, Istanbul* Aug. 25-29, 2014.
- Frankel, N.A. and Acrivos, A., (1967). "On the viscosity of a concentrated suspension of solid spheres." *Chemical Engineering Science*, 22(6), pp.847-853.
- Gaimster, R., Dixon, N., (2003). "Self Compacting Concrete, in Advanced concrete technology," Newman, J., Choo, B. S. (eds), Oxford, *Elsevier*, 3, pp.202-223.
- Gandage, A.S., Rao, V.V., Sivakumar, M.V.N., Vasani, A., Venu, M. and Yaswanth, A.B., (2013). "Effect of perlite on thermal conductivity of Self Compacting Concrete." *Procedia-Social and Behavioural Sciences*, 104, pp.188-197.
- Gardner, N.J. (1969), "Triaxial behaviour of concrete", in *Proceedings of ACI Journal*, volume 66, pp.136–158.
- Gencil, O., Ozel, C., Brostow, W., & Martinez-Barrera, G. (2011). "Mechanical properties of Self Compacting Concrete reinforced with polypropylene fibres." *Materials Research Innovations*, 15(3), pp.216-225.
- Gesoğlu, M., Güneyisi, E. and Özbay, E., (2009). "Properties of Self Compacting Concretes made with binary, ternary, and quaternary cementitious blends of fly ash, blast



- furnace slag, and silica fume.”*Construction and Building Materials*, 23(5), pp.1847-1854.
- Ghanbari, A. and Karihaloo, B.L., (2009). “Prediction of the plastic viscosity of Self Compacting steel fibre reinforced concrete.”*Cement and Concrete Research*, 39(12), pp.1209-1216.
- Ghanbari, A., (2011). “Self Compacting high and ultra-high performance concretes” (Doctoral dissertation, Cardiff University (United Kingdom)).
- Grégoire, D., Rojas-Solano, L. B., & Pijaudier-Cabot, G. (2013). “Failure and size effect for notched and unnotched concrete beams.” *International Journal for Numerical and Analytical Methods in Geomechanics*, 37(10), pp.1434-1452
- Grzeszczyk, S., & Lipowski, G. (1997). “Effect of content and particle size distribution of high-calcium fly ash on the rheological properties of cement pastes.” *Cement and concrete research*, 27(6), pp.907-916.
- Guinea, G., Planas, J. and Elices, M.(1992), “Measurement of the fracture energy using three-point bend tests: Part 1-Influence of experimental procedures”, *Materials and Structures*, 25(4), pp.212–218.
- Güneysi, E., Gesoğlu, M., & Özbay, E. (2010). “Strength and drying shrinkage properties of Self Compacting Concretes incorporating multi-system blended mineral admixtures.”*Construction and Building Materials*, 24(10), pp.1878-1887.
- Hanson, J. H., & Ingraffea, A. R. (2003). “Using numerical simulations to compare the fracture toughness values for concrete from the size-effect, two-parameter and fictitious crack models.” *Engineering fracture mechanics*, 70(7), pp.1015-1027.
- Hillerborg, A., Moder, M. and Petersson, P.E., (1976). “Analysis of crack formation and crack growth in concrete by means of fracture mechanics and finite elements”, *Cement and concrete research*, 6(6), pp.773–782.
- Hočevar, A., Kavčič, F. and Bokan-Bosiljkov, V., (2012). “Rheological parameters of fresh concrete—comparison of rheometers,”*GRADEVINAR* 65 (2), pp.99-109

- Hofstetter, B. V. (2013). "Review and enhancement of 3D concrete models for large-scale numerical simulations of concrete structures." *International Journal for Numerical and Analytical Methods in Geomechanics*, 37(3), pp.221-246.
- Hsu, L.S. and Hsu, C.T. (1994), "Stress-strain behaviour of steel-fibre high-strength concrete under compression", *ACI Structural Journal*, 91(4), pp.448–457.
- Hu, X.Z. and Wittmann, F. (1992), "Fracture energy and fracture process zone", *Materials and Structures*, 25(6), pp.319–326.
- Ibrahim, A., El-Chabib, H. and Eisa, A. (2012). "Ultra-strength Flowable Concrete Made with High Volumes of Supplementary Cementitious Materials." *Journal of Materials in Civil Engineering*, 25(12), pp.1830-1839.
- Ibrahim, H.A. and Razak, H.A. (2016). "Effect of palm oil clinker incorporation on properties of pervious concrete." *Construction and Building Materials*, 115, pp.70-77.
- ICT-Self Compacting Concrete, "Successful projects demonstrate the strengths of Self Compacting Concrete", Concrete Construction Industry Critical Technology Committee on Self Compacting Concrete, USA, October, 2011.
- Instruments, B. (1999). "User Manual for Bohlin Rheometers." *Bohlin Instruments*, (1.0)
- IS: CED2 (11290) \_ 30012017 - Concrete Mix Design. Draft Code.
- Jefferson, A. D. (2002). "Constitutive modelling of aggregate interlock in concrete." *International journal for numerical and analytical methods in geomechanics*, 26(5), pp.515-535.
- Juan Rodriguez (2014). "Uses, Benefits and Drawbacks of Fly Ash in Construction", <<https://www.thebalance.com/fly-ash-applications-844761>> (Accessed on April 7<sup>th</sup>, 2017).
- Kamal, M. M., Safan, M. A., Etman, Z. A., & Kasem, B. M. (2014). "Mechanical properties of self-compacted fibre concrete mixes." *HBRC Journal*, 10(1), pp.25-34.
- Kanadasan, J. and Abdul Razak, H., 2015. "Utilization of palm oil clinker as cement replacement material." *Materials*, 8(12), pp.8817-8838.

- Kanadasan, J. and Razak, H.A., (2014). "Mix design for Self Compacting palm oil clinker concrete based on particle packing." *Materials & Design*, 56, pp.9-19.
- Kanojia, A. and Jain, S.K. (2017). "Performance of coconut shell as coarse aggregate in concrete." *Construction and Building Materials*, 140, pp.150-156.
- Kar, A., Ray, I., Unnikrishnan, A. and Davalos, J.F., (2012). "Microanalysis and optimization-based estimation of C–S–H contents of cementitious systems containing fly ash and silica fume." *Cement and Concrete Composites*, 34(3), pp.419-429
- Karihaloo, B., Abdalla, H. and Imjai, T. (2003), "A simple method for determining the true specific fracture energy of concrete", *Magazine of concrete research*, 55(5), pp.471–481.
- Khaleel, O.R. and Razak, H.A., (2014). "Mix design method for Self Compacting metakaolin concrete with different properties of coarse aggregate." *Materials & Design*, 53, pp.691-700.
- Khan, A., Do, J., & Kim, D. (2016). "Cost effective optimal mix proportioning of high strength Self Compacting Concrete using response surface methodology." *Computers & Concrete*, 17(5), pp.629-638.
- Khatib, J.M., (2008). "Performance of Self Compacting Concrete containing fly ash." *Construction and Building Materials*, 22(9), pp.1963-1971.
- Khayat, K., Hu, C., & Monty, H. (1999). "Stability of self-consolidating concrete, advantages, and potential applications." In *Self Compacting Concrete: Proceedings of the First International RILEM Symposium*, pp. 143-152.
- Khayat, K.H. and Guizani, Z., (1997). "Use of viscosity-modifying admixture to enhance stability of fluid concrete." *ACI Materials Journal*, 94(4), pp.332-340.
- Khayat, K.H., (1999). "Workability, testing, and performance of self-consolidating concrete." *ACI materials journal*, 96, pp.346-353.
- Kim B-G, Jiang S, Aitcin P-C. "Influence of molecular weight of PNS superplasticizers on the properties of cement pastes containing different alkali contents." In:

- International RILEM conference. The role of admixtures in high performance concrete. Monterrey, Mexico; 1999. pp.69–96.
- King, D., Fict, H., Dip, M. and Chartered, M.C.I.M. (2012). August. “The effect of silica fume on the properties of concrete as defined in concrete society report 74, cementitious materials.” In *37th Conference on our world in concrete and structures*, Singapore pp. 29-31.
- Kmiecik, P. and Kamin’ski, M. (2011), “Modelling of reinforced concrete structures and composite structures with concrete strength degradation taken into consideration”, *Archives of Civil and Mechanical Engineering*, 11(3), pp.623–636.
- Kotsovos, M. and Newman, J. (1977), “Behaviour of concrete under multiaxial stress”, in *ACI Journal Proceeding*, volume 74, pp.443–446.
- Krieger, I.M. and Dougherty, T.J., (1959). “A mechanism for non-Newtonian flow in suspensions of rigid spheres.” *Transactions of the Society of Rheology*, 3(1), pp.137-152.
- Kumar P. and Kaushik S., "Some trends in the use of concrete: Indian scenario", *Indian Concrete Journal*, 77(12), 2003, pp. 1503-1508
- Kumar, K.S. and Baskar, K. (2015). “Recycling of E-plastic waste as a construction material in developing countries.” *Journal of Material Cycles and Waste Management*, 17(4), pp.718-724.
- Kumar, P. and Mittal, K.L. eds., (1999). “Handbook of microemulsion science and technology.” *CRC press*.
- Kumar, R. (2017). “Influence of recycled coarse aggregate derived from construction and demolition waste (CDW) on abrasion resistance of pavement concrete.” *Construction and Building Materials*, 142, pp.248-255.
- Kupfer, H., Hilsdorf, H.K. and Rusch, H. (1969), “Behaviour of concrete under biaxial stresses”, *Proceedings of ACI Journal*, volume 66, pp.656–666.
- Kupfer, H.B. and Gerstle, K.H. (1973), “Behaviour of concrete under biaxial stresses”, *Journal of the Engineering Mechanics Division*, 99(4), pp.853–866.

- Kurita, M., & Nomura, T. (1998). "Highly-flowable steel fibre-reinforced concrete containing fly ash." *Special Publication*, 178, pp.159-176.
- Kwak, H.G. and Filippou, F.C. (1990), *Finite element analysis of reinforced concrete structures under monotonic loads*, Department of Civil Engineering, University of California Berkeley, CA.
- Kwon, S. H., Zhao, Z., & Shah, S. P. (2008). "Effect of specimen size on fracture energy and softening curve of concrete: Part II. Inverse analysis and softening curve." *Cement and Concrete Research*, 38(8), pp.1061-1069.
- L'opez-Almansa, F., Alfarah, B. and Oller, S. (2014), "Numerical simulation of RC frame testing with damaged plasticity model. Comparison with simplified models", *Second European Conference on Earthquake Engineering and Seismology, Istanbul, Turkey*,
- Le, H.T., Müller, M., Siewert, K. and Ludwig, H.M., (2015). "The mix design for Self Compacting high performance concrete containing various mineral admixtures." *Materials & Design*, 72, pp.51-62.
- Lee, S.K., Song, Y.C. and Han, S.H. (2004), "Biaxial behaviour of plain concrete of nuclear containment building", *Nuclear Eng. Des.*, 227(2), pp.143-153.
- Li, F. X., Yu, Q. J., Wei, J. X., & Li, J. X. (2011). Predicting the workability of SELF COMPACTING CONCRETE using artificial neural network. In *Advanced Materials Research*, 168, pp.1730-1734.
- Liu, M., (2010). "Self Compacting Concrete with different levels of pulverized fuel ash." *Construction and Building Materials*, 24(7), pp.1245-1252.
- Long, G., Gao, Y. and Xie, Y., (2015). "Designing more sustainable and greener Self Compacting Concrete." *Construction and Building Materials*, 84, pp.301-306.
- Long, W. J., Gu, Y., Liao, J., & Xing, F. (2017). "Sustainable design and ecological evaluation of low binder Self Compacting Concrete." *Journal of Cleaner Production*, 167, pp.317-325.

- M. Collepari. (1998)“Admixtures used to enhance placing characteristics of concrete.”*Cement Concrete Composites*, 20, pp.103-112.
- Madandoust, R., Ranjbar, M. M., Ghavidel, R., & Shahabi, S. F. (2015). “Assessment of factors influencing mechanical properties of steel fibre reinforced Self Compacting Concrete.” *Materials & Design*, 83, pp.284-294.
- Mahdikhani, M., & Ramezani-pour, A. A. (2014). “Mechanical properties and durability of self-consolidating cementitious materials incorporating nano silica and silica fume.”*Computers & Concrete*, 14(2), pp.175-191.
- Majewski, S. (2003), “The mechanics of structural concrete in terms of elasto-plasticity”, *Silesian Polytechnic Publishing House, Gliwice*.
- Manasi Phadke (2016). “In 300-km range of any power plant: Fly ash mandatory for constructing new buildings”, <<https://www.epa.gov/smm/beneficial-uses-spent-foundry-sands>> (Jul 29, 2016).
- Manjunath, B.A. (2016). “Partial replacement of e-plastic waste as coarse-aggregate in concrete.” *Procedia Environmental Sciences*, 35, pp.731-739.
- Mather, B. (1967). ‘Field and laboratory studies of the sulfate resistance of concrete”. *Army Engineer Waterways Experiment Station Vicksburg MS*
- Mathew, G. and Paul, M.M., (2012). “Mix design methodology for laterized Self Compacting Concrete and its behaviour at elevated temperature.” *Construction and Building Materials*, 36, pp.104-109.
- Mehta, P. K., and Monteiro P. J. M. (2006). *Concrete Microstructure, Properties and Materials*. McGraw Hill, San Francisco, US, pp.475-476.
- Mills, L.L. and Zimmerman, R.M. (1970), “Compressive strength of plain concrete under multiaxial loading conditions”, *Journal of American Concrete Institute*, 67(10), pp.802–807.
- Mindess, S., Young, J.F. and Darwin, D., (2003). *Concrete*. Prentice Hall.

- Mohebbi, A., Shekarchi, M., Mahoutian, M., & Mohebbi, S. (2011). "Modeling the effects of additives on rheological properties of fresh self-consolidating cement paste using artificial neural network." *Computers & Concrete*, 8(3), pp.279-292.
- Mukhopadhyay, A. K., & Jang, S. (2009). "Using cement paste rheology to predict concrete mix design problems: Technical Report" (No.FHWA/TX-09/0-5820-1). *Texas Transportation Institute, Texas A & M University System*.
- Mundra, S., Sindhi, P.R., Chandwani, V., Nagar, R. and Agrawal, V. (2016). "Crushed rock sand—An economical and ecological alternative to natural sand to optimize concrete mix." *Perspectives in Science*, 8, pp.345-347.
- Muralidhara, S., Prasad, B. R., & Singh, R. K. (2013). "Size independent fracture energy from fracture energy release rate in plain concrete beams." *Engineering Fracture Mechanics*, 98, pp.284-295.
- Murthy, A.R., Karihaloo, B.L., Iyer, N.R. and Prasad, B.R. (2013), "Determination of Size independent specific fracture energy of concrete mixes by two methods", *Cement and concrete research*, 50, pp.19–25.
- Muthadhi, A. and Kothandaraman, S. (2013). "Experimental investigations of performance characteristics of rice husk ash–blended concrete." *Journal of Materials in Civil Engineering*, 25(8), pp.1115-1118.
- Muthukumar G and Manoj Kumar (2014) " Failure criteria of concrete- A review", *Computers and Concrete*, Vol. 14, No. 5, pp.503-526.
- N. Mitra and L.N. Lowes "Factors Influencing Continuum Simulation of Three point Bend test of a concrete Notched Beam" *The 14th world conference on earthquake Engineering*, October 12-17, 2008, Beijing, China
- Naik, B.T.R., Canpolat, F. and Chun, Y. (2003). "Limestone powder use in cement and concrete." Department of Civil Engineering and Mechanics College of Engineering and Applied Science the university of wisconsin–Milwaukee.

- Naik, T.R., Patel, V.M., Parikh, D.M. and Tharaniyil, M.P. (1994). "Utilization of used foundry sand in concrete." *Journal of Materials in Civil Engineering*, 6(2), pp.254-263.
- NBMCW (2012). "Influence of Marble Powder on Mechanical Properties of Mortar and Concrete Mix", <<https://www.nbmcw.com/concrete/29107-influence-of-marble-powder-mortar-and-concrete-mix.html>> (Jun, 2012).
- Nehdi, M., & Rahman, M. A. (2004). "Estimating rheological properties of cement pastes using various rheological models for different test geometry, gap and surface friction." *Cement and concrete research*, 34(11), pp.1993-2007.
- Nepomuceno, M.C., Pereira-de-Oliveira, L.A. and Lopes, S.M.R., (2014). "Methodology for the mix design of Self Compacting Concrete using different mineral additions in binary blends of powders." *Construction and Building Materials*, 64, pp.82-94.
- Nijansh chingari (2013). "Use of Plastics and E-waste in concrete", <<https://www.slideshare.net/nijansh/chingari-idp-presentation>> (Nov 13, 2013).
- Nikbin, I. M., Beygi, M. H. A., Kazemi, M. T., Amiri, J. V., Rahmani, E., Rabbanifar, S., & Eslami, M. (2014). "A comprehensive investigation into the effect of aging and coarse aggregate size and volume on mechanical properties of Self Compacting Concrete." *Materials & Design*, 59, pp.199-210.
- Nikbin, I. M., Beygi, M. H. A., Kazemi, M. T., Amiri, J. V., Rahmani, E., Rabbanifar, S., & Eslami, M. (2014). "Effect of coarse aggregate volume on fracture behaviour of Self Compacting Concrete." *Construction and Building Materials*, 52, pp.137-145.
- Norchem (2011). "How does Silica Fume work in concrete?", <<http://www.norchem.com/silica-fume-concrete.html>> (Accessed on June 17<sup>th</sup>, 2017).
- Okamura, H. and Ouchi, M., (2003). Self Compacting Concrete. *Journal of advanced concrete technology*, 1(1), pp.5-15.



- Okamura, H., Ouchi, M., (1999). “Self Compacting Concrete. Development, present use and future.” In 1st International RILEM Symposium on SELF COMPACTING CONCRETE,
- Okamura, H., Ozawa, K., (1995). “Mix design for Self Compacting Concrete.” *Concrete Library of JSCE*, 25, pp. 107-120.
- Ouchi, M., Hibino, M., Ozawa, K. and Okamura, H., 1998. “A rational mix-design method for mortar in Self Compacting Concrete.” *Structural Engineering & Construction: Tradition, Present and Future.*, 2, pp.1307-1312.
- Ouchi, M., Nakamura, S., Osterson, T., Hallberg, S., Lwin, M., (2003). “Applications of Self Compacting Concrete in Japan, Europe and the United States.” *International Symposium on High Performance Computing (ISHPC)*. pp. 1–20.
- Pagé, M., & Spiratos, N. (2000, April). “The role of superplasticizers in the development of environmentally-friendly concrete.” *CANMET/ACI International Symposium on Concrete Technology for Sustainable Development*, Canada.
- Pai, B. H. V., & Sujith Kumar, C. P. (2009). “Experimental study on steel fibre reinforced Self Compacting Concrete with silica fume as filler material.” In *34th Conference on Our World In Concrete & Structures*, Singapore.
- Pająk, M., & Ponikiewski, T. (2013). “Flexural behaviour of Self Compacting Concrete reinforced with different types of steel fibres.” *Construction and Building Materials*, 47, pp.397-408.
- Pathak, S. S., Sharma, S., Sood, H., & Khitoliya, R. K. (2012). “Prediction of Compressive Strength of Self Compacting Concrete with Flyash and Rice Husk Ash using Adaptive Neuro-fuzzy Inference System.” *Editorial Preface*, 3(10).
- PCA. “Ultra-High Performance Concrete”, <<http://www.cement.org/learn/concrete-technology/concrete-design-production/ultra-high-performance-concrete>>
- Peter Grassl and Milan Jirasek “Damage-plastic model for concrete failure.” *International Journal of Solids and Structures* 43 (2006),pp.7166–7196

- Phan-Thien, N. and Karihaloo, B.L., (1994). "Materials with negative Poisson's ratio: A qualitative microstructural model." *Journal of applied mechanics*, 61(4), pp.1001-1004.
- Phelan W. S., "Self-Consolidating Concrete (Self Compacting Concrete): Today and Tomorrow", *STRUCTURE magazine*, Michigan city, USA, Sept. 2011, pp. 33-35.
- Planas, J., Elices, M. and Guinea, G.(1992), "Measurement of the fracture energy using three-point bend tests: Part 2-Influence of bulk energy dissipation", *Materials and Structures*, 25(5), pp.305–312.
- Ponikiewski, T., & Gołaszewski, J. (2013). "Properties of steel fibre reinforced Self Compacting Concrete for optimal rheological and mechanical properties in precast beams." *Procedia Engineering*, 65, pp.290-295.
- Prabhu, G.G., Hyun, J.H. and Kim, Y.Y. (2014). "Effects of foundry sand as a fine aggregate in concrete production." *Construction and Building Materials*, 70, pp.514-521.
- Prusty, J.K. and Patro, S.K. (2015). "Properties of fresh and hardened concrete using agro-waste as partial replacement of coarse aggregate—A review." *Construction and Building Materials*, 82, pp.101-113.
- Raheman, A., & Modani, P. O. (2013). "Prediction of Properties of Self Compacting Concrete Using Artificial Neural Network." *International Journal of Engineering Research and Applications (IJERA)* ISSN, pp.2248-9622.
- Ramezani pour, A.A. (2014). "Fly ash." In *Cement replacement materials*. Springer Berlin Heidelberg, pp.47-156
- Ramezani pour, A.A., Ghiasvand, E., Nickseresht, I., Mahdikhani, M. and Moodi, F. (2009). "Influence of various amounts of limestone powder on performance of Portland limestone cement concretes." *Cement and Concrete Composites*, 31(10), pp.715-720.
- Rao, A. (2010). "Rheology of fluid and semisolid foods: principles and applications." Springer Science & Business Media.

- Rao, A., Jha, K.N. and Misra, S. (2007). “Use of aggregates from recycled construction and demolition waste in concrete.” *Resources, conservation and Recycling*, 50(1), pp.71-81.
- Rao, G. A., &Raghu Prasad, B. K. (2002). “Fracture energy and softening behaviour of high-strength concrete.” *Cement and Concrete Research*, 32(2), pp.247-252.
- Ricehuskash.com (2008). “Rice Husk Ash”, <<http://www.ricehuskash.com/application.htm>> (2008).
- RILEM Technical Committee 50-FMC (1985), “Draft Recommendation: Determination of the fracture energy of mortar and concrete by means of three-point bend tests on notched beams”, *Materials and Structures*, (106), pp.285–290.
- S. V. Chaudhari and M. A. Chakrabarti “Modelling of Concrete for nonlinear analysis using Finite Element Code ABAQUS.” *International Journal of Computer Applications* (0975 – 8887) Volume 44– No.7, April 2012.
- Saenz, L. (1964), “Discussion of equation for the Stress-Strain Curve of Concrete, by P. Desayi and S. Krishnan”, *ACI Journal*, 61, pp.1229–1235.
- Saitô, N., (1950). “Concentration dependence of the viscosity of high polymer solutions.” *I. Journal of the Physical Society of Japan*, 5(1), pp.4-8.
- Seleem, M. H., Sallam, H. E. M., Attwa, A. T., Heiza, K. T., & Shaheen, Y. B. (2008). “Fracture toughness of Self Compacting Concrete.” *MesoMechanics. HBRC*, Giza, Egypt, Jan 28 – Feb. 1, 2008.
- Senthil Kumar, K. and Baskar, K. (2014). “Development of ecofriendly concrete incorporating recycled high-impact polystyrene from hazardous electronic waste.” *Journal of Hazardous, Toxic, and Radioactive Waste*, 19(3), pp.04014042.
- Sharma, N.K., Kumar, P., Kumar, S., Thomas, B.S. and Gupta, R.C. (2017). “Properties of concrete containing polished granite waste as partial substitution of coarse aggregate.” *Construction and Building Materials*, 151, pp.158-163.
- Shenoy, A.V., (2013). “Rheology of filled polymer systems.” *Springer Science & Business Media*.

- Shi, C., Wu, Z., Lv, K. and Wu, L., (2015). "A review on mixture design methods for SELF COMPACTING CONCRETE." *Construction and Building Materials*, 84, pp.387-398.
- Shyam Prakash, K. and Rao, C.H. (2016). "Study on Compressive Strength of Quarry Dust as Fine Aggregate in Concrete." *Advances in Civil Engineering*, pp. 1-5.
- Siddique, R., & Kaur, G. (2016). "Strength and permeation properties of Self Compacting Concrete containing fly ash and hooked steel fibres". *Construction and Building Materials*, 103, pp.15-22.
- Siddique, R., Aggarwal, P., & Aggarwal, Y. (2011). "Prediction of compressive strength of SELF COMPACTING CONCRETE containing bottom ash using artificial neural networks." *Advances in Engineering Software*, 42(10), pp.780-786.
- Silica Fume Association (2014). "What is Silica Fume?", <<http://www.silicafume.org/general-silicafume.html>> (Accessed on August 20<sup>th</sup>, 2017).
- Singh, G. and Siddique, R. (2012). "Effect of waste foundry sand (WFS) as partial replacement of sand on the strength, ultrasonic pulse velocity and permeability of concrete." *Construction and Building Materials*, 26(1), pp.416-422.
- Singh, M. and Siddique, R. (2013). "Effect of coal bottom ash as partial replacement of sand on properties of concrete." *Resources, conservation and recycling*, 72, pp.20-32.
- Singh, M. and Siddique, R. (2016). "Effect of coal bottom ash as partial replacement of sand on workability and strength properties of concrete." *Journal of Cleaner Production*, 112, pp.620-630.
- Singh, M., Chaudhary, K., Srivastava, A., Sangwan, K.S. and Bhunia, D. (2017). "A study on environmental and economic impacts of using waste marble powder in concrete." *Journal of Building Engineering*, 13, pp.87-93
- Singh, S., Nande, N., Bansal, P. and Nagar, R. (2017). "Experimental Investigation of Sustainable Concrete Made with Granite Industry By-Product." *Journal of Materials in Civil Engineering*, 29(6), pp.04017017-1 to 04017017-13.

- Snehith devasani (2015). "Utilization of Sugarcane Bagasse Ash in concrete", <<https://www.slideshare.net/snehithdevasani/utilization-of-sugarcane-bagasse-ash-in-concrete-52550175>> (Sep 8, 2015).
- Struble, L. and Sun, G.K., (1995). "Viscosity of Portland cement paste as a function of concentration." *Advanced Cement Based Materials*, 2(2), pp.62-69.
- Su, N., Hsu, K.C. and Chai, H.W., (2001). "A simple mix design method for Self Compacting Concrete." *Cement and concrete research*, 31(12), pp.1799-1807.
- Surya, M., VVL, K.R. and Lakshmy, P. (2013). "Recycled aggregate concrete for transportation infrastructure." *Procedia-Social and Behavioural Sciences*, 104, pp.1158-1167.
- Tattersall, G. H. (2003). "Workability and quality control of concrete." *CRC Press*.
- Team WFM (2014). "What are the advantages and disadvantages of using Fly ash in Concrete?", <<https://www.wfm.co.in/advantages-disadvantages-using-fly-ash-concrete/>> (Aug 31, 2016)
- Tennent, R. M. (Ed.). (2004). *Science data book*. Oliver & Boyd.
- Thrane, L. N., Szabo, P., Geiker, M., Glavind, M., & Stang, H. (2004). "Simulation of the test method "L-Box" for Self Compacting Concrete." *Annual Transactions of the NORDIC rheology society*, 12(1), pp.47-54.
- Tim Raud (2014). "Uses for Limestone Powder", <<http://sciencing.com/uses-limestone-powder-8271568.html>> (Apr 24, 2017).
- Tomasz Jankowiak and Tomasz Lodygowski. "Identification of parameters of Concrete Damage Plasticity Constitutive model." *Publishing House of Poznan University of Technology, Poznan* 2005, ISSN 1642-9303.
- Toumi, A., & Bascoul, A. (2002). "Mode I crack propagation in concrete under fatigue: microscopic observations and modelling." *International journal for numerical and analytical methods in geomechanics*, 26(13), pp.1299-1312.

- Ulubeyli, G.C. and Artir, R. (2015). “Properties of Hardened Concrete Produced by Waste Marble Powder.” *Procedia-Social and Behavioural Sciences*, 195, pp.2181-2190.
- Upreti, G., Murthy, A.R., Goptinath, S., Iyer, N.R. and Venkat, L. (2016), “Strength and ductility of RC beams strengthened with ultra-high strength cementitious composite overlay”, *Journal of Structural Engineering (Madras)*, 43(2), pp.190–198.
- Utracki, L.A. and Wilkie, C.A. eds., (2002). “Polymer blends handbook (Vol. 1, p. 2).” *Dordrecht: Kluwer academic publishers*.
- Uysal, M., & Sumer, M. (2011). “Performance of Self Compacting Concrete containing different mineral admixtures.” *Construction and Building materials*, 25(11), pp.4112-4120.
- Uysal, M., & Tanyildizi, H. (2012). “Estimation of compressive strength of Self Compacting Concrete containing polypropylene fibre and mineral additives exposed to high temperature using artificial neural network.” *Construction and Building Materials*, 27(1), pp.404-414.
- Uysal, M., Yilmaz, K., & Ipek, M. (2012). “Properties and behaviour of Self Compacting Concrete produced with GBFS and FA additives subjected to high temperatures.” *Construction and Building Materials*, 28(1), pp.321-326.
- Uysal, M., Yilmaz, K., & Ipek, M. (2012). “The effect of mineral admixtures on mechanical properties, chloride ion permeability and impermeability of Self Compacting Concrete.” *Construction and Building Materials*, 27(1), pp.263-270.
- Van Der Vurst, F., Grünewald, S., Feys, D., Lesage, K., Vandewalle, L., Vantomme, J., & De Schutter, G. (2017). “Effect of the Mix Design on the Robustness of Fresh Self Compacting Concrete.” *Cement and Concrete Composites*, 82, pp.190-201.
- Vand, V., (1948). “Viscosity of solutions and suspensions. II. Experimental determination of the viscosity–concentration function of spherical suspensions.” *The Journal of Physical Chemistry*, 52(2), pp.300-314.

- Vivek, S.S. and Dhinakaran, G. (2017). “Fresh and hardened properties of binary blend high strength SELF COMPACTING CONCRETE.” *Engineering Science and Technology, an International Journal*. 20(3), pp.1173-1179.
- Wahalathantri, B.L. (2012), “Damage assessment in reinforced concrete flexural members using modal strain energy based method”, (Doctoral Dissertation, Queensland University of Technology).
- Wallevik, O.H. and Wallevik, J.E., (2011). “Rheology as a tool in concrete science: The use of rheographs and workability boxes.” *Cement and Concrete Research*, 41(12), pp.1279-1288.
- Wongkeo, W., Thongsanitgarn, P., Ngamjarrojana, A. and Chaipanich, A., (2014). “Compressive strength and chloride resistance of Self Compacting Concrete containing high level fly ash and silica fume”. *Materials & Design*, 64, pp.261-269.
- Yahia, A., Tanimura, M., Shimabukuro, A., & Shimovama, Y. (1999). “Effect of rheological parameters on self-compactability of concrete containing various mineral admixtures.” In *International RILEM symposium on Self Compacting Concrete*, pp. 523-535.
- Zhao, Z., Kwon, S. H., & Shah, S. P. (2008). “Effect of specimen size on fracture energy and softening curve of concrete: Part I. Experiments and fracture energy.” *Cement and Concrete Research*, 38(8), pp.1049-1060.

---

## PUBLICATIONS FROM THE PRESENT STUDY

---

### Journal Publications

1. **Kalyana Rama J. S.**, Sivakumar M. V. N., Vasana A., Sai Kubair K. and Ramachandra Murthy A. (2017). "Plastic Viscosity based mix design of SCC with Crushed Rock Fines", *Computers and Concrete*, 20(4), pp.461-468.
2. **Kalyana Rama J. S.**, D.R. Chauhan, Sivakumar M. V. N., Vasana A. and Ramachandra Murthy A. (2017). "Fracture properties of concrete using damaged plasticity model-A parametric study", *Structural Engineering and Mechanics*, 64(1), pp.59-69
3. George J., **Kalyana Rama J S.**, Sivakumar M V N and Vasana A. (2017). "Behaviour of Plain Concrete Beam subjected to Three Point Bending using Concrete Damaged Plasticity (CDP) Model". *Materials Today: Proceedings*, 4(9), pp.9742-9746.

### Book Chapters

1. **Kalyana Rama, J. S.**, Sivakumar, M. V. N., Vasana, A., Garg, C., & Walia, S. (2015). "A Review on Studies of Fracture Parameters of SCC". In *Advances in Structural Engineering* (pp. 1705-1716). Springer, New Delhi.
2. **Kalyana Rama, J. S.**, Reshmi, N., Sivakumar, M. V. N., & Vasana, A. (2015). Experimental Investigation and Numerical Validation on the Effect of NaOH Concentration on GGBS Based Self Compacting Geopolymer Concrete. In *Advances in Structural Engineering* (pp. 1673-1686). Springer, New Delhi.

### Conference Proceedings

1. **Kalyana Rama J S**, Saikrishna Pallerla, MVN Sivakumar, A Vasana, A Ramachandra Murthy "Parametric study on the influence of cement replacement materials on the rheology of cement paste using Brookfield Viscometer", *RILEM 71st Week, International Conference on Advances in Construction Materials and Systems (ICACMS-2017)*, IIT Madras, September-2017.
2. **Kalyana Rama, J. S.**, Sivakumar, M. V. N., Vasana, A., Ritesh Reddy K. (2014) "A Review on Influence of superplasticizers on the strength characteristics of Self-Compacting Concrete", *International Conference on Sustainable Civil Infrastructure (ICSCI)*, Hyderabad, 286-293.
3. George J., **Kalyana Rama J S.**, Sivakumar M V N and Vasana A. (2016) "Influence of notch to depth ratio on fracture process parameters of plain concrete beam using concrete damaged plasticity model", *International Congress on Computational Mechanics and Simulation (ICCMS)*, Mumbai, 510-513.



**Dr M. V. N Sivakumar** is currently an Assistant Professor in the Department of Civil Engineering at NIT Warangal. He worked under Prof B. N. Rao for his Doctoral research at IIT Madras. His fields of interests are fracture mechanics steel and concrete, reliability analysis and finite element modelling of structures. He has authored more than 40 peer-reviewed papers in international journals and reputed conferences. He serves as a reviewer for a number of reputed scientific journals.

**Prof. A.Vasan** is currently an Associate Professor in the Department of Civil Engineering as well as Associate Dean of Instruction Division at BITS Pilani, Hyderabad Campus. He has been actively involved in teaching, research and academic administration for the past seventeen years. He worked under the guidance of Prof. Slobodan P. Simonovic for his Post-Doctoral Fellowship at The University of Western Ontario, London, Canada. His research interests include asystems approach to planning and management of complex water resources systems using evolutionary algorithms such as differential evolution, genetic algorithms, firefly algorithm, particle swarm optimization, harmony search, cuckoo search; water distribution network design optimization and multi criterion decision making methods. He has completed several research projects sponsored by CSIR and ABG. He has authored more than 50 peer-reviewed papers in international journals and reputed international and national conferences. He serves as areviewer for a number of reputed scientific research journals.

**Mr Sri Kalyana Rama J** is currently working as a Lecturer in the Department of Civil Engineering at BITS Pilani, Hyderabad Campus. He has obtained his Post Graduate degree from V R Siddhartha Engineering College affiliated to JNTU Kakinada. He has an academic experience of 6.5 years and he is actively involved in teaching and research. His fields of interest are scientific ways of mix design for geopolymers concrete/SCC incorporating sustainable materials, non-linear behaviour of concrete structures with different plasticity models, and fracture mechanics of concrete and metals. He has authored more than 15 peer-reviewed papers in international journals and reputed conferences. He serves as a reviewer for 7 reputed international journals.

# APPENDIX A

## C++ CODE FOR PROPORTIONING SCC MIXES WITH AND WITHOUT FIBRES

```
#include<stdio.h>
#include<stdlib.h>
#include<math.h>
int main()
{
    FILE *fp;
    fp=fopen("SCCtrial_fib_mod.txt","w");

    double t1,t2,pfa,pca,x,pfib,pfib_mix,totvol,pvol;
    double cement, water, SP, GGBS, FLA ,cementmaterial,wc,u,v,ld,nmix;
    int fcu;
    printf("*****");
    printf("\n");
    printf(" ** **");
    printf("\n");
    printf(" **      SCFRC MIX DESIGN      **");
    printf("\n");
    printf(" ** **");
    printf("\n");
    printf("*****");
    printf("\n");
    printf("\n");
    printf("\n");
    printf("* Please enter the following parameters: ");
    printf("\n");
    printf("\n");
    printf("1. Enter Water in Kg/m3: ");scanf("%lf",&water);
    printf("2. Enter Strength of concrete in MPa: ");scanf("%d",&fcu);
    printf("3. Enter Desired plastic viscosity in Pa-s: ");scanf("%lf",&nmix);
```

```

printf("4. Enter the volume fraction of fibres to be added in percentage:
");scanf("%lf",&pfib);
printf("5. Enter Aspect Ratio of Fibres: ");scanf("%lf",&ld);

//calculation of fibre contribution factor

double f1=pow(ld,2.0);
double f2=2.0*ld;
double f3=log(f2);
double Kfib=((3.141592654*f1)/(3.0*f3))-1.0;
    wc= log(132.77/fcu)/log(11.00);

    cementmaterial=water/wc;
    cement=roundf(1.00*cementmaterial*100)/100;
    GGBS=roundf(0.00*cementmaterial*100)/100;
    FLA=roundf(0.00*cementmaterial*100)/100;
    SP=roundf(0.0125*cementmaterial*100)/100;

double npaste = 0.24;
pfib_mix=pfib/100;
v=(nmix/(npaste*(1+(Kfib*pfib_mix))))*4.2629741;
u=pow(v,-0.52632);
x=pow(u,0.5);
//calculation of t1 & t2

                                //t1*t2=1

/*Varying t1 and generating t2*/

double lb1=(-0.37/x);
double lb2=(-0.26/x);
double ub1=(0.63/x);
double ub2=(0.74/x);
double r1;
for(r1=0;r1<=1;r1=r1+0.001)

```

```

{
t1=lb1+(r1*(ub1-lb1));
t2= 1/(t1);
pfa=0.63-(t1*x);
pca=0.74-(t2*x);
double deno1= cement/3150 + GGBS/2850 + FLA/2160 + water/1000 + SP/1070 + 0.02;
double FA= (deno1*pfa*2610)/(1-pfa);
double deno2= deno1 + FA/2610;
double CA= (deno2*pca*2710)/(1-pca);
pvol= cement/3150 + GGBS/2850 + FLA/2160 + water/1000 + SP/1070 + FA/2610 +
CA/2710 + 0.02;

double Fibres=((pvol*pfib_mix*7000)/(1-pfib_mix));

totvol=cement/3150 + GGBS/2850 + FLA/2160 + water/1000 + SP/1070 + FA/2610 +
CA/2710 + 0.02;

/*Modified pfa,pca values (total volume correction)*/

pfa=(FA/(totvol*2610)) / ( (cement/(totvol*3150)) +
(GGBS/(totvol*2850)) + (FLA/(totvol*2160)) + (water/(totvol*1000))
+ (SP/(totvol*1070)) + 0.02 + (FA/(totvol*2610)) );
pca=(CA/(totvol*2710)) / ( (cement/(totvol*3150)) +
(GGBS/(totvol*2850)) + (FLA/(totvol*2160)) + (water/(totvol*1000))
+ (SP/(totvol*1070)) + 0.02 + (FA/(totvol*2610)) +
(CA/(totvol*2710)) );

/*New Plastic Viscosity of the mix*/

double h = 1.0 - (pfa/0.63);
double a = 1.0 - (pca/0.74);
double s = 1.0 + (Kfib*pfib_mix);

double nmod = npaste * pow(h,-1.9) * pow(a,-1.9) * s;

```

```

double delta = (nmod - nmix)*100/nmix;

if ((Fibres/totvol)>=0 && (Fibres/totvol)<=100 && ((cement+FLA+GGBS)/totvol)<=600
&& (water/totvol)<220 && (CA/totvol)<=1000 && (CA/totvol)>=750 &&
(FA/totvol)<=1000 && delta>=0 && nmod>=0 && FA/CA>=1)
{
    fprintf(fp,"t1=%lf t2=%lf CA=%lf FA=%lf water=%lf cement=%lf GGBS=%lf FLA=%lf
Fibres=%lf pfib_mix=%lf Kfib=%lf SP=%lf pvol=%lf totvol=%lf nmod=%lf
delta=%lf",t1,t2,CA/totvol,FA/totvol,water/totvol,cement/totvol,GGBS/totvol,FLA/totvol,Fib
res/totvol,pfib_mix,Kfib,SP/totvol,pvol,totvol,nmod,delta);
        if((water/totvol)>210)
            fprintf(fp,"**");
            if(delta<-5.0 || delta>5.0)
                fprintf(fp,"##");
                fprintf(fp,"\n");
}
}

/*Varying t2 and generating t1*/

double r2;
for(r2=0;r2<=1;r2=r2+0.001)
{
    t2=lb2+(r2*(ub2-lb2));
    t1= 1/(t2);
    pfa=0.63-(t1*x);
    pca=0.74-(t2*x);

double deno1= cement/3150 + GGBS/2850 + FLA/2160 + water/1000 + SP/1070 + 0.02;
double FA= (deno1*pfa*2610)/(1-pfa);

double deno2= deno1 + FA/2610;
double CA= (deno2*pca*2710)/(1-pca);

```

```
pvol= cement/3150 + GGBS/2850 + FLA/2160 + water/1000 + SP/1070 + FA/2610 +
CA/2710 + 0.02;
```

```
double Fibres=((pvol*pfib_mix*7000)/(1-pfib_mix));
```

```
totvol= cement/3150 + GGBS/2850 + FLA/2160 + water/1000 + SP/1070 + FA/2610 +
CA/2710 + 0.02;
```

```
/*Modified pfa,pca values (total volume correction)*/
```

```
pfa=(FA/(totvol*2610)) / ( cement/(totvol*3150) +
(GGBS/(totvol*2850)) + (FLA/(totvol*2160)) + (water/(totvol*1000))
+ (SP/(totvol*1070)) + 0.02 + (FA/(totvol*2610)) );
```

```
pca=(CA/(totvol*2710)) / ( cement/(totvol*3150) +
(GGBS/(totvol*2850)) + (FLA/(totvol*2160)) + (water/(totvol*1000))
+ (SP/(totvol*1070)) + 0.02 + (FA/(totvol*2610)) +
(CA/(totvol*2710)) );
```

```
/*New Plastic Viscosity of the mix*/
```

```
double h = 1.0 - (pfa/0.63);
```

```
double a = 1.0 - (pca/0.74);
```

```
double s = 1.0 + (Kfib*pfib_mix);
```

```
double nmod = npaste * pow(h,-1.9) * pow(a,-1.9) * s;
```

```
double delta = (nmod - nmix)*100/nmix;
```

```
if ((Fibres/totvol)>=0 && (Fibres/totvol)<=100 && ((cement+FLA+GGBS)/totvol)<=600
&& (water/totvol)<220 && (CA/totvol)<=1000 && (CA/totvol)>=750 &&
(FA/totvol)<=1000 && delta>=0 && nmod>=0 && FA/CA>=1)
```

```
{
```

```
fprintf(fp,"t1=%lf t2=%lf CA=%lf FA=%lf water=%lf cement=%lf GGBS=%lf FLA=%lf
Fibres=%lf pfib_mix=%lf Kfib=%lf SP=%lf pvol=%lf totvol=%lf nmod=%lf
delta=%lf",t1,t2,CA/totvol,FA/totvol,water/totvol,cement/totvol,GGBS/totvol,FLA/totvol,Fib
res/totvol,pfib_mix,Kfib,SP/totvol,pvol,totvol,nmod,delta);
```

```
if((water/totvol)>210)
    fprintf(fp,"**");
if(delta<-5.0 || delta>5.0)
    fprintf(fp,"##");
    fprintf(fp,"\n");
}
}
}
```

# APPENDIX B

## MATLAB CODES FOR GENERATING COMPRESSION AND TENSION DATA FOR CONCRETE DAMAGE PLASTICITY MODEL

MainCode:CompressiveBehaviour.m

```
1  %%%CodeforCompressionDataGeneration
2
6
7  clearall
8  clc
9
10 fck=input('InputcharacteristiccompressivestrengthofconcreteinMPa:');
11
12 if(fck==10||fck==15)
                                %%assumedstandarddeviationaccordi
    ngtoIS456:2000
13     std_dev=3.5;
14 elseif(fck==20||fck==25)
15     std_dev=4;
16 else
17     std_dev=5;
18 end
19
20 density=2400;%kg/m3
21 EcmACI=(33*((density*0.062428)^1.5)*((fck*145.038)^0.5))
    *0.00689476;%ACI,1992
22 fcm=fck+1.65*std_dev;%%Meancompressivestrengthofconcrete
23 EcmEURO=round(22*((0.1*fcm)^0.3)*1000,4);%%longitudanal
```



```

        modulusofelasticityasperthepaper(EUROCODE)
24 EcmIS=5000*(fck^0.5);%%asperIS456:2000Code
25 EcmNEW=9500*(fcm^(1/3));%%CEB-FIB
26
27 %%%---HSUandHSU---%%
28 sigma_cu=fcm*0.145037743;
29 eps_0=((8.9e-5)*sigma_cu)+(2.114e-3);
30 %E_0=((1.2431e2)*sigma_cu)+(3.28312e3);%%AsperWahalathantrithesis
31 E_0=0.145037743*EcmIS;
32 EcmWahala=E_0/0.145037743;
33 beta=(1/(1-(sigma_cu/(E_0*eps_0))));
34 eps_crit=round(((0.5*sigma_cu)/E_0),5);
35
36 %%%---SAENZFormula---%%
37 ec1=round(0.0014*(2-exp(0.0024*fcm)-exp(-0.140*fcm)),4);%%strainatmax.stress
38 ecu=round(0.004-0.0011*(1-exp(-0.0215*fcm)),4);%%finalstrain
39 optimum_factor=Optimum_Multiplication_Factor(fcm,EcmIS,ec1,ecu)
    ;
40 fcu=optimum_factor*fcm;%%fcuisthestressatfinalstrain
41 P1=ecu/ec1;
42 P2=fcm/fcu;
43 P3=EcmIS*ec1/fcm;
44 P4=((P3*(P2-1))/((P1-1)^2))-(1/P1);
45
46 A=1/EcmIS;
47 B=(P3+P4-2)/(P3*fcm);
48 C=-((2*P4)-1)/(P3*fcm*ec1);
49 D=(P4-1)/(P3*fcm*ec1);
50
51 eps_ref=1e-4*[11.7922886819012.6270815765513.89756717738
    14.1492365954714.5607431993514.9281300779215.25717211713
    15.55585634485];
52 aa=(fck-15)/5;
53

```

```

54  forii=2:10000
55      %---HsuandHsuExpesstion---%
56      eps_c(ii)=(ii-1)*1e-5;
57      ifeps_c(ii)<=eps_crit
58          sigma_c(ii)=(eps_c(ii)*E_0);
59      else
60          sigma_c(ii)=sigma_cu*((beta*eps_c(ii)/eps_0)/(beta-1
              +((eps_c(ii)/eps_0)^beta)));
61      end
62
63      eps_c_elas=sigma_c(ii)/E_0;
64      eps_c_in(ii)=eps_c(ii)-eps_c_elas;
65      E_secant(ii)=sigma_c(ii)/eps_c(ii);
66      d_c(ii)=(1-(E_secant(ii)/E_0));
67      eps_c_pl(ii)=eps_c_in(ii)-((d_c(ii)/(1-d_c(ii)))*(sigma_c(ii)/E_0));
68
69      %---SaenzExpression---%
70      ifeps_c(ii)<=eps_ref(aa)
71          sigma_saenz(ii)=EcmIS*eps_c(ii);
72      else
73
              sigma_saenz(ii)=(eps_c(ii)*(A+(B*eps_c(ii))+(C*eps_c(ii)^2)+
              (D*eps_c(ii)^3))^(-1));
74      end
75
76
              sigma_saenz_unmodified(ii)=(eps_c(ii)*(A+(B*eps_c(ii))+(C*eps_c(ii)^2)+
              (D*eps_c(ii)^3))^(-1));
77
78      eps_c_el_saenz=sigma_saenz(ii)/EcmIS;
79      eps_c_in_saenz(ii)=eps_c(ii)-eps_c_el_saenz;
80
81      ifsigma_c(ii)<(0.3*sigma_cu)&&eps_c(ii)>eps_0
              %%Conditonforstoppingiterations
82          break

```

```

83     end

84 end

85

86 eps_c_full=[0eps_c];
87 sigma_c_full=[0sigma_c]/0.145037743;
88 d_c_full=[0d_c];
89 eps_c_inel=[0eps_c_in];
90 eps_c_plas=[0eps_c_pl];
91 eps_c_inel_saenz=[0eps_c_in_saenz];
92 sigma_saenz_full=[0sigma_saenz];
93 Youngs_sigma=round((EcmIS.*eps_c_full(1:100)),1);
94 sigma_saenz_unmodified_full=[0sigma_saenz_unmodified];
95

96 forjj=1:length(eps_c_full)
97     d_c_Wala(jj)=eps_c_inel(jj)/eps_c_full(ii+1);
98     eps_plas_wala(jj)=eps_c_inel(jj)-((d_c_Wala(jj)/(1-
99         d_c_Wala(jj)))*(sigma_c_full(jj)/(E_0/0.145037743)));
100    d_c_saenz(jj)=eps_c_inel_saenz(jj)/eps_c_full(ii+1);
101    eps_plas_saenz(jj)=eps_c_inel_saenz(jj)-((d_c_saenz(jj)
102        /(1-d_c_saenz(jj)))*(sigma_saenz_full(jj)/(EcmIS)));
103 end

104

105 %%%forreducingtheno.ofobservations%%%
106 forabc=1:(floor((length(eps_c_inel))/50)+1)
107     xyz=((abc-1)*50)+1;
108     eps_c_inel1(abc)=eps_c_inel(xyz);
109     sigma_c_full1(abc)=sigma_c_full(xyz);
110     d_c_Wala1(abc)=d_c_Wala(xyz);
111     eps_plas_wala1(abc)=eps_plas_wala(xyz);
112     eps_c_inel_saenz1(abc)=eps_c_inel_saenz(xyz);
113     sigma_saenz_full1(abc)=sigma_saenz_full(xyz);
114     d_c_saenz1(abc)=d_c_saenz(xyz);
115     eps_plas_saenz1(abc)=eps_plas_saenz(xyz);
116 end
117
118

```

```

behaviour_Hsu_Comp=[eps_c_inel1'sigma_c_full1'd_c_Wala1'eps_plas_wal
a1'eps_c_inel_saenz1'sigma_saenz_full1'd_c_saenz1'eps_plas_saenz1'];

116

117 f_ctm=0.3*(fck^(2/3))                %%%MaximumTensilestress
118 Moduli_Values=[EcmWahalaEcmISEcmACIEcmEUROEcmNEW]
119

120 figure;
121 plot(eps_c_full,sigma_c_full);
122 %holdon
123 %plot(eps_c_full,sigma_saenz_full);
124 legend('\sigma_c-\epsilon_cHSU','\sigma_c-\epsilon_cSAENZ')
125 xlabel('\epsilon_c');ylabel('\sigma_c');
126

127 sigma_C_wahalan=[1624.729.731.63223.31916.214.413.1
12.1];
128 eps_C_wahalan=1e-4*[03.047.0711.91785.4153220286353
420];
129 d_c_wahalan=[00.00440.01030.01730.02480.1240.2220.32
0.4170.5130.61];

130

131 figure;
132 plot(eps_c_inel1,d_c_Wala1);
133 holdon
134 plot(eps_c_inel_saenz1,d_c_saenz1);
135 iffck==25
136     holdon
137     plot(eps_C_wahalan,d_c_wahalan)
138     legend('d_c-inelastic\epsilon_c','d_cWalahan-inelastic
\epsilon_c','d_cSaenz','DataforM25-Buddhi')
139 else
140     legend('d_c-inelastic\epsilon_c','d_cWalahan-inelastic
\epsilon_c','d_cSaenz')
141 end
142 xlabel('Inelastic\epsilon_c');ylabel('CompressiveDamage');

```

```

143
144 figure;
145 plot(eps_plas_wala1,sigma_c_full1);
146 holdon
147 plot(eps_plas_saenz1,sigma_saenz_full1);
148 legend('\sigma_c-Walahanplastic\epsilon_c','\sigma_c-Saenzplastic\epsilon_c')
149 xlabel('Plastic\epsilon_c');ylabel('\sigma_c');
150
151 X=[00.00040.00080.00120.00160.0020.00240.00360.005
      0.01];
152 Yse=[24.0129.2131.732.35831.76830.37928.50721.90714.897
      2.95];
153 figure;
154 plot(eps_c_inel1,sigma_c_full1)
155 holdon
156 plot(eps_c_inel_saenz1,sigma_saenz_full1)
157 iffck==25
158     holdon
159     plot(eps_C_wahalan,sigma_C_wahalan)
160     legend('\sigma_c-\epsilon_cinelasticHSU','\sigma_c-
            \epsilon_cinelasticSAENZ','dataforM25-Buddhi');
161 else
162     legend('\sigma_c-\epsilon_cinelasticHSU','\sigma_c-
            \epsilon_cinelasticSAENZ');
163 end
164 xlabel('Inelastic\epsilon_c');ylabel('\sigma_c');
165
166 xref=[ec1ecu];
167 yref=[fcmfcu];
168 figure;
169 plot(eps_c_full,sigma_saenz_unmodified_full);
170 holdon
171 plot(eps_c_full,sigma_saenz_full);
172 holdon
173 scatter(xref,yref);
174 xlabel('CompressiveStrain,\epsilon_c');ylabel('CompressiveStress,\sigma_c(MPa)')

```

```

175 legend('\sigma_c-\epsilon_cSAENZUnmodified', '\sigma_c-
    \epsilon_cSAENZModified', 'ReferencePoints')
Function:Optimum _ MultiplicationFactor.m

1 function optimum_factor=Optimum_Multiplication_Factor(fcm,Ecm,ec1,ecu)
2
3 %%%%%%%%%SaenzFormulationforCompressionCurve%%%%%%%%%
4 range=0.4:0.0001:0.7;
5
6 for ii=1:length(range)
7
8     fcu=range(ii)*fcm; %%fcu isthe stressatfinalstrain
9     P1=ecu/ec1;
10    P2=fcm/fcu;
11    P3=Ecm*ec1/fcm;
12    P4=((P3*(P2-1))/((P1-1)^2))-(1/P1);
13
14    A=1/Ecm;
15    B=(P3+P4-2)/(P3*fcm);
16    C=-((2*P4)-1)/(P3*fcm*ec1);
17    D=(P4-1)/(P3*fcm*ec1);
18
19    eps=[ec1 ecu];
20
21    for i=1:length(eps);
22        sigma(i)=eps(i)*(A+(B*eps(i))+(C*eps(i)^2)+(D*eps(i)^3))^(-1);
23    end
24    error(ii)=((sigma(1)-fcm)^2)+((sigma(2)-fcu)^2);
25 end
26
27 [~,index]=min(error);
28 optimum_factor=0.4+(index*0.0001);

```